Author:
Hares, Edward

Title:
The effect of creep strain rate on damage accumulation in type 316H austenitic stainless steel

THE EFFECT OF CREEP STRAIN RATE ON DAMAGE ACCUMULATION IN TYPE 316H AUSTENITIC STAINLESS STEEL

By

Edward Hares

May 2019

A thesis submitted to the University of Bristol in accordance with requirements of the degree of Doctor of Philosophy in the Department of Mechanical Engineering in the Faculty of Engineering

42000 words

Summary

With the constant growth in technology, there is an ever-growing demand on the power generation industry. This has made extending the life of conventional and nuclear power plants critical. Components operating at high temperatures can be subject to a variety of different loading conditions which include constant load creep, stress relaxation and creep-fatigue. This research highlights the impact these conditions have on the structural integrity of Type 316H stainless steel, which is a material commonly used to fabricate components in nuclear power plants e.g. pipes and other vessels. Laboratory experiments exploring different creep modes are typically conducted on uniaxial specimens. However, since service components in plants tend to experience multiaxial states of stress, the experimental and computational work reported within this thesis are predominantly on notched bar specimens. Adding a notch to standard specimens allows a multiaxial state of stress to be applied within standard uniaxial test rigs. It also allows creep failure data to be obtained more rapidly because of the increased stress concentration. The material used in this research was an ex-service austenitic stainless-steel Type 316H.

Constant load creep, stress relaxation and creep-fatigue all result in an increase in creep strain within components. It has been postulated that the more slowly creep strain is accumulated the more damaging it can be to service components. This rather unintuitive postulation has been made due to failures occurring within components with low levels of creep strain that have been in operation for several decades. The damaging effect of creep strain can be assessed by conducting constant load creep tests comparing the creep strain on failure and time to rupture for a variety of different applied net section stresses. A range of net section stresses were tested and it was subsequently found that the greater the net section stress, the greater the creep strain on failure and the shorter the time to rupture. This showed that equal amounts of creep strain accumulated more slowly were more damaging to notched specimens under constant load creep conditions. The damaging effects of creep strain rate can be assessed in repeat relaxation tests with varying dwell lengths as short-term relaxation tests can isolate the effects of the rapid accumulation of creep strain and the longer-term dwell tests can isolate the effect of creep strain accumulated more

slowly. Creep fatigue experiments allow the effect of reverse plasticity on subsequent creep to be explored.

Two different creep damage models were validated and assessed using the experimental data obtained in this work. The models were the "Spindler damage model" and the "Stress Modified Ductility Exhaustion" damage model. The Spindler damage model is a ductility exhaustion model where failure is deemed to have occurred when a finite limit to ductility is reached. The stress modified model is similar, but the ductility of the material is a function of the strain rate and applied stress. Once these models had been validated they were used to understand what was happening locally at the notch as this could not be monitored during testing for all the experiments.

One significant aspect of the results obtained from this research is that they can contribute to decisions whether nuclear power plants' stainless-steel components service lives can be prolonged, and they allow for accurate predictions of when components will fail based on their creep strain history. The experimental results show that the material being tested has a strain rate dependent ductility (a given amount of creep strain is less damaging the faster it is accumulated). The results add further characterisation to a commonly used service material and validate existing creep damage models for use on this material.

The novelty of this work is that results from laboratory and finite element experiments showed this material to exhibit a clear strain rate dependent ductility. All experiments conducted showed this material had an increased creep ductility at increased strain rates. The experimental methods used for conducting repeat relaxation and creep fatigue experiments of type 316H stainless steel were also novel.

Acknowledgements

One of the joys of reaching the end of this PhD is remembering all the friends and family who have supported me throughout.

Firstly, I would like to thank my supervisors, Chris Truman and Mahmoud Mostafavi for providing me with this opportunity and assisting me throughout. I am highly indebted to my supervisor Rick Bradford from EDF Energy for his continuous support, wealth of experience, guidance and time during the last three years. It certainly would not have been possible without his help.

I would like to thank all members of the Solid Mechanics Research Group for making the last three years so enjoyable and helping with the problems I've had along the way. I would like to give special thanks to Nader Zentuti, Andrew James, Satyajit Dey and Sam Oliver for helping me understand various analytical techniques, proof reading my work and always making time for me.

I would like to thank EDF Energy for funding this work and being supportive throughout. I am very grateful to Mike Spindler for all his help with both experimentation and analysis.

Finally, I would like to thank my friends and family for their love and support throughout this PhD. I would like to thank my friend and housemate Tom Bridgewater for his company and support throughout, for always being willing to have a tennis/sport break when I need to burn off some steam. I am very grateful to Emily Jelly for making the last few years the most enjoyable I've had with her company and love. I would like to thank both my parents for their support not only throughout this PhD but throughout my entire life. They have always gone above and beyond to support me and help me achieve everything I have set out to do.

I would also like to thank all those who have helped me directly in indirectly throughout the last three years that haven't been named in this acknowledgement.

Publications

Journal

1. Hares E, Mostafavi M, Bradford R, Truman C. "The effect of creep strain rate on damage accumulation in Type 316H austenitic stainless steel." *International Journal of Pressure Vessels and Piping* 168 (2018): 132-141.
2. Hares E, Mostafavi M, Bradford R, Truman C. "Repeat stress relaxation of notched bars and the dependence of creep damage on relaxation rate." *International Journal of Pressure Vessels and Piping* 169 (2019): 115-124.
3. Hares E, Mostafavi M, Bradford R, Truman C. " Creep-Fatigue of Notched Bars to Identify the Effects of Creep Strain Rate and Reversed Plasticity on Creep Damage" **(Under Review).**

Conference

4. Hares E, Mostafavi M, Bradford R, Truman C. The Influence of Creep Strain Rate on Creep Damage Formation in Austenitic Stainless Steel. ASME. Pressure Vessels and Piping Conference, *Volume 6A: Materials and Fabrication*: V06AT06A055. doi:10.1115/PVP2018-84635.
5. Hares E, Mostafavi M, Bradford R, Truman C. Creep Fatigue of Notched Bars. International Conference on Experimental Mechanics, *Brussels 2018*.
6. Hares E, Mostafavi M, Bradford R, Truman C. Creep Rupture of Notched Bars. International Conference on Fracture, Rhodes 2017.

Author’s Declaration

I declare that the work in this dissertation was carried out in accordance with the requirements of the University’s Regulations and Code of Practice for Research Degree Programmes and that it has not been submitted for any other academic award. Except where indicated by specific reference in the text, the work is the candidate’s own work. Work done in collaboration with, or with the assistance of, others, is indicated as such. Any views expressed in the dissertation are those of the author.

Signed: Date:

Contents

List of Figures

List of Tables

Nomenclature

Nomenclature from the literature review has been omitted as some symbols are used to define different variables in different damage models (stated for every damage model reviewed in the literature review). Beyond the literature review the following symbols are used to define the stated variables.

A	Primary creep constant
a	Radius of specimen at notched section
b	Radius of specimen at unnotched section
C	Secondary creep constant
C_f	Coefficient of fitted power law for fatigue calculation
D_0	Diameter after load up
d_c/D_c	Creep damage
D_f	Diameter on failure
d_f/D_f	Fatigue damage
E'	Augmented Youngs modulus
E	Youngs modulus
E_0	Extension after load up
E_f	Extension on failure
ε	strain
$\dot{\varepsilon}_c$	Creep strain rate
$\bar{\varepsilon}_c$	Accumulated von Mises creep strain
$\bar{\varepsilon}_f$	von Mises strain on failure
$\bar{\varepsilon}_{skf}$	Skeletal von Mises creep strain on failure
ε_c	Creep strain

ε_e	Elastic strain
ε_{fu}	Uniaxial lower shelf ductility
ε_h	Surface hoop creep strain
ε_{pl}	Plastic strain
ε_p	Primary creep strain
ε_s	Secondary creep strain
L	Length of specimen
m	Primary creep exponent (time)
n	Primary creep exponent (stress)
n_1	Secondary creep exponent (stress)
n_f	Exponent of fitted power law for fatigue calculation
N_f	Number of cycles to failure
η	Stress triaxiality (stress triaxiality is the hydrostatic stress divided by the von Mises Stress)
p	Cast specific material constant in triaxial correction to creep ductility
q	Cast specific material constant in triaxial correction to creep ductility
R	Radius of curvature of the notch
σ	Stress
$\bar{\sigma}$	von Mises equivalent stress
$\sigma_{0.2\%}$	0.2% proof stress
σ_1	Maximum principal stress
σ_p	Hydrostatic stress
T	Temperature

t	Time
t_r	Time to rupture
Z	Elastic follow-up factor

CHAPTER 1

Introduction

“What is not started will never get finished” – Johann Wolfgang von Goethe

Chapter 1 Introduction

1.1 Project background and aims

Advanced Gas Cooled Reactors (AGR) in the United Kingdom commonly have sections of the boilers including headers, pipework and tubing, fabricated from Type 316H austenitic stainless steel [1]. Austenitic steels show increased resistance to corrosion and creep as well as greater ease of welding and forming [2]. With the growing demand for the generation of more and cheaper electrical power in the UK the need to increase the life of nuclear power plants has grown significantly. There have been several unpredicted failures occurring within components fabricated from Type 316H stainless steel in the last 30 years in AGR plants operating at temperatures between 480 and 520˚C. These include the pressure tube failures in the UK between 1967 and 1972 which resulted in loss of fluid reviewed in [3]. It is important to be able to predict when failures are likely to occur for reasons of safety and economy.

It is currently common practice to conduct laboratory experiments to study the deformation and damage accumulation of austenitic steels used in power plants. However, these experiments tend to be accelerated creep tests because conducting tests at the low stress levels (0-80MPa) experienced by plant components takes decades and is not feasible within the time frame required to determine the fitness for service for operation of the UK's power plants. Recent findings have led to the belief that austenitic stainless steels could show a time dependent ductility at high temperature [4]. This means they will fail at a lower creep strain when subjected to lower stresses for very large periods of time. This phenomenon could explain some of the failures in austenitic steel components which have occurred significantly before best predictions.

Research has also indicated that when components are operating at high temperatures a varying load can have a damaging effect. This varying load can be due to a number of things such as power shutdown and plant restart, relaxation of residual stresses and cyclic behaviour of operation.

Given these considerations the main aim of this thesis was to determine the damaging effect of creep strain rate on equal amounts of creep strain accumulation. This aim was addressed by consideration of the following project objectives:

1) To perform experimental creep testing on notched bar specimens under constant load conditions at 550˚C at a range of different applied loads.

2) To perform experimental creep testing on uniaxial and notched specimens under displacement-controlled stress relaxation conditions at 515˚C and 550˚C with a range of different dwell times and start of dwell stresses.
3) To perform experimental creep fatigue tests on notched bar specimens at 550˚C with a range of different dwell times.
4) To conduct known methods of finite element analysis on all experiments conducted including creep damage models with strain rate dependence.
5) To analyse all data from experiments and finite element models and establish the effect creep strain rate has on damage accumulation in austenitic Type 316H stainless steel.

1.2 Thesis Structure

There are 8 chapters in this thesis. Chapter 1 is an introduction which provides the objectives and structure of the thesis.

Chapter 2 reviews the literature around topics related to this thesis. The topics covered include austenitic stainless-steel Type 316H, prior service history (heat treatment and pre-straining), different types of creep of notched bar specimens (creep rupture, stress relaxation and creep fatigue) and creep damage models.

Chapter 3 describes the common methodology across all experiments. The specimen geometry, details of the experimental rigs, derivations of material constants and finite element methodologies are stated.

Chapter 4 details creep rupture of Type 316H stainless-steel. Existing uniaxial creep data is reported. This leads into the primary focus of this chapter – creep rupture of notched bars. The test experimental results and results from various creep damage models are detailed. The effect of creep strain rate accumulation on subsequent creep damage was explored.

Chapter 5 details stress relaxation of Type 316H stainless-steel. Uniaxial stress relaxation tests are reported at various loads and compared with results from various finite element models. The main focus of this chapter was the repeat stress relaxation experiments conducted on notched bar

specimens. These tests were conducted to investigate the relative damaging effects of creep strain accumulated rapidly at the start of the dwell and equal amounts of creep strain accumulated much more slowly towards the end of the dwell. Effects of lower test stress and temperature were also explored. Experimental results were then compared with results from different finite element creep damage models.

Chapter 6 focuses on creep fatigue of Type 316H stainless-steel notched bar specimens. The experimental methodology is detailed before the experimental results are reported. The main aim of the work described in this section was to isolate the effect of a fatigue cycle between stress relaxation dwells. The results from the creep fatigue tests are compared with the results from the repeat stress relaxation tests as well as results from various finite element creep damage models and R5 assessments.

Chapter 7 provides an overall discussion of this research, linking all the main findings and experimental results.

Chapter 8 states the main conclusions from this work and suggests potential future work in this area.

CHAPTER 2

Literature Review

"It always seems impossible until it's done." – Nelson Mandela

Chapter 2 Literature Review

2.1 Introduction

Many different types of steel are used in nuclear power plants, including austenitic stainless-steel type 316H (cast 69431), which is the main subject of this study. Some of these plants have been operating at high temperature for decades. This means that structural integrity assessments for the components are key and understanding the thermo-mechanical history of a material vital to the meaningful prediction of service life. The material used in this thesis has been thermally aged during prior service history. The first area of interest in this literature review is the material that is being used for all testing within this Thesis - the chemical composition of the material and how previous service history affects its creep properties.

The second area of focus in this literature review is creep rupture. Creep rupture tests are also known as forward creep tests and refer to a specimen subject to a constant load at a constant temperature until the specimen ruptures. The review starts by detailing uniaxial tests which have been conducted on the material used in the study and on similar materials. Thereafter experiments conducted on notched bar specimens are reviewed.

The third topic covered in this review is stress relaxation, otherwise known as displacement-controlled creep. In stress relaxation tests a displacement or load is applied to the specimen and then the displacement is fixed, followed by the specimen being allowed to relax for a set dwell time. During this time the overall displacement will remain constant and the stress on the specimen will drop as it is subject to creep. Uniaxial tests are reviewed initially and then experiments on notched bar specimens are reviewed.

Creep fatigue is the fourth topic reviewed in this work. Experiments are reviewed where fatigue is applied to the specimen followed by the applicated of creep (pre-strained). Thereafter experiments where creep dwells and fatigue dwells are alternately applied to specimens are discussed.

The fifth area of interest in this review is the finite element models which have been used for creep damage modelling, what their assumptions and limitations are and which is the most effective available model. Creep damage is a phenomenon that commonly occurs in metals and alloys with prolonged exposure to stress at elevated temperatures. It tends to be associated with the tertiary stage of creep and brings about the onset of creep failure. It is possible for creep damage to initiate

at the relatively early stages of creep and gradually develop throughout a material's creep life. The manifestation of creep damage is often voids or cavities being formed within the microstructure of the material [5]. However, it is not clear that creep damage is always manifest in the form of cavities, and in this work the signature of creep is time dependent failure which is sensitive to temperature, i.e., an engineering level perspective.

These areas of interest were chosen because the aim of this work was to explore whether Type 316H stainless steel exhibited a strain rate dependent creep ductility. It was of interest to know if this behaviour had been seen in constant load and constant displacement creep as well as creep fatigue as these are all conditions commonly occurring in plant life. Notched bars were of particular interest because they are more representative of plant components (e.g. weld toes).

2.2 Type 316H Austenitic Stainless-Steel Cast 69431

Type 316H stainless steel is an austenitic stainless steel that is regularly used in the power generation industry. 316H is used widely in the British nuclear industry and is a major constituent in Advanced Gas-Cooled Reactors (AGR). The present alloying elements in type 316 are Chromium (Cr), Nickel (Ni) and Molybdenum (Mo) with quantities of approximately 17, 11 and 2-4% respectively (by weight). Ni is alloyed in these percentages as it helps with the stabilisation of the austenite phase at room temperature with the removal of most of the ferritic phase, this rules out any ductile to brittle transition [6]. Cr forms an oxide layer on the surface of the steel which prevents corrosion [7]. The main difference between 316H and similar steels (316L, 316N) is the increased amount of carbon [8]. The chemical composition of the cast of steel used in this research is shown in Table 2.1.

Table 2.1- Chemical composition of cast 69431 by weight % [9].

C	Si	Mn	S	P	Ni	Cr	Mo	Co	B
0.06	0.4	0.98	0.014	0.021	11.83	17.17	2.19	0.1	0.005

Austenitic steels have very different properties to ferritic steels. These include:

- Lower yield strength than ferritic steels
- High ductility in terms of both plasticity and creep, however the creep ductility is not always high, especially over long timescales.
- significant changes in plastic strain for small stress changes

The lower yield strength means that austenitic steels have a greater capacity for work hardening than ferritic steels [10]. The high ductility allows plant components to experience high plastic strains on loading as well as large residual stresses after cyclic loading. Pre straining before creep causes a decrease in ductility despite the increase in strength due to work hardening [11].

Most of the work done in AGR plants with 316H stainless steel is limited to temperature values in the range of 480˚C to 600˚C, because of this most of the research has been performed at these temperatures [12-14].

EDF Energy provided Type 316H stainless steel from cast 69431 for the experiments conducted in this thesis. The material was from an ex-service header, header 2C2/3. This material had a previous service history, 51000 hours at temperatures between 480˚C and 510˚C. This prior service history will have thermally aged the material.

2.2.1 Prior Heat Treatment/Thermal Ageing (TA)

The material studied in this thesis has previously been exposed to high temperature conditions while in service. This has caused a thermal ageing process that altered its microstructure and changed its material properties. It has been previously shown that long term ageing of 316 austenitic stainless steels produces a complex microstructure, it also changes the mechanical properties of the material.

The most well documented change is the material embrittlement, this is not caused by the formation of a sigma phase but arises from dense $M_{23}C_6$ precipitates at the grain boundaries [15]. This is due to the very heavy carburisation (up to 0.5mm) due to CO_2 effects in AGRs. This embrittlement causes the steel to be very sensitive to work hardening effects. This means thin specimens can complicate testing as different failure modes can arise (brittle failure). Larger, round notched bar specimens are used for experiments conducted within this thesis so there are limited surface effects.

Previous research has established that the temperature at which steel is thermally aged has a dramatic effect on its end properties. When 316 stainless steel was thermally aged at 450˚C for 50,000 hours there was no effect towards the fracture toughness of the material, whereas when it was thermally aged for the same duration at 550˚C the fracture toughness was reduced [16].

2.3 Creep Rupture

2.3.1 Creep Rupture of Uniaxial Specimens

The material used in this study (Type 316H stainless steel cast 69431 header 2C2/3) has previously been tested under uniaxial creep in unpublished work by M. Spindler of EDF Energy [17]. Eight constant load tests were conducted at 550˚C with applied net section stress values ranging from 160-360MPa. The time to rupture for the highest stress value (360MPa applied stress) was 79 hours, the test at 230MPa had a rupture time of 11204 hours (the test at 160MPa was stopped once secondary creep was reached). It was found that the time to rupture increased rapidly with a decrease in applied stress. The deformation data from these experiments were used to calculate the primary and secondary constants for this cast of material for finite element analysis (discussed later).

Uniaxial forward creep (constant load) experiments were conducted at 550˚C by Kim et al [18]. All the specimens were fabricated from Type 316H austenitic stainless-steel. The specimens tested had a diameter of 6.68mm and a gauge length of 36mm. The stresses applied to the specimen were 290MPa, 308MPa, 349MPa, 359MPa and 366MPa. These led to rupture times of 6000hours, 3200hours, 950hours, 700hours and 550hours respectively. There was no significant trend between the creep strain on failure and the applied stress, the creep strains on failure varied between 6% and 8%.

2.3.2 Creep Rupture of Notched Bars

When designing structures that will experience creep the problem that is currently least well understood is creep rupture, which is brought about by the accumulation of creep damage. The main difficulty is the prediction of crack growth and propagation due to stress. When cracks occur, a decision needs to be made to repair the defect or continue operation. Repairing cracks can be very expensive but predicting component life requires very accurate techniques.

Methods of assessing creep damage under homogenous, uniaxial states of stress have been developed and tested. These laws have not been rigorously tested for a triaxial state of stress. They have been implemented to analyse semi-circular notched bar specimens but not to the same extent and accuracy as with standard un-notched creep specimens with a uniaxial state of stress.

Adding a notch to a standard creep specimen allows a stress triaxiality to be obtained using a standard dead weight creep rig. This gives a more accurate representation of plant behaviour and reduces the duration of the testing time. However it also greatly increases the complexity of analysing the results obtained during creep experimentation.

Mike Spindler of EDF Energy conducted creep rupture experiments on notched bar specimens fabricated from Type 316H stainless-steel, cast 69431, the same material used within the work in this thesis. Double notched bar specimens were fabricated with varying notch acuities [4] (notch acuity is defined as a/R where a is the radius of specimen at the notched section and R is the radius of the notch). Notch acuities of 1.5, 2.41, 5 and 15 were tested, all tests were conducted at 550˚C. It was unsurprisingly found that increasing the notch acuity reduced the time to rupture (due to the increased stress triaxiality and increased local stress) and increased the hoop creep strain on failure. Increasing the applied stress reduced the time to rupture and increased the hoop creep strain on failure. For the tests conducted at a notch acuity of 5 the maximum hoop creep strain on failure occurred at the highest stress test (500MPa) and was 2.7%. The lowest hoop creep strain on failure occurred at the lowest stress test (320MPa) and was 0.96%. The creep strain was almost 3 times as large at the higher stress test where the test duration was 15 hours as opposed to the lower stress test where the test duration was 5718 hours. The same trends were apparent in the other tests with different notch acuities.

Takahashi et al [19] conducted tests at 550˚C on notched bar specimens fabricated from Type 316FR stainless steel, a similar material to the one used in this study. They found that with an increase in net section stress the time to rupture was greatly reduced. With a notch acuity of 2 and a net section stress of 353MPa the time to rupture was 218 hours. Using an identical specimen with a net section stress of 245MPa the time to rupture was 94,177 hours. They found that extension of the specimens on failure increased with an increase in net section stress. With a net section stress of 353MPa the extension on failure was 39% and with a net section stress of 245MPa

the extension on failure was 28%, these extension values did not include the loading phase (plastic strain). These results also showed a greater reduction in cross sectional area of the specimens at the notch with increased net section stress. The reduction of area at the notch on failure for the test with a net section stress of 353MPa was 52% and 45% with a net section stress of 245MPa. These values for reduction in area did not include plastic loading strain.

Creep rupture experiments were conducted by Kim et al. on three different notch acuity specimens fabricated from Type 316H stainless steel [18]. The notch acuities tested were 1.5, 5 and 15. The minimum diameter of the notched bars was 5.64mm and the gauge length 36mm in all tests. All tests were conducted at 550˚C. The tests were conducted to determine the effect of stress triaxiality on multi-axial creep ductility. The researchers found the same trends as Spindler. With an increase in test stress the time to rupture reduced and the creep strain on failure increased. With an increase in notch acuity the time to failure reduced and the creep strain on failure increased.

2.4 Stress Relaxation

2.4.1 Stress Relaxation of Uniaxial Specimens

One repeat stress relaxation test of a uniaxial specimen fabricated from the same material used in this study was conducted by EDF Energy at 550˚C. In this experiment a net section stress (start of dwell stress) of 300MPa was applied and then allowed to relax for 500-hour dwells before being re-applied. The specimen ruptured after 35 dwells (17,500 hours). It was found the creep strain on failure was 3.25% for this experiment.

Researchers at the University of Bristol and EDF Energy conducted stress relaxation experiments on the same cast of Type 316H stainless steel used within this work (69431) [20]. However, the specimens were fabricated from a different header which had a different history, header 2D2/3. This had been subject to the same prior service history as the material used within this thesis but had also been subsequently heat treated for 21,000hours at 550˚C, causing additional ageing. The stress relaxation tests were conducted on dead weight creep rigs. The strain was kept constant by manually removing the load while monitoring the strain. Eight stress relaxation tests were conducted at temperatures ranging between 475˚C and 600˚C and initial stress ranging from 125MPa to 230MPa. It was found that the stress relaxation behaviour was strongly dependent on

the test temperature. It was also found that the higher the test temperature the lower the stress value at which the test plateaus. At a test temperature of 600˚C the stress relaxed to 45MPa but at 475˚C the test only relaxed to 140MPa even when maintained for over 10,000hours. It was found that at temperatures above 500˚C the stress relaxation rate was strongly dependent on the initial stress. At temperatures of 550˚C and above it was found that the stresses would converge at a fixed value after 100 hours of relaxation regardless of the initial stress. It was found in all tests that the creep stress relaxation rates continuously reduced with time.

Stress relaxation tests were conducted at 550˚C on uniaxial test specimens fabricated from Type 316H stainless steel by Fookes et al [21]. Stress relaxation tests were conducted at fixed strain values of 0.2%, 0.3%, 0.4% and 0.5%. It was found that the stress relaxed more in a 50 hour dwell at higher test strains than lower test strains. The end of dwell stresses came close to converging with each other regardless of initial applied strain at the end of a 50-hour dwell, as was seen in previous work conducted by Wang et al [22].

2.4.2 Stress Relaxation of Notched Bars

Many repeat relaxation notched bars tests conducted on Type 316H stainless steel have been performed in unpublished work by EDF energy. These tests have been conducted with temperatures ranging from 475-550˚C, start of dwell stresses from 350-390MPa, notch acuity values ranging from 1.06 to 30 and dwell times of 100-500 hours. These experiments were performed on parent, HAZ and welded HAZ. It was found that the sharper the notch (higher the notch acuity) the shorter the time to failure (faster damage accumulation) and the higher the mean ductility [23]. The results showed that temperatures below 515˚C led to substantially longer times to failure. Varying the temperature between 515-550˚C appeared to have no effect on the duration of the experiments although only one test was performed at each temperature other than 550˚C. (We shall see later that this can be explained by a lower ductility at 515ºC compensating for the lower creep rate at this temperature). Raising the start of dwell stress led to shorter rupture times and increased ductility. Increasing the notch acuity led to a shorter time to rupture and an increased creep strain on failure. The final finding from these tests was that the parent material had a greater rupture life than the HAZ material.

2.5 Creep and Fatigue

Creep damage and fatigue damage can occur separately and progressively during plant operation [24]. Fatigue damage is related to the magnitude and number of load cycles whereas creep damage is related to steady load levels and operating temperature. There are commonly occurring circumstances under which fatigue damage and creep damage can interact leading to the sudden onset of cracking and much reduced component endurance [24]. Creep-fatigue experiments typically have alternating fatigue cycles and creep dwells applied to a specimen until rupture. In pre-straining/prior plasticity experiments a number of fatigue cycles are applied to the material and it is subsequently subject to creep testing. In fatigue damage you see transgranular cracking where the crack follows a relatively straight path compared with creep failures which are mainly intergranular and the crack follows the edges of the lattices. Creep and creep fatigue failures can both show regions of both transgranular and intergranular behaviour making them hard to categorize.

2.5.1 Creep-Fatigue

The combination of creep and fatigue deformation is known to be one of the most important problems for design of high-temperature components [25]. This is often simulated in laboratories by conducting high-temperature low-cycle fatigue (HTLCF) experiments. These experiments tend to include hold periods at either a constant strain or stress. There has been considerable effort made to characterise the HTLCF behaviour of structural materials. It has been found that frequency, strain rate, hold position, hold period and strain range are key factors in the outcome of these HTLCF experiments.

In [26] the researchers investigate the development of intergranular strains and stresses in Type 316H austenitic stainless steel during cyclic loading at high temperature. Experiments were conducted at 650˚C with 2-hour displacement-controlled creep dwells at maximum strains every cycle. An in-situ neutron diffraction monitoring system was used at a time of flight facility. It was found that intergranular strains during the first dwell remained unchanged but relaxed over time in later dwells. The start of dwell intergranular strains increased cycle upon cycle, but the rate of increase reduced each cycle.

In [27] long term creep-fatigue tests were conducted at 550 and 600˚C on Type 316FR stainless steel. Creep-fatigue lives under a biaxial state of stress were obtained using cruciform test

specimens. Using the von Mises strain range as a governing parameter the fatigue lives could be conservatively predicted for all strain ranges. A more accurate lifetime prediction was given using a version of the ductility exhaustion approach where only the creep strain is assumed damaging and minimum rupture elongation is taken as the ductility. The introduction of a strain rate dependent ductility had little effect on the results.

Creep-fatigue experiments were conducted on uniaxial welded specimens made from the same material as the material used within this work by Spindler [28]. It was found that tensile residual stresses could be of a similar magnitude to the yield magnitude of the material. Displacement controlled tests were conducted, and it was found that the presence of tensile residual stresses within welded components accelerated the crack growth rate and reduced the time to rupture.

Previous creep fatigue experimentation on Type 316 stainless steels has focused on uniaxial specimens [25, 26, 29, 30]. Creep fatigue experimentation has been conducted on weldments [28, 31], varying hold times [32, 33] and life predictions [27, 34, 35]. Equations have been developed for predicting lifetime of these uniaxial fatigue tests [36]. A gap in the literature for creep-fatigue of notched bars has been identified. This is relevant to industry because service components experience high stress triaxiality factors which can exceed the 0.33 value which is representative of un-notched bars. Stress triaxiality, η, accelerates structural degradation of components during creep, it is the hydrostatic stress divided by the von Mises stress [37, 38]. Component failure strains are greatly affected by stress triaxiality [39]. Ductility exhaustion states failure will occur when the accumulated strains equal the available ductility.

2.5.2 Prior Fatigue (Pre-straining) then Creep

2.5.2.1 316 Stainless Steel

Wei and Dyson [40] conducted experiments to determine the effect of prior cyclic loading on subsequent creep tests. Tubular specimens of 316 stainless steel were pre-strained to creep strain values of 0.5%, 1.0% and 1.5%. It was found that the sample that had been subjected to the greater pre-strain showed a lower minimum creep rate, longer life and a higher ductility than the samples pre-strained to a lesser strain.

Murakami et al [41] also conducted creep tests with tubular specimens that had been pre-strained. These specimens were heat treated for an hour at 920°C. The subsequent pre-straining and creep tests were conducted at 600°C. These specimens had been subject to a uniaxial cyclic pre-strain strain of 0.8%. The samples then had a uniaxial stress applied of either 230, 252 or 270MPa which was terminated after 100hours. The main findings were that uniaxially pre-strained samples that were subject to creep in tension experienced a greater strain rate than unstrained (virgin) material. Samples in tension-torsion experienced very similar values of strain rate whether pre-strained or not, this was a significantly faster strain rate than the samples under pure torsion. It was concluded that at low creep stresses the anisotropicity (has a different value when measured in a different direction) introduced by the pre-straining controls the creep behaviour but at high stresses this is overcome and the pre-straining has little effect [41].

Tavassoli et al [42] cyclically pre-strained type 316L stainless steel. This cyclic pre-strain was conducted at 600˚C, the pre-straining had a range of 0.7 or 1% and was fully reversed. On completion of the pre-straining the sample was immediately held at a constant stress (stress values of 300MPa and 250MPa were used). The analysis of experiments concluded that a reduction of creep rupture lives of pre-strained samples only occurs when prior fatigue damage exceeds $N/N_F=0.5$ (the proportion of fatigue life experienced by the sample). Some of the pre-strained samples had creep lives up to 5 times that of the virgin material whereas others had very similar creep lives to the virgin material. It was thought that the material work hardened at low levels of pre-strain.

Fookes et al [43] conducted tests on type 316L stainless steel. They used specimens with a 10mm diameter and a gauge length of 22mm prior to their cyclic pre-straining which was conducted at 600˚C. The pre-straining was conducted at strain ranges of 1 and 1.6%, the rate of pre-straining was $0.1\%s^{-1}$. The specimens were re-machined post pre-straining into creep specimens with a 6mm diameter and 16mm gauge length. It was found that the pre-straining considerably reduced the creep strain rates when compared to results with the virgin material. Primary creep was eliminated in the pre-straining process.

Skelton and Horton [44] conducted creep tests on samples of Type 316 stainless steel at 625˚C that had been cyclically pre-strained. The specimens had a diameter of 12.7mm and a gauge length of 25mm. The pre-straining was at a rate of $0.01\%s^{-1}$ to a strain range of 0.2%. (Between 705 and

710 cycles). The specimens were then re-machined into creep specimens with a diameter of 3.8mm and a gauge length of 25mm. Constant load creep tests were conducted at a temperature of 625˚C and a stress of 140MPa. The ductility (axial strain on failure) was greatly reduced (from 52 to 13.5%) and the creep life was greatly increased (from 6,000 to 25,000 hours). It should be noted that the pre-straining conducted in these experiments was completed in a vacuum.

Rezgui [45, 46] conducted experiments on type 316L stainless steel to determine the effects of prior cyclic loading at 600˚C (for both pre-straining and subsequent creep experiments). Specimens were pre-strained to a strain range of 1.4% and creep tests were conducted at 200 and 300MPa. It was found that the creep rupture life doubled with pre-straining and the minimum creep strain rate halved. The sample with pre-straining had a shorter secondary creep phase and a reduced amount of creep strain at the end of the secondary phase when compared to the virgin material. The pre-straining had very little effect on the creep strain at failure.

The research of most relevance was conducted by a previous researcher at the University of Bristol on the same cast of material (with additional thermal ageing) used in this Thesis on the same apparatus (Tim Joseph). Joseph investigated the effects of prior heat treatment on the creep properties of type 316H stainless steel (cast 69431 from an ex-service header 2D2/3). Solid creep specimens with a diameter of 5.65mm and a gauge length of 28.25mm were used. This cast had a previous service history and had then undergone subsequent heat treatment at 550°C for 21,000 hours. Six uniaxial creep tests were conducted in the University of Bristol creep lab with varying applied loads. The results from these experiments were compared to those obtained from British Energy [47] with the same material with the previous service history but no subsequent heat treatment.

When Joseph compared the results of his experiments to the results obtained by British Energy with the same material without prior heat treatment he found:

- Creep life and duration of primary creep were not significantly affected by heat treatment.
- Plastic strain was slightly lower in the specimens post heat treatment.
- The minimum strain rate in the samples that were heat treated was higher than that in the untreated samples.

- The most significant change was the relatively large increase in creep ductility with heat treatment. With heat treatment the true creep strain was in the range of 25-33% at the end of testing and in the untreated material only 5-16%.

As well as the samples taken to failure, Joseph conducted a creep test with the same dimension specimen with the same material but with a strain range of 1.2% (±0.6%). The results from this experiment were compared with those obtained by British Energy at strain ranges of 1.5, 0.9, and 0.6% (±0.75, 0.45 and 0.3%). The material from Joseph's experiments (cast 69431, header 2D2/3) exhibited a higher stress range at the start of the test (±218 vs ±190MPa) but underwent significantly less hardening during the experiment, in terms of both stress per cycle and number of cycles until peak stress. The material from Joseph's header failed at a lower number of cycles (1015 vs 1378). This indicated that heat treatment may make the material more susceptible to damage from cyclic loading in strain control. The final experiments that Joseph ran were creep tests with prior heat treatment and prior straining. He observed that a significant reduction in creep strain rate was found in all areas of the test matrix and that the observed minimum strain rate decreased with increases in both N/Np (Np was the number of cycles to peak hardening) and strain range.

2.5.2.3 Summary

The common conclusion drawn from the experiments reviewed on type 316 and 304 stainless steels was a decrease in the minimum true creep strain and an increase in the creep rupture life of the material with pre-straining. The minimum creep strain rate tends to reduce by a factor of between 2 and 6 and there is also an increase of a factor between 2 and 6 for the observed creep rupture life of the material. Joseph also confirmed that prior cyclic loading drastically reduces creep strain rates with his experimentation at the University of Bristol. He found that this decrease in minimum strain rate was associated with an increased number of cycles in the pre-straining.

One of the experiments on type 316 stainless steel [48] found there was an increase of a factor between 2 and 5 in the final creep ductility of the sample. The tests by British Energy showed inconclusive results; in one there was an increase in creep ductility but in the other the creep ductility remained unchanged. These tests were on type 304 stainless steel. In a further experiment conducted by Skelton and Horton [44] it was found that the final ductility decreased by a factor of

4 after cyclic pre-straining under a vacuum but was restored after heat treatment. Other experiments showed that pre-straining had little effects on ductility [45].

As expected type 304 and 316 stainless steels exhibited cyclic hardening.

2.6 Creep Damage Models

Creep damage is a phenomenon that occurs in metals and alloys. Creep damage is caused by prolonged exposure to stress at high temperatures. In general it is associated with tertiary creep and brings about creep failure [49, 50]. This is not always the case, sometimes it can develop in the early stages of creep and develop more gradually throughout a component's creep life. The onset of creep damage can be caused by the formation of creep cavities or voids within the material's microstructure [5, 51]. The damage models that have been most successfully used to analyse steel components under creep conditions are detailed below.

2.6.1 Kachanov Model

Hyde, Becker, Sun and Williams created a creep damage model for the analysis of P91 pipes. This was developed at the University of Nottingham [52]. The finite element analysis calculations were conducted through the use of a user sub-routine. Material constants were added for the P91 steel at a given temperature. Finite element modelling of notched bar creep rupture tests were conducted to obtain the material constants for the one and three state variable equations [53, 54].

This finite element model utilized the Kachanov type equations [55]. Both the one and three state variable equations have been implemented within Abaqus. The equations for the one state equation were as follows for a uniaxial form [56, 57]:

$$\frac{d\varepsilon^c}{d_t} = A'(\frac{\sigma}{1-\omega})^n t^m \qquad (2.1)$$

$$\frac{d\omega}{d_t} = B'\frac{\sigma}{(1-\omega)^{\emptyset}} t^m \qquad (2.2)$$

where A, B, n and m were material constants, σ was the applied stress, ω was the damage variable, t was the time and ø the ageing damage parameter.

And the uniaxial form of the three state variable equations were as follows:

$$\frac{d\varepsilon^c}{d_t} = Asinh(\frac{B\sigma(1-H)}{(1-\emptyset)(1-\omega_2)}) \quad (2.3)$$

$$\frac{dH}{d_t} = \frac{h}{\sigma}\frac{d\varepsilon^c}{dt}(1-\frac{H}{H^*}) \quad (2.4)$$

$$\frac{d\emptyset}{d_t} = \frac{k_c}{3}(1-\emptyset)^4 \quad (2.5)$$

$$\frac{d\omega_2}{d_t} = D\frac{d\varepsilon^c}{d_t} \quad (2.6)$$

where k_c was another material constant, D was the damage, ε^c was the creep strain, H was the strain hardening variable and H* was the strain hardening variable at saturation.

When the researchers at the University of Nottingham used these damage equations in their finite element analysis of notched bar P91 stainless steel specimens they found the peak stress occurred at the root of the notch where the stress raising feature was most severe. The notch radius was 2.5mm and the diameter of the bar 12.5mm in these simulations. Implementing this model, it was found that the time to failure for the one variable equations with a nominal stress of 93MPa was approximately 996 hours and with the three-variable equation 1127 hours. These were simulated at 650˚C. Comparing these results with the experiments gave very good agreement, under the same conditions an actual test sample failed after 1050 hours. When the simulations were conducted with an applied stress of 82MPa the opposite trends were found with the one state variable equations giving a slight overestimation of time to failure and the three state variable equations giving a slight underestimate of the time to failure.

2.6.2 Spindler (Ductility Exhaustion and Stress Modified Ductility Exhaustion Models)

There is a simple formula for calculating fatigue damage, D_f, in ASME [58], RCC-MR and R5, it is

$$D_f = \sum_i \frac{N^{(i)}}{N_o^{(i)}} \quad (2.7)$$

$N^{(i)}$ is the number of cycles of type i, $N_o^{(i)}$ is the corresponding continuous cycling fatigue endurance at the same total strain range. When using this equation it is usual to define N_o as $N_{5\%}$ of continuous cycling tests where [59]

$$\log(N_{5\%}) = 1.8655 + \frac{0.9370}{\Delta\varepsilon_T} \tag{2.8}$$

To estimate creep damage, a time fraction rule can be applied. It is used in design codes such as ASME and RCC-MR, using this rule the total creep damage is given by [60]

$$D_c^{TF} = \sum_i N^{(i)} \int_0^{t_h^{(i)}} \frac{dt}{t_f(\sigma, T)} \tag{2.9}$$

where t_f is the creep rupture time at a temperature, T and stress, σ.

In R5 a ductility exhaustion approach is used to calculate the total creep damage, D_c^{R5}, this equation is given by

$$D_c^{R5} = \sum_i N^{(i)} \int_0^{t_h^{(i)}} \frac{\dot{\varepsilon}_c}{\varepsilon_f(\dot{\varepsilon}_c, T)} dt \tag{2.10}$$

Where ε_f is the multiaxial ductility given by equation 2.11 for the Spindler damage model

$$\frac{\bar{\varepsilon}_f}{\varepsilon_{fu}} = \exp\left[p\left(1 - \frac{\sigma_1}{\bar{\sigma}}\right)\right] \exp\left[q\left(\frac{1}{2} - \frac{3\sigma_p}{2\bar{\sigma}}\right)\right] \tag{2.11}$$

where $\bar{\varepsilon}_f$ and ε_{fu} are the von Mises equivalent and uniaxial strains to failure, respectively. σ_1, $\bar{\sigma}$ and σ_p are the maximum principal, von Mises equivalent and hydrostatic stresses, respectively. p and q are constants based on the material and test temperature. They were calibrated to give the best fit for Type 316 stainless steel at 550˚C using notched bars with a notch acuity 5 in previous research conducted by Spindler[61]. The values of p and q established by Spindler were 1.2 and 1.0 respectively for the material used in this study. These values were assumed at both test temperatures, 550ºC and 515ºC.

Another method for measuring creep damage in R5 is the stress modified ductility exhaustion scheme, which is a slight modification on the ductility exhaustion approach. This modification means that the effect of stress on creep damage is included, this is achieved by treating the ductility as a function of both stress and strain rate. The new expression for the total creep damage, D_c^{SM}, is given by

$$D_c^{SM} = \sum_i N(i) \int_o^{t_h^{(i)}} \frac{\dot{\varepsilon}_c}{\varepsilon_f(\dot{\varepsilon}_c, \sigma, T)} dt \tag{2.12}$$

where $\varepsilon_f(\dot{\varepsilon}_c, \sigma, T)$ is the multiaxial creep ductility at a given temperature as a function of stress and strain rate (given by equation 2.13).

$$\varepsilon_f(\dot{\varepsilon}_c, \sigma, T) = \mathrm{MAX}\left\{ \begin{array}{c} \mathrm{A_1 exp}\left(\frac{\mathrm{Q_1}}{\mathrm{T}}\right) \dot{\bar{\varepsilon}}_{\mathrm{in}}{}^{\mathrm{n_1}} \sigma_1{}^{-\mathrm{m}}, \\ \mathrm{MIN}\left[\varepsilon_{\mathrm{L}}, \mathrm{A_2 exp}\left(\frac{\mathrm{Q_2}}{\mathrm{T}}\right) \sigma_1{}^{-\mathrm{m_2}}\right] \end{array} \right\} . \left[\frac{\bar{\sigma}}{\sigma_1} \exp\left(\frac{1}{2} - \frac{3\sigma_{\mathrm{p}}}{2\bar{\sigma}}\right)\right] \tag{2.13}$$

where $\varepsilon_f(\dot{\varepsilon}_c, \sigma, T)$ is the von Mises inelastic strain at failure at the appropriate temperature as a function of both the von Mises inelastic strain rate, $\dot{\bar{\varepsilon}}_{\mathrm{in}}$, and the maximum principal stress, σ_1. In addition, ε_L is a lower shelf creep ductility (which is independent of stress and strain rate). A_1, n_1, m_1, Q_1, A_2, m_2, and Q_2, are material parameters for regions 1 and 2 respectively (region 1 is the transition region and region 2 is the lower shelf region). $\bar{\sigma}$ is the von Mises stress and σ_{p} the hydrostatic stress. The units are strain in mm/mm, stress in MPa and temperature in Kelvin.

Whilst a strain controlled creep dwell is ongoing the instantaneous creep strain is constantly falling as the stress reduces, the creep damage is calculated via the creep ductility for every increment. However it is typical to use the average creep strain rate, ε_f/t_f, when fitting data [62].

2.6.3 Liu and Murakami

The model designed by Liu and Murakami [63] is as shown

$$\dot{\varepsilon}_{ij}^{c} = \frac{3}{2} C \sigma_{eq}^{n2} \frac{S_{ij}}{\sigma_{eq}} exp \frac{2(n_2 + 1)}{\pi \sqrt{1 + \frac{3}{n_2}}} \cdot \left(\frac{\sigma_1}{\sigma_{eq}} \right) \cdot \omega^{\frac{3}{2}} \quad (2.14)$$

where

$$\dot{\omega} = D \frac{(1 - e^{-q2})}{q_2} {\sigma_r}^p e^{q2\omega} \quad (2.15)$$

and

$$\sigma_r = \alpha \sigma_1 + (1 - \alpha) \sigma_{eq} \quad (2.16)$$

the material constants were A, n, B, q_2, and p were material constants. σ_r was the rupture stress, $\dot{\varepsilon}_{ij}^{c}$ was the equivalent strain, σ_{eq} was the equivalent stress, S_{ij} was the deviatoric stress and

ω was the damage variable [64].

In the study conducted by Hyde et al. [65] crack growth is assumed to have occurred when the damage variable reaches 0.99. Simulations were conducted for Type 316H stainless steel at 600'C and compared with experimental data. The derivation of the above equations can be found in [63]. The material constants A, n, B, q_2, and p can be determined from uniaxial creep data.

One of the advantages with Liu's damage model when compared to the Kachanov damage model is that in finite element analysis the time steps do not become impractically small. The results tend to be quite insensitive to element size near the crack tip. The damage model was implemented using a user subroutine in Abaqus [65, 66].

2.6.4 Dyson

The Dyson creep damage model has a sinh relationship between the creep strain rate and stress as opposed to the power law relationship in the Liu and Kachanov models [67]. The multiaxial form of the Dyson damage model is given below [68].

$$\frac{d\varepsilon_{ij}^{c}}{d_t} = \frac{A}{(1-\omega_2)^n}\left(\frac{S_{ij}}{\sigma_{eq}}\right) sinh\left[\frac{B\sigma_{eq}(1-H)}{1-\emptyset}\right] \quad (2.17)$$

$$\frac{dH}{dt} = \frac{h}{\sigma_{eq}}\frac{A}{(1-\omega_2)^n} sinh\left[\frac{B\sigma_{eq}(1-H)}{1-\emptyset}\right]\left[1-\frac{H}{H^*}\right] \quad (2.18)$$

$$\frac{d\emptyset}{dt} = \frac{K_c}{3}(1-\emptyset)^4 \quad (2.19)$$

$$\frac{d\omega_2}{dt} = \frac{DAK_c}{(1-\omega_2)^n}\left(\frac{\sigma_1}{\sigma_{eq}}\right)^v Nsinh\left[\frac{B\sigma_{eq}(1-H)}{1-\emptyset}\right] \quad (2.20)$$

The Dyson model has 3 state variables:

1. H, the strain hardening variable
2. ∅, the ageing damage parameter
3. ω_2, the cavitation damage parameter

The other parameters are all constants or as defined in the Liu model.

The strain hardening variable H evolves throughout the primary creep stage, it has a saturation value of H^* [69].

The Dyson model has a multiaxiality constant, v, which is part of the expression for cavitation damage ($(\sigma_1/\sigma_{eq})^v$). The Liu and Murakami model uses the multiaxiality constant, α and is included in the function in the form ($\alpha\sigma_1+(1-\alpha)\sigma_{eq}$). The material constants A, B, H^*, h, K_c and D can be determined via a method detailed in [68]. The key starting point is that during the early part of secondary creep, H will have reached the saturation value of H^*, also at this point both ∅ and ω_2 are very small so can be assumed to be zero for a first approximation [70, 71].

2.7 Concluding Remarks

The literature review showed that previous repeat relaxation experiments had been conducted with different notch acuities and start of dwell stresses but not with different dwell lengths, so this was decided as being an area of key interest. The literature review also highlighted that creep fatigue experiments on notched bar specimens had not previously been conducted so this was marked as another area of interest. The experimental results surrounding the material being used for testing

in this work suggested this material had a strain rate dependent ductility. Stuart Holdsworth, a leading researcher in the field of creep, proposed that the reason that this material exhibits a strain rate dependent ductility is because at low creep strain rates specimens fail via constrained cavity growth [72]. As creep strain rate is increased they start to fail via diffusion controlled cavity growth and these cavities are larger and result in more deformation before failure. At very high strain rates/approaching plastic failure then plastic holes appear in the specimen which result in a very large ductility on failure. One of the main aims of this work was to determine whether this material did exhibit a strain rate dependent ductility experimentally.

With this in mind it was decided three areas of experimental testing would be focussed on.

1. Constant load creep
2. Displacement controlled creep
3. Creep-Fatigue

Constant load uniaxial creep tests had already been conducted on the material available to the researchers conducting this study. They would be used to derive creep constants for finite element modelling. Constant load creep tests would be conducted on notched bar specimens.

Uniaxial stress relaxation (displacement controlled) creep tests would be conducted to verify the behaviour of the finite element model under displacement control. Then repeat stress relaxation tests would be conducted on notched bar specimens, these experiments would be run to failure to allow for verification of the creep damage models.

Creep-fatigue experiments would be conducted on notched bar specimens. These creep-fatigue experiments would be the same as the repeat stress relaxation tests on notched bar specimens except the stress would be removed after relaxation dwells before being re-applied creating a creep fatigue cycle at the notch of the specimen.

It was decided that the Spindler damage model and the Stress Modified Ductility Exhaustion (SMDE) damage models would be used within this research. The Spindler model was selected as it has been previously used to model this cast of Type 316H stainless steel to great effect. The SMDE model was selected as it was part of the High Temperature Behaviour of Austenitic

Stainless Steels (HTBASS) program which is of great relevance to the material being used within this work.

CHAPTER 3

Methodology

“Man must evolve for all human conflict a method which rejects revenge, aggression and retaliation. The foundation of such a method is love.”- Martin Luther King, Jr.

Chapter 3 Methodology

This Chapter describes the experimental and finite element methodology for all experiments conducted. First the geometry of all the notched specimens is given, followed by descriptions of the experimental test rigs, then derivations of material properties for the specific cast of Type 316H stainless steel used in all the experiments being conducted to determine whether the material in question exhibits a strain rate dependent ductility and finally the methodology of the creep damage models being assessed used for finite element analysis and verification of experimental behaviour.

3.1 Specimens

The same notch geometry was used for all creep tests conducted on notched bar specimens in this work (creep rupture, stress relaxation and creep fatigue). All specimens were cylindrical specimens and were machined to meet codes of practice for conducting experiments with notched bars [72]. Dimensions are shown graphically in Figure 3.1 and stated in Table 3.1. All specimens had a notch acuity of 5 [4, 73, 74]. This was to ensure that the notch was sharp enough to create a suitably increased stress triaxiality while remaining within machining limits. The only difference between the specimens used for constant load creep and constant displacement creep tests was the gauge length. The gauge length for specimens subject to constant load creep was 28.25mm and 50mm for specimens subject to constant displacement creep. The difference in gauge length was required due to the extensometry attaching directly to the specimens on the constant load rigs and attaching to the specimen grips on the constant displacement rigs.

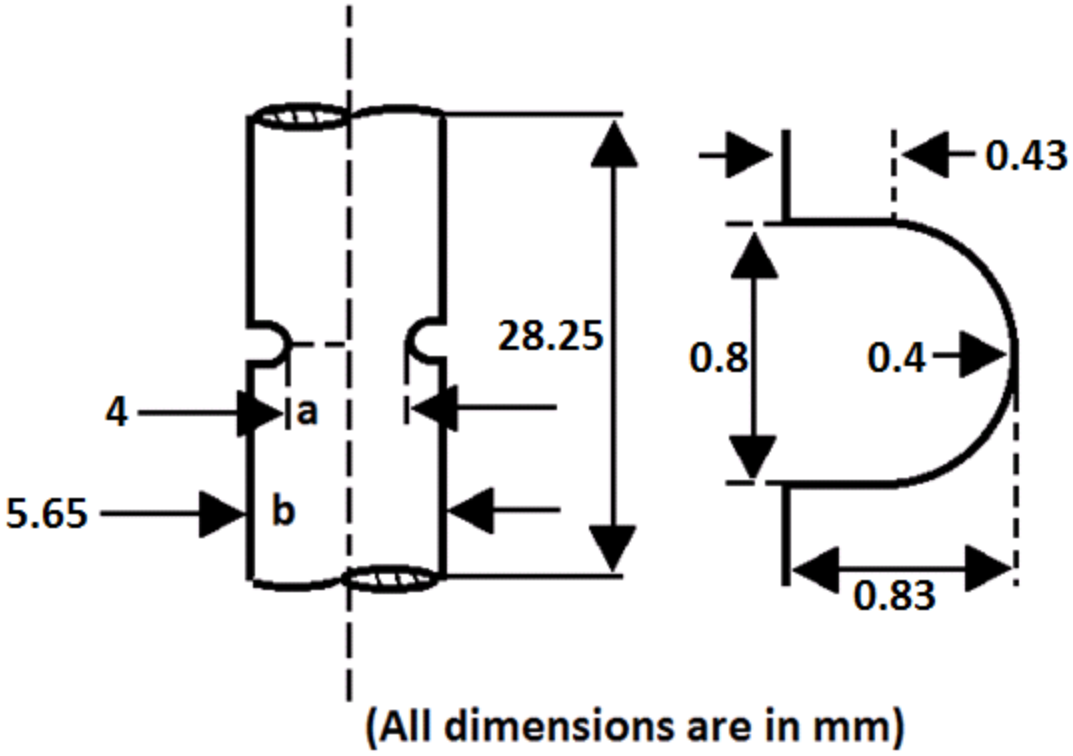

Figure 3.3.1- Specimen Dimensions (tolerances of 0.01mm for machining)

Table 3.1– Specimen dimensions for constant load creep rupture of notched bars experimentation.

Notch Acuity (a/R)	R (mm)	a (mm)	b (mm)	L (mm) (constant load/constant displacement)
5.0	0.40	2.00	2.83	28.25/50

where R was the radius of the notch, a was the radius of the specimen at the notch, b was the radius of the specimen away from the notch and L was the gauge length of the specimen.

3.2 Experimental test rigs

3.2.1 Constant load creep

Standard dead weight creep machines were used to conduct constant load creep experiments. Two different types of creep rig were used; one design was automatically levelled and the other manually levelled. The automatically controlled test rigs were connected to capstans that kept the lever arms horizontal during a creep test. The manually levelling rigs were adjusted in accordance to the spirit levels attached to them. On both rig designs the specimens were connected at the middle of the rig and attached to the lever arm at the top of the specimen and a 25kN load cell at the bottom. On the manually controlled rigs the load cell was attached to the manual levelling device and on the automatic rigs it was connected to the capstan. The load cell, which was at the base of the rigs, measured the applied load and connected to the data logger. Thermocouples measured the temperature at the top, middle and bottom of the sample together with the room temperature. A schematic of the experimental test rig is shown in Figure 3.3.3a.

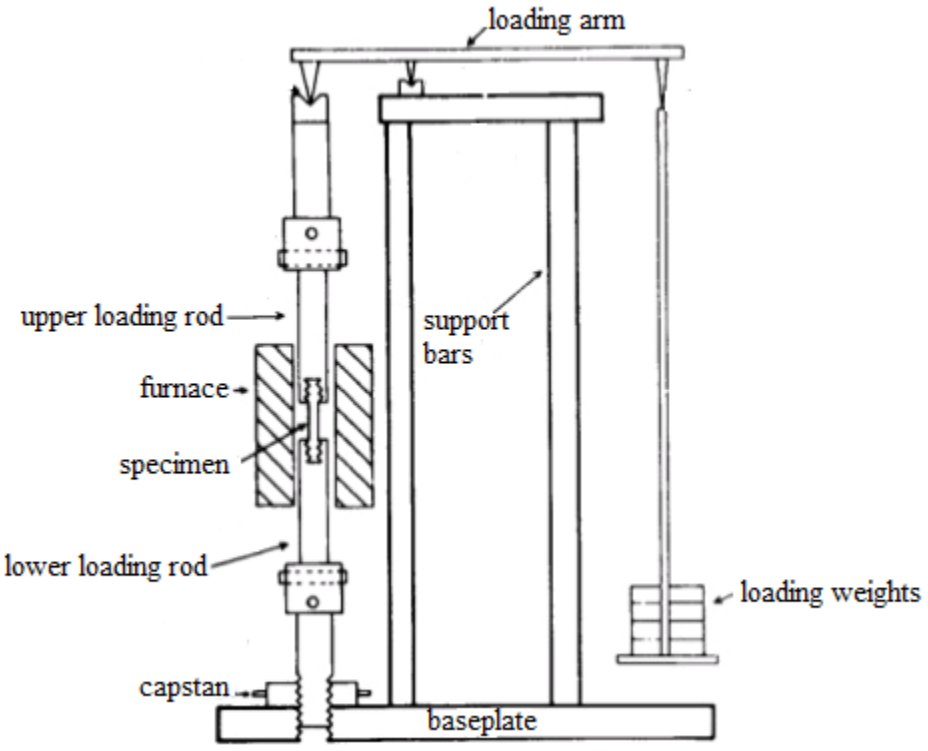

Figure 3.3.2a – Schematic of constant load test rig with capstan

The extension of the gauge length of the specimens (starting value 28.25mm) was measured using an extensometer and linear variable differential transformer (LVDTs). On two tests the specimen diameter was also measured. A diametric extensometer provided a measurement at the notch. A data logger captured temperature, load and extension data throughout the test together with diameter when available. As an alternative to the diametric extensometer a camera system allowed measurement of the complete notch profile. A USB camera (Logitech C270, 1280 X 720 pixels) was adapted to take a zoom lens (Tokina TV lens 7900754, 1:2.5/22-88mm) and imaged the specimen though a 14mm diameter hole in the furnace. The sample was illuminated with a ring of light emitting diodes positioned around the optical axis. The camera was read out into a laptop and images were captured every 5 minutes. Analysis of these images provided the diameter of the specimen and the notch together with the notch profile throughout the test. This method was chosen because the images from the camera allowed the reduction in notch diameter, the notch opening and deformation of the specimen to be measured. The camera set up is shown in Figure 3.3.2b.

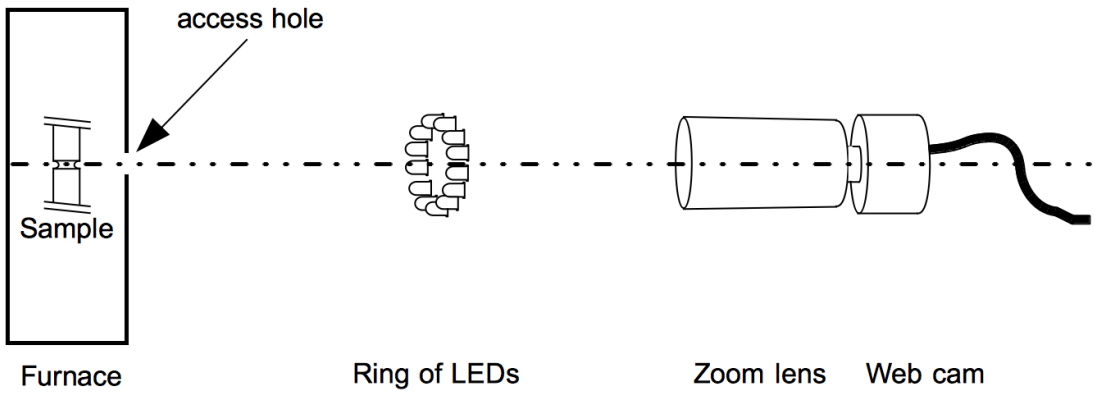

Figure 3.3.2b- Camera set up for notch imaging

3.2.2 Constant displacement creep

A guide for setting up experiments on the displacement-controlled test rig was written and is included in Appendix 2.

Constant displacement creep experiments (stress relaxation and creep fatigue) were conducted on a three-bar structure with only the central bar of this structure contained within the furnace (shown in Figure 3.3). The stiffness of the parallel bars ensured the effects of elastic follow-up were insignificant (discussed in Chapter 5). The central bar was made up of a bottom series bar and a top series bar that screwed into either end of the specimen. The bottom series bar was divided into two parts with different diameters, this increased the stiffness of the bar and reduced the amount of heat transfer through the bar and into the load cell. The load cell screwed into the bottom series bar which was in turn screwed into the specimen allowing the load in the specimen to be measured directly.

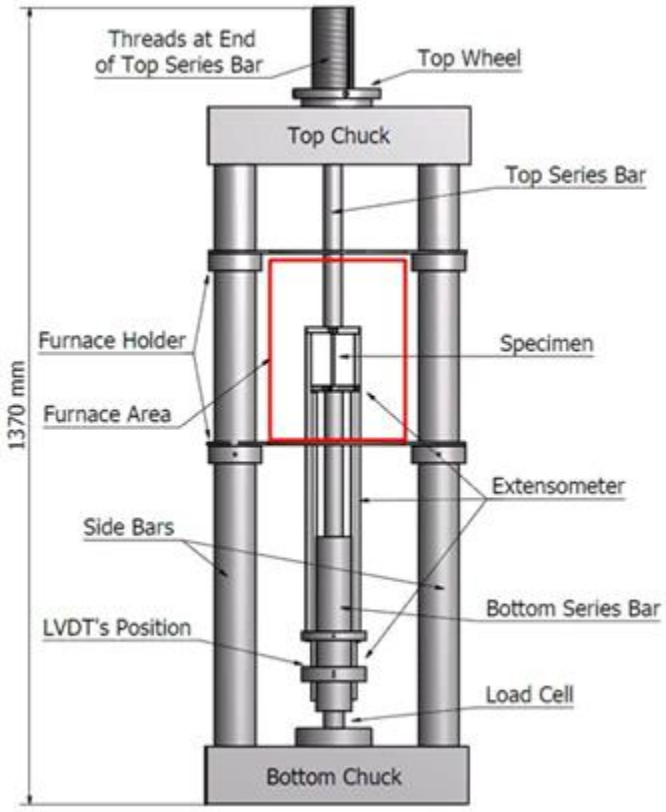

Figure 3.3.3- Stress Relaxation Test Rig [9].

The side bars were 1m long with a 70mm diameter, they weighed over 40kg and were very stiff. This meant that a load could not be applied over the whole structure and so load was applied to

the specimen via a misfit. When the top was rotated the top bar was moved upwards applying a tensile load to the specimen which was measured by the load cell. This loading mechanism allowed the displacement to be fixed when the top wheel was stationary. Once the displacement of the specimen was fixed the stress started to relax as the specimen's notch redistributes under the applied load. On the stress relaxation rig, LVDTs were used to measure the extension of the specimen's gauge length (local notch measurements could not be taken), three thermocouples were used to measure the temperature of the specimen and to ensure the temperature was constant across the gauge length.

3.3 Material Constants

A single cast of Type 316H austenitic stainless steel was used to fabricate all creep specimens tested within this research. It is important to note that the variation of creep behaviour between different casts can be large and the use of a single cast (from a single header) was deliberate to remove this source of uncertainty.

Tensile tests were conducted at both 515°C and 550°C within this thesis. Uniaxial creep rupture tests were conducted on this material with varying applied stresses by Spindler and used to determine creep constants for modelling.

To determine all constants needed for modelling creep experiments, tensile and uniaxial creep data are both needed. The results of the tensile test at 550°C can be seen graphically in Figure 3.4 and are tabulated in Table 3.2. The tabular stress strain results inputted into Abaqus can be seen in Appendix 3. The material had no definite yield stress and so the 0.2% proof stress (0.002 absolute strain) was taken as the point where the termination of the elastic region occurs.

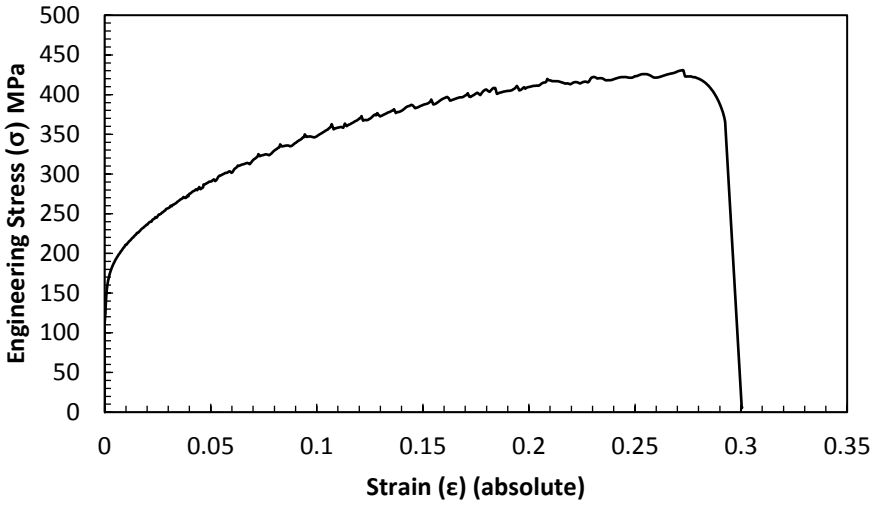

Figure 3.3.4- Engineering stress vs strain curve for Type 316H (cast 69431) steel at 550˚C from a tensile test

Table 3.2- Tensile properties of Type 316H austenitic stainless steel (cast 69431) at 550˚C.

E (GPa)	$\sigma_{0.2\%}$ (MPa)	UTS	Failure Strain (%)
165	160	430.8	30.05

The power law creep constants for this material had not been calculated prior to this thesis. EDF energy provided uniaxial creep data for this specific header to allow these constants to be calculated. Secondary creep constants were calculated first. Secondary creep strain rate was of the form:

$$\dot{\varepsilon}_c = C\sigma^{n1} \qquad (3.1)$$

The minimum secondary creep constants were calculated by integrating the true creep strain vs normalised time curve to obtain the strain rate against time curve as shown in Figure 3.5. This had

to be done for all of the uniaxial creep data provided by EDF energy at 550°C [47]. From the strain rate against time graphs the minimum creep strain rates for each applied stress value could be identified and these results are plotted in Figure 3.6.

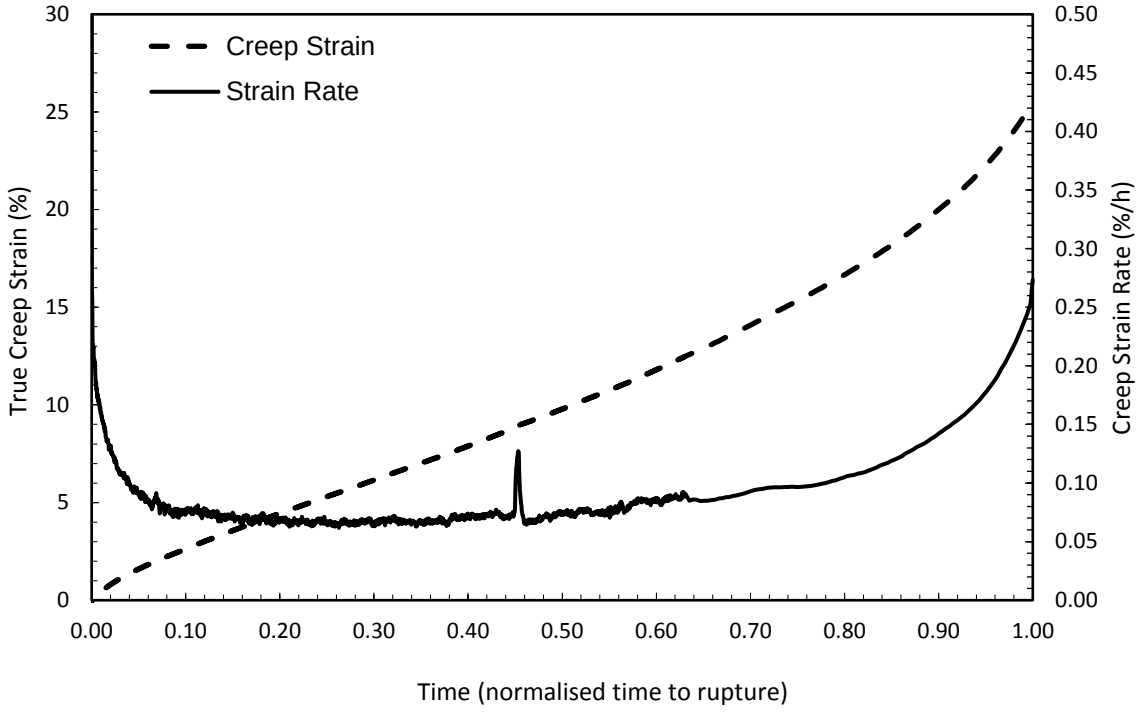

Figure 3.3.5- Creep strain/strain rate vs time at 320MPa. Experimental values at 550˚C given.

These results were plotted on a log scale so that it was possible to obtain a straight line fit where the intercept and gradient were the values for C ($MPa^{1/n}h^{-1}$) and n1 in the creep law respectively.

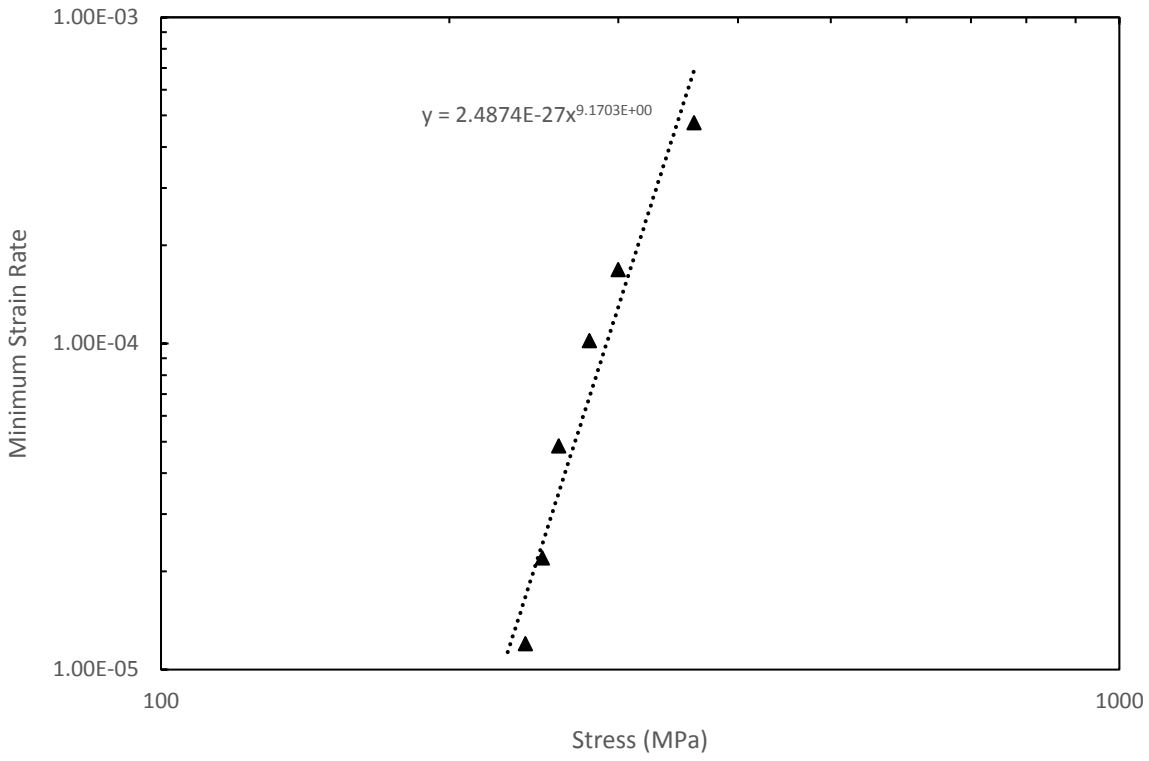

Figure 3.3.6- Experimental stress vs minimum strain rate (% per hour) for Type 316H (cast 69431) at 550˚C.

The average creep constants could be calculated by dividing the creep strain on failure by the time to rupture for each of the data sets. The average strain rate values were then plotted against the corresponding applied stress values as shown in Figure 3.7. The C and n1 creep constants were the intercept and gradient of this fit.

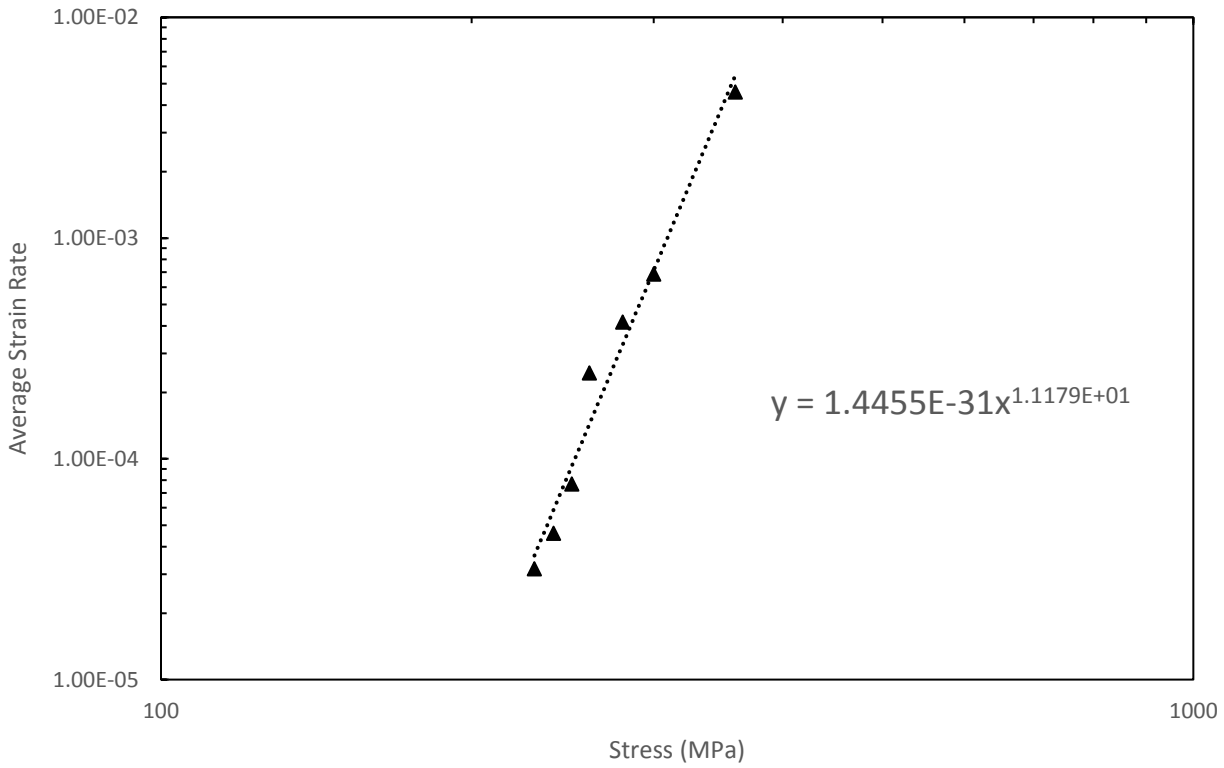

Figure 3.3.7- Stress vs average strain rate for Type 316H (cast 69431) at 550˚C.

The minimum and average secondary creep constants are shown in Table 3.3.

Table 3.3 - Minimum and average secondary creep constants for cast 69431 stainless-steel at 550˚C.

	$C(MPa^{1/n}h^{-1})$	n_1
$\dot{\varepsilon}_{min}(h^{-1})$	2.4874×10^{-27}	9.1703
$\dot{\varepsilon}_{average}(h^{-1})$	1.4455×10^{-31}	11.179

Primary Creep

$$\varepsilon_{c(abs.)} = A\sigma^n t^m \qquad (3.2)$$

where ε_c is creep strain (abs.), σ is stress, t is time and n and m are material constants. Note that creep strain has been fitted in primary creep, in contrast to the fitting of strain rate in secondary creep.

The first step was to calculate m. This was achieved by plotting the material data of strain against time at a fixed stress within the primary creep region, this plot was on a log log scale and the index of the trendline was the value of m for each relevant stress as can be seen graphically in Figure 3.8 and numerically in Table 3.4.

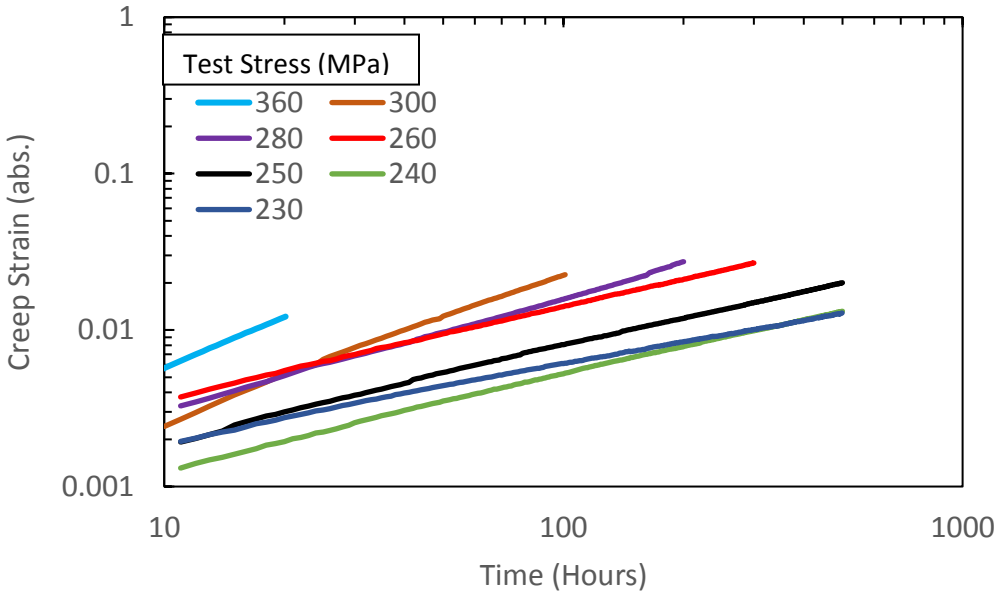

Figure 3.3.8 - Experimental primary creep rate for Type 316H (cast 69431) stainless steel at 550˚C

Table 3.4 – Values of the primary creep constant m for various constant load experiments conducted at 550˚C.

Stress	m
360	0.4825
300	0.4331
280	0.4216
260	0.4185
250	0.4035
240	0.3947
230	0.3901

The value for m varied with stress, it was averaged over the range to give a value of m = 0.421.

Once m had been determined plots of stress against strain were displayed on a log log scale at different fixed time intervals. This can be seen graphically in Figure 3.9 and numerically in Tables 3.5 and 3.6 (these plots were performed at a time of 100, 200, 300 and 500 hours for each creep curve).

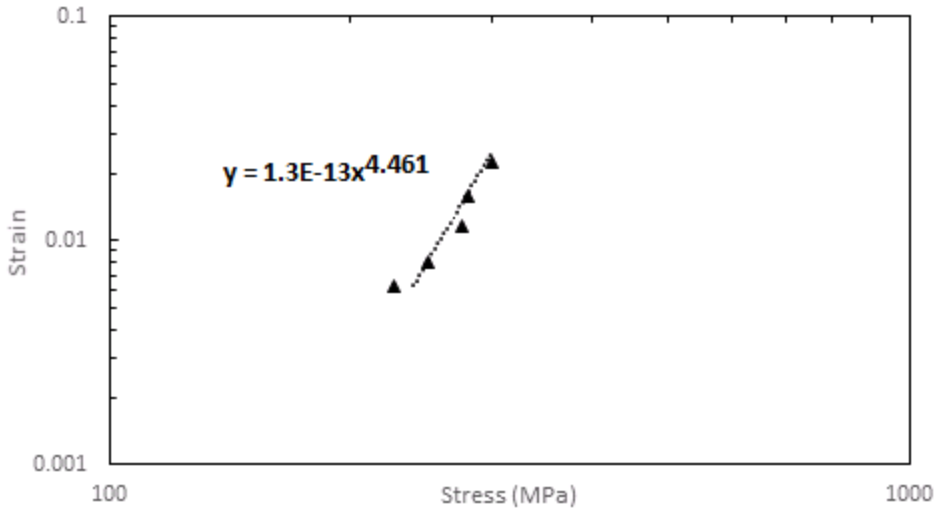

Figure 3.3.9- Stress against strain after 100 hours of primary creep at 550˚C under various loads

Table 3.5 - Strain values of stainless steel cast 69431 at varying stresses after 100 hours of primary creep at 550˚C.

Time (Hours)	Stress (MPa)	Strain
100	300	0.022599573
100	280	0.015753446
100	260	0.014139286
100	250	0.008075001
100	240	0.00525357

Table 3.6 - Strain values of stainless steel cast 69431 at varying stresses after 200 hours of primary creep at 550˚C.

Time (Hours)	Stress (MPa)	Strain
200	280	0.027355136
200	260	0.021067866
200	250	0.011921424
200	240	0.007855356

The gradient of this plot was divided by t^m to get A and the intercept of these plots was n. These values were similar for each time plot but not identical, so these values were also averaged to give the following initial primary creep constants.

Table 3.7– Primary creep constants (abs. strain) for austenitic stainless steel Type 316 (cast 69431) at 550˚C.

m	A	n
0.421	1.84×10^{-14}	4.5

These constants were then used with the Norton Bailey creep law to evaluate how the predicted creep curves using these constants compared with the actual data. It can be seen in Figure 3.10 that these values accurately captured primary creep behaviour for this material. The first 10 hours of creep have been ignored as the experimental scatter was very large in the early stages of creep and no meaningful fit could be found.

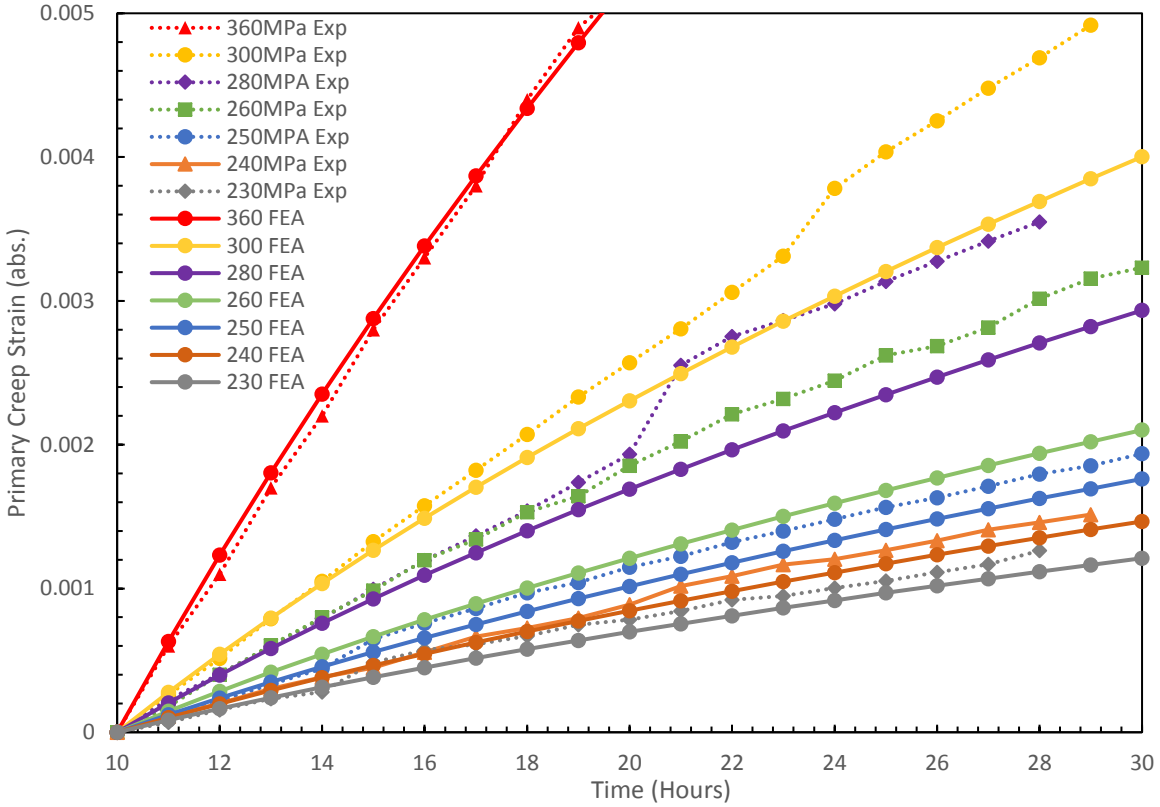

Figure 3.3.10- Primary creep predicted using derived creep constants vs experimental values at 550˚C (the first 10 hours of creep have been ignored as the experimental scatter was very large in the early stages of creep and no meaningful fit could be found).

The creep constants determined for modelling creep of cast 69431 header 2C2/3 (stainless steel Type 316H) at 550˚C are given in Table 3.8.

It should be noted that the minimum secondary creep constants were used instead of the average creep constants when using a model with both primary and secondary creep. This is because when the average creep constants are calculated they are calculated over the whole creep life of the specimen including the primary and tertiary creep phases, whereas the minimum secondary creep constants are calculated using the minimum strain rate which is when secondary creep occurs. If modelling were to have been conducted on a single parameter creep model with no differentiation

between primary and secondary creep, then the average creep constants would have been used. Also, a correction for tertiary creep is introduced below.

Table 3.8- Constants used in finite element simulations of Type 316H stainless steel (cast 69431) at 550˚C.

Temperature (˚C)	E (MPa)	ν	A	n	m	C	n_1	Uniaxial (lower shelf) Ductility, ε_{fu}
550	165,000	0.3	1.84E-14	4.5	0.421	2.49E-27	9.17	10.69%
515	169,000	0.3	1.88E-12	4.1	0.401	4.72E-28	9.06	4%

(Units of A and C are such that strain rates result in absolute per hour for stress in MPa and time in hours).

The purpose of this research is to confirm the theory that the material being tested has a strain rate dependent ductility. This strain rate dependent ductility was inputted into the FEA to see if better agreement with the experimental data was found. The material being used has previously been found to have an upper shelf ductility of 28% (strain rates exceeding $3.232h^{-1}$) and a lower shelf ductility of 10.69% (strain rates below $1E\text{-}5h^{-1}$) at 550˚C with a transition period in between as shown in Figure 3.11 [4]. It was found this material had a significantly smaller lower shelf multiaxial ductility at 515˚C than 550˚C in unpublished repeat stress relaxation experiments conducted on notched bar specimens by EDF Energy. These previous tests suggested a ductility at 515˚C of roughly 40% of that at 550˚C. This was accounted for in the model with a reduced lower shelf ductility at 515˚C than 550˚C as shown in Figure 3.11 (a lower shelf ductility of 4% was used for simulations at 515˚C).

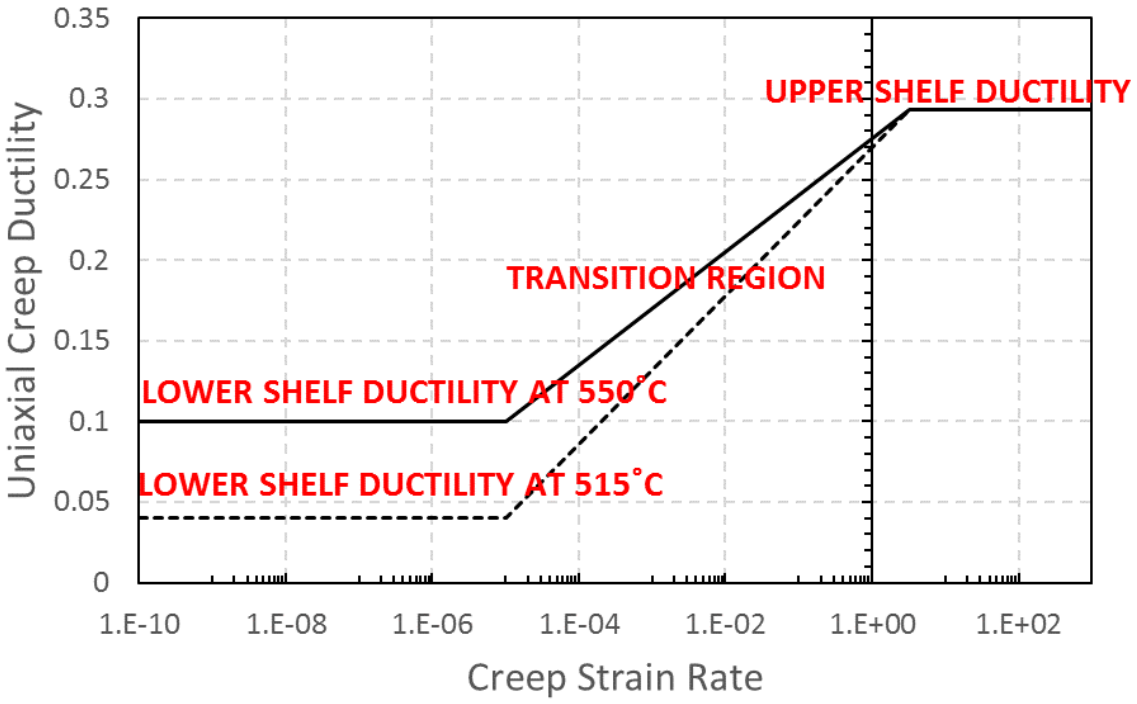

Figure 3.3.11- Upper and lower shelf creep ductilities for 316H (strain rate in absolute per hour).

3.4 Finite Element Analysis Methodology

Finite element simulations were conducted using Abaqus version 6.14 [75]. Initial simulations were conducted on a round bar specimen to ensure that elastic and plastic loading conditions could be accurately captured in the model. These simulations were compared with experimental data for the load up of uniaxial creep tests at varying stresses. Then primary and secondary creep were added to the model and again validated against experimental data.

The next step of the simulation was the introduction of the notched specimen used in the tests conducted for this research. A mesh sensitivity study found that the elements at the notch tip needed to be 0.01mm or smaller for the result to be mesh independent as shown in Figure 3.12.

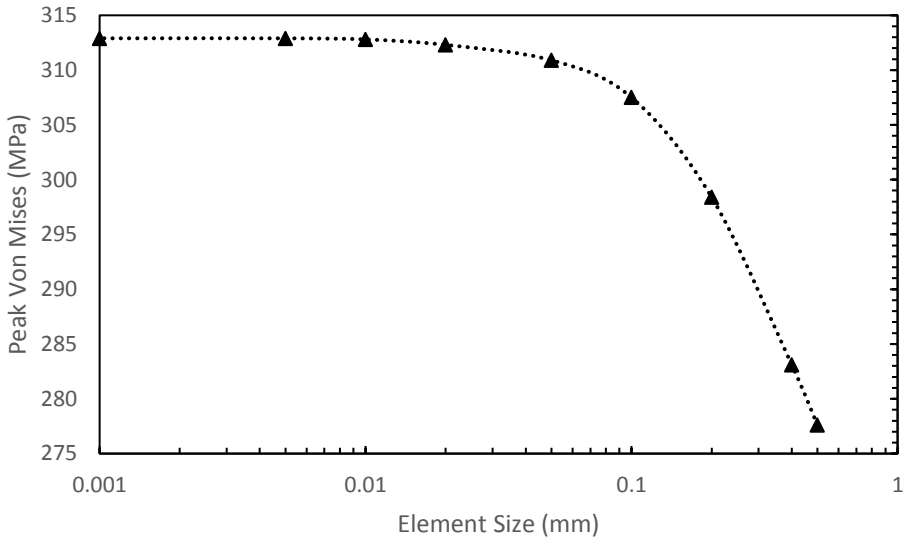

Figure 3.3.12- Mesh sensitivity for a notch bar specimen, acuity 5, at 550˚C.

Approximately 1000 structured quadratic elements were used. The part was axisymmetric, a further plane of symmetry was added along the centre line of the notch in the yy plane. The load was applied as a constant pressure on the top edge of the specimen as shown in Figure 3.13 (in the constant displacement experiments this top edge was then fixed in a constant position after the initial load up). The analysis was conducted assuming 'large displacements' (NLGEOM ON) since the notch geometry changes substantially under load.

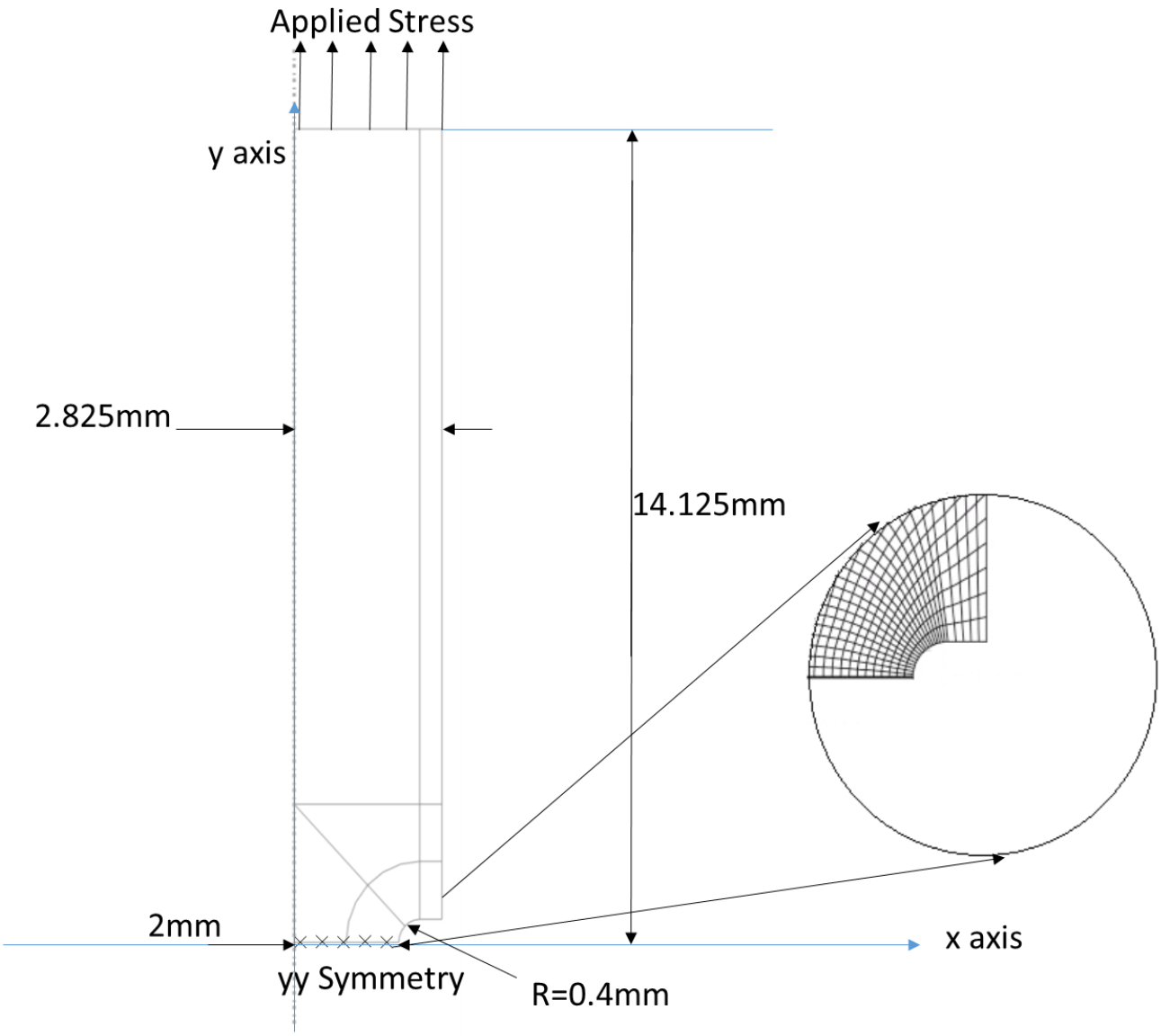

Figure 3.3.13- Partitioning and meshing used at notch tip for finite element modelling of notched bars.

Modelling creep of notched bars was done via employing a user subroutine to incorporate the empirical constants for primary and secondary creep. Two different user subroutines were used to conduct simulations using two different creep damage models, the Spindler damage model and the stress modified ductility exhaustion (SMDE) damage model. Both creep damage models used isotropic hardening.

Spindler derived an empirical equation from multi-axial creep data of Type 316 stainless steel that incorporates cavity nucleation within creep behaviour[76]. This equation is used in the Spindler damage model is given in equation 3.3 and the equation used in the SMDE model is given in equation 3.4:

$$\frac{\bar{\varepsilon}_f}{\varepsilon_{fu}} = \exp\left[p\left(1-\frac{\sigma_1}{\bar{\sigma}}\right)\right]\exp\left[q\left(\frac{1}{2}-\frac{3\sigma_p}{2\bar{\sigma}}\right)\right] \qquad (3.3)$$

where $\bar{\varepsilon}_f$ and ε_{fu} are the von Mises equivalent and uniaxial strains to failure, respectively. σ_1, $\bar{\sigma}$ and σ_p are the maximum principal, von Mises equivalent and hydrostatic stresses, respectively. p and q are constants based on the material and test temperature. They were calibrated to give the best fit for Type 316 stainless steel at 550˚C using notched bars with a notch acuity 5 in previous research conducted by Spindler[61]. The values of p and q established by Spindler were 1.2 and 1.0 respectively for the material used in this study. These values were assumed at both test temperatures, 550ºC and 515ºC.

$$\bar{\varepsilon}_f(\dot{\bar{\varepsilon}}_{in}, \sigma_1, T) = MAX\left\{\begin{matrix} A_1\exp\left(\frac{Q_1}{T}\right)\dot{\bar{\varepsilon}}_{in}{}^{n_1}\sigma_1{}^{-m}, \\ MIN\left[\varepsilon_L, A_2\exp\left(\frac{Q_2}{T}\right)\sigma_1{}^{-m_2}\right]\end{matrix}\right\}.\left[\frac{\bar{\sigma}}{\sigma_1}\exp\left(\frac{1}{2}-\frac{3\sigma_p}{2\bar{\sigma}}\right)\right] \qquad (3.4)$$

Where $\bar{\varepsilon}_f(\dot{\bar{\varepsilon}}_{in}, \sigma_1, T)$ is the von Mises inelastic strain at failure at the appropriate temperature as a function of both the von Mises inelastic strain rate, $\dot{\bar{\varepsilon}}_{in}$, and the maximum principal stress, σ_1. In addition, ε_L is a lower shelf creep ductility (which is independent of stress and strain rate). A_1, n_1, m_1, Q_1, A_2, m_2, and Q_2, are material parameters for regions 1 and 2 respectively (region 1 is the transition region and region 2 is the lower shelf region). $\bar{\sigma}$ is the von Mises stress and σ_p the hydrostatic stress. The units are strain in mm/mm, stress in MPa and temperature in Kelvin.

Tertiary creep was simulated by factoring the nominal strain rate by $1/(1-D_C{}^3)$ in both damage models, where D_C is the damage defined by equation 3.5 for the Spindler damage model and by equation 3.6 for the SMDE damage model. This factor has been implemented successfully in previous research by Spindler on this material [77]. Both damage models were based on ductility

exhaustion and the triaxiality factors given by equation 3.3 for the Spindler model and 3.4 for the SMDE model. The stress modified ductility exhaustion (SMDE) creep damage model is a recent adaption to the Spindler damage model. This modification means that the effect of stress on creep damage is included, this is achieved by treating the ductility as a function of both stress and strain rate (as shown in equation 3.6). These simulations were used to determine the stress, strain and damage across the notched section.

$$\mathrm{D_C} = \frac{\bar{\varepsilon}_\mathrm{c}}{\bar{\varepsilon}_\mathrm{f}} \tag{3.5}$$

where $\bar{\varepsilon}_\mathrm{c}$ was the accumulated von Mises creep strain and $\bar{\varepsilon}_\mathrm{f}$ was given by equation 3.3 for the Spindler damage model and 3.4 for the SMDE model.

$$D_c^{SM} = \sum_i N(i) \int_o^{t_h^{(i)}} \frac{\dot{\varepsilon}_c}{\varepsilon_f(\dot{\varepsilon}_c, \sigma, T)} dt \tag{3.6}$$

where $\varepsilon_f(\dot{\varepsilon}_c, \sigma, T)$ is the creep ductility at a given temperature as a function of stress and strain rate.

The creep constants used for both finite models are given in Table 3.8 previously (simulations with both damage models were also conducted with the strain dependent ductility shown in Figure 3.11):

Two different failure cases were modelled. In the first case failure was deemed to have occurred when the node of maximum damage reached a D_C value of 1. In this work these failures were referred to as the Type 1 failure criterion. In the second case failure was deemed to have occurred when all nodes along the yy line of symmetry reached a D_C value of 1. These were referred to as the Type 2 failure criterion. When elements reach a damage value of 1 (unity) the damage level does not increase any more, but the creep strain continues to increase towards infinity and so the load held by these elements falls and the stress is concentrated elsewhere, similar to methods used by previous researchers to simulate progressive failure [12, 78]. This causes an effect similar to that of the elements losing stiffness. This is an approximate allowance for the initiation and propagation of a crack, although the crack tip field is not modelled.

CHAPTER 4

Constant Load Creep

Work from this chapter was presented at the 14th International Conference on Fracture in Rhodes, 2017.

It has also been published in the International Journal of Pressure Vessels and Piping.

"Research is what I'm doing when I don't know what I'm doing." - Wernher von Braun

Chapter 4 Creep Rupture

The main aim of this Chapter was to determine the effect of creep strain rate on creep damage accumulation in notched bar specimens fabricated from Type 316H austenitic stainless steel and tested under constant load. Initially creep rupture equations were used to estimate the life of uniaxial creep rupture experiments for specimens fabricated from Type 316H stainless steel, these results were compared with tests conducted by Mike Spindler of EDF Energy on the material used within this study. Creep rupture experiments were then conducted on notched bar specimens. The experimental results were then analysed using finite element analysis. The material constants derived in the last chapter were used within the various finite element models.

4.1 Creep rupture of round bars

Initial calculations were conducted to estimate the time to rupture (tr) in forward creep tests. Three creep rupture equations were utilised. All the equations were based on experimental data for generic Type 316H stainless steel, they are not cast specific equations. Equations 4.1 and 4.2 were obtained by curve fitting to experimental data, these equations were derived by EDF energy. Equation 4.1 is for predicting creep rupture in the temperature range 400-550˚C, equation 4.2 is for predicting creep rupture in the temperature range 550-700˚C. Equation 4.3 is the most recent equation, also derived from experimental data and is in the AGR materials data handbook [79]. All the equations are for forward creep tests conducted at 550˚C, the same test temperature to be used in this work.

$$\ln(\mathrm{tr}) = 1924.17554 - 557.164551\log(\mathrm{T}) - 41.2390327\log(\sigma) - \frac{164848.156}{\mathrm{T}} + 26.3856277 * \frac{\sigma}{\mathrm{T}} \quad (4.1)$$

$$\ln(\mathrm{tr}) = -352.731628 + 96.765976\log(\mathrm{T}) - 7.55743979\log(\sigma) + \frac{85672.6406}{\mathrm{T}} - 20.2565994 * \frac{\sigma}{\mathrm{T}} \quad (4.2)$$

$$\begin{aligned} tr = VTC\_Int * Exp(&-13.8171453 - 7.75643206 * \log(\sigma) - VTC\_H \\ &* 0.0467775278 * \sigma * \log(\sigma) + VTC\_L * 122.272964 \\ &* (\log(\sigma))/\sigma - VTC\_L * 1490.80469 * (\log(\sigma))/T + VTC\_H \\ &* 89.4402466 * (\sigma/T) + 35809.1992/T) \end{aligned} \quad (4.3)$$

(stress, σ , in MPa, temperature, T, in K and time to rupture, tr, in Hours.

where at 823K/550˚C

VTC_H = 0.5

VTC_L = 0.5

VTC_Int = 1

Table 4.1 shows the predicted rupture times generated from the three equations for a range of different stress values (200-400MPa). These predicted times to rupture are for uniaxial test specimens.

Table 4.1- Uniaxial creep rupture predictions under constant load conditions at 550˚C based on equations 4.1, 4.2 and 4.3.

	Equation 4.1		Equation 4.2		Equation 4.3
Stress (MPa)	ln(tr)	tr (hours)	ln(tr)	tr (hours)	tr (hours)
200	11.04	62000	11.17	71000	39000
225	9.73	17000	10.16	26000	18000
250	8.64	5700	9.20	9900	8700
275	7.74	2300	8.27	3900	4300
300	6.98	1100	7.37	1600	2100
325	6.35	570	6.50	660	1100
350	5.82	340	5.64	280	540
375	5.39	220	4.79	120	280
400	5.03	150	3.97	53	140

Figure 4.1 shows the results from Table 4.1 graphically along with experimental data from tests conducted by EDF Energy on the specific cast used for all tests conducted within this Thesis (internally referred to as cast 69431). Figure 4.1 shows that all equations give a slight overestimate of the time to rupture for this material, suggesting that this material is below average for an austenitic stainless-steel Type 316H based on its creep life. This is unsurprising as the material being used is an ex-service material that has already been subject to 51,000 hours of service at temperatures between 480 and 510˚C.

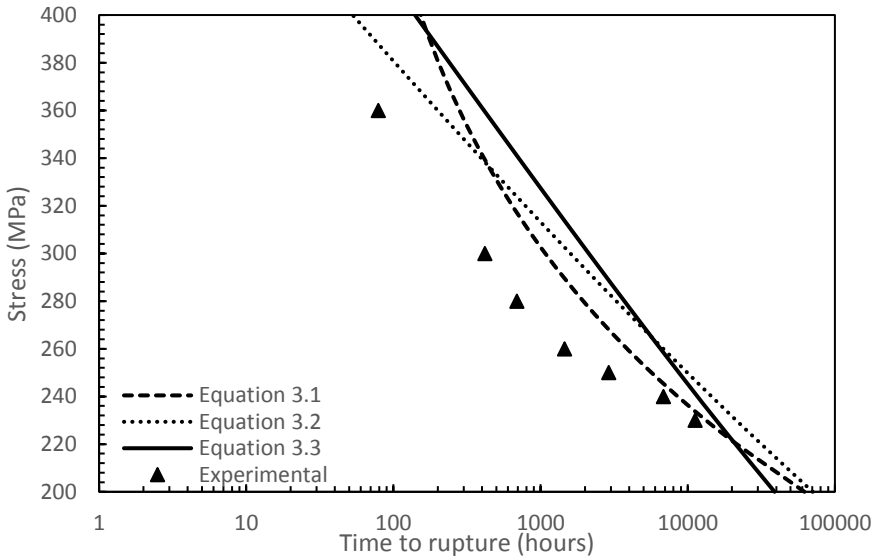

Figure 4.1 - Time to rupture for uniaxial specimens fabricated from Type 316H stainless-steel at various stresses at 550˚C. Experimental and predictions based on best fit equations shown.

4.1.2 Finite element analysis of creep rupture of round bars

Initial simulations were conducted on a round bar specimen to ensure that elastic and plastic loading conditions could be accurately captured within Abaqus. Following this primary and secondary creep were added to the model. The results from the model were then compared with uniaxial creep data [28]. Table 4.2 shows the experimental data for loading strain and secondary creep strain rates as well as that calculated from the finite element model. Figure 4.2 shows the loading strain data graphically along with the tensile test conducted on this material to determine

constants for modelling. Unsurprisingly all the values of strain after load-up from the finite element model match the tensile curve as this curve was explicitly used within Abaqus to capture the elastic-plastic behaviour of the material. Figure 4.2 shows that there is significant experimental variation in the plastic loading phase experimentally. For the test conducted at a stress of 260MPa there is a 32% difference (0.013% strain) between the experimental value and the values from the tensile test and the finite element simulation. Figure 4.3 shows the secondary creep strain rate experimentally and also from the finite element model. Here it can be seen that creep strain rate value experimentally can vary by up to 31% of the value predicted by the finite element model in either direction.

Table 4.2- Loading strains and secondary creep rates for constant load creep tests conducted at 550˚C (from both experimental and finite element analysis tests).

Test Stress (MPa)	Strain after load-up, %		Secondary creep strain rate, h^{-1}	
	Experimental	FEA	Experimental	FEA
230	0.023	0.015	9.35E-6	1.13E-5
240	0.031	0.018	1.20E-5	1.67E-5
250	0.032	0.024	2.20E-5	2.43E-5
260	0.041	0.028	4.85E-5	3.49E-5
280	0.036	0.040	1.02E-4	6.88E-5
300	0.055	0.051	1.68E-4	1.29E-4
360	0.115	0.110	4.75E-4	6.89E-4

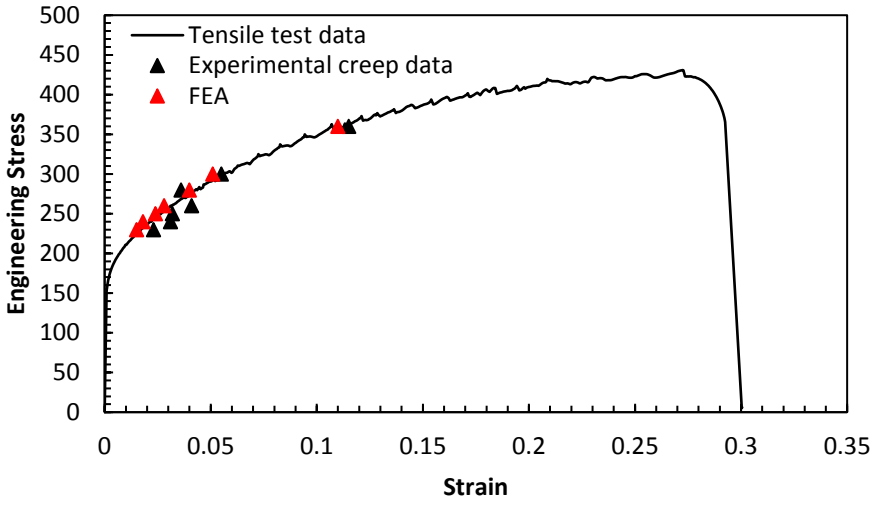

Figure 4.2- Loading strains experimentally and from FEA shown against tensile test data all at 550˚C.

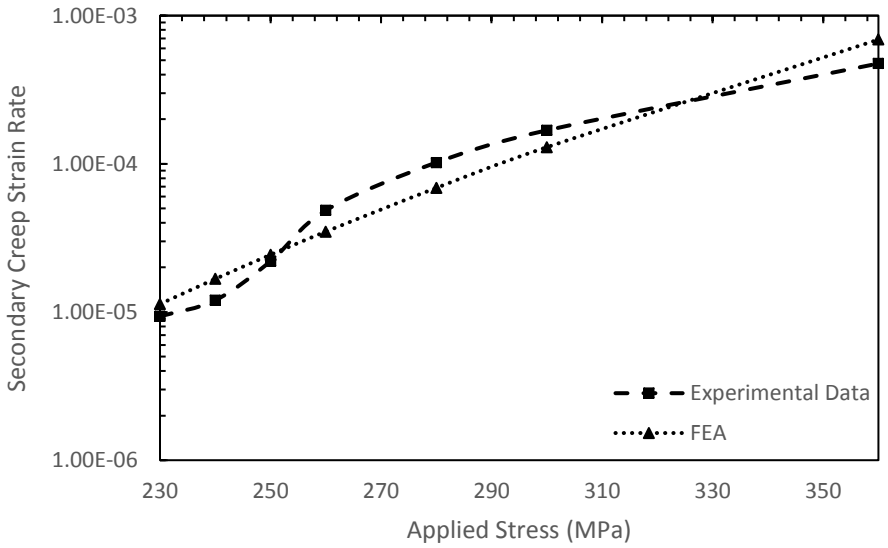

Figure 4.3- Secondary creep strain rate at various applied stresses for a round bar specimen at 550˚C.

Figure 4.4 shows a strain against time curve for a specimen under constant load creep at 230MPa. The experimental and finite element results are shown. Figure 4.4 shows that the model accurately predicted Elastic-Plastic Primary-Secondary (EP-PS) creep.

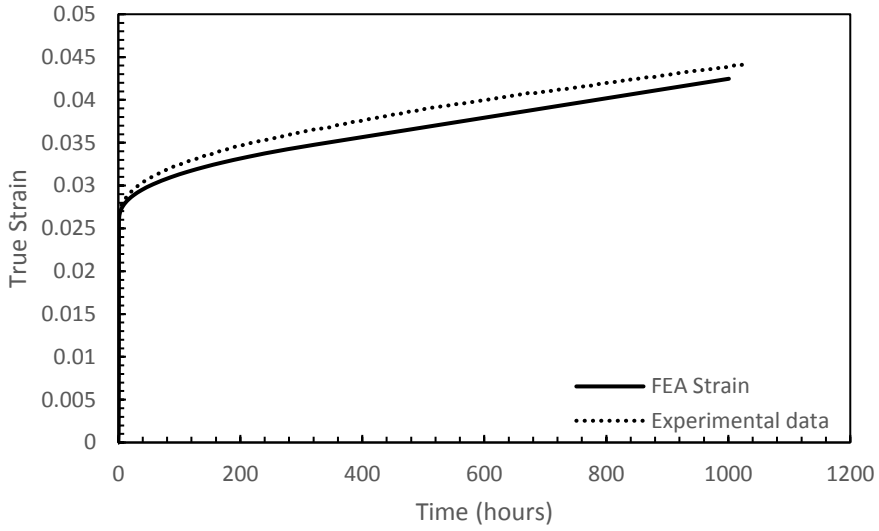

Figure 4.4-230MPa applied stress, round bar specimen at 550˚C, FEA vs experimental [80].

4.2 Creep rupture of notched bars

4.2.1 Introduction

Uniaxial forward creep behaviour has been investigated in previous research by Spindler [17]. Uniaxial loading conditions are not truly representative of plant operating conditions because complex geometries and loading conditions are often present. Notched bar tests have been conducted by previous researchers to determine the multiaxial effect on creep ductility [62, 81, 82], defining creep ductility as the creep strain on failure. In this research notched bar specimens have been used to introduce a stress triaxiality [83-86].

4.2.2 Methodology

Experimental methodology can be found in Chapter 3.

4.2.3 Experimental Results

(Published, see #1 in Publication list (taken directly from a paper published by the author))

The results of the tests are reported in Table 4.3 and shown graphically in Figures 4.5 to 4.7. Nine creep rupture tests were conducted on notched bar specimens with various stresses and a notch acuity of 5. The test with a net section stress of 260MPa was interrupted by a power cut which resulted in the structural integrity of the specimen being lost.

Table 4.3– Creep rupture of notched bars experimental results at 550˚C (test at 260MPa was interrupted by a power cut which led to damage of specimen).

Net Section Stress (MPa)	Rupture Time	E_0 (mm)	E_f (mm)	d_0 (mm)	d_f (mm)	ε_h (abs)	$\bar{\varepsilon}_{skf}$ (abs.)	Magnitude of diametric creep strain (abs.)
260	>4320	0.055	-	3.95	-	-	-	-
342	11097	0.11	0.43	3.91	3.79	-0.0312	0.0391	0.0312
390	480	0.29	0.60	3.80	3.70	-0.0267	0.0334	0.0267
432	175	0.58	1.00	3.80	3.68	-0.0321	0.0402	0.0321
436	307	0.70	1.19	3.63	3.54	-0.0251	0.0315	0.0251
469	231	0.41	0.84	3.60	3.46	-0.0397	0.0497	0.0397
500	16	1.18	1.73	3.65	3.51	-0.0391	0.0490	0.0391
500	23	-	-	3.82	3.61	-0.0565	0.0708	0.0565
515	35	0.56	1.13	3.49	3.32	-0.0499	0.0625	0.0499

E_0 and E_f were the extension after initial loading and on failure respectively. d_0 and d_f were the diameter after initial loading and on failure respectively. ε_h was the surface hoop creep strain. For a notched bar this was calculated using the following expression (noting that it is the hoop strain which is related to the measured diameter of the specimens):

$$\varepsilon_h = \ln\left(\frac{d_f}{d_0}\right) \qquad (4.4)$$

$\bar{\varepsilon}_{skf}$ was the skeletal Mises strain on failure (this is the Mises strain at the skeletal point). The skeletal point is the point where the stress state is insensitive to the power law stress dependence of creep (1.42mm from the centre of the specimen in this case). It has been determined in previous work that for a notched bar with notch acuity 5 that $\bar{\varepsilon}_{skf}/\ \varepsilon_h$=-1.253 [73]. This value was validated within the finite element analysis conducted within this work. It was found that after 300 hours of creep with a net section stress of 350MPa $\bar{\varepsilon}_{skf}$ was 3.9E-3 and ε_h was -3.1E-3, these values agreed with the conversion factor calculated previously by Spindler. The skeletal point is often used as the point of analysis in notched bar testing [88].

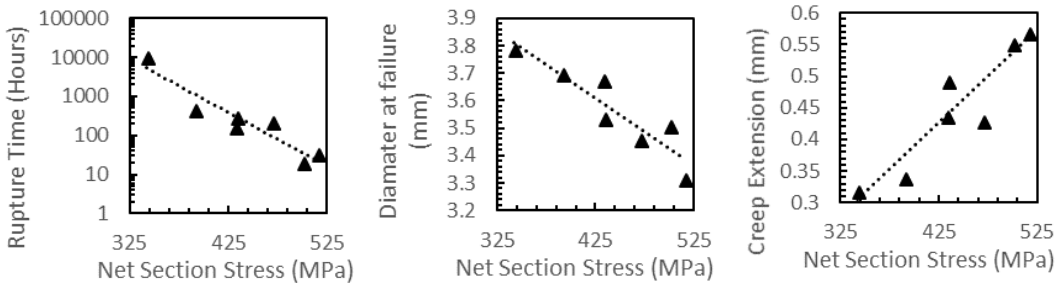

Figure 4.5(a,b,c) Rupture time, diameter on failure and extension during creep for various net section stresses (initial diameter 4mm for all specimens)

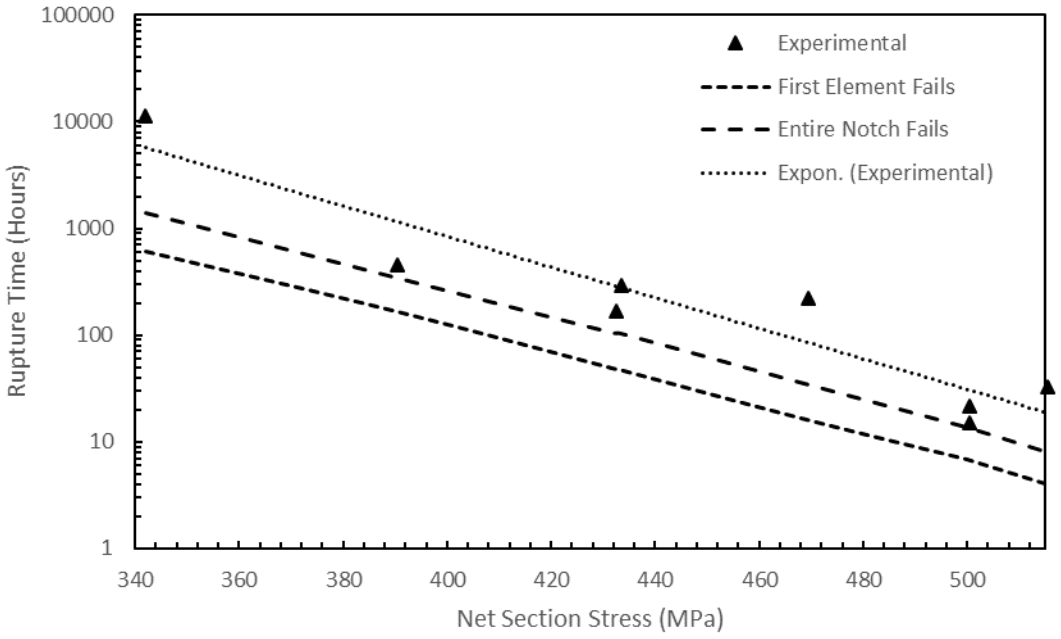

Figure 4.6- Time to rupture for various net section stresses on notched bar specimens at 550˚C (experimental and finite element analysis with the Spindler damage model).

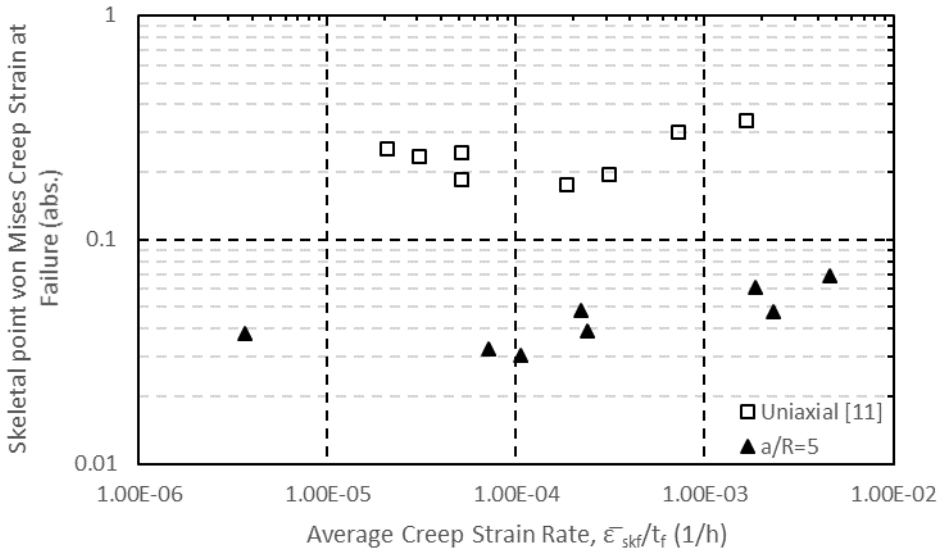

Figure 4.7- Ductility of uniaxial and multiaxial Type 316H stainless steel specimens (cast 69431) at 550˚C.

The rupture time reduced with an increase in net section stress as shown in Figure 4.5a, the maximum time to rupture was 11,097 hours with a net section stress of 342MPa, the minimum time to rupture was 23 hours with a net section stress of 500MPa. The diameter on failure reduced with an increase in net section stress (this was because there was more creep strain accumulated at higher net section stress experiments before failure due to this materials strain rate dependent ductility), this can be seen graphically in Figure 4.5b. The maximum diameter on failure was on the lowest stress completed test, the diameter was 3.79mm on failure with a net section stress of 342MPa and the smallest diameter on failure was from the highest stress test, 3.32mm on failure at a net section stress of 515MPa. The relation between diameter on failure and net section stress was linear. With every 1MPa of stress added the diameter on failure was reduced by 0.0026mm. Extension during creep was increased with an increased net section stress as highlighted in Figure 4.5c. The maximum extension during creep was 0.57mm and the minimum was 0.31mm. The relationship between overall specimen extension during creep and net section stress was linear, with every 1MPa of stress added the increase in length of specimen during creep was 0.0016mm. Figure 4.6 shows the time to rupture for various net section stresses. Figure 4.7 shows the creep ductility on failure for the notched specimens (with a/R=5), defined as the skeletal point Mises creep strain, as well as the creep ductility on failure for uniaxial specimens with the same cast, conducted in previous research [73]. The uniaxial specimens had a significantly larger creep ductility on failure.

The lower creep ductility and reduced plastic strain during the lower net section stress experiments is the reason for the reduced extension on failure and less of a reduction in diameter.

Figures 4.8 – 4.10 show the test conducted at a net section stress of 433MPa. They show the reduction in diameter during load up, the reduction in diameter during creep and the extension of the specimen during creep respectively. Figure 4.11 shows images taken by the camera set-up during the experiment conducted at a net section stress of 500MPa. The unstressed notch, notch after load-up, notch just before failure and notch after failure are shown.

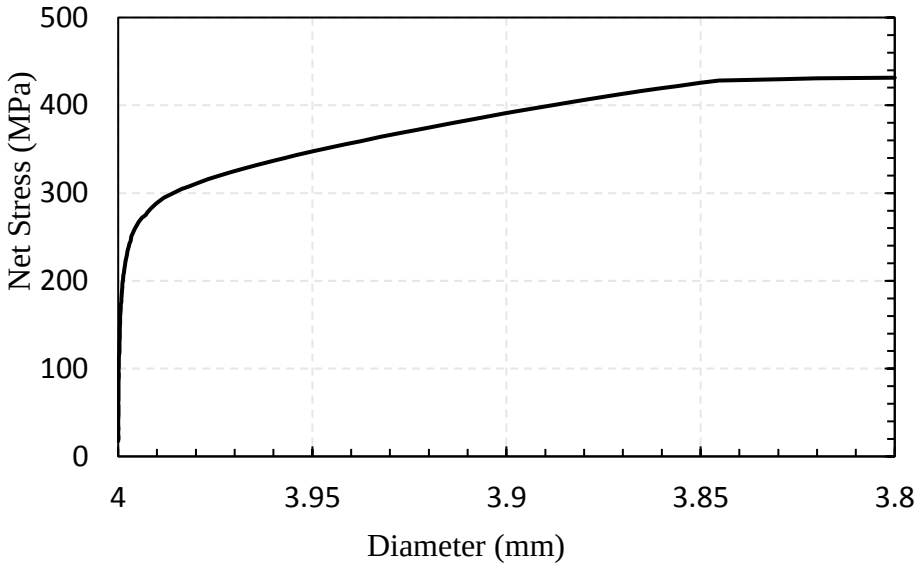

Figure 4.8- Net section stress vs reduction in diameter for a notched bar at 550˚C during load up (loaded to 433MPa).

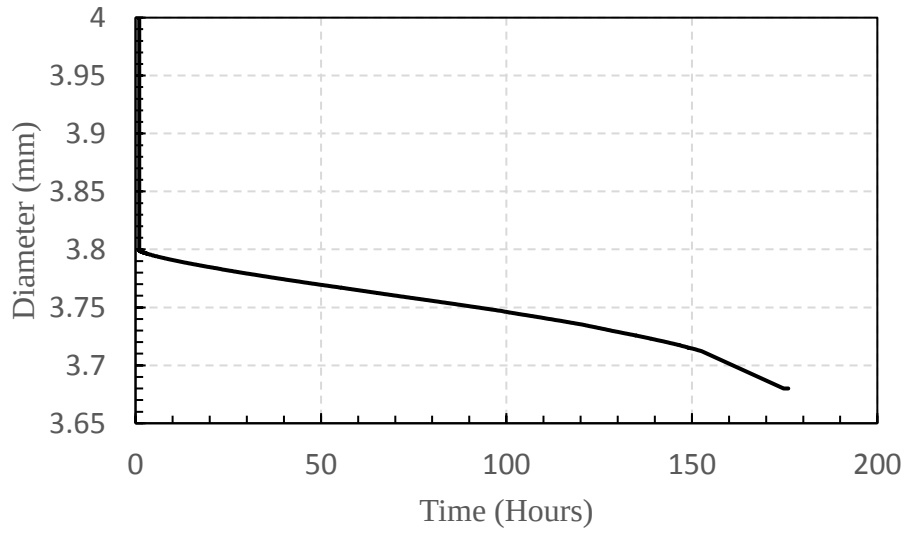

Figure 4.9- Reduction in diameter for a notched bar at 550˚C (loaded to 433MPa) during creep.

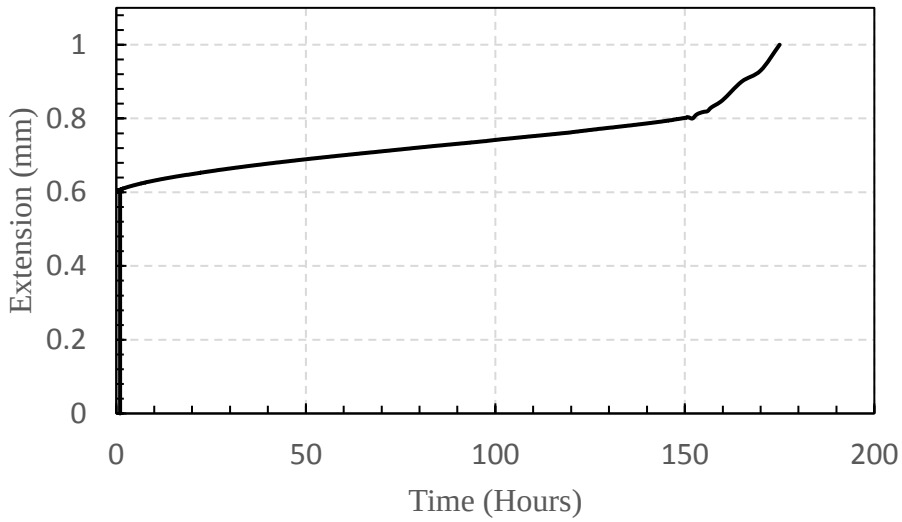

Figure 4.10- Overall creep extension for a notched bar at 550˚C (loaded to 433MPa).

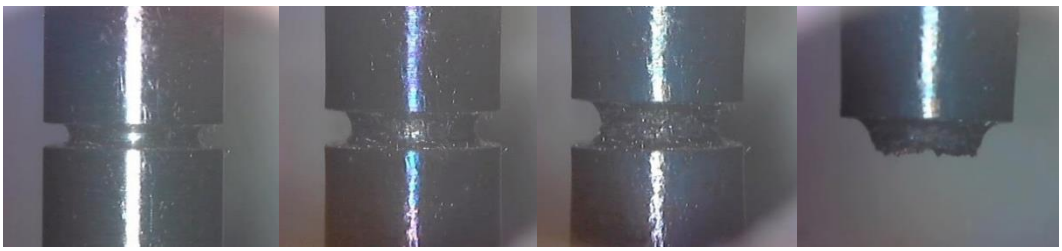

Figure 4.11- A notched bar specimen before load up, after load up, just before failure and just after failure under constant load creep conditions (500MPa net section stress) at 550˚C.

4.2.4 Spindler Damage Model

4.2.4.1 Spindler Damage Model Methodology

(Published, see #1 in Publication list (taken directly from a paper published by the author))

The Spindler damage model was used to assess creep rupture of notched bars. Details of the Spindler damage model can be found in Chapter 3.

4.2.4.2 Spindler Damage Model Results

The results from the Spindler finite element model were compared with uniaxial creep data [73]. The model accurately predicted Elastic-Plastic Primary-Secondary (EP-PS) creep. The model accurately captured the creep behaviour of round bar specimens subject to constant load creep.

An elastic plastic simulation was conducted with the notched specimen, the hydrostatic, von Mises equivalent, maximum principal and net section stresses can be seen along the notched diameter in Figure 4.12. The stress triaxiality (Hydrostatic stress/Mises stress) and Spindler Fraction (equation 3.2) along the notched diameter can be seen in Figure 4.13.

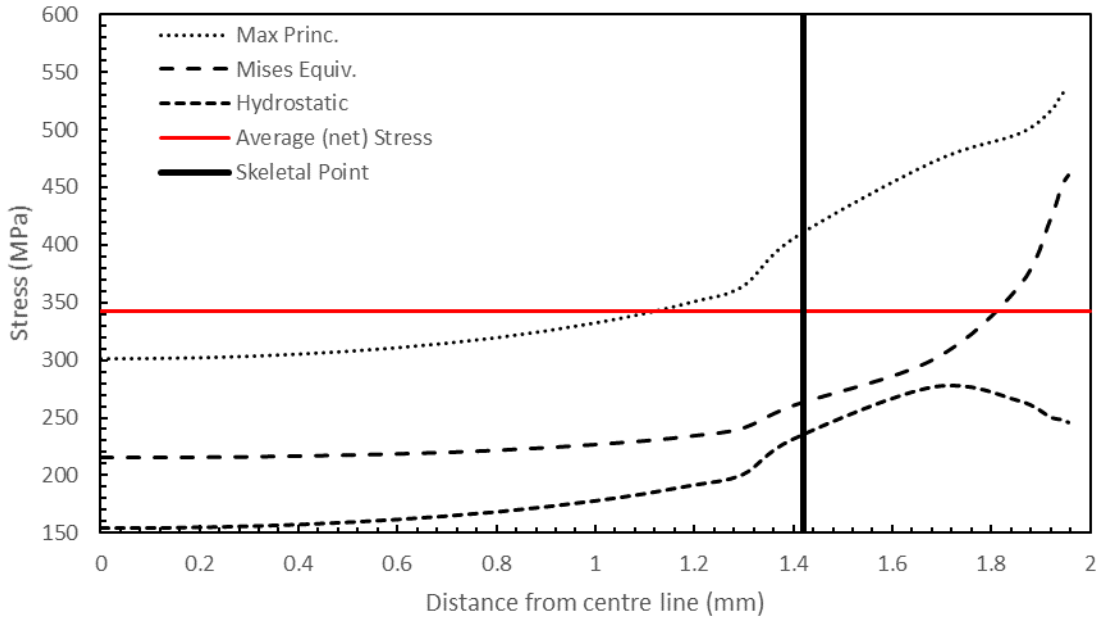

Figure 4.12- Maximum principal, von Mises equivalent, hydrostatic and net section stresses along the centre line after loading up to 342MPa (no creep)

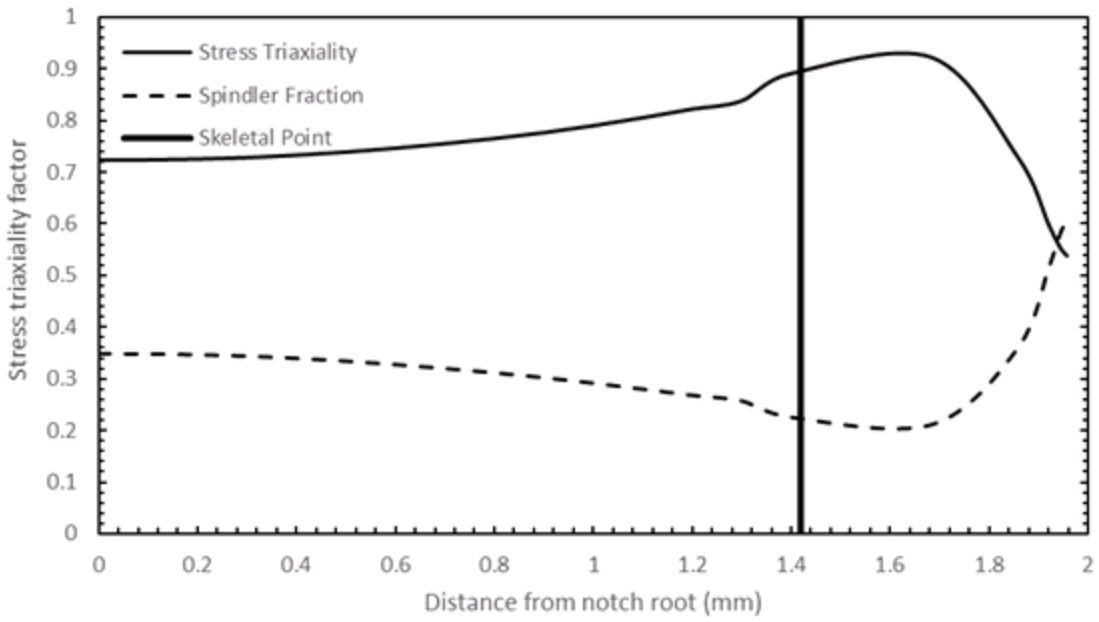

Figure 4.13- Stress triaxiality and Spindler Fraction along the centre line after loading up to 342MPa (no creep).

Figure 4.14 shows extension against time for the test at 390MPa. Figure 4.14 shows that the experimental and FEA results were in good agreement regarding to extension at failure. The extension on failure was 2% higher in the experiment than the FEA, but the time to rupture was 28% longer in the experiment than the FEA. This showed the model was within the margin of error expected within creep tests and on the conservative side (the two experiments conducted at 500MPa were 43% different in time to rupture). In reality a crack might initiate upon Type 1 failure, and the physical process between this and ultimate failure would then be by crack growth. This has only been crudely modelled in the FEA presented here by virtue of the failed elements having no strength. A crack will also propagate due to the intense stress and strain fields near the sharp crack tip, but this has not been modelled.

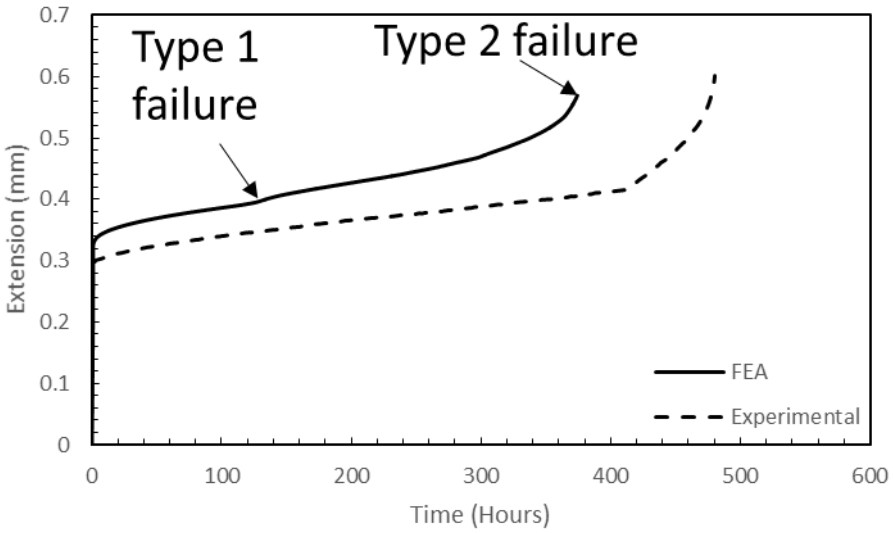

Figure 4.14- Notched bar with applied net section stress 390MPa at 550˚C (finite element analysis and experimental results shown).

Figure 4.15 shows that in the finite element model the Mises creep strain on failure (Type 2 FEA failure plotted) at the point of maximum damage increases with the average experimental Mises creep strain rate (defined here as failure strain/time to rupture).

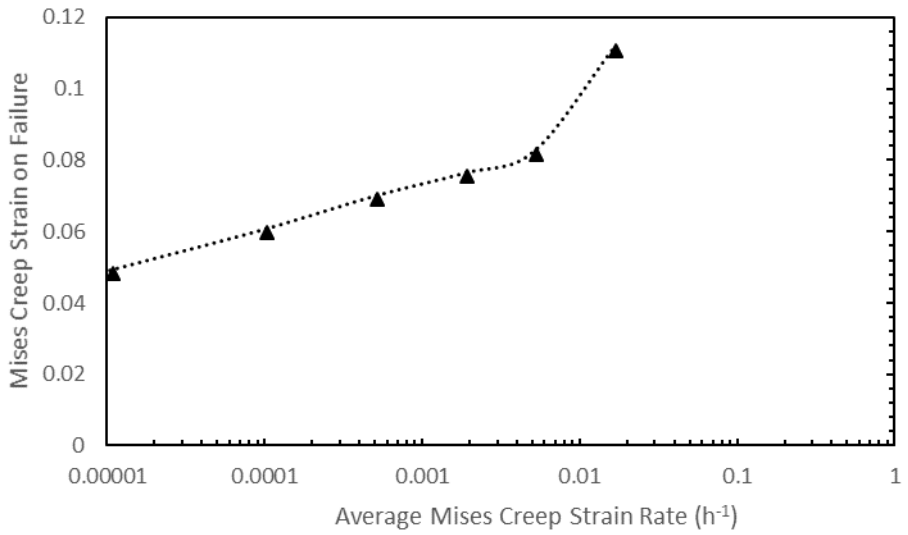

Figure 4.15- Mises creep strain on failure against average Mises creep strain rate (FEA) at the point of maximum damage (Type 2 FEA failure).

Figure 4.16 shows how damage is accumulated over time at the elements of maximum and minimum damage across the notch ligament. Type 1 failure is defined as when the element of maximum damage reaches a damage value of 1. Type 2 failure is defined as when all elements along the notched diameter reach a damage value of 1.

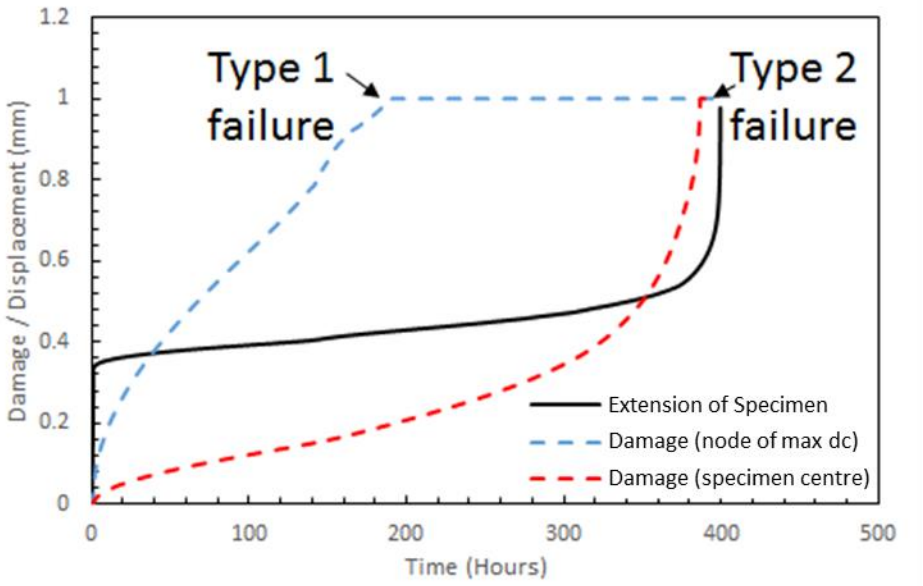

Figure 4.16- Creep damage accumulation over time leading to failures (Net section stress 390MPa (FEA extension shown)).

Figure 4.17 shows the distribution of creep damage and creep strain across the notch ligament. Figure 4.17 predicts failure will have occurred at the surface earlier than it did at the Skeletal point. This agrees with previous notched bar FEA conducted by Spindler [73]. Other research on notched bars has used the Skeletal point as a focal point for analysis [88]. This shows that using the Skeletal point may give us an underestimate of creep damage.

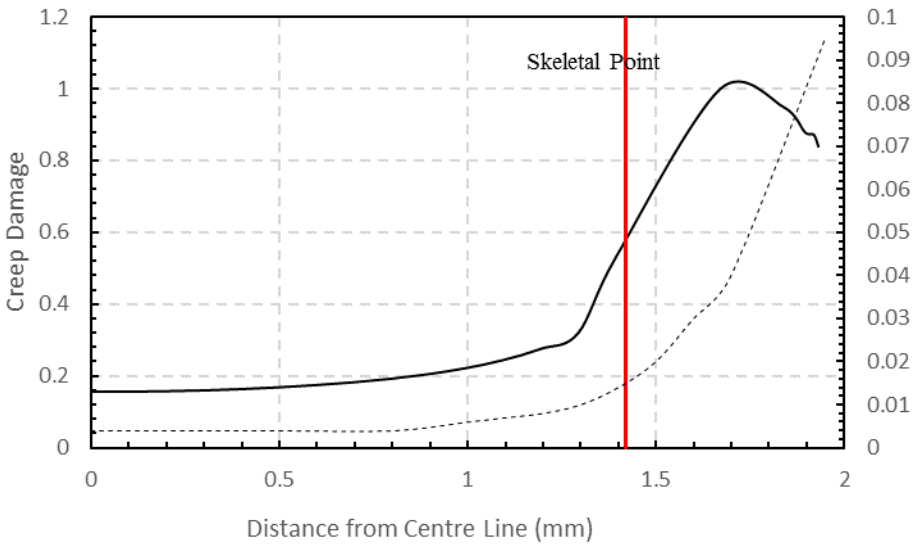

Figure 4.17- Creep damage and creep strain predicted across ligament as first element fails (Type 1 failure distribution). Testing conditions were a 500MPa net section stress at 550˚C.

Figure 4.18 shows the experimental reduction in diameter of this specimen compared with the reduction in diameter obtained from the finite element model, both plotted against time. From this comparison, it can be seen that the reduction in diameter after loading up is captured very well by the finite element model as is the reduction in diameter during subsequent creep.

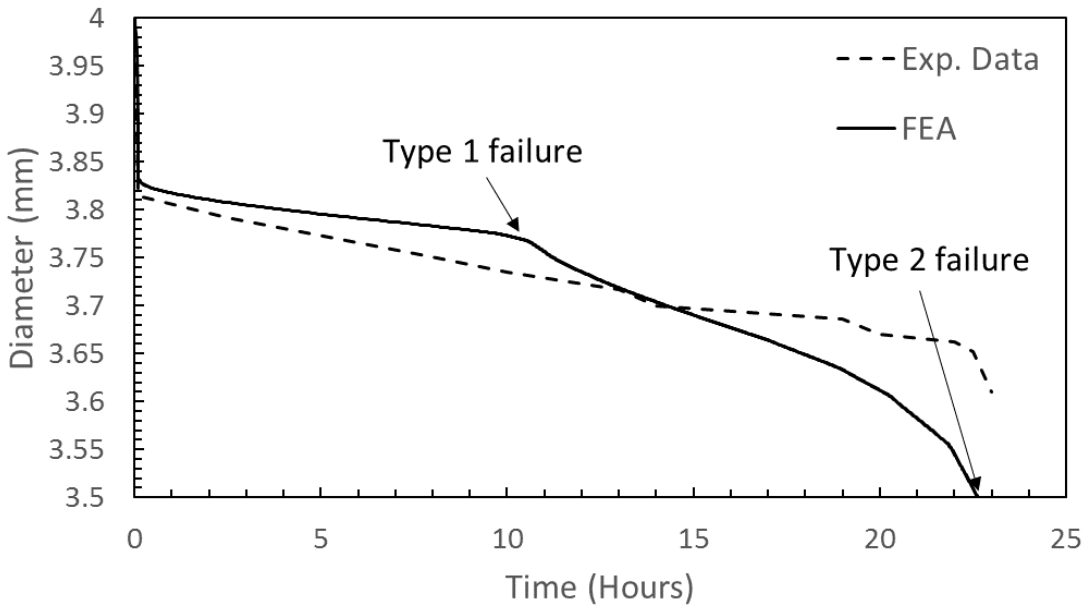

Figure 4.18- Reduction in diameter, 500MPa net section stress (data from camera and finite element analysis) at 550˚C.

Figure 4.19 shows the notch opening of the same specimen from the same creep test (net section stress 500MPa, 550˚C) again plotted alongside the finite element simulation. Again, it can be seen that the finite element model accurately captures the behaviour of the specimen. Figure 4.19 shows how the overall extension of the specimen is predominantly coming from the notch. For the test with a 500MPa net section stress the overall extension on failure was 1.73mm of which 1.48mm was notch opening. 85% of the specimen's extension is from the notch, given that the notch only accounts for 3% of the overall length of the specimen it is clear that the notch is the area of greatest interest where the highest stresses and strains are apparent. This was confirmed by the experimental and finite element work.

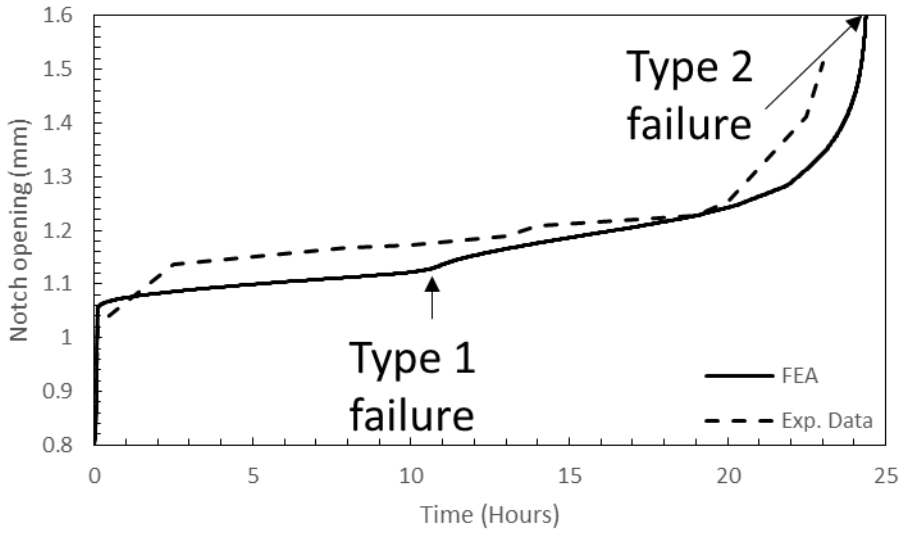

Figure 4.19- Notch opening, 500MPa net section stress at 550˚C (experimental data from camera set up and finite element values shown).

Figure 4.20 shows the final image captured before failure of the specimen from the experiment overlayed with the corresponding FEA simulation (500MPa net section stress). This Figure shows the deformation of the specimen was captured by the model and the damage throughout the specimen can be seen. Figure 4.6 (in the experimental section) shows the finite element times to failure plotted with the experimental data for a range of stresses.

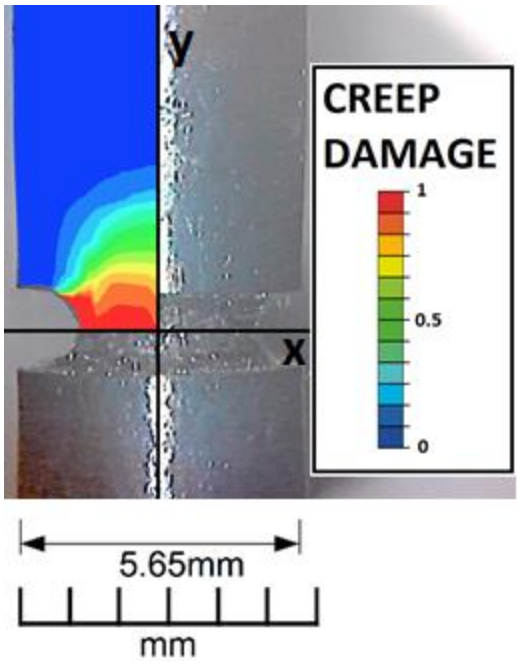

Figure 4.20- 500MPa net section stress test, FEA (Type 2 failure) and experimental (last image taken before failure of the specimen) at 550˚C.

4.2.5 SMDE

The stress modified ductility exhaustion (SMDE) creep damage model is a recent adaption to the Spindler damage model. This modification means that the effect of stress on creep damage is included, as detailed in Chapter 3. This model incorporates the strain rate dependent ductility. The SMDE model leads to large variations in the distribution of creep damage and creep strain on failure (otherwise gives similar results and trends for creep rupture experiments as the Spindler damage model). Figures 4.21 and 4.22 show the creep damage and creep strain on failure respectively for a notched bar specimen (acuity 5) at 550˚C for various constant load net section stress rupture tests. Figure 4.21 shows that for the SMDE model the initial failure location where damage = 1 first shifts further away from the notch tip the greater the applied stress. Figure 4.22 shows that the maximum creep strain on failure at the tip of the notch can be 6 times greater depending on the applied stress. Type 2 failures are predicted on a similar time scale for the SMDE and Spindler damage model in creep rupture of notched bars. However, for the SMDE model Type

1 failures occur in approximately 10% of the time as the corresponding type 2 failure as opposed to 40% of the corresponding Type 2 failure for the Spindler damage model.

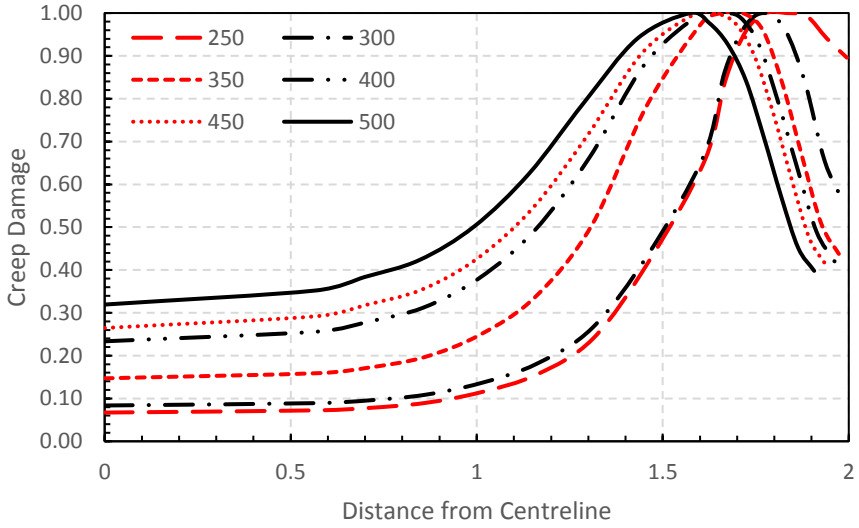

Figure 4.21– Failure location changing with stress SMDE model at 550˚C (Type 1 failure).

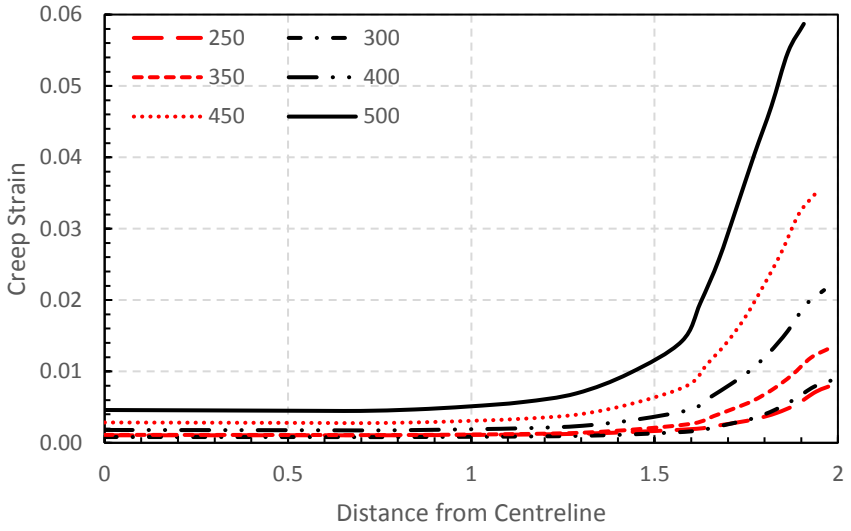

Figure 4.22- Creep strain on failure changing in the SMDE model with applied stress at 550˚C (Type 1 failure).

4.3 Discussion

(Published, see #1 in Publication list (taken directly from a paper published by the author))

The uniaxial creep data for this cast of austenitic stainless steel showed that this material exhibits a large scatter under plastic load up and creep conditions at 550˚C. However, this was to be expected as there is an inherently large scatter in the data from creep of stainless steels at high temperature. The creep constants derived from uniaxial data accurately captured the behaviour of both uniaxial and multiaxial specimens under constant load conditions.

Unsurprisingly, all the specimens failed at the notch. This was because the cross-sectional area was lowest at the notched section, so the net section stress was the highest at this area. Furthermore a small radius notch was used which generated a high stress concentration factor (approximately 3) and induced triaxiality, which together reduce the time to rupture in a specimen [89]. The triaxiality at the notch peaked after initial load, the ratio of hydrostatic to Mises stress being almost 3 times the uniaxial value [17]. Figure 4.7 shows that the creep strain on failure is increased with an increase in creep strain rate. This was a key to this work and further work in this thesis involved testing whether this behaviour was the same in constant displacement creep of notched bars.

As the net section stress applied to the specimens was increased the time to rupture was decreased, the extension on load up was increased and the creep extension on failure was increased. This agrees with research conducted on similar materials that found that creep ductility is a function of stress, temperature and loading rates [90].

The finite element model used showed very good agreement with the experimental data in the case of uniaxial specimens. This was expected as the constants used in the FEA had been derived from the uniaxial test data. When the FEA was compared to the experimental results of the notched bar rupture tests it was found to be within the range of the experimental data but towards the conservative side rather than being the average as with the uniaxial data. Agreement between the data and the model was strong with the model able to predict the notch opening and reduction in area of the notched specimen accurately when compared to the data obtained experimentally (with the camera set-up). The model found that damage reaches 1 (first element fails (Type 1 failure) approximately 40% of the way into the creep life of the specimen then propagates progressively faster through the specimen as creep continues until rupture of the specimen when all elements along the root of the notch fail (Type 2 failure).

The test results and the FEA are consistent with an approximately exponential relationship between stress and rupture time. A test was started with a net section stress of 260MPa on the same specimen geometry and was run for over 4,000 hours and was predicted to be approximately one tenth of the way through its creep life from the data till that point but a power shutdown in the lab interrupting the furnace and integrity of the specimen led to termination of the test before rupture of the specimen.

The creep strain at failure was almost twice as large for the higher stress tests than for the lower stress tests. This suggests that creep strain is not always equally damaging, the results suggest that for a fixed amount of creep strain, the slower it is accumulated the more damaging it is to the specimen. This implies where damage is predicted from creep-fatigue cycles, and hence repeat relaxations, the initial, faster, phase of relaxation may be less damaging than the same strain accumulated slowly. Direct demonstration of this effect is the subject of Chapters 5 and 6.

4.4 Concluding Remarks

(Published, see #1 in Publication list (taken directly from a paper published by the author))

Nine experiments with varying net section stresses were conducted on notched bar specimens (All specimens had a notch acuity of 5). Notched bar specimens were used to introduce a stress triaxiality and reduce failure times, notched bar specimens are particularly representative of weld toes. Finite element simulations were conducted using Abaqus to determine the behaviour at the notch of the specimens. The conclusions drawn from this work were that in creep rupture as the net section stress increases the time to failure reduces but the creep ductility on failure increases implying the material has a time or strain rate dependent creep ductility. As net section stress is increased the overall extension of the specimen on failure is increased and specimen diameter on failure is reduced. Moreover, the extension and diameter change attributable to creep also increase as the net section stress is increased, further confirming this material has an increased creep ductility at higher strain rates/stresses. As net section stress is increased, hoop and skeletal creep strains on failure are also increased. It has been shown that using creep constants derived from uniaxial creep data it is possible to accurately capture creep behaviour of notched bar specimens with a notch acuity of 5. The Spindler damage model also performed well in predicting rupture times and their trend with increasing stress. The highest stress triaxiality factor (hydrostatic

stress/Mises stress) occurs just away from the notch tip, 1.65mm from the centre line (15% of the distance from the edge of the notch to the centre line), the same point on the specimen where damage reaches 1 (unity) first. The higher the net section stress and therefore the higher the average creep strain rate in creep rupture tests, the higher the extension and creep ductility of the specimens on failure. This leads to the key conclusion drawn from this work which is that a given creep strain is less damaging the faster it is accumulated in creep rupture of Type 316H stainless steel. Smaller effective creep ductilities may therefore apply at the very slow strain rates relevant to plant operating for several decades.

CHAPTER 5

STRESS RELAXATION

Work from this chapter was presented and published at the Pressure Vessels and Piping conference in Prague, 2018.
It has also been published in the International Journal of Pressure Vessels and Piping.

"A diamond is merely a lump of coal that did well under pressure." – Will Rogers

Chapter 5 Stress Relaxation

In Chapter 3 creep constants were derived for finite element modelling of the specific cast of Type 316H stainless steel used within this work. It was then shown in Chapter 4 that creep ductility is strain rate dependent in constant load creep experiments conducted on notched bar specimens. In practical situations components are often subjected to cyclic/relaxing loads. The purpose of this Chapter was to determine whether the creep strain accumulated very quickly at the start of a stress relaxation dwell is just as damaging as an equal amount of creep strain accumulated much more slowly during the later stages of a relaxation dwell. This aim was achieved by conducted repeat stress relaxation experiments on notched bar specimens with varying dwell lengths. Initial stress relaxation experiments were conducted on uniaxial specimens to ensure that the creep damage model being used could accurately capture the stress relaxation behaviour of this material.

5.1 Elastic follow-up

Many previous stress relaxation studies have focussed on the effect of elastic follow-up (Z) [37, 92-96]. Elastic follow-up is a measure of the relative stiffness of the rig compared to the stiffness of the specimen. The elastic follow-up factor in forward creep tests is infinite ($Z = \infty$) (illustrated in Figure 5.1) because the specimen is in series with the loading arms and the load is applied from a hanging weight. As seen in Figure 5.1, in forward creep tests the stress is increased during the load up then when creep occurs the stress stays constant while the strain increases throughout the experiment. In a pure displacement controlled stress relaxation test where the rig is completely rigid and does not deform when stress is applied to the specimen, the elastic follow-up factor is 1($Z = 1$) [97]. In a stress relaxation test after initial load up when the displacement becomes fixed the stress drops with time but the strain/displacement remains at the same level [98-100]. Figure 5.1 shows the stress strain curves for creep tests with varying elastic follow-up factors. The experiments conducted in this investigation were performed on a 3-bar structure with very thick outer bars. These bars were made from Nimonic steel (which exhibits very high stiffness) and the notched specimens used had a relatively low stiffness. This led to a low elastic follow-up factor of $Z = 1.1$. This meant the rig provided excellent displacement control and the effects of elastic follow-up were negligible [20, 101].

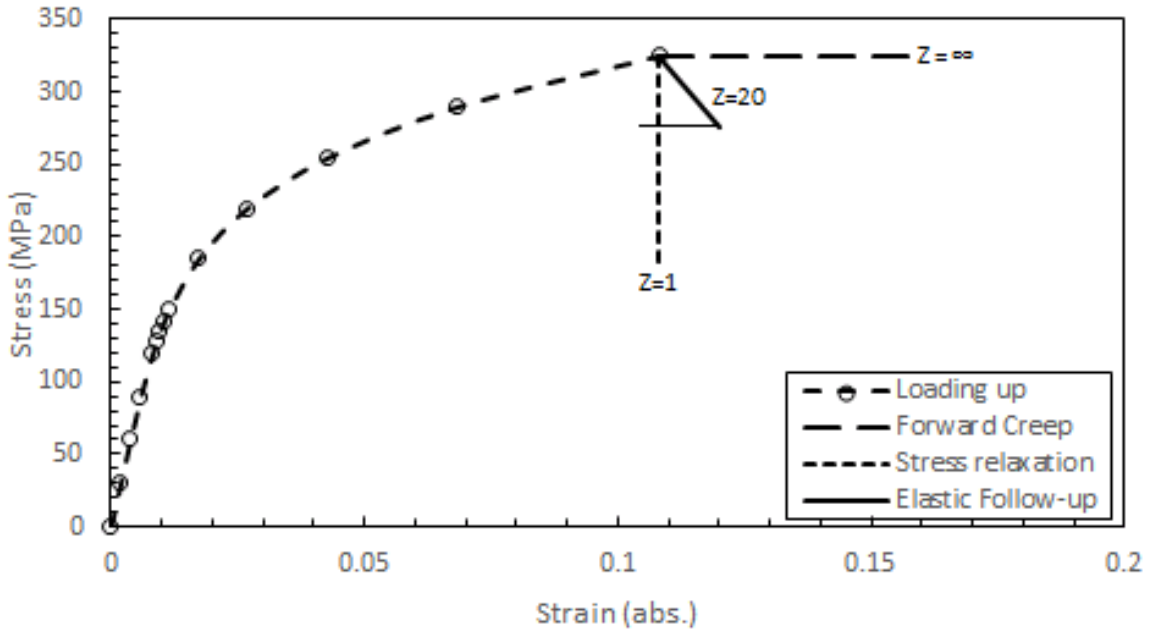

Figure 5.1- Stress-strain trajectories with loading associated with forward creep (Z=∞), elastic follow up (Z=20) and stress relaxation (Z=1).

5.2 Uniaxial Stress Relaxation

5.2.1 Experimental Methodology

Details of the test rig can be found in Chapter 3.

Stress relaxation tests were conducted with different initial stresses on uniaxial creep specimens. In these stress relaxation tests a stress was applied, then the displacement (and strain) was fixed and the stress relaxed for 100 hours and the stress drop behaviour was recorded. Initial stress values of 75, 125, 150, 250, 300 and 350MPa were used so that stress relaxation behaviour with and without plasticity on loading could be observed.

5.2.2 Experimental Results

The results from the 7 uniaxial stress relaxation experiments conducted can be seen in Table 5.1 and graphically in Figures 5.2-5.4. The specimens had a gauge length of 50mm and a diameter of 5.65mm.

Table 5.1 - Stress relaxation results summary.

Initial Stress (MPa)	Stress after 100 hours (MPa)	Stress Drop (MPa)	Stress Drop as a Percentage of Initial Stress (%)	Extension (mm)	Total Strain (%) (elastic + plastic)
75	61	14	19	0.02	0.04
125	111	14	11	0.04	0.08
150	134	16	11	0.05	0.10
250	183	67	27	1.21	2.42
300	199	101	34	2.97	5.94
350	215	135	38	6.22	12.44

Figure 5.2 shows the stress relaxation behaviour with respect to time for all experiments conducted. Here it can be seen that there is a very limited stress drop seen below the yield stress of the material and significantly larger amounts of stress drop when an initial stress above the yield stress is applied. This behaviour is shown in Figure 5.3 where the total stress drop in a 100 hour relaxation dwell is shown vs the start of dwell stress for each experiment.

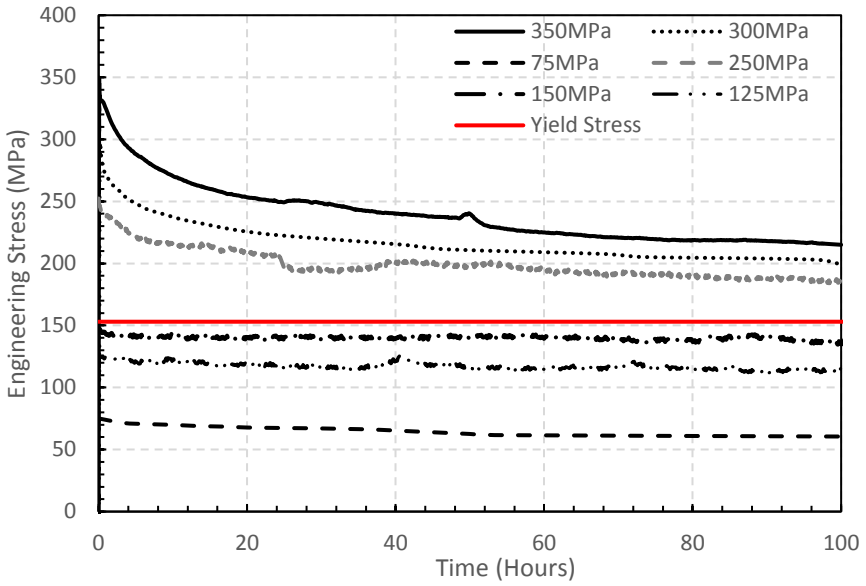

Figure 5.2- Stress relaxation against time

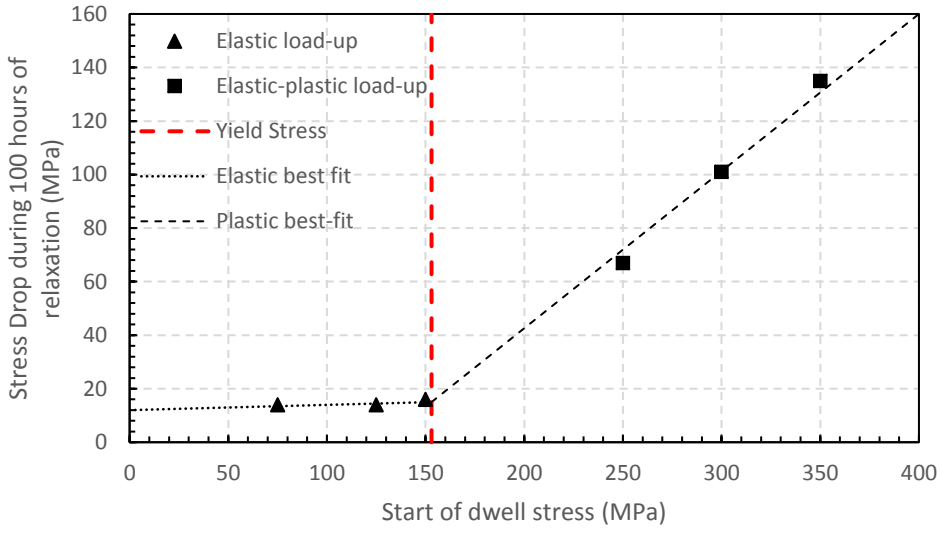

Figure 5.3- Stress drop vs start of dwell stress.

Figure 5.4 shows the stress strain curve for the material used in this study at 550˚C from a tensile test conducted in this work. Also shown in Figure 5.4 are the strains (strain is calculated as the change in length of the specimens gauge length divided by the original gauge length of the specimen) after load up for each of the tests conducted, here it can be seen that 3 relaxation experiments were conducted below the yield stress of the material and 3 above.

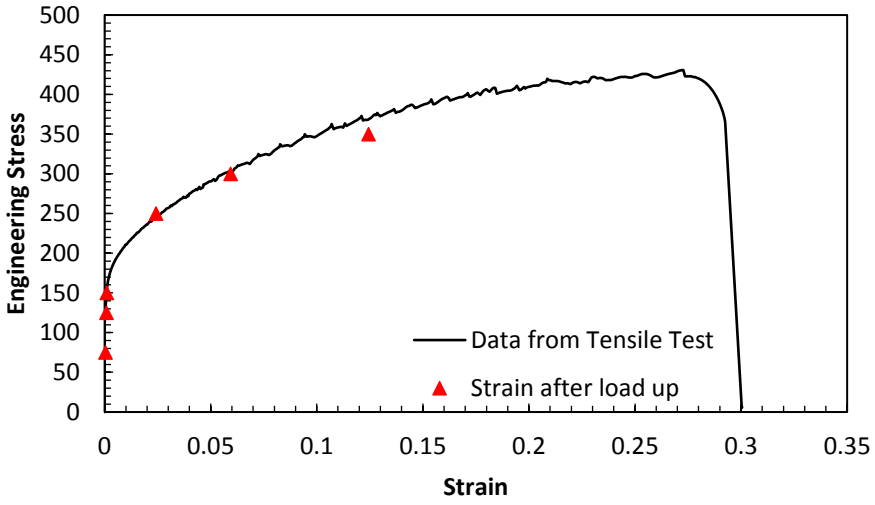

Figure 5.4- Stress against strain curve.

5.2.3 Finite Element Analysis

Uniaxial stress relaxation predictions were conducted in Abaqus using the material constants detailed in Chapter 3. Simulations with primary creep and simulations without primary creep were used. The model without primary creep has been used as it is thought this stress drop during load up could exhaust the primary creep. It was found that for the tests below the yield stress of the material (150MPa, 125MPa and 75MPa start of dwell stresses) there was very little stress relaxation and both models captured this behaviour. The three tests above the yield stress (350MPa, 300MPa and 250MPa) can be seen in Figures 5.5-5.8. Figure 5.5 shows all 3 tests with both creep models and experimental data. Figures 5.6, 5.7 and 5.8 show the tests at start of dwell stresses of 350MPa, 300MPa and 250MPa respectively. ST in the key represents a model with

secondary and tertiary creep. PST in the key represents a model with primary, secondary and tertiary creep.

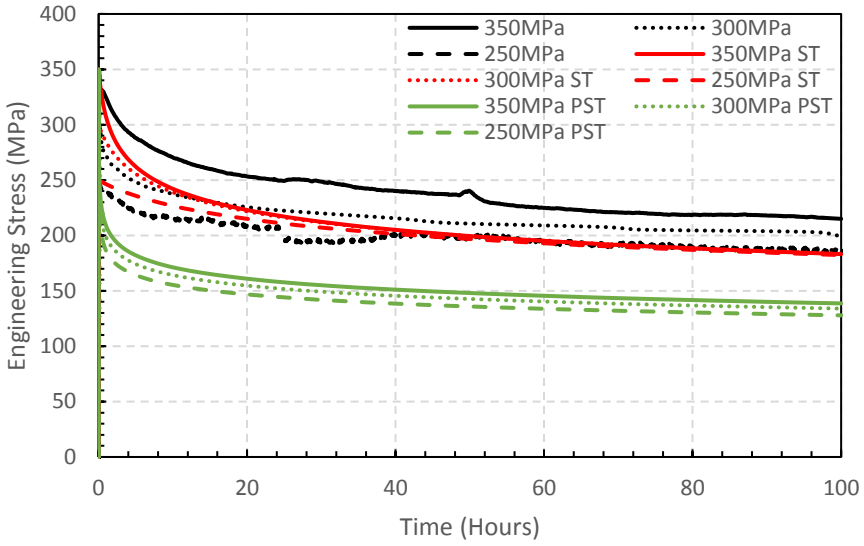

Figure 5.5- Uniaxial stress relaxation behaviour experimentally and with finite element analysis at 550˚C at different start of dwell stresses.

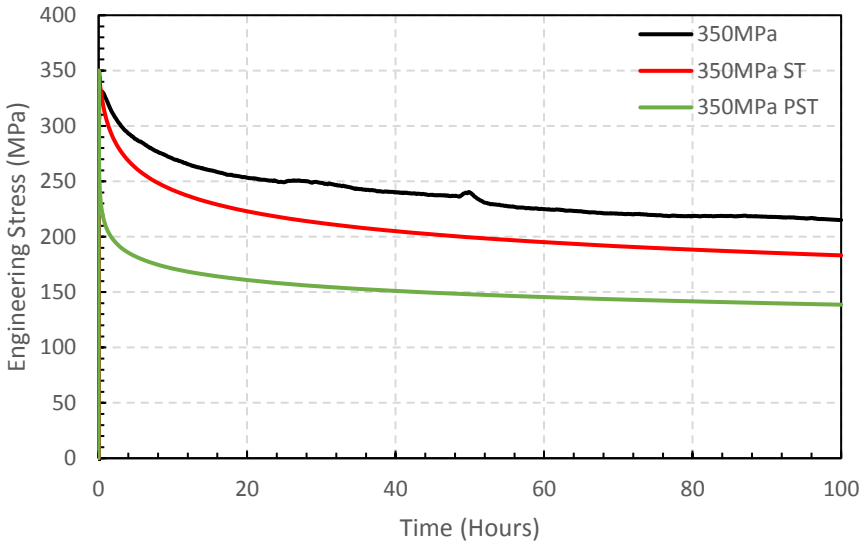

Figure 5.6- Uniaxial stress relaxation behaviour experimentally and with finite element analysis at 550˚C with a 350MPa start of dwell stress.

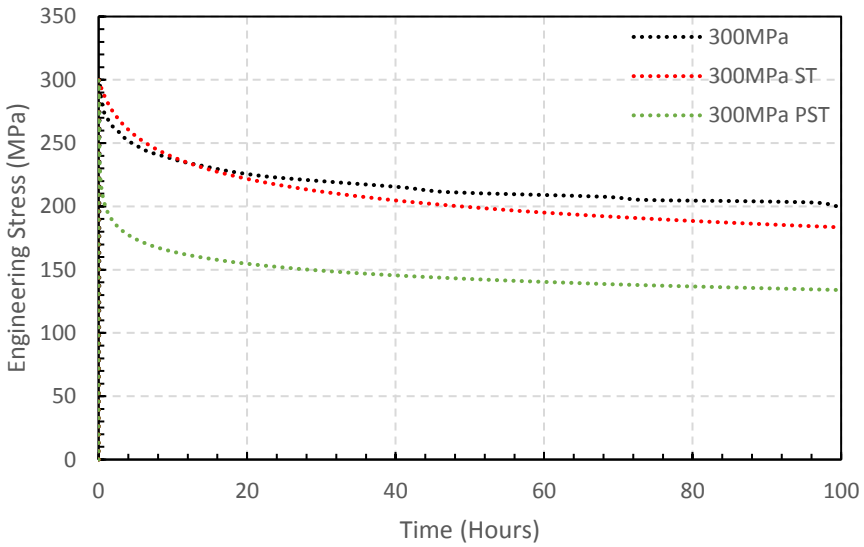

Figure 5.7- Uniaxial stress relaxation behaviour experimentally and with finite element analysis at 550˚C with a 300MPa start of dwell stress.

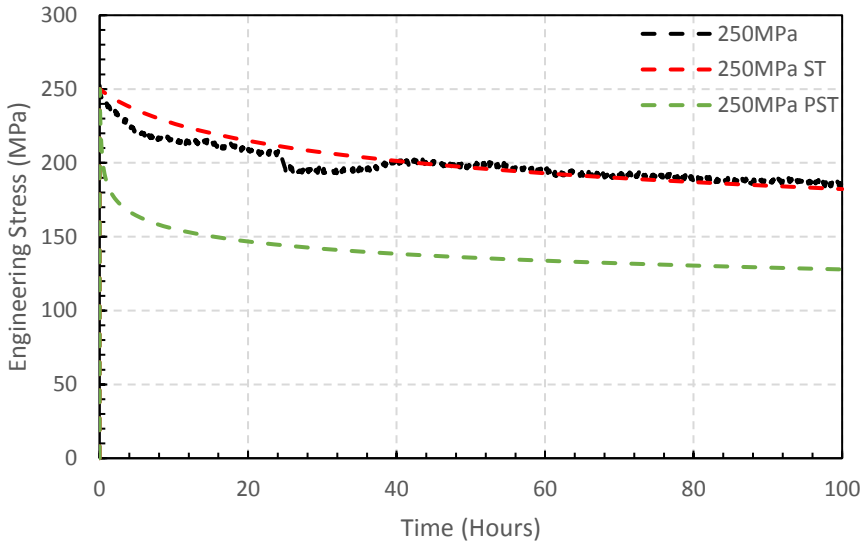

Figure 5.8- Uniaxial stress relaxation behaviour experimentally and with finite element analysis at 550˚C with a 250MPa start of dwell stress.

From these figures it can be seen that the finite element model without primary creep more accurately captures the stress drop behaviour at high stresses than the model with primary creep. This agrees with previous researchers who have noted that Type 316H does not exhibit primary creep during stress relaxation at high start of dwell stresses [102]. This is likely due to the primary creep being exhausted during the loading of the specimens because of the duration of time taken to load the specimens manually. In between rotations of the loading wheel the specimen relaxes and several rotations of the top wheel are required to take the specimen to high stresses.

5.3 Stress Relaxation of Notched Bars

5.3.1 Experimental Methodology

(Published, see #2 in Publication list (taken directly from a paper published by the author))

Details of the notched specimens and test rig used can be found in Chapter 3.

Repeat stress relaxation tests were conducted with different dwell times on notched bar specimens at 550˚C and 515˚C. In these repeat relaxation tests a net section axial stress of 500MPa was applied to the specimen (based on initial specimen diameter). The displacement of the specimen was then fixed for a certain dwell time (1, 12, 24, 168 or 500 hours) and the stress could relax. At the end of the dwell the initial load was again applied to the specimen and it was fixed at its new displacement. It was then allowed to relax for its prescribed dwell time. This was repeated until rupture of the specimens. Experiments were also conducted with a start of dwell stress of 440MPa at 550˚C, the same dwell times were used as in the other experiments.

5.3.2 Experimental Results

(Published, see #2 in Publication list (taken directly from a paper published by the author))

An example of the stress against time (5.9a) and extension against time curves (5.9b) can be seen in Figure 5.9. This shows how the displacement is fixed during dwells when stress is dropping, it also shows how the extension of the specimen is increased at the end of each dwell to ensure the start of dwell stress is 500MPa for every dwell (strictly this is the engineering stress, based on re-establishing the original load).

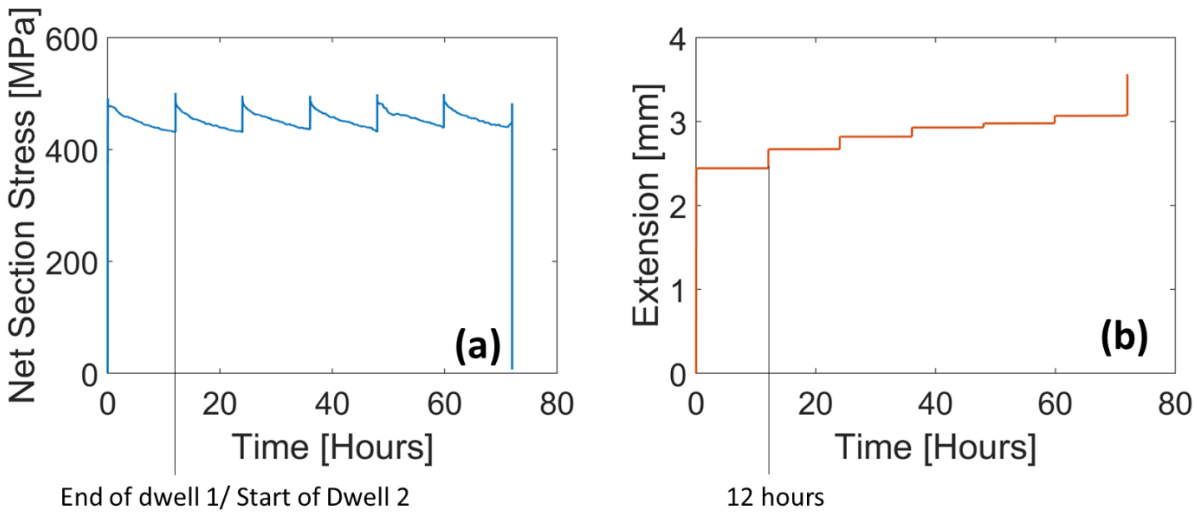

Figure 5.9a and b- 12-hour repeat stress relaxation dwells at 550˚C.

Tables 5.2 and 5.3 show the results for all the different dwell times during these repeat relaxation tests at 550˚C with a net section start-of-dwell stress of 500MPa and 440MPa respectively. The magnitude of the diametric creep strain was calculated by dividing the change in diameter during creep by the specimen diameter after initial load up. The notched diameter after load up was 3.74mm for tests at 550˚C with a net section stress of 500MPa, 3.85mm with a net section stress of 440MPa and 3.80mm for tests at 515˚C with a net section stress of 500MPa. The hoop creep strain was calculated via equation 4.4. The results show the shorter the length of the dwell time, the more dwells to failure, the larger the extension on failure, the larger the creep strain on failure, the larger the stress drop summed over all dwells, but the shorter the test duration. This highlights that the early part of the dwell is when most damage is accumulated within the specimen and then the rate of damage accumulation slows the further into the dwell you go, this can be seen because the experiments with lots of short term dwells fail in far less time than the experiments conducted with longer relaxation dwells. This is unsurprising because most of the creep strain is accumulated early in the creep dwell. However, the results indicate also that the damaging effect of a given level of creep strain is less when accumulated quickly, i.e., for the short dwell tests which therefore accumulate greater creep strain at failure.

Table 5.4 shows the results for the same set of experiments as Table 5.2 but conducted at 515˚C instead of 550˚C. These temperatures were chosen because they are common temperatures within power plant operation and it is believed from previous unpublished work by EDF energy that this stainless steel has a lower creep ductility at 515˚C than it does at 550˚C (Table 3.8). The same trends are apparent in the data at 515˚C that were previously seen at 550˚C. As expected, the creep strains at failure are smaller at the lower temperature. The total drop in net section stress included in the tables was calculated by adding the stress drop for each dwell, for example the 1-hour dwell test conducted at 550˚C with a start of dwell net section stress of 440MPa lasted for 55 stress drop cycles and in each of these cycles the stress dropped by approximately 20MPa hence the total stress drop of close to 1000MPa over the specimens lifetime.

Table 5.2- Repeat stress relaxation tests with a 500MPa start of dwell stress at 550˚C.

Dwell Length (hours)	Number of Load Cycles to Failure	Failed on loading?	Time to failure (hours)	Extension on failure (mm)	Total drop in net section stress during relaxation (MPa)	Magnitude of Diametric Creep strain on failure (%)	Hoop creep strain on failure, ε_h (abs.)	Unnotched Diameter on failure (mm)	Notched Diameter on failure (mm)
1	17	Yes	16	3.48	420	13.6	-0.147	5.32	3.23
12	7	Yes	72	3.34	366	11.5	-0.122	5.27	3.31
24	5	Yes	96	3.25	363	10.2	-0.107	5.34	3.36
168	3	Yes	336	3.14	277	6.2	-0.063	5.33	3.51
500	2	No	507	3.13	163	4.5	-0.047	5.37	3.57

Table 5.3 - Repeat stress relaxation tests with a 440MPa start of dwell stress at 550˚C.

Dwell Length (hours)	Number of Load Cycles to Failure	Failed on loading?	Time to failure (hours)	Extension on failure (mm)	Total drop in net section stress during relaxation (MPa)	Magnitude of Diametric Creep strain on failure (%)	Hoop creep strain on failure, ε_h (abs.)	Unnotched Diameter on failure (mm)	Notched Diameter on failure (mm)
1	56	Yes	55	2.44	980	12.2	-0.130	5.27	3.38
12	13	Yes	144	2.42	420	10.6	-0.113	5.35	3.44
24	8	Yes	168	2.25	350	10.1	-0.107	5.36	3.46
168	5	Yes	672	2.24	320	7.8	-0.081	5.42	3.55
500	4	Yes	1500	1.77	390	4.4	-0.045	5.43	3.68

Table 5.4- Repeat stress relaxation tests with a 500MPa start of dwell stress at 515˚C.

Dwell Length (hours)	Number of Load Cycles to Failure	Failed on loading?	Time to failure (hours)	Extension on failure (mm)	Total drop in net section stress during relaxation (MPa)	Magnitude of Diametric Creep strain on failure (%)	Hoop creep strain on failure, ε_h (abs.)	Unnotched Diameter on failure (mm)	Notched Diameter on failure (mm)
1	32	Yes	31	3.47	407	11.3	-0.120	5.48	3.37
12	9	Yes	96	3.11	256	9.5	-0.100	5.38	3.44
24	6	Yes	120	2.81	243	7.4	-0.077	5.42	3.52
168	3	Yes	336	2.79	168	4.8	-0.049	5.49	3.62
500	2	Yes	500	2.17	89	0.5	-0.005	5.44	3.78

Comparing the data at 515˚C and 550˚C (500MPa start of dwell tests) the number of dwells to failure was very similar for the tests with long dwell times, but as the duration of dwell time is reduced the number of dwells to failure at 515˚C becomes significantly larger than at 550˚C. This is shown in Figure 5.10. The tests conducted at a lower start of dwell stress consistently require 2-3 times the number of dwells to failure as the tests conducted at the higher test stress at 550˚C.

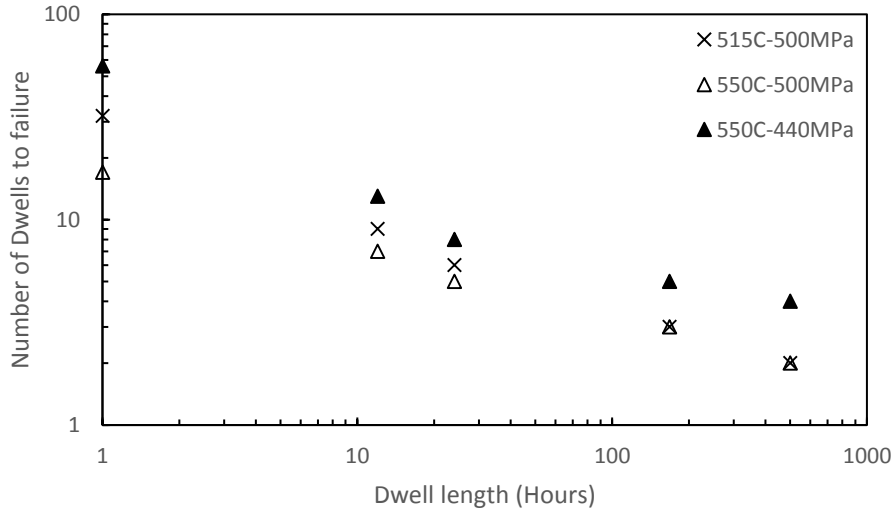

Figure 5.10- Number of dwells vs dwell length for repeat relaxation tests with varying dwell times.

5.3.3 Strain rate dependent Spindler Model

(Published, see #2 in Publication list (taken directly from a paper published by the author))

5.3.3.1 Methodology

The Spindler damage model is detailed in Chapter 3.

Simulations were conducted using the Spindler damage model with 5 different variations:

1. A fixed uniaxial ductility with primary/secondary/tertiary creep
2. A fixed uniaxial ductility without primary creep
3. A strain rate dependent ductility with primary/secondary/tertiary creep
4. A strain rate dependent ductility with primary creep factored to ignore the stress drop occurring during loading up of the specimen
5. A strain rate dependent ductility without primary creep.

5.3.3.2 Results

The stress relaxation behaviour experimentally at 550˚C can be seen in Figure 5.11, along with the stress relaxation at 550˚C predicted from the FEA model with primary, secondary and tertiary creep, and without primary creep. Also shown is an adjusted primary, secondary and tertiary creep simulation, it has been factored to ignore the first 140MPa of relaxation of experiments with a start of dwell stress of 500MPa at 550˚C (60MPa at 515˚C) and the first 100MPa of relaxation for tests with a start of dwell stress of 440MPa. This adjustment has been made because the stress relaxes by this amount during the load up due to the manual nature of the loading between rotations of the top wheel. The manual loading process takes a relatively large amount of time for the initial load up (approx. 2 mins) and involves multiple rotations of the top wheel where the loading bars need to be removed and reinserted after each rotation. During this time there is some stress relaation, when all this relaxation is summed over the loading period it comes out at approximately 140MPa, hence the correction. This effect during load up experimentally can be seen graphically in appendix II. It is believed that this very rapid, almost instantaneous stress drop/strain accumulation is not damaging to the specimen. This belief is justified below and reinforces our main finding that very rapidly accumulated creep strains are not damaging, or far less damaging than creep strains accumulated more slowly. The model without primary creep has been used as it is thought this stress drop during load up could exhaust the primary creep.

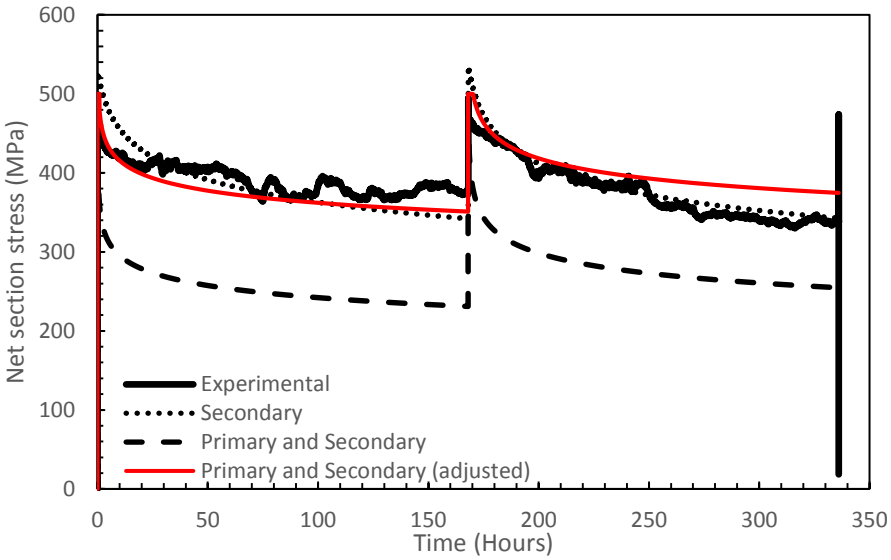

Figure 5.11- 168-hour stress relaxation dwells at 550˚C.

Figure 5.12 shows the maximum von Mises equivalent creep strain on failure at the notch root for all the strain rate dependent models used and the diametric creep strain obtained experimentally. Here it can be seen that the same trend in creep strain on failure is apparent both experimentally and from the finite element models, namely increasing in the shorter term, higher average creep strain rate experiments. In the case of the finite element models, this is because in the longer term experiments the creep strain rate decreases with time and so the creep ductility shifts lower down the transition region and ultimately onto the lower shelf ductility as shown in Figure 5.13 (the height of the arrows has no bearing, they are there to show the stress range experienced at the notch tip at dwells of different durations). This Figure shows that the shorter dwells (1 and 12 hours) are within the transition region throughout, whereas the longer dwells spend an increasing proportion of their time on the lower shelf, and hence have a smaller strain at failure.

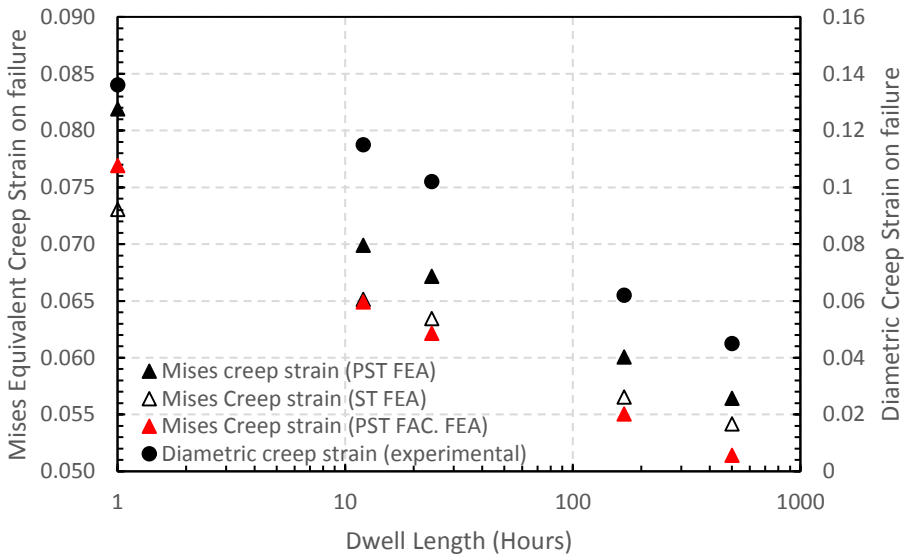

Figure 5.12- Creep strain on failure. Experimental and FEA (FEA at the notch tip and Type 1 failure), 500MPa start of dwell stress at 550˚C.

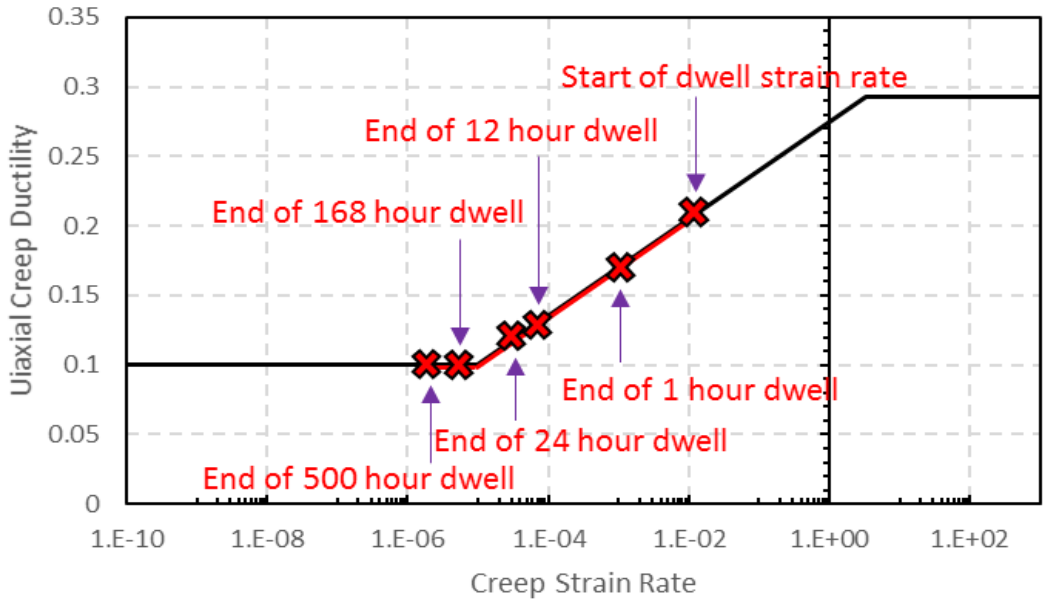

Figure 5.13- Strain rate ranges for experiments with a 500MPa start of dwell stress at 550˚C (strain rate in absolute per hour).

The following discussion and Figures illustrate the analysis for the 168-hour dwell tests with a start of dwell stress of 500MPa at 550˚C (Type 1 failure). The model demonstrated is the strain rate dependent model without primary creep, however all the trends noted were the same for all the models and both failure modes. The model without primary creep has been used for demonstration as it most closely matched the stress relaxation behaviour and number of dwells to failure from the experiments conducted.

Figure 5.14 shows the distribution of creep damage across the notch ligament as the first node reaches a damage level of 1 at 550˚C being subject to repeating 168-hour dwells. Figure 5.14 predicts failure occurred at the surface earlier than it did at the Skeletal point. (Creep damage, D_C, of 1 equates to failure). The skeletal point is the point where the stress state is insensitive to the power law stress dependence of creep, it is often used as the point of analysis in notched bar testing [88].

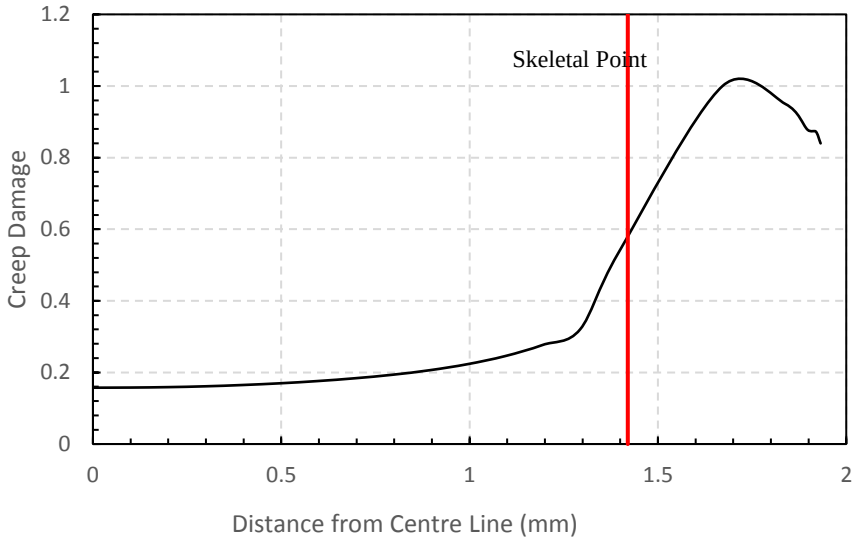

Figure 5.14- Creep damage predicted across ligament as first node fails (From FEA simulation at 550˚C with 168-hour dwells (Type 1 failure)).

Figures 5.15, 5.16, 5.17 and 5.18 show the axial stress, triaxiality, local elastic follow-up and Mises creep strain respectively across the notch ligament at varying points throughout creep life. On the key A denotes axial stress, T denotes triaxiality, Z denotes elastic follow-up, CS denotes creep strain, numbers represent the dwell number, E denotes end of dwell, S denotes start of dwell and F denotes failure. Here the elastic follow-up relates to points on the reduced (notched) section and is not to be confused with the gross specimen elastic follow-up. Triaxiality, η, was calculated diving the hydrostatic stress by the von Mises stress and local elastic follow-up via equation 5.1:

$$\text{Elastic follow} - \text{up, Z} = \frac{\varepsilon_c * E'}{\Delta\sigma_{axial}} \tag{5.1}$$

where ε_c is the creep strain, E' is the augmented Youngs modulus (defined in equation 5.2) and $\Delta\sigma_{axial}$is the drop in local axial stress.

$$\text{E}' = \frac{3E}{2(1+\nu)} \tag{5.2}$$

where E is the Youngs modulus and v is the Poisson's ratio.

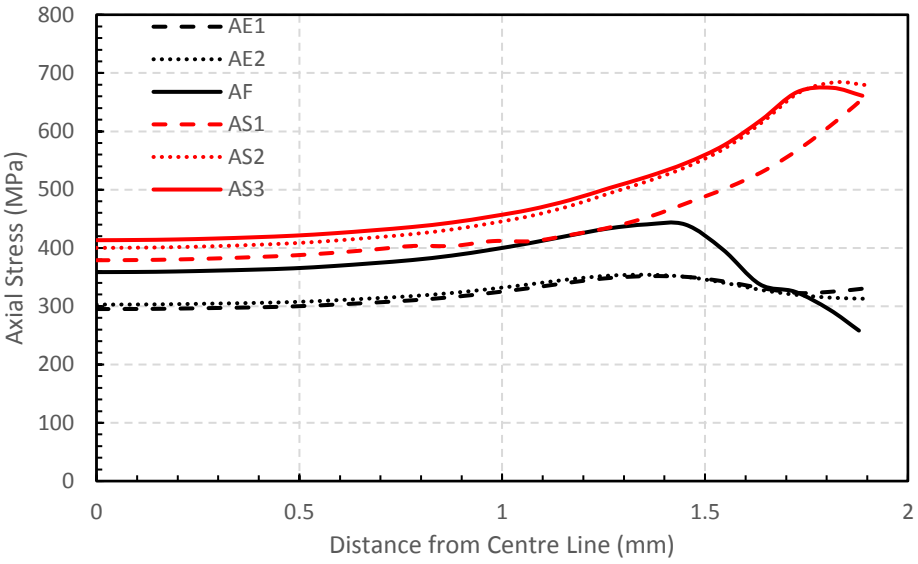

Figure 5.15- Axial stress across the notch ligament (From FEA simulation at 550˚C with 168-hour dwells).

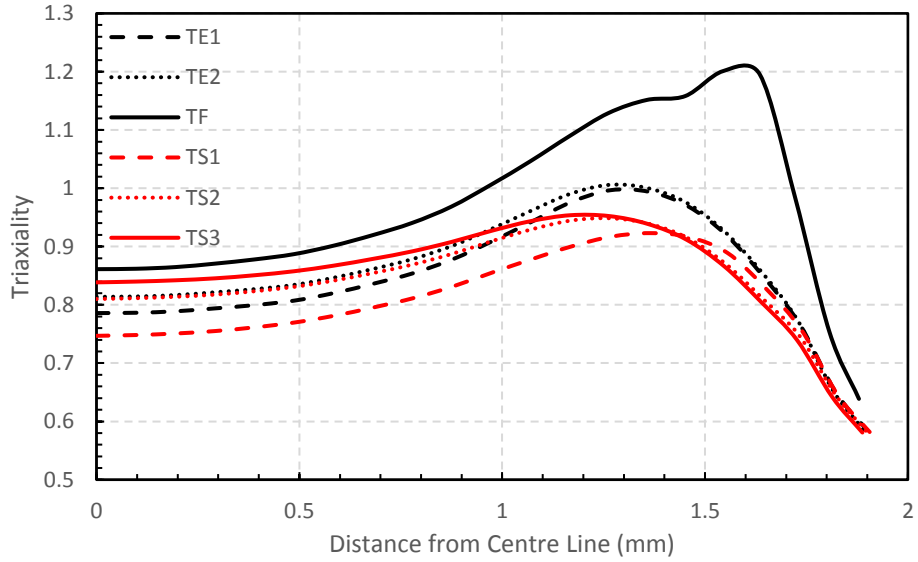

Figure 5.16- Triaxiality across the notch ligament (From FEA simulation at 550˚C with 168-hour dwells).

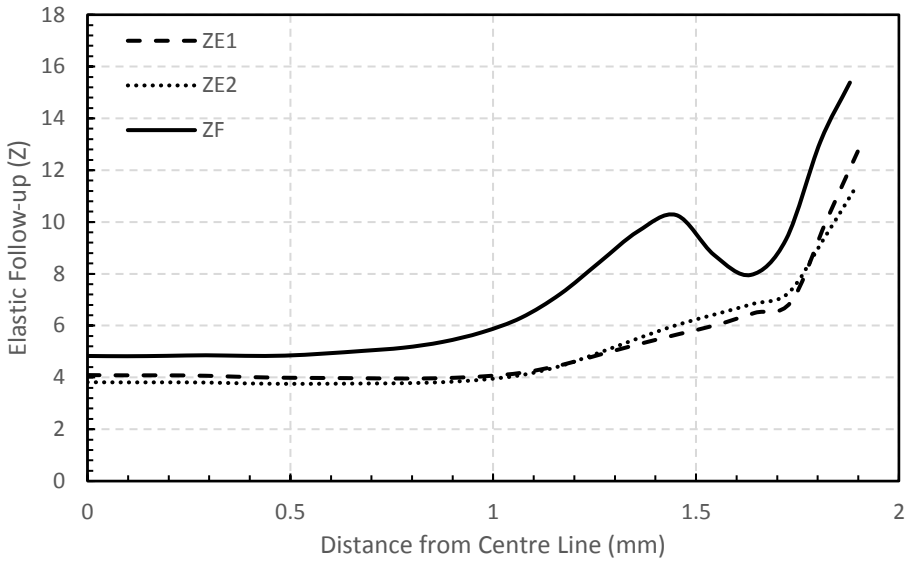

Figure 5.17- Elastic follow-up across the notch ligament (From FEA simulation at 550˚C with 168-hour dwells).

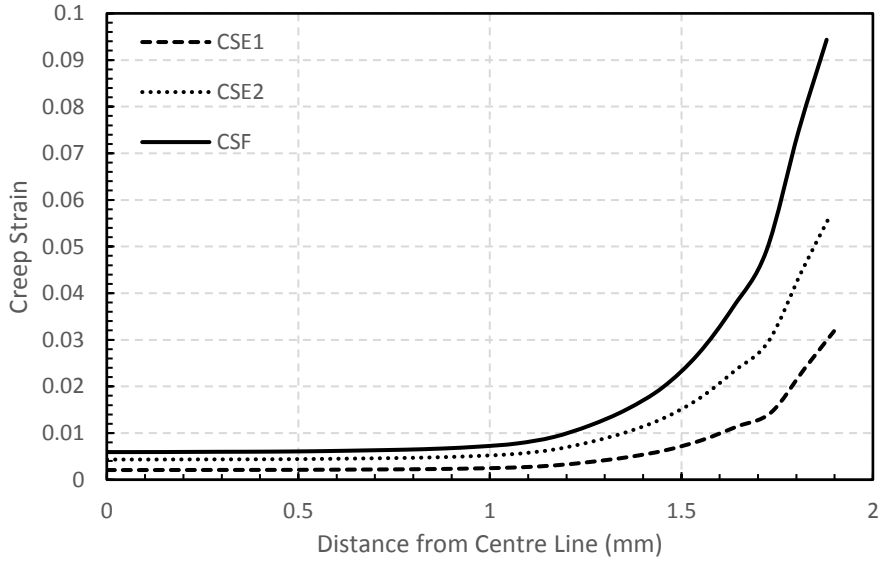

Figure 5.18- Mises equivalent creep strain across the notch ligament (From FEA simulation at 550˚C with 168-hour dwells).

Figures 5.19, 5.20, 5.21, 5.22 and 5.23 show the axial stress, Mises stress, hydrostatic stress, Mises equivalent creep strain and triaxiality respectively against time. Three points are given against time for all variables, the dotted line represents what is happening at the centerline, the dashed line represents what is happening at the tip of the notch and the solid line shows what

is happening at the node of maximum damage (From Figure 5.14). Note that Figure 5.18 shows that the equivalent creep strain is greater at the notch root than at the point of maximum predicted damage. This is because of the more severe stress triaxiality at the latter (Figures 5.16 and 5.23).

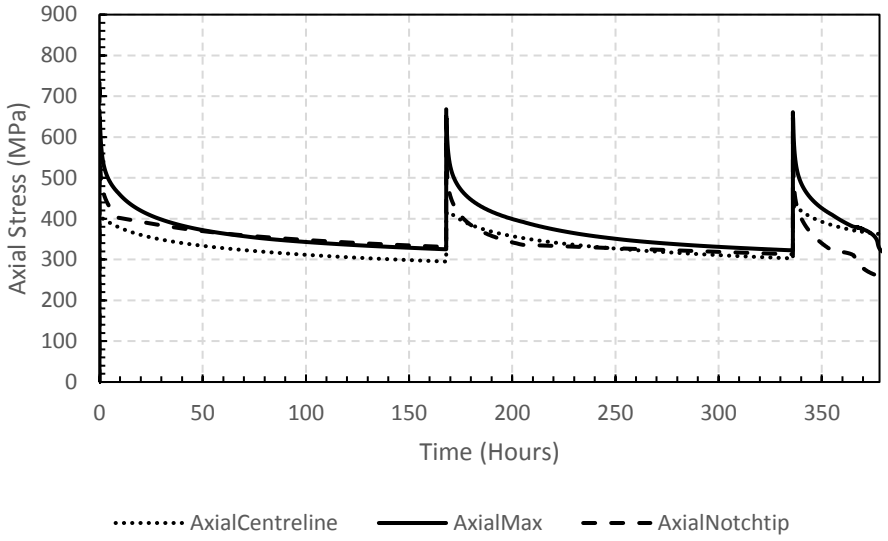

Figure 5.19- Axial stress against time (From FEA simulation at 550˚C with 168-hour dwells).

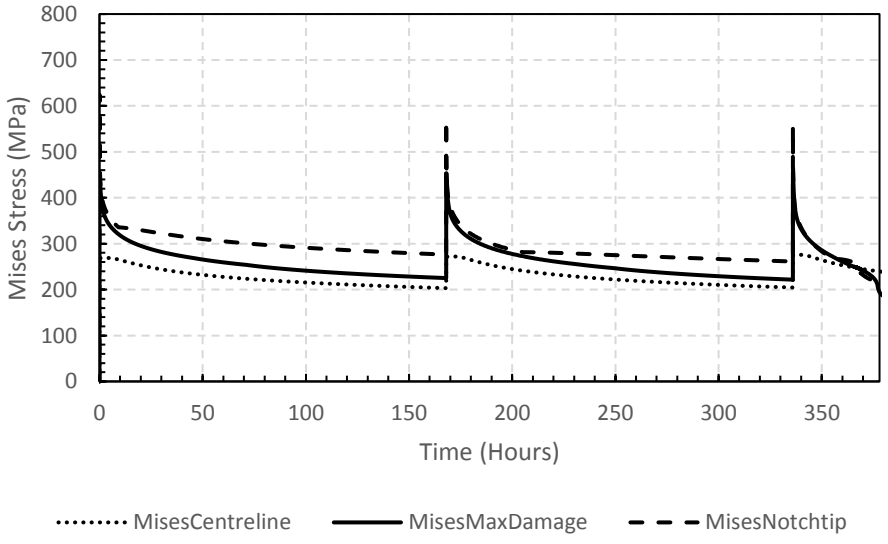

Figure 5.20- Mises stress against time (From FEA simulation at 550˚C with 168-hour dwells).

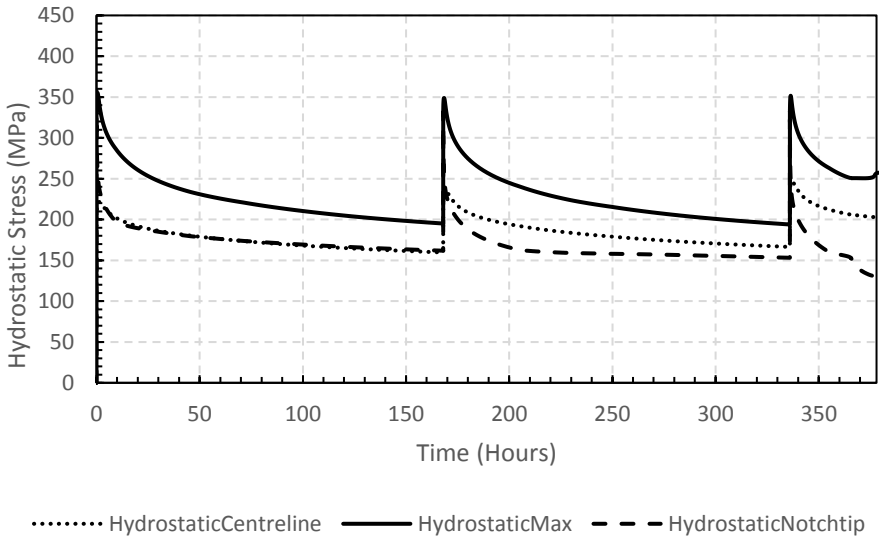

Figure 5.21- Hydrostatic stress against time (From FEA simulation at 550˚C with 168-hour dwells).

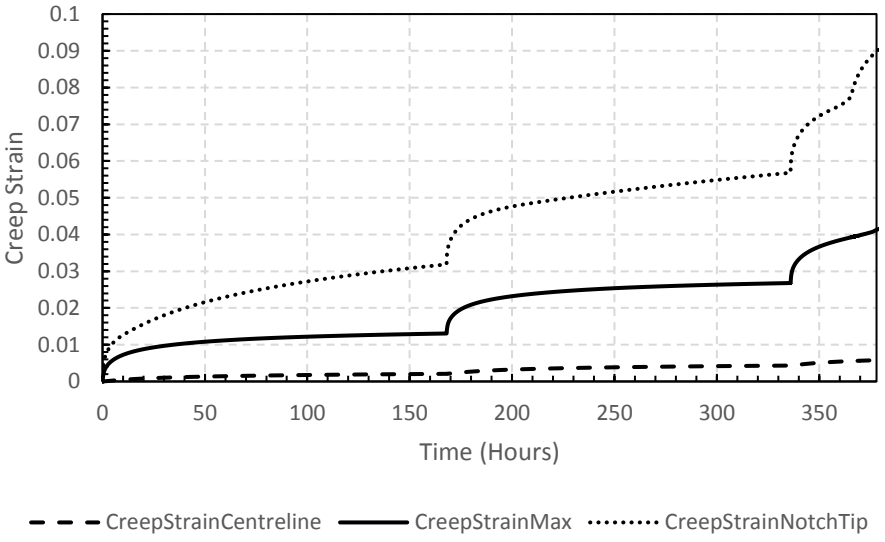

Figure 5.22- Creep strain against time (From FEA simulation at 550˚C with 168-hour dwells).

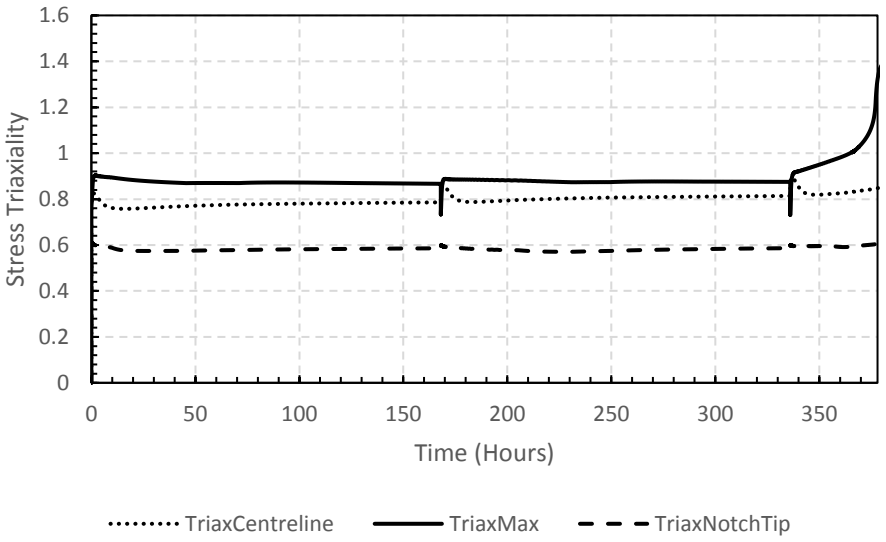

Figure 5.23- Triaxiality against time (From FEA simulation at 550˚C with 168-hour dwells).

Figure 5.24 shows the creep damage accumulation at the node of maximum damage for all three of the finite element models used.

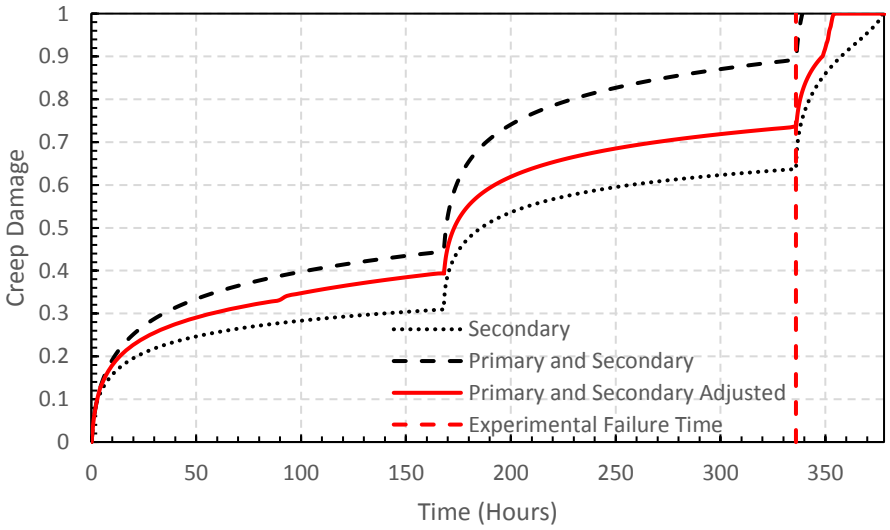

Figure 5.24- Creep Damage against time (From FEA simulation at 550˚C with 168-hour dwells).

Tables 5.5, 5.6 and 5.7 show the number of dwells to failure predicted for all the experiments for all damage models used and also the experimental results. Table 5.5 shows the results with

a start of dwell stress of 500MPa at 550˚C, Table 5.6 with a start of dwell stress of 440MPa at 550˚C and Table 5.7 with a start of dwell stress of 500MPa at 515˚C. Figure 5.25 shows the dwells to failure with a start of dwell stress of 500MPa at 550˚C graphically. Figure 5.25 shows finite element models without a strain rate dependency (fixed lower shelf ductility of 10.69%) with and without primary creep and also with a strain rate dependency (From 5.13) with and without primary creep (Type 1 failures).

Table 5.5- Dwells to failure predicted at 550˚C with a 500MPa start of dwell stress.

Duration of dwells (Hours)	Dwells to Failure						
	Experimental	FEA					
		Prim., sec. & ter. creep		Adjusted Prim., sec. & ter		Secondary & tertiary creep	
		Type 1	Type 2	Type 1	Type 2	Type 1	Type 2
1	17	12	29	14	31	21	44
12	7	5	12	6	13	6	13
24	5	4	9	5	10	5	10
168	3	3	7	3	7	3	6
500	2	3	5	3	5	3	4

Table 5.6- Dwells to failure at 550˚C with a 440MPa start of dwell net section stress.

Duration of dwells (Hours)	Dwells to Failure						
	Experimental	FEA					
		Prim., sec. & ter. creep		Adjusted Prim., sec. & ter		Secondary & tertiary creep	
		Type 1	Type 2	Type 1	Type 2	Type 1	Type 2
1	56	29	73	34	80	52	107
12	13	9	22	10	24	11	25
24	8	7	18	8	20	8	20
168	5	5	11	5	11	5	11
500	4	4	9	4	9	4	9

Table 5.7- Dwells to failure at 515˚C with a 500MPa start of dwell net section stress.

Duration of dwells (Hours)	Dwells to Failure						
	Experimental	FEA					
		Prim., sec. & ter. creep		Adjusted Prim., sec. & ter		Secondary & tertiary creep	
		Type 1	Type 2	Type 1	Type 2	Type 1	Type 2
1	32	23	51	26	59	34	81
12	9	10	22	11	25	12	27
24	6	9	19	10	21	10	21
168	3	5	11	6	13	6	13
500	2	4	9	5	11	5	11

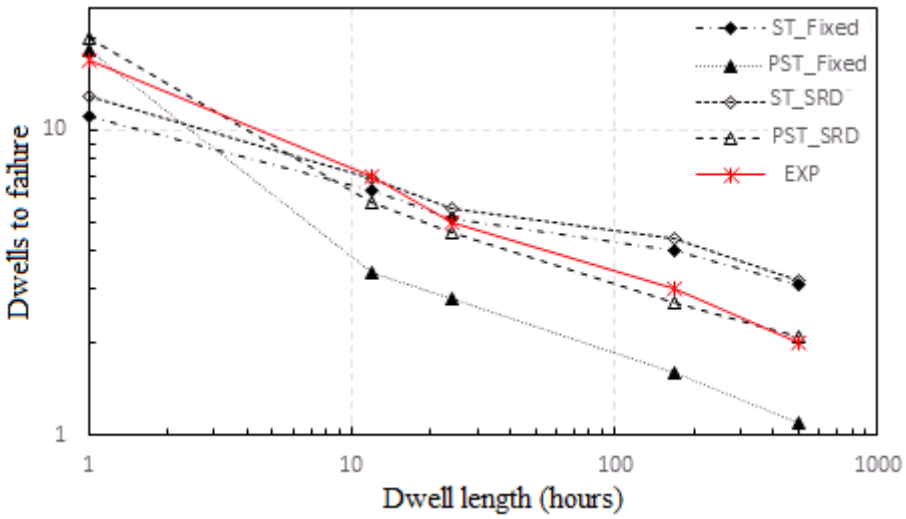

Figure 5.25 - Dwells to failure from all finite models and experimentally for tests with a start of dwell stress of 500MPa at 550˚C (Type 1 failures) (PST = primary, secondary and tertiary creep. ST = secondary and tertiary creep. SRD = strain rate dependent model. Fixed = Fixed uniaxial ductility model (10%)).

5.3.3.3 Discussion

Figure 5.10 shows the number of dwells to failure against the dwell length. As expected this shows that the longer the duration of the dwell the fewer dwells required for the specimen to fail at both 515˚C and 550˚C. This is because the longer the duration of the dwell the more creep strain is accumulated. The same Figure shows that in the tests with the longer duration dwells (168 and 500 hours with a start of dwell stress of 500MPa) the tests at 515˚C and 550˚C fail at the same time. However, as the dwell time is reduced the tests at 515˚C start to take significantly longer before rupture of the specimen is achieved than at 550˚C. This is simply because creep is slower at the lower temperature. Despite longer times to failure at the lower temperature, the creep strain at failure is smaller, i.e., the creep ductility at 515˚C is lower than at 550˚C. This has been noted in earlier tests. Lowering either the test temperature or test start of dwell stress lowered the creep strain rate and reduced the creep strain on failure, implying that creep strain accumulated more slowly was more damaging.

Figure 5.11 shows the stress relaxation behaviour experimentally alongside the 3 finite element models used. It can be seen in Figure 5.11 that the model with primary, secondary and tertiary

creep significantly overpredicts the amount of stress relaxation during dwells, particularly in the early stages. This was because the stress relaxes significantly during load up due to the time taken to carry out the manual loading using the top wheel. In the adjusted primary, secondary and tertiary model the first 140MPa of relaxation is ignored in Figure 5.11 as that is how much the stress relaxed experimentally during the load up stage. This model more accurately captures the experimental behaviour, but still slightly overpredicts the stress drop in the early stages. Some researchers believe that primary creep is not apparent in stress relaxation at high stresses [16]. In this work this is likely due to the relatively long duration of the loading period (2 minutes) where the primary creep is likely exhausted and hence the rapid stress drop associated with primary creep is not seen in the experimental results. The model without primary creep most accurately matches the experimental curve. The reason primary creep is not apparent could be because it is active only during the load up.

Figures 5.14-5.23 are all from the model without primary creep for a 168-hour repeat stress relaxation test at 550˚C with a start of dwell net section stress of 500MPa. Figure 5.14 predicts that failure occurs initially just away from the notch tip and not at the skeletal point. This agrees with previous notched bar rupture experimentation and research conducted by Spindler [4]. Other research on notched bars has used the skeletal point as a focal point for analysis. Figure 5.14 shows that using the skeletal point gives an underestimate of the creep strain at failure.

Figure 5.17 shows that the local ligament elastic follow-up factor remains constant throughout dwells up until the dwell where failure occurs where it increases, in particular at the node of maximum damage. Prior to the failure cycle, the elastic follow-up on the centre line of the ligament is about 4, rising to about 12 at the notch root. The peak elastic follow-up factor seen at the notch tip was 15.4 on failure. The elastic follow-up of the bulk material away from the notch was below 1.1.

Figure 5.23 shows that the maximum triaxiality occurs at the node of maximum damage. This triaxiality increases gradually throughout creep life until tertiary creep where it starts to increase rapidly reaching a peak value of 1.38.

Figure 5.25 shows that assuming a creep model without a strain rate dependency, for which all creep strains are assumed to be equally damaging and using a fixed lower shelf uniaxial ductility of 10.69%, the number of dwells to failure is significantly underpredicted.

Tables 5.5, 5.6 and 5.7 show that using the Type 1 failure mode gives a more realistic estimate to the number of dwells to failure experimentally that using the Type 2 failure mode. It was

thought that this was because when Type 1 failures occur are when experimentally cracks would be appearing in the specimen and then practically the specimen would likely fail on the next load up as the stress would be concentrated over a smaller area.

It can be seen from the figure that the model that is most representative of the experimental data in terms of dwells to failure is the model without primary creep and including the strain rate dependency (using Type 1 failures) detailed in Chapter 3 (ST_SRD model). This model most accurately captures the experimental data in terms of stress drop throughout testing and predicted cycles to failure. This use of a strain rate dependent ductility is consistent with the experimental findings that creep ductility does indeed reduce at slower strain rates, at least as far as some lower shelf. The contribution of various parts of the ductility transition curve and lower shelf to the tests of differing dwell length is nicely illustrated by Figure 5.13.

5.3.4 Stress Modified Ductility Exhaustion Model

Details of the SMDE damage model are given in Chapter 3.

5.3.4.1 Results

Figure 5.26 shows the stress drop behaviour from the SMDE with (PST) and without (ST) primary creep. The model without primary creep most accurately captures the experimental stress drop whereas the model with primary creep most accurately predicts the number of dwells to failure (it was thought that the model with primary creep was lucky to capture the number of dwells to failure and due to this models lack of match with the experimental macroscopic response it would not be recommended for use). For that reason, both models are looked at in the following analysis. The test focussed on for the following analysis was the test with a start of dwell stress of 500MPa at 550˚C with 24-hour dwells. Figures 5.27-5.31a show the axial stress, von Mises stress, creep strain, creep damage and triaxiality respectively against time for the SMDE model without primary creep. Figures 5.27-5.31b show the axial stress, von Mises Stress, creep strain, creep damage and triaxiality respectively against time for the SMDE model with primary creep. All graphs show the variable displayed at 3 key points along the specimen, the notch tip, the element of maximum damage and the centre of the specimen (centreline). Table 5.8 shows the number of dwells to failure for all the repeat relaxation experiments experimentally and with all variation and failure modes of the SMDE damage model.

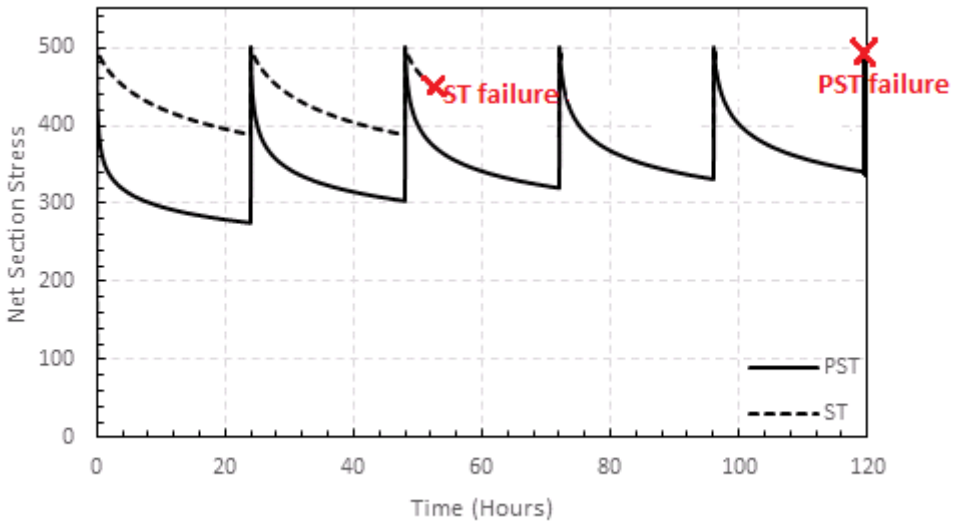

Figure 5.26- Stress relaxation behaviour for SMDE models with and without primary creep at 550˚C (Type 2 failures).

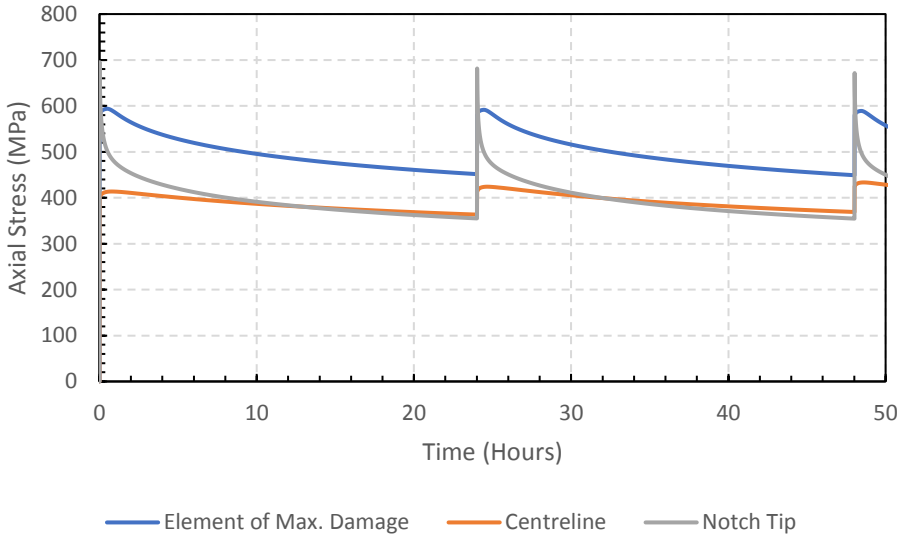

Figure 5.27a- Axial stress relaxation at various points for SMDE model without primary creep at 550˚C.

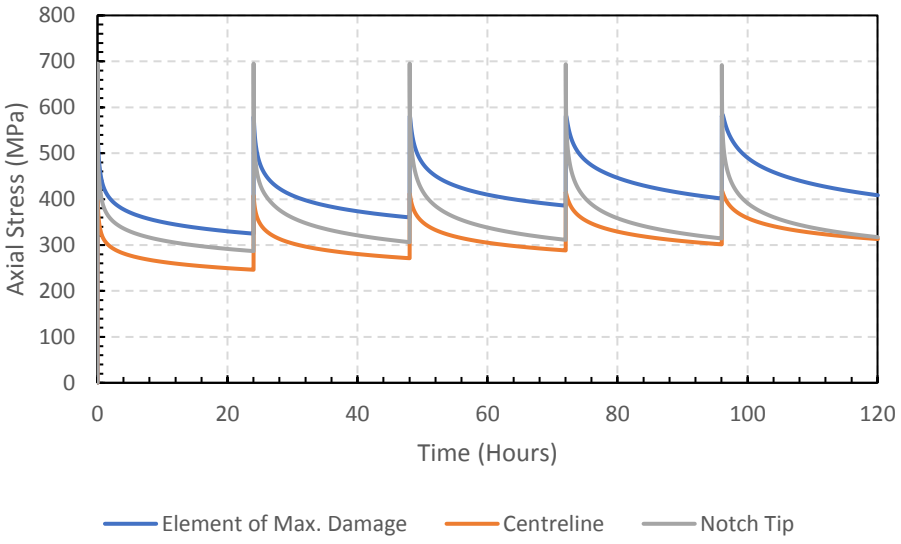

Figure 5.27b – Axial stress relaxation at various points for SMDE model with primary creep at 550˚C

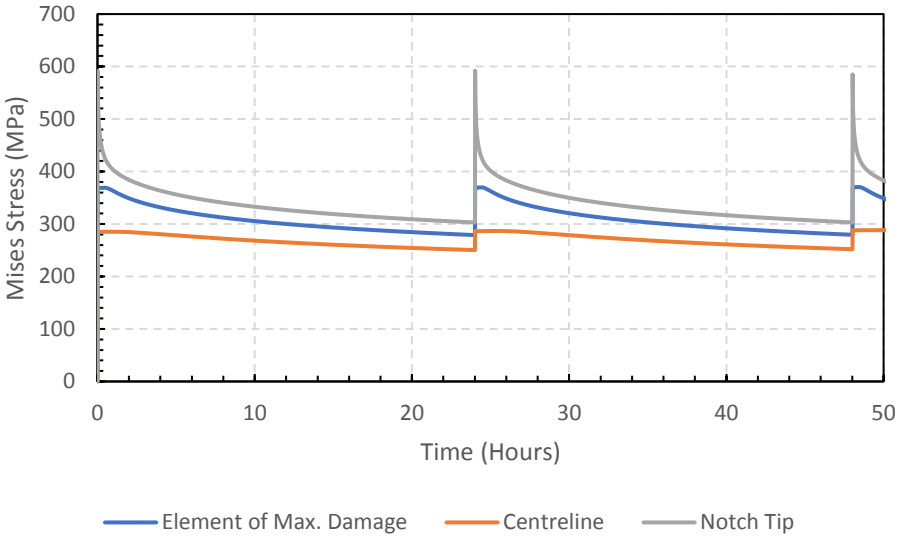

Figure 5.28a – Mises stress relaxation at various points for SMDE model without primary creep at 550˚C.

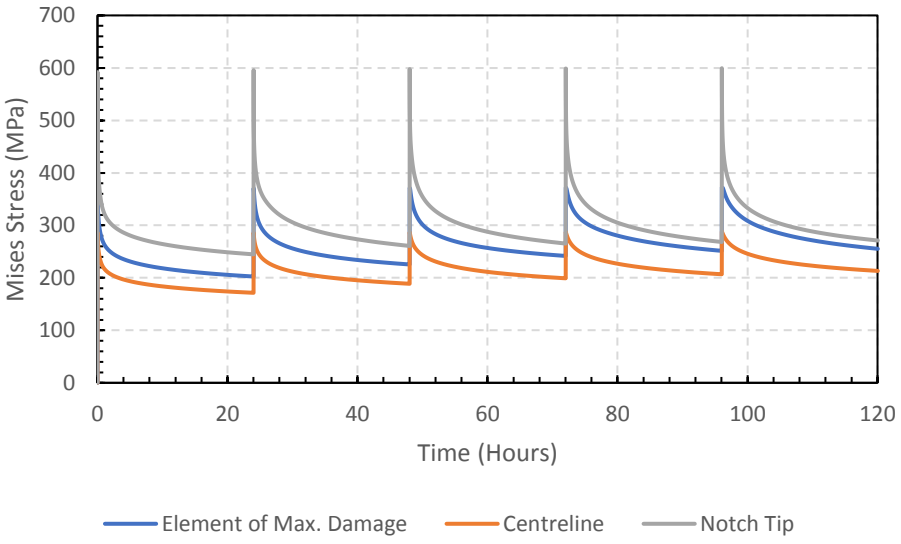

Figure 5.28b – Mises stress relaxation at various points for SMDE model with primary creep at 550˚C

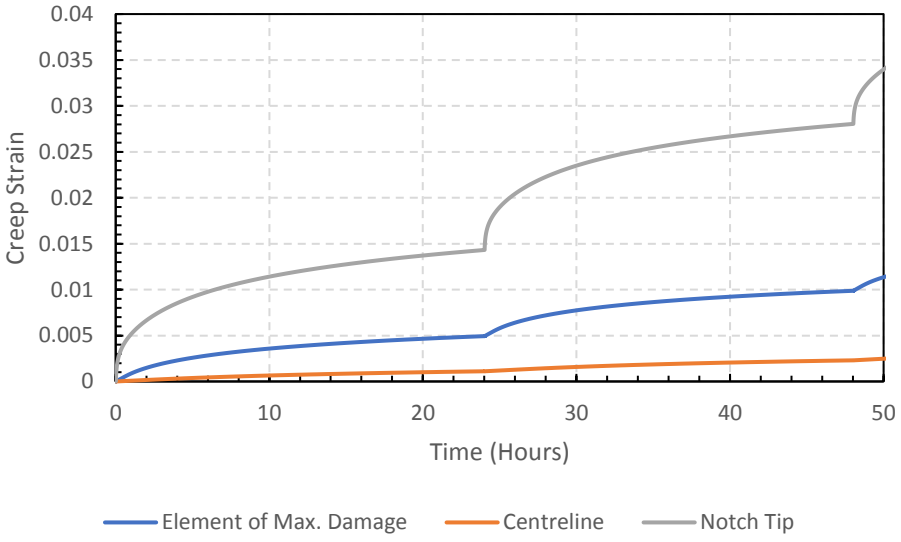

Figure 5.29a - Creep strain accumulation at various points for SMDE model without primary creep at 550˚C.

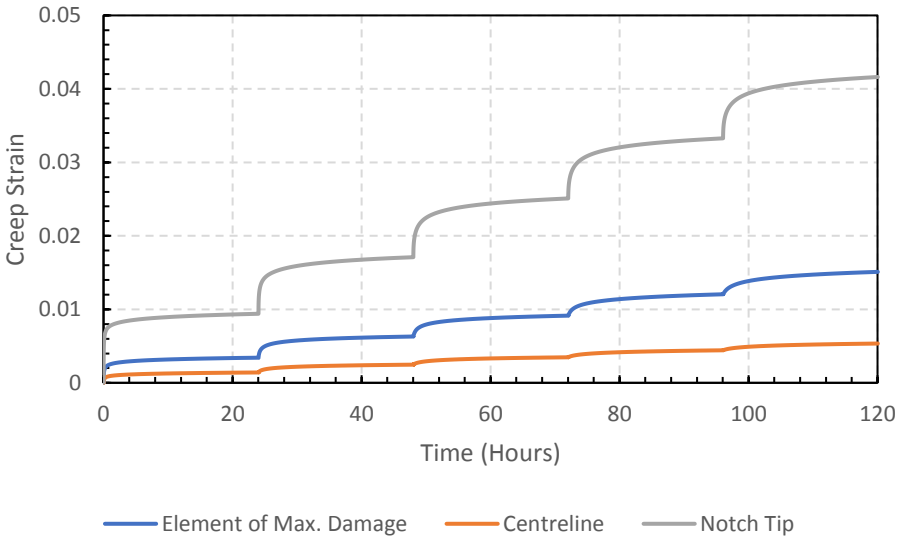

Figure 5.29b – Creep strain accumulation at various points for SMDE model with primary creep at 550˚C

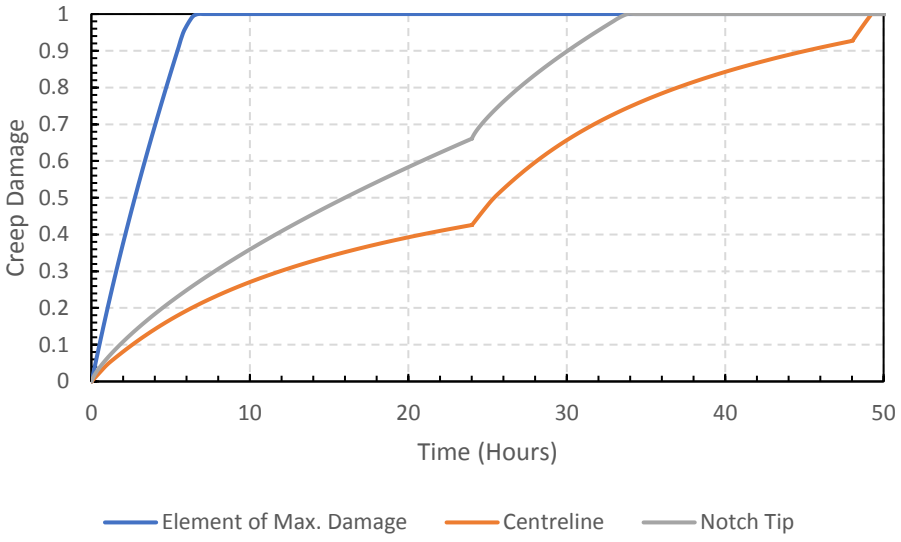

Figure 5.30a – Creep damage accumulation at various points for SMDE model without primary creep at 550˚C.

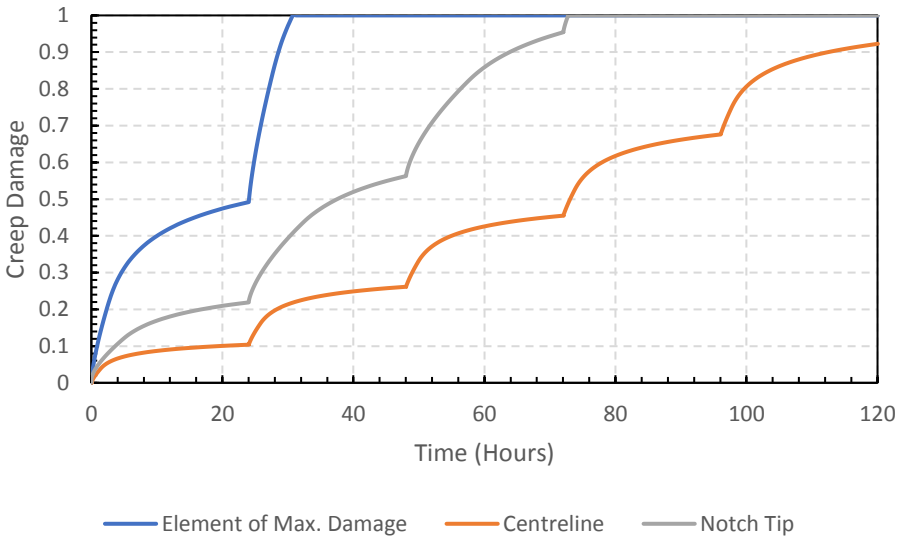

Figure 5.30b – Creep strain accumulation at various points for SMDE model with primary creep at 550˚C

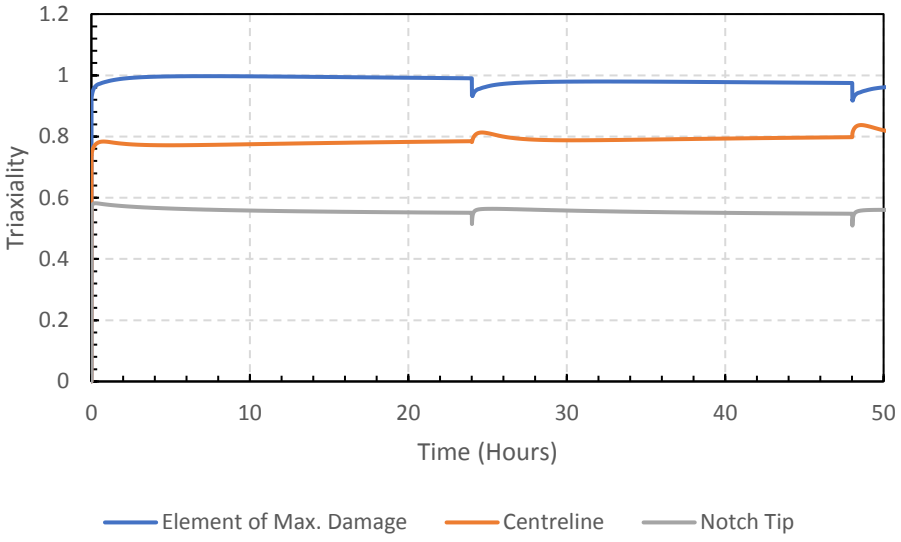

Figure 5.31a – Triaxiality over time at various points for SMDE model without primary creep at 550˚C.

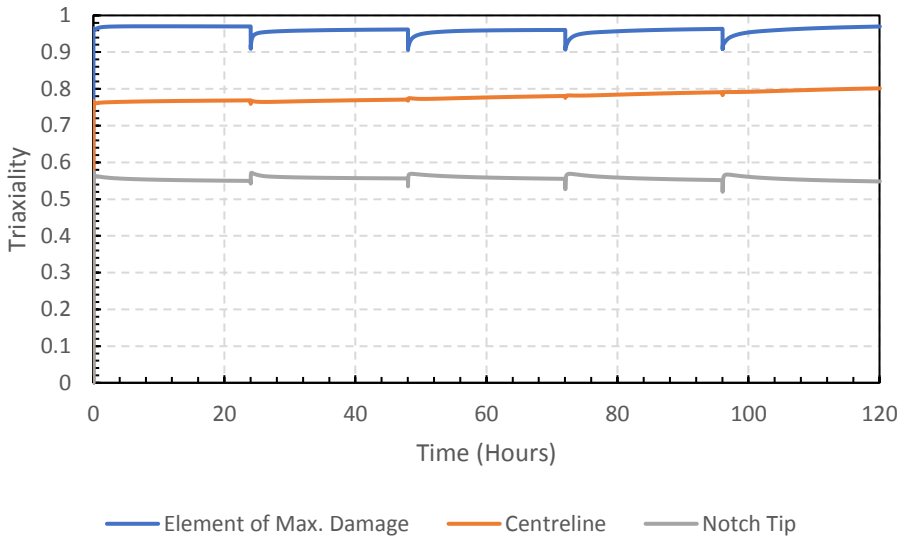

Figure 5.31b – Triaxiality over time at various points for SMDE model with primary creep at 550˚C

Table 5.8– Summary of repeat relaxation dwells to failure experimentally and from SMDE damage models.

Dwell Duration (hours)	Test Temperature, T (˚C)	Start of Dwell Stress, σ (MPa)	Dwells to Failure				
			Exp	PST		ST	
				Type 1	Type 2	Type 1	Type 2
1	550	440	56	8.8	30.9	7.0	34.9
12	550	440	13	2.1	7.7	0.7	4.5
24	550	440	8	1.8	6.3	0.3	3.1
168	550	440	5	1.1	4.6	0.1	1.2
500	550	440	4	1.1	4.1	0.1	1.1
1	550	500	17	7.4	19	5.1	15.1
12	550	500	7	1.9	5.5	0.5	2.5
24	550	500	5	1.3	5.1	0.3	2.1
168	550	500	3	1.1	3.5	0.1	1.1
500	550	500	2	1.1	3.1	0.1	1.1
1	515	500	32	16.0	65.6	19.4	88.4
12	515	500	9	1.5	17.5	1.8	25.1
24	515	500	6	1.0	13.9	1.1	21.1
168	515	500	3	0.2	5.1	0.2	10.0
500	515	500	2	0.1	5.1	0.1	3.9

5.3.4.3 Discussion

Figure 5.26 shows the net section stress relaxation behaviour over time for the SMDE models with and without primary creep. The model without primary creep accurately captures the experimental stress relaxation behaviour. However, it under predicts the number of dwells to failure significantly. The model with primary creep over predicts the amount of stress relaxation experienced by the specimen every dwell but predicts the number of dwells to failure more accurately.

Figures 5.27a and b show the axial stress over time for models without and with primary creep respectively. Here it can be seen the axial stress is the highest at the notch tip at the start of the dwell in the model without primary creep but by the end of the dwell the highest axial stress occurs at the element of maximum damage and the notch tip experiences the lowest axial stress drop as the axial stress drop at the notch tip during the dwell is so large. In the model with primary creep, displayed in Figure 5.28b, the notch tip again has the highest axial stress at the start of the dwell and the notch tip has the highest axial stress at the end of the dwell. However, the centre of the specimen is always subject to the lowest axial stress in this model. Figures 5.28a and b show the von Mises equivalent stress over time for the models without and with primary creep respectively. It can be seen in both Figures that the highest Mises stress always occurs at the notch tip and the lowest Mises stress always occurs at the centreline.

Figures 5.29a and b show the creep strain over time for the models without and with primary creep respectively. In both models the maximum creep strain occurs at the notch tip and the lowest creep strain occurs at the centreline. In the model without primary creep the maximum creep strain on failure was 0.034 and the minimum 0.003. In the model with primary creep the maximum creep strain on failure was 0.042 and the minimum 0.005. Figures 5.30a and 4b show the creep damage for both models. In both models the damage is rather unsurprisingly largest at the element of maximum damage. Type 1 failures occur very early in both SMDE models and then Type 2 failures occur at a more realistic time. Here it can be seen that in the model without primary creep where there is less of a stress drop during the dwell and the stress the specimen is subject to remains higher throughout the dwell the specimen is predicted to fail more quickly. Figures 5.31a and b show the triaxiality over time for both SMDE damage models. Here it can be seen that in both models the stress triaxiality is significantly higher at the element of maximum damage than it is at the notch tip, which is why this element was the first to fail despite the highest stresses occurring at the notch tip.

Table 5.8 shows the dwells to failure predicted for all failure modes and damage models using the stress modified ductility exhaustion approach. This table shows that for both damage models (with and without primary creep) the Type 1 failure criterion (failure occurs when first element reaches D_C value of 1) was overly conservative. The most accurate predictions in terms of number of dwells to failure came from the model with primary creep using the Type 2 failure criteria (all elements along notch root reach a D_C value of 1). This gave a good fit to the data for the tests at 550˚C with a start of dwell stress of 500MPa. For the tests at the same temperature with a start of dwell stress of 440MPa the dwells to failure were underpredicted

with this model and for the tests with a start of dwell stress of 500MPa at 515˚C the dwells to failure were overpredicted.

Based on the fact that neither version of the SMDE model (with and without primary creep) gave good agreement with the experimental results in terms of dwells to failure and in terms of macroscopic response (stress drop behaviour) it was concluded that it was not as reliable a model for predicting stress relaxation of Type 316H stainless steel notched bars as the Spindler damage model.

5.4 Concluding Remarks

(Published, see #2 in Publication list (taken directly from a paper published by the author))

The uniaxial relaxation tests showed that at high start of dwell stress values Type 316H stainless steel does not display primary creep behaviour in relaxation and a finite element model with just secondary and tertiary creep most accurately captures the stress relaxation behaviour.

The experiments showed that austenitic stainless-steel type 316H has a lower creep ductility at 515˚C than at 550˚C. Creep strain accumulated rapidly at the start of the dwell is less damaging to a notched bar specimen than creep strain accumulated more slowly towards the end of a dwell. Creep strain accumulated more slowly because of the lower test temperature was also more damaging than creep strain accumulated at the higher temperature. This was shown in the longest dwell repeat relaxation tests (500-hour dwells) where the tests at 515˚C and 550˚C failed at the same time but the tests at 515˚C had accumulated significantly less creep strain. It was also found that lowering the creep strain rate by reducing the start of dwell stress led to specimens failing with a lower accumulation of creep strain suggesting creep strain is more damaging when accumulated slowly due to a lower test stress or temperature. These quantitative results and conclusions, in concert with previous unpublished work by M. Spindler, provide corroboration that the materials' ductility is strain rate dependent, regardless of whether the strain rate is altered by changing the test temperature or stress.

It was found that when modelling stress relaxation of notched bars with an acuity of 5 with a high initial net section stress, a Spindler model with secondary and tertiary creep more accurately predicts the behavior than one with primary, secondary and tertiary creep. It was also found that an adjusted model with the stress drop lost through load up ignored in the finite

element model and assumed to not be damaging gives much better agreement than a model with primary, secondary and tertiary creep. This shows that strain accumulated very quickly during the rapid stress drop present in the load up between rotations of the top wheel is not damaging to the specimen. It was found that when using a SMDE model the stress drop behaviour was most accurately predicted with a model without primary creep but the number of dwells to failure was best predicted with a model with primary creep. For other researchers' future work on conducting stress relaxation tests the authors would recommend the Spindler model without primary creep with a strain rate dependent ductility but without the stress modified ductility exhaustion approach. This is because best agreement between observed and predicted cycles to failure (when using Type 1 failures) was obtained with the secondary plus tertiary creep model together with an assumed strain-rate dependent uniaxial creep ductility (Chapter 3), consistent with test findings that creep ductility is rate dependent. It was also found that an adjusted model with the stress drop lost through load up ignored in the finite element model and assumed not to be damaging gives much better agreement than a model with primary, secondary and tertiary creep. This implies that strain accumulated very quickly during the rapid stress drop present in the load up between rotations of the top wheel is not damaging to the specimen, consistent with the main test findings.

CHAPTER 6

CREEP FATIGUE

Work from this chapter was presented at the International Conference on Experimental Mechanics in Brussels, 2018.

“If there is no struggle, there is no progress” Frederick Douglas

Chapter 6 Creep Fatigue

The main aim of these experiments was to determine whether taking the net section stress to zero at the end of each cycle has a significant effect on the lifetime of notched specimens. The fatigue cycle was applied by unloading the net section stress of the specimen at the end of a relaxation dwell causing compressive stresses near the notch root, before re-applying the load and thus causing a local fatigue cycle at the notch tip. The results of these fatigue experiments were then compared with the repeat relaxation experiments to isolate the effect of the fatigue cycles and local stress reversal. Creep fatigue experiments were the load was taken to zero were of interest because they imitate situations in plant operation such as power outages.

6.1 Introduction

In repeat relaxation tests the load is re-established repeatedly after relaxation dwells of equal duration. The creep fatigue tests of this chapter were conducted similarly on the same test rig, the only difference being that the net section stress was taken to 0MPa (load completely removed) at the end of stress relaxation dwells, before the re-establishment of the load for the next cycle. The motive was the expectation that taking the net section stress to zero would result in a compressive stress at the tip of the notch without causing buckling of the specimen, so causing fatigue behaviour. Applying a net compressive stress was initially considered but was rejected due to concerns about specimen buckling. The dwell times used for the various experiments were 1, 12, 24, 168 and 500 hours. The experiments were conducted at 550℃ and with stress-of-dwell net section stresses of 500MPa. Hence the temperature, the stress and the dwell times were as previously addressed in the repeat relaxation tests, permitting like-for-like comparison.

In between dwells, when the net section stress is taken zero, the specimen experiences a compressive stress at the notch tip so the notch tip can undergo reverse plasticity between dwells. The purpose of these experiments is to see whether fatigue damage or reverse plasticity interacts with creep damage. If so the tests may be expected to fail sooner than the comparative repeat stress relaxation tests, especially the 1-hour dwell test where the number of cycles will be larger and the amount of fatigue damage accumulated is greater. These tests may also help validate the theory that creep strain is less damaging the faster it is accumulated.

6.2 Experimental

The same displacement-controlled test rig was used for the creep fatigue tests in this chapter that was used for the stress relaxation tests in Chapter 5. Details of the rig are in Chapter 3.

All creep-fatigue experiments were conducted at 550˚C.

6.3 Experimental Results

Dwell times of 1, 12, 24, 168 and 500 hours were used for experiments at 550˚C. A start of dwell net section stress of 500MPa was re-established on each cycle. These 5 experiments with different dwell times were conducted with the same dwell times as previous repeat relaxation experiments so that the effects of the fatigue cycle could be isolated. An example net section stress against time curve can be seen in Figure 6.1a (24-hour dwells) and an example extension against time curve can be seen in Figure 6.1b (24-hour dwells). These figures show how, after the initial load up, the stress drops as the displacement is fixed. Thereafter, at the end of the relaxation period, there is a slight negative displacement as the net section stress is taken to zero, then a significant positive displacement as the net section stress is taken to the start of dwell stress.

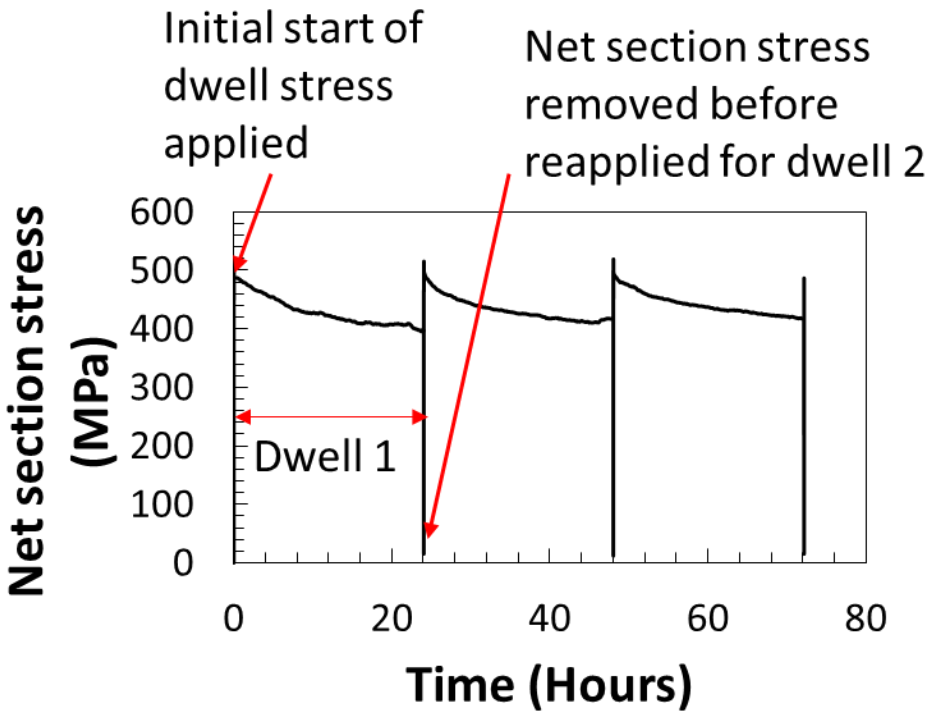

Figure 6.1a - Net section stress against time for 24-hour creep fatigue dwells.

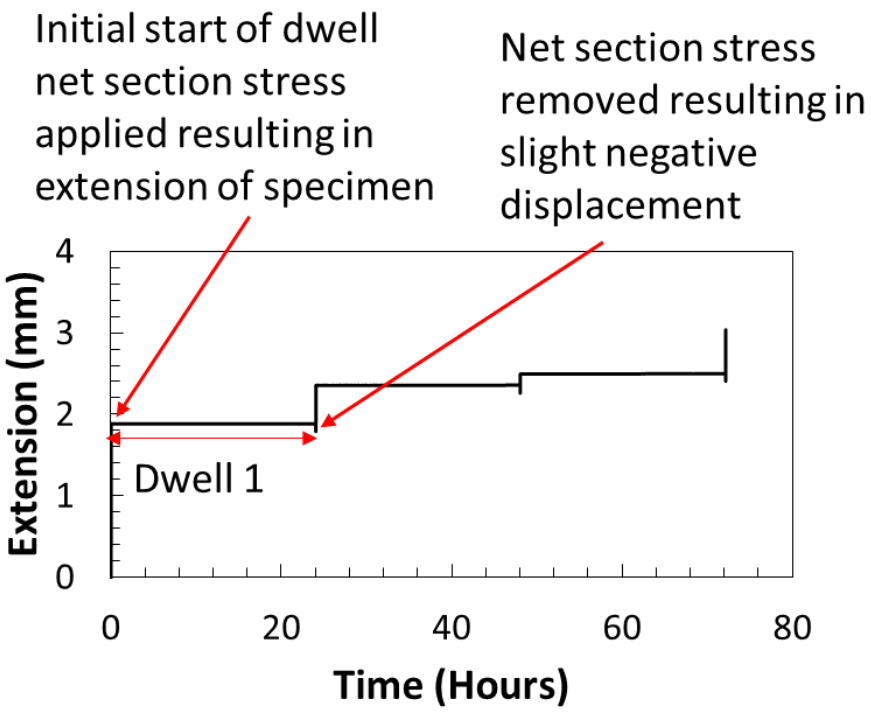

Figure 6.1b - Extension against time for 24-hour creep fatigue dwells

Table 6.1 shows the results for all creep fatigue tests with different dwell times. Diametric strain was calculated by dividing the change in diameter during testing by the original diameter. Hoop creep strain was calculated via equation 4.4. The results show that the longer the duration of dwell, the lower the number of dwells to failure, the longer the time to failure, the greater the notched diameter on failure and the lower the diametric strain on failure. Figure 6.2 shows the net section stress against normalised time to rupture for all the creep fatigue experiments conducted. The time to rupture has been factored so that a value of one represents when failure occurred. Figure 6.3 shows the diametric strain on failure against dwell.

Table 6.1- Creep fatigue at 550˚C results summary.

Dwell length (Hours)	Dwells to failure	Failed on loading?	Time to failure (Hours)	Notched diameter on failure	Magnitude of Diametric strain on failure (%)	Hoop creep strain on failure, ε_h (abs.)
1	8	Yes	7	3.09	23	-0.191
12	6	Yes	60	3.28	18	-0.131
24	4	Yes	72	3.43	14	-0.087
168	2	No	301	3.52	12	-0.061
500	2	Yes	500	3.67	8	-0.019

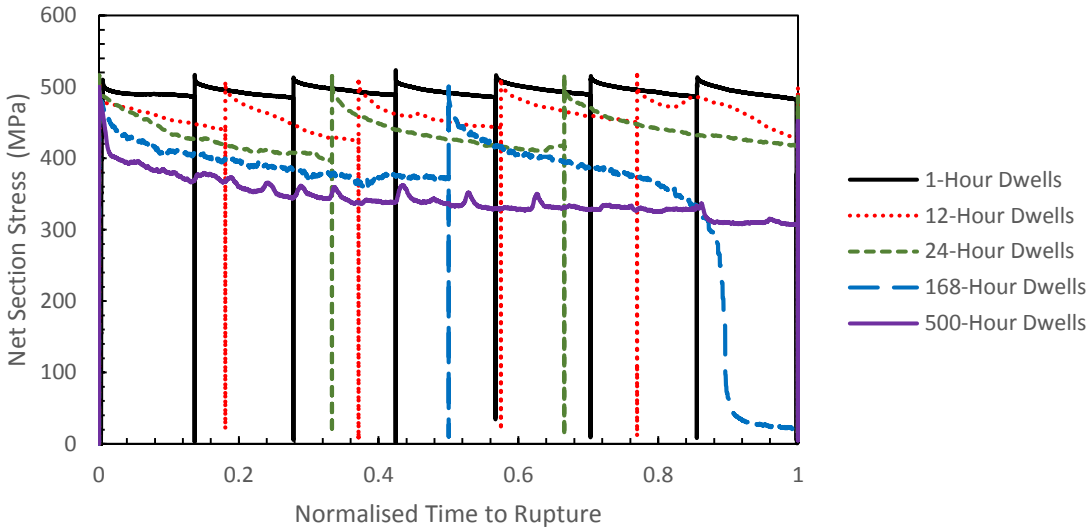

Figure 6.2- Stress vs Normalised time to rupture.

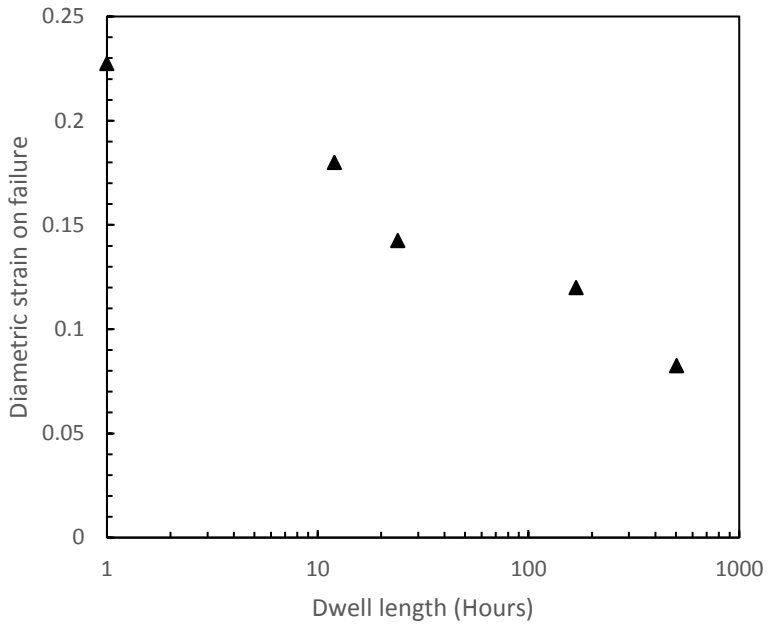

Figure 6.3- Diametric strain on failure against dwell length.

6.4 Comparisons with Repeat Stress Relaxation Experiments

Figure 6.4 shows the number of dwells to failure experimentally for the creep fatigue tests and the corresponding repeat stress relaxation experiments. All of the tests were conducted at 550˚C with a start of dwell stress of 500MPa. Figure 6.5a shows the diametric creep strain on failure for both the creep fatigue and repeat stress relaxation tests, Figure 6.5b shows the diametric creep strain on failure against the average diametric creep strain rate throughout the experiments. The diametric creep strain on failure was calculated as the diameter change during creep divided by the diameter after initial load up. This was not the same as the total diametric strain on failure showed in Figure 6.3.

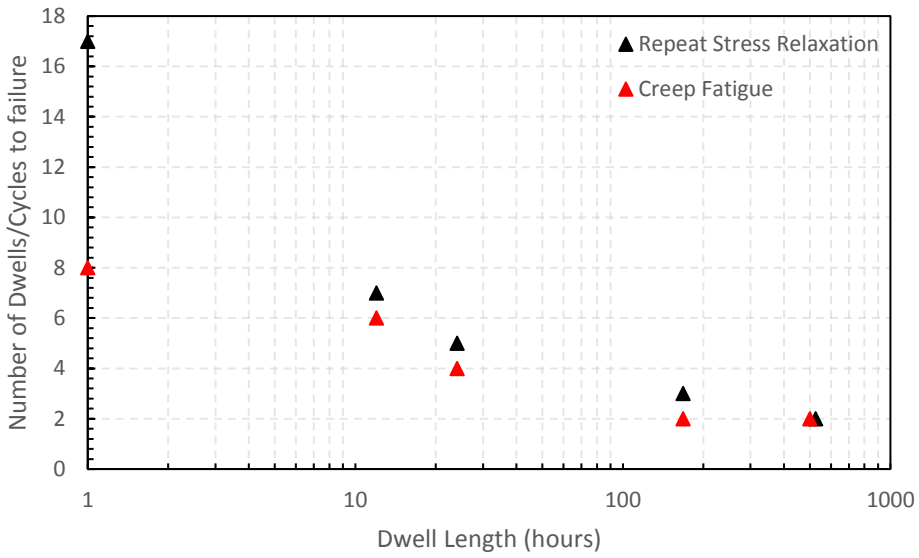

Figure 6.4- Dwells to failure at 550˚C with a 500MPa start of dwell stress for repeat stress relaxation tests and creep fatigue tests with varying dwell lengths.

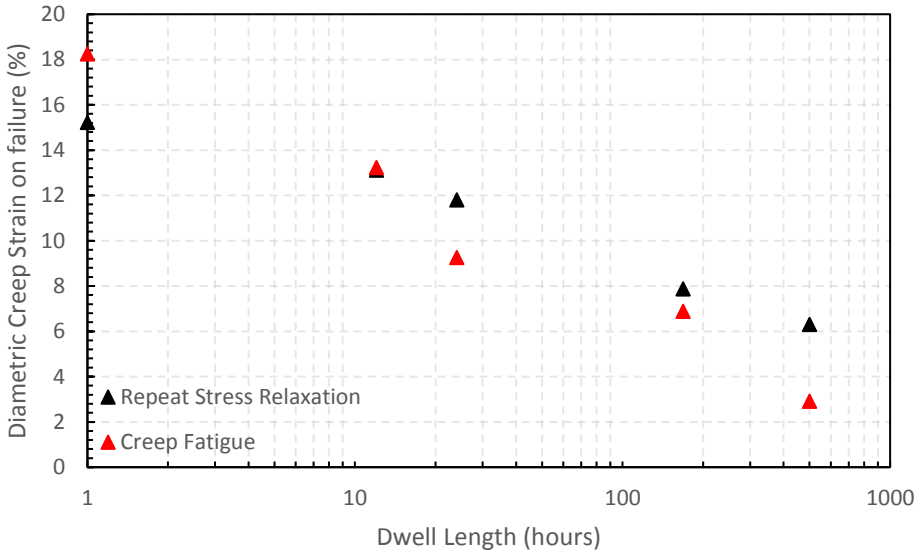

Figure 6.5a- Diametric creep strain on failure at 550˚C with a 500MPa start of dwell stress for repeat stress relaxation tests and creep fatigue tests with varying dwell lengths.

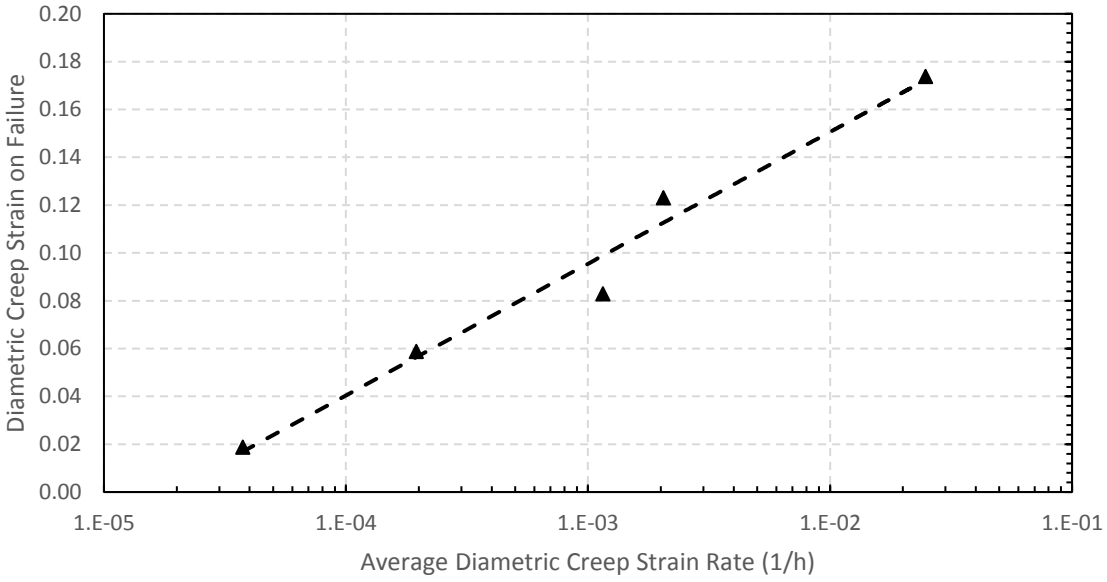

Figure 6.5b - Diametric creep strain on failure at 550˚C shown against the average diametric creep strain rate for all creep fatigue experiments conducted.

6.5 Creep and Fatigue Damage Calculations

6.5.1 Spindler Damage Model

The net section stress behaviour experimentally can be seen in Figure 6, along with the FEA with just secondary and tertiary creep (ST) and primary, secondary and tertiary creep (PST).

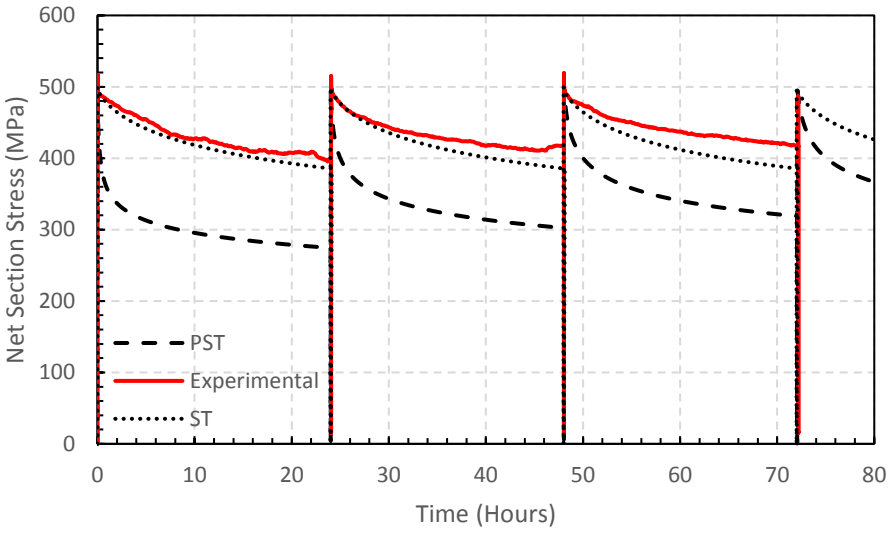

Figure 6.6 - Stress relaxation behaviour during a creep fatigue experiments with 24-hour relaxation dwells. Finite element models with and without primary creep shown along with experimental results.

Figures 6.7-6.16 are all for a creep fatigue experiment with 24-hour relaxation dwells with a start of dwell stress of 500MPa at 550˚C, simulated with the model without primary creep. Both creep models and all dwell lengths showed the same trends. Figure 6.7 shows the creep damage and creep strain across the notched section of the specimen as failure occurs. Figure 6.8 shows the triaxiality (hydrostatic stress/von Mises equivalent stress) across the notched section of the specimen as failure occurs.

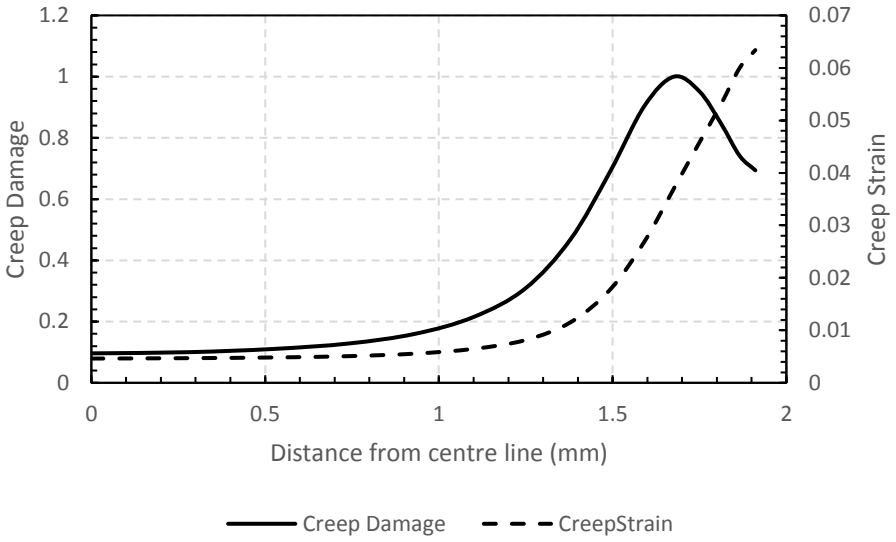

Figure 6.7 – Creep damage and creep strain across the ligament at the notched section on failure (24-hour dwell creep fatigue experiment modelled without primary creep)

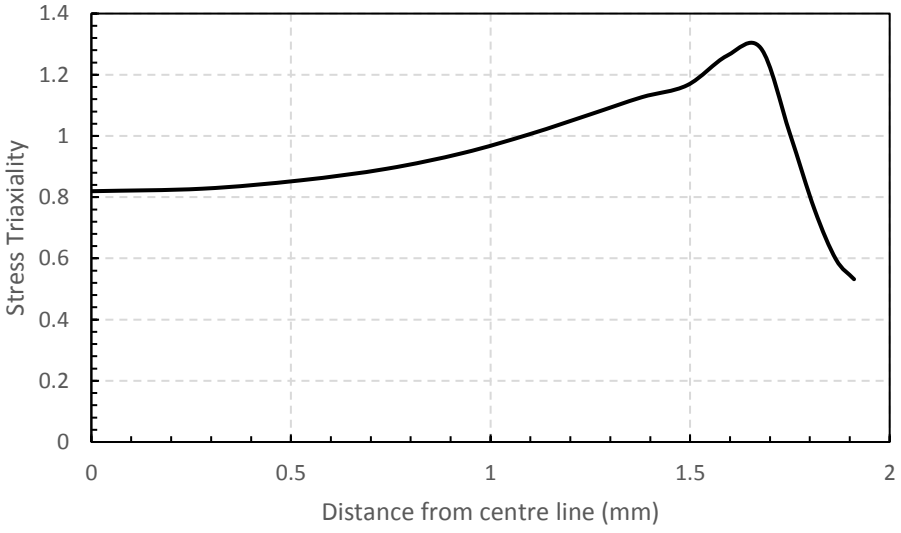

Figure 6.8– Triaxiality across the ligament at the notched section on failure (24-hour dwell creep fatigue experiment modelled without primary creep)

Figures 6.9-6.13 show the von Mises equivalent stress, axial stress, creep damage, creep strain, triaxiality and elastic follow-up respectively at three key points in the specimen against time. The three key points displayed in every Figure are the centre of the specimen, the element of maximum damage and the notch tip.

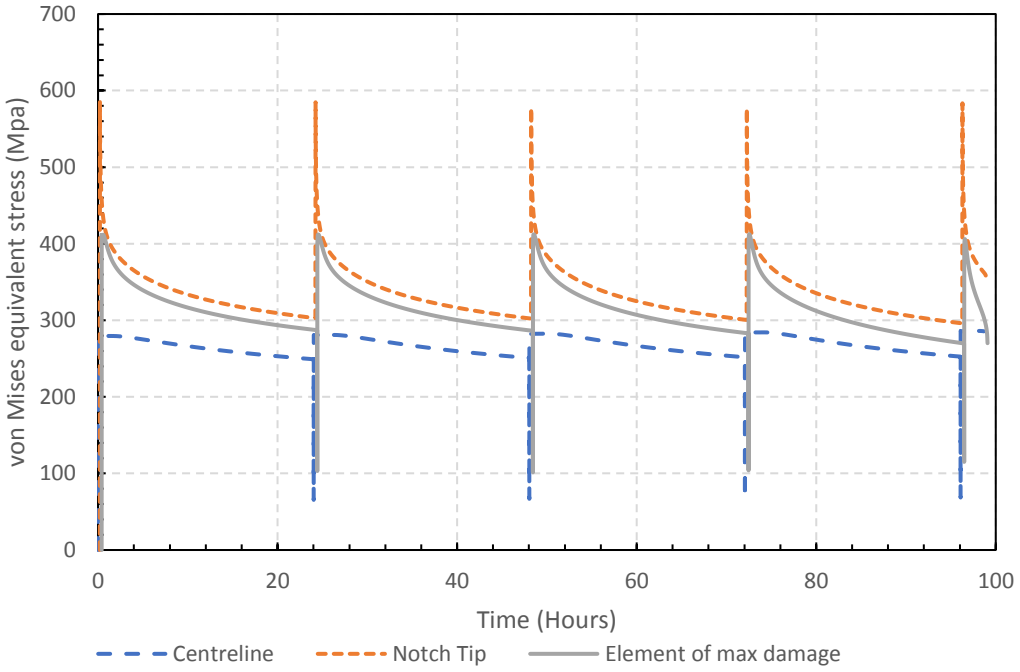

Figure 6.9– von Mises equivalent stress over time at the notch tip, element of maximum damage and centre line of the specimen (24-hour creep fatigue dwell experiment)

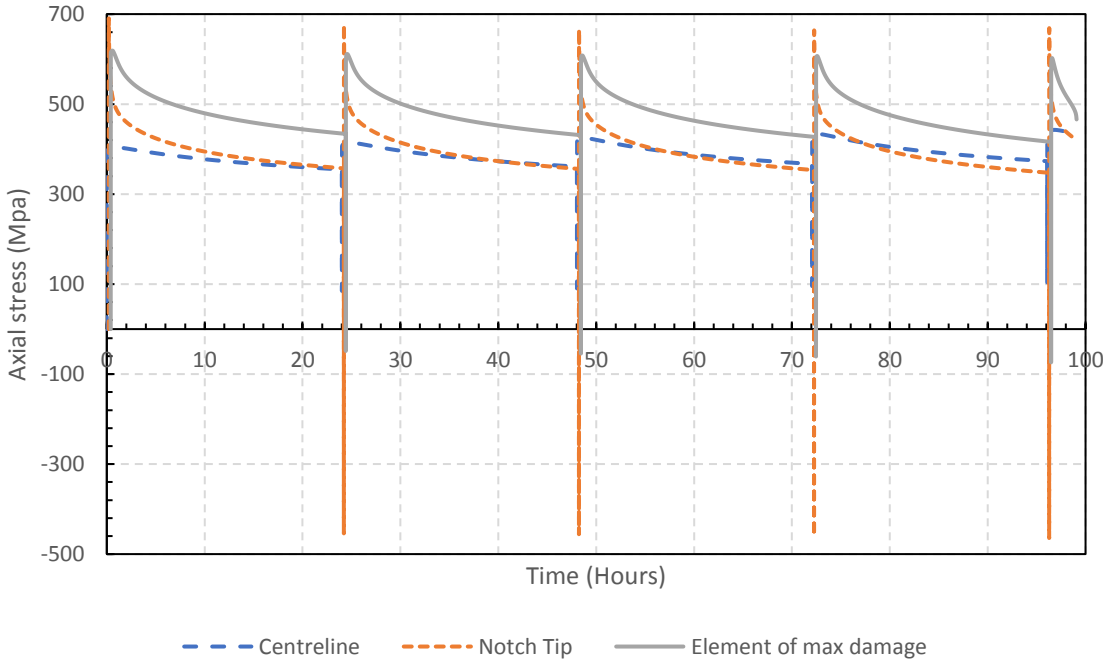

Figure 6.10– Axial stress over time at the notch tip, element of maximum damage and centre line of the specimen (24-hour creep fatigue dwell experiment)

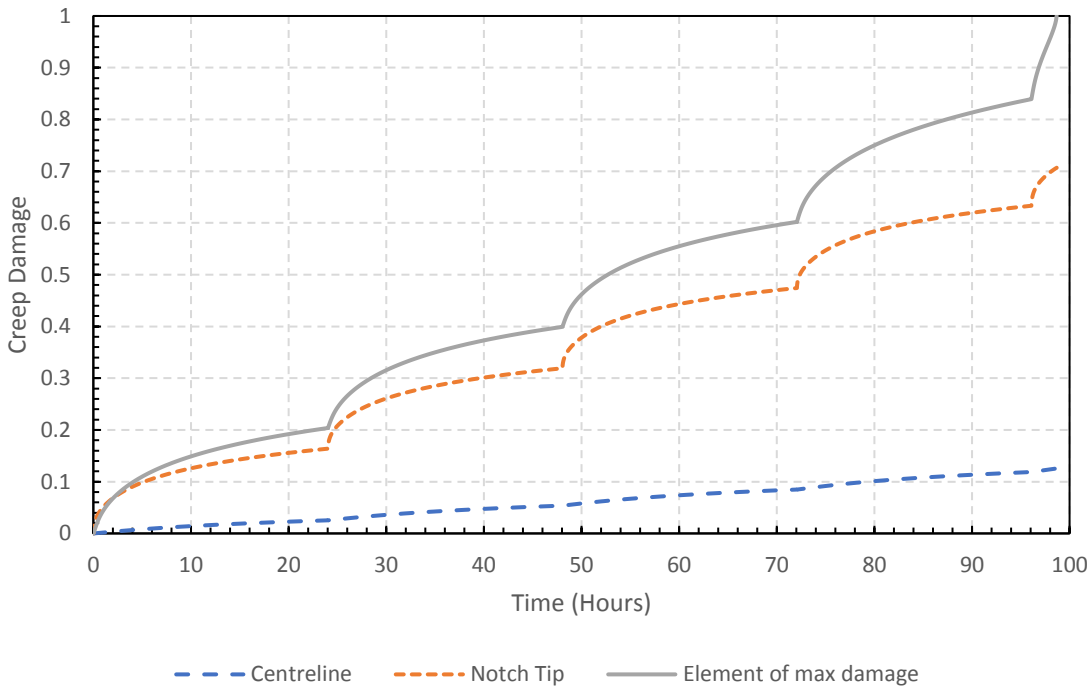

Figure 6.11 – Creep damage over time at the notch tip, element of maximum damage and centre line of the specimen (24-hour creep fatigue dwell experiment)

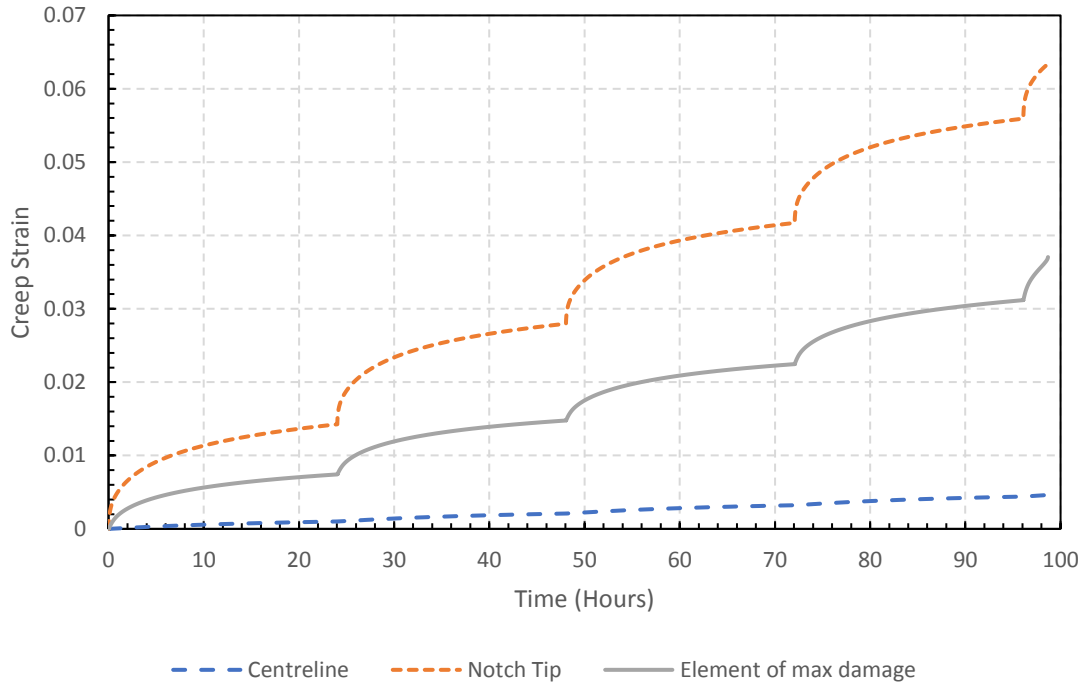

Figure 6.12– Creep strain over time at the notch tip, element of maximum damage and centre line of the specimen (24-hour creep fatigue dwell experiment)

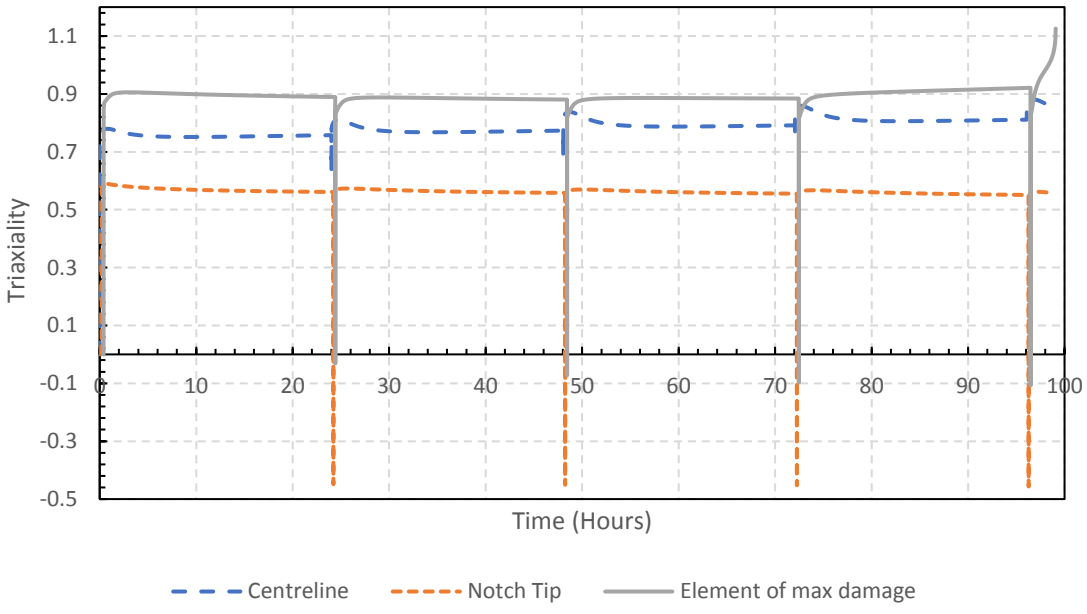

Figure 6.13– Triaxiality over time at the notch tip, element of maximum damage and centre line of the specimen (24-hour creep fatigue dwell experiment) (where triaxiality is defined as the hydrostatic stress/von Mises equivalent stress)

Figures 6.14-6.16 show the hydrostatic stress, von Mises stress, axial stress and triaxiality respectively across the notch ligament at three key times during the first complete cycle. The key times are the start of the relaxation dwell after initial load-up, the end of the relaxation dwell and during the unload (fatigue) cycle where the net section stress is taken to 0MPa.

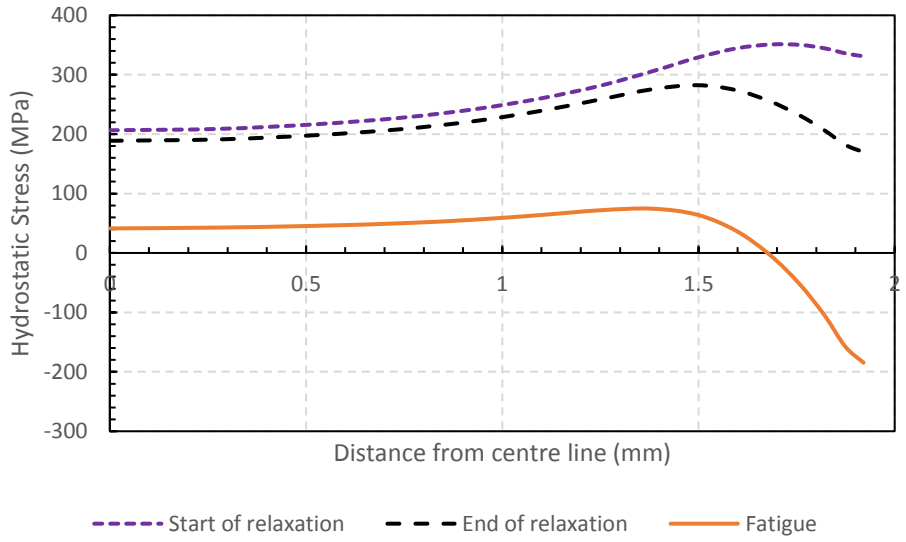

Figure 6.14– Hydrostatic stress across the ligament at the notched section at the start of the relaxation dwell, end of relaxation dwell and at unload (peak fatigue) (24-hour creep fatigue dwell experiment)

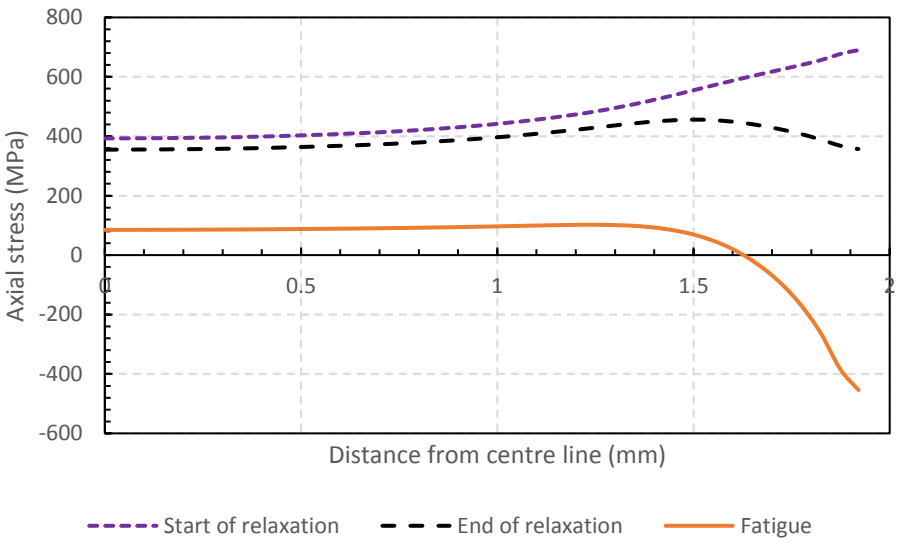

Figure 6.15– Axial stress across the ligament at the notched section at the start of the relaxation dwell, end of relaxation dwell and at unload (peak fatigue) (24-hour creep fatigue dwell experiment)

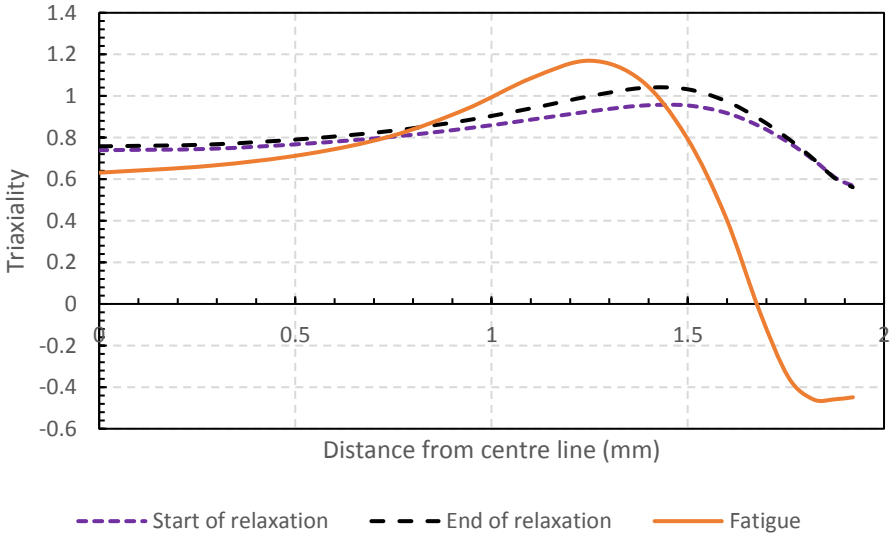

Figure 6.16– Triaxiality across the ligament at the notched section at the start of the relaxation dwell, end of relaxation dwell and at unload (peak fatigue) (24-hour creep fatigue dwell experiment) (where triaxiality is defined as the hydrostatic stress/von Mises equivalent stress)

It is worth noting that Figures 6.10, 6.13, 6.14, 6.15 and 6.16 confirm the presence of a substantial compressive stress near the notch tip, as expected. Figure 6.15 shows that reverse plasticity was occurring at the notch of the specimen.

Table 6.2 compares the experimental cycles to failure for the creep-fatigue and repeat relaxation tests. As expected, the introduction of the fatigue cycle, and reverse plasticity, reduces the number of cycles to failure, especially for the shortest dwell (i.e., the largest number of cycles). Table 6.2 also shows the dwells to failure predicted by both variations of the Spindler damage model used (accounting for creep damage only). Despite the finite element model showing that the specimen was subject to local compressive stresses during the fatigue cycle/unload of the specimen, the number of dwells to failure predicted by the model was almost the same as for the corresponding repeat relaxation experiments. This was because compressive stresses were assumed non-damaging in the creep damage model, creep damage was only accumulated under a positive load throughout modelling and fatigue damage was not calculated within the damage model but was present in the laboratory experiments (consistent with the R5V2/3 procedure).

Table 6.2– Dwells to failure for repeat relaxation tests from all damage models used.

Dwell length (Hours)	Dwells to failure experimentally		Spindler			
	Repeat Relaxation	Creep Fatigue (this work)	PST		ST	
			Type 1	Type 2	Type 1	Type 2
1	17	8	12.8	29.1	20.0	42.1
12	7	6	6.9	12.2	5.7	12.2
24	5	4	5.5	9.1	4.6	9.4
168	3	2	4.4	7.0	2.6	6.2
500	2	2	3.2	5.0	2.1	4.1

6.5.2 SMDE Damage Model

The net section stress behaviour experimentally can be seen in Figure 6.17, along with the FEA with just secondary and tertiary creep (ST) and primary, secondary and tertiary creep (PST).

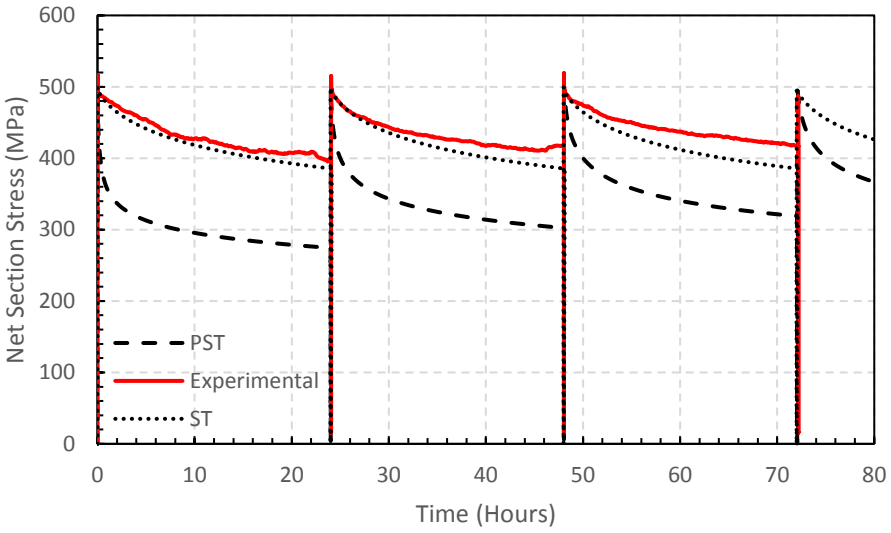

Figure 6.17 - Stress relaxation behaviour during a creep fatigue experiments with 24-hour relaxation dwells. Finite element models with and without primary creep shown along with experimental results.

Figure 6.18 shows the time to rupture for the damage model with primary creep for both failure types. Type 1 failures are when the first node fails, this is representative of a crack occurring experimentally. Type 2 failures are when all nodes along the notch root have failed, this is representative of fracture of a specimen. Here it can be seen that the model predicts failure of the first element early on in the creep life of the specimen and then total failure significantly later, suggesting cracks initiate in the early stages of creep and then take time to propagate throughout the specimen. This model showed poor macroscopic agreement with the experimental results so the usefulness of the finite element results from this model are debateable.

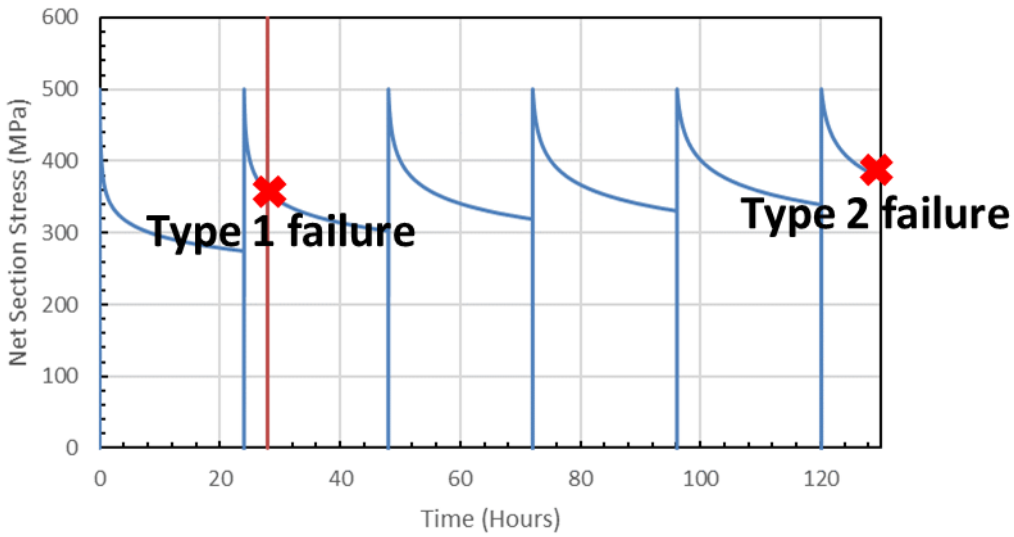

Figure 6.18 – Type 1 and type 2 failures for a 24-hour dwell creep fatigue experiment modelled with primary creep

Figures 6.19-32 are all for a creep fatigue experiment with 24-hour relaxation dwells with a start of dwell stress of 500MPa at 550˚C, simulated with the model including primary creep. Both creep models and all dwell lengths showed the same trends. Figures 6.19-23 show the creep damage, creep strain, axial stress, von Mises stress and stress triaxiality respectively across the notched section of the specimen as Type 1 and Type 2 failures occur.

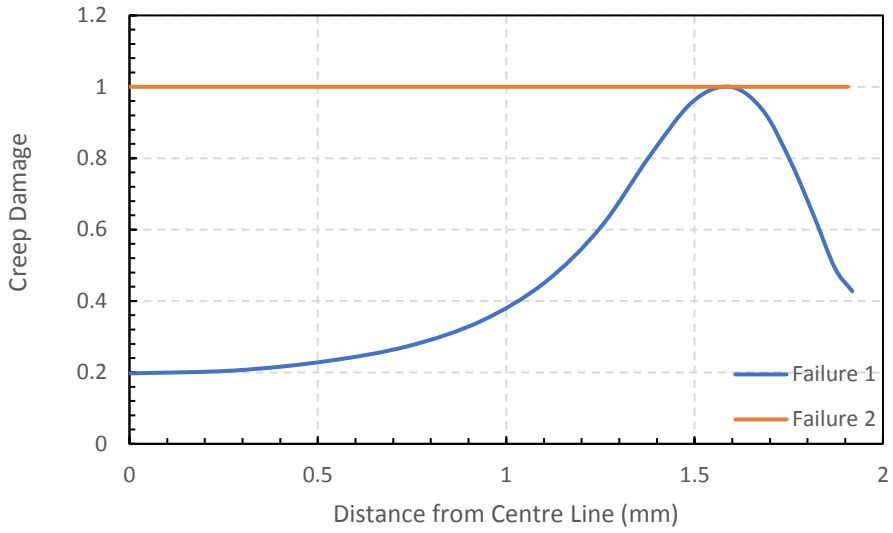

Figure 6.19– Creep damage across the notch for type 1 and type 2 failures (24-hour dwell creep fatigue experiment modelled with primary creep)

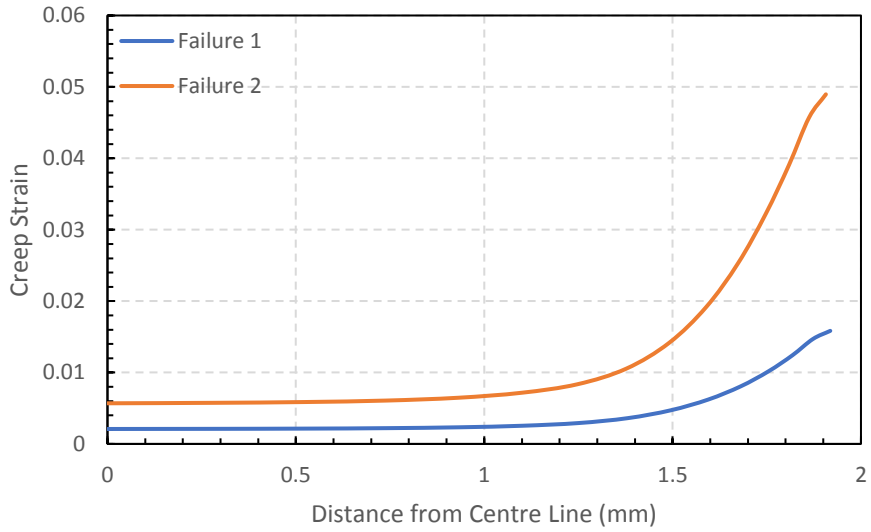

Figure 6.20– Creep strain across the notch for type 1 and type 2 failures (24-hour dwell creep fatigue experiment modelled with primary creep)

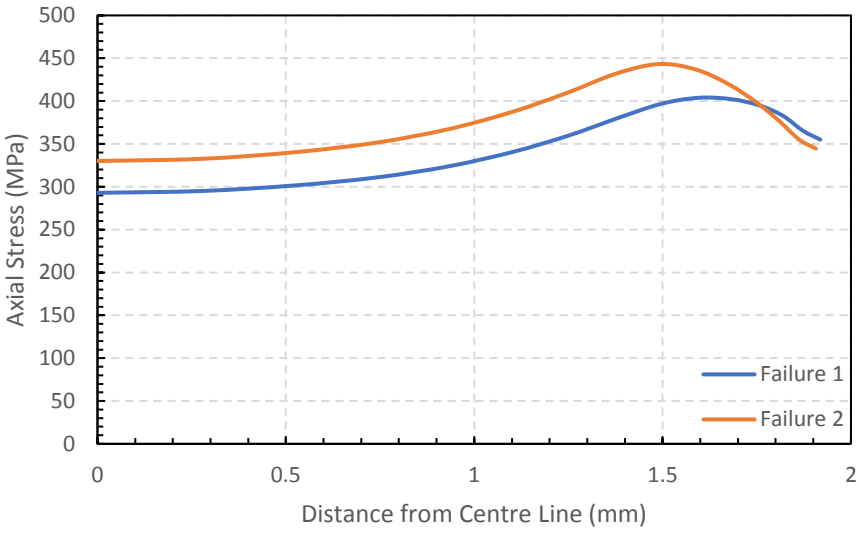

Figure 6.21– Axial stress across the notch for type 1 and type 2 failures (24-hour dwell creep fatigue experiment modelled with primary creep)

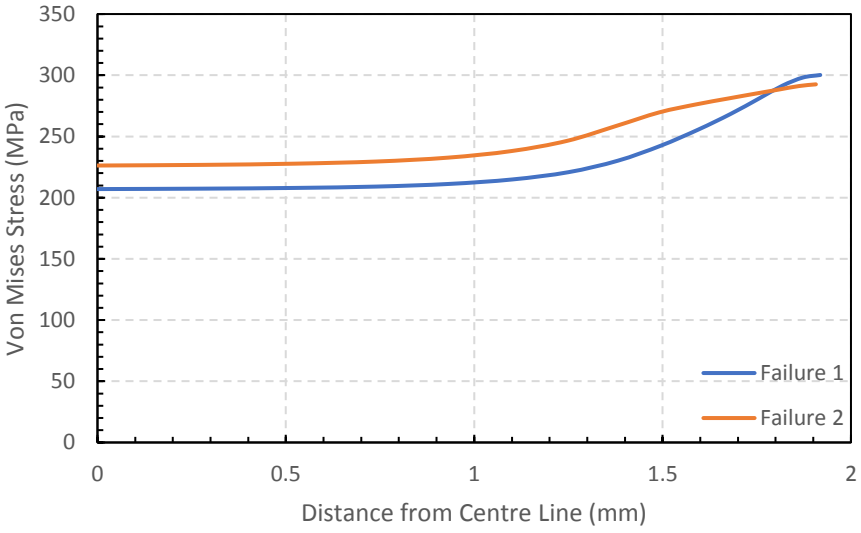

Figure 6.22– Von Mises stress across the notch for type 1 and type 2 failures (24-hour dwell creep fatigue experiment modelled with primary creep)

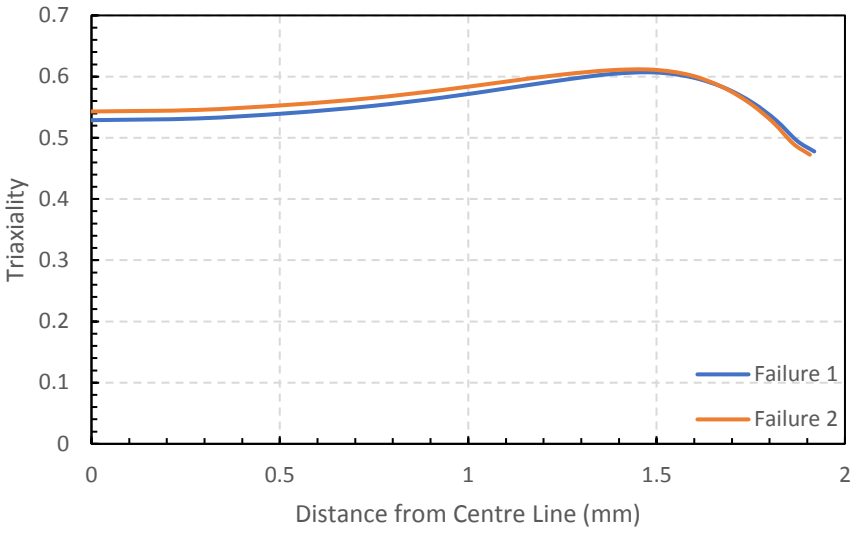

Figure 6.23– Triaxiality across the notch for type 1 and type 2 failures (24-hour dwell creep fatigue experiment modelled with primary creep)

Figures 6.24-6.28 show the von Mises equivalent stress, axial stress, creep damage, creep strain, triaxiality and elastic follow-up respectively at three key points in the specimen against time. The three key points displayed in every Figure are the centre of the specimen, the element of maximum damage and the notch tip.

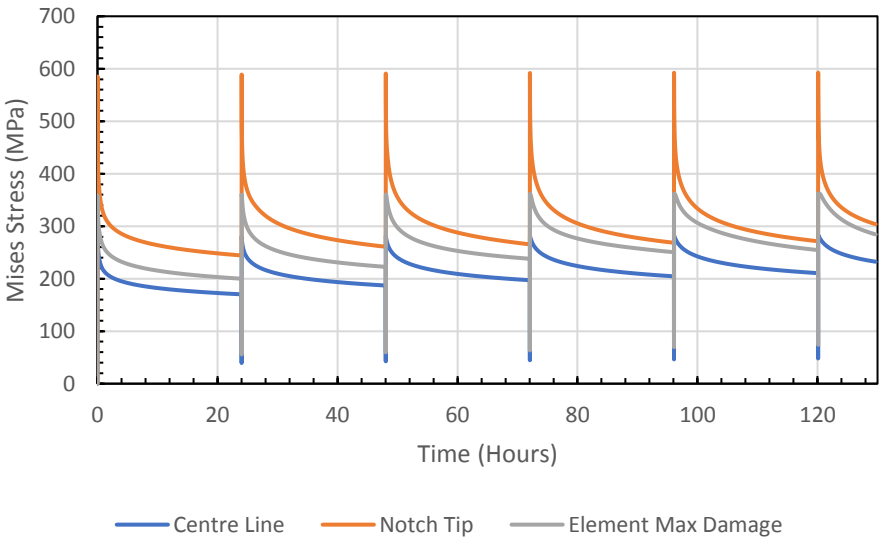

Figure 6.24– von Mises equivalent stress over time at the notch tip, element of maximum damage and centre line of the specimen (24-hour creep fatigue dwell experiment)

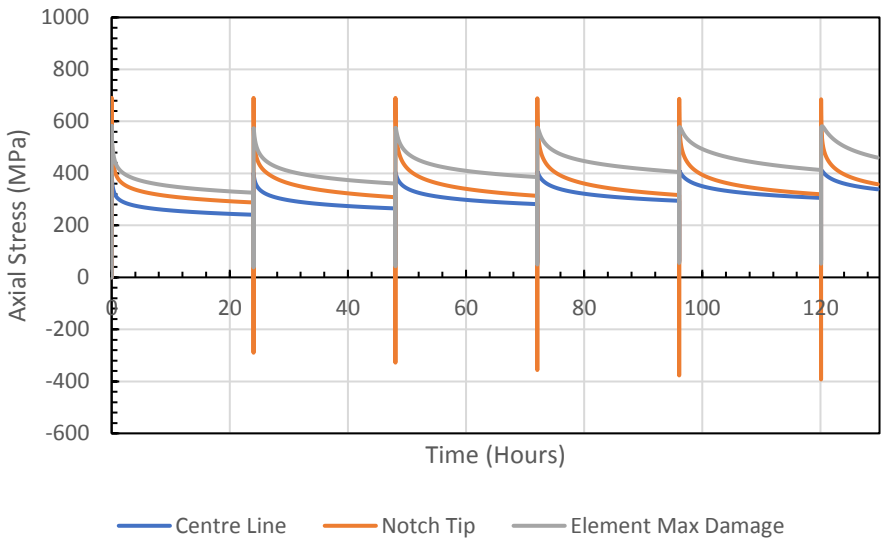

Figure 6.25– Axial stress over time at the notch tip, element of maximum damage and centre line of the specimen (24-hour creep fatigue dwell experiment)

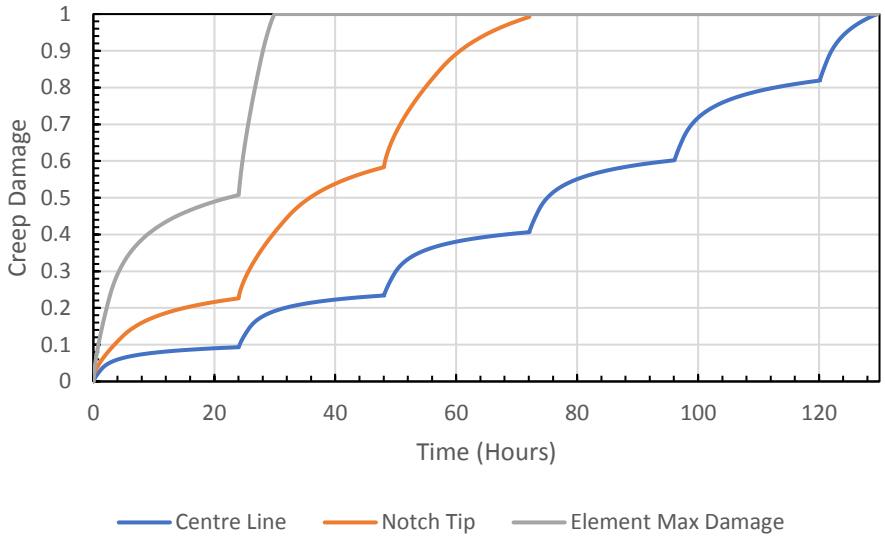

Figure 6.26– Creep damage over time at the notch tip, element of maximum damage and centre line of the specimen (24-hour creep fatigue dwell experiment)

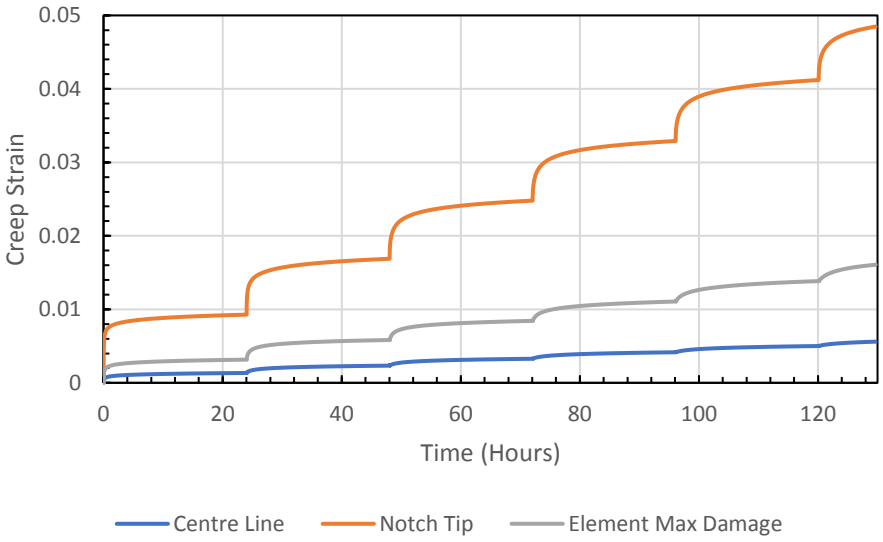

Figure 6.27– Creep strain over time at the notch tip, element of maximum damage and centre line of the specimen (24-hour creep fatigue dwell experiment)

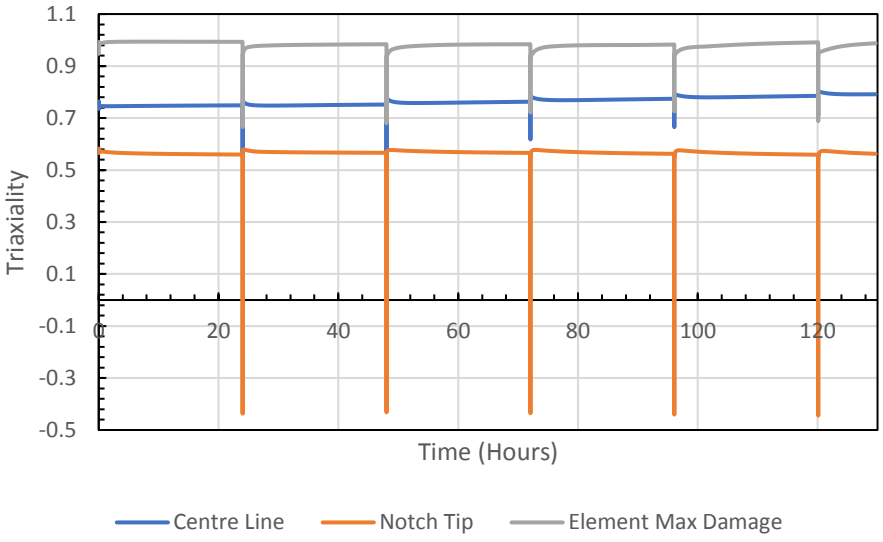

Figure 6.28– Triaxiality over time at the notch tip, element of maximum damage and centre line of the specimen (24-hour creep fatigue dwell experiment) (where triaxiality is defined as the hydrostatic stress/von Mises equivalent stress)

Figures 6.29-6.32 show the hydrostatic stress, von Mises stress, axial stress and triaxiality respectively at three key points during the first complete cycle. On the Figure keys S stands for the distribution of the variable at the start of the relaxation dwell after initial load up. E denotes the distribution of the variable at the end of the relaxation dwell and F denotes the distribution at the unload of the specimen during the fatigue cycle. 1 denotes that this analysis was for the first cycle the specimen was subject to.

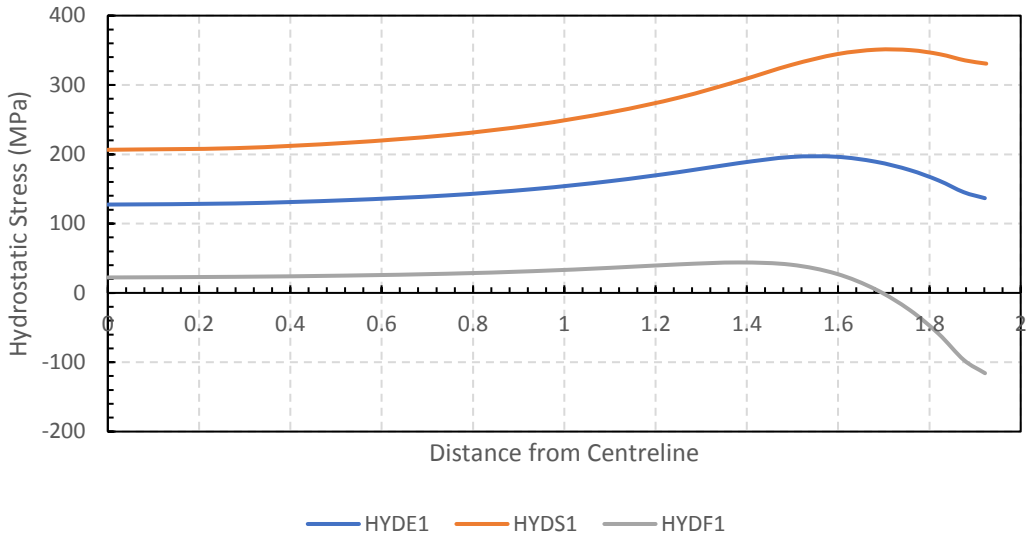

Figure 6.29– Hydrostatic stress across the notch at the start of the relaxation dwell, end of relaxation dwell and at unload (peak fatigue) (24-hour creep fatigue dwell experiment)

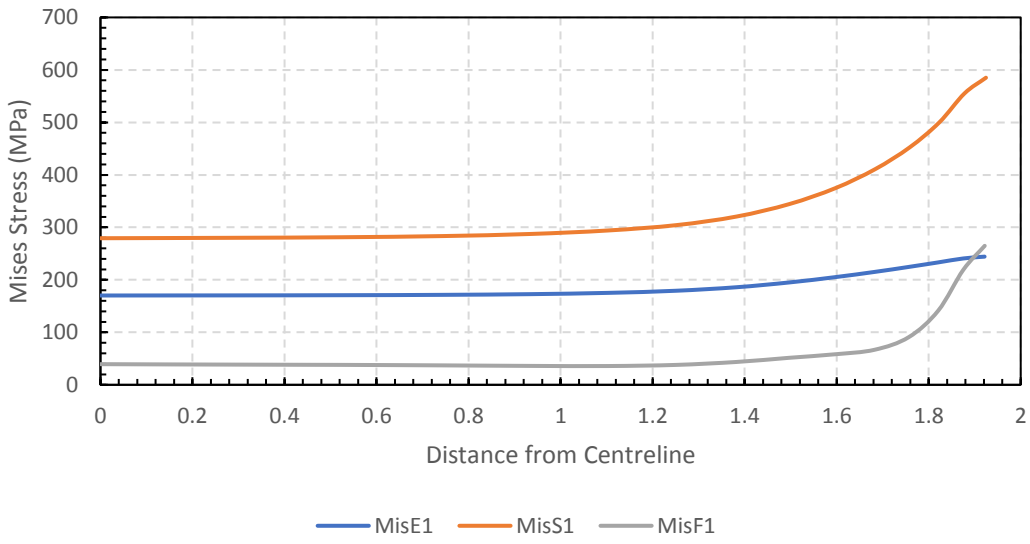

Figure 6.30– von Mises equivalent stress across the notch at the start of the relaxation dwell, end of relaxation dwell and at unload (peak fatigue) (24-hour creep fatigue dwell experiment)

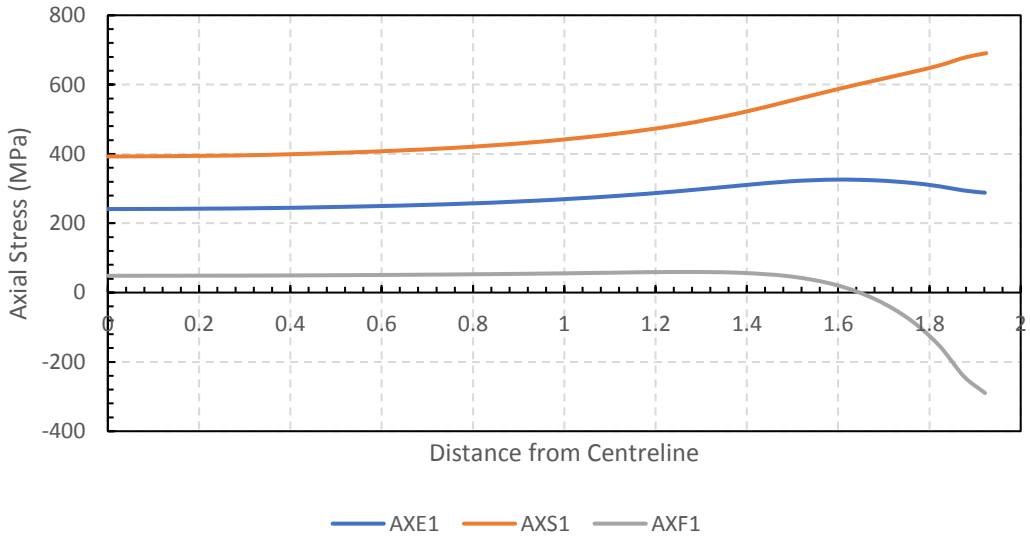

Figure 6.31– Axial stress across the notch at the start of the relaxation dwell, end of relaxation dwell and at unload (peak fatigue) (24-hour creep fatigue dwell experiment)

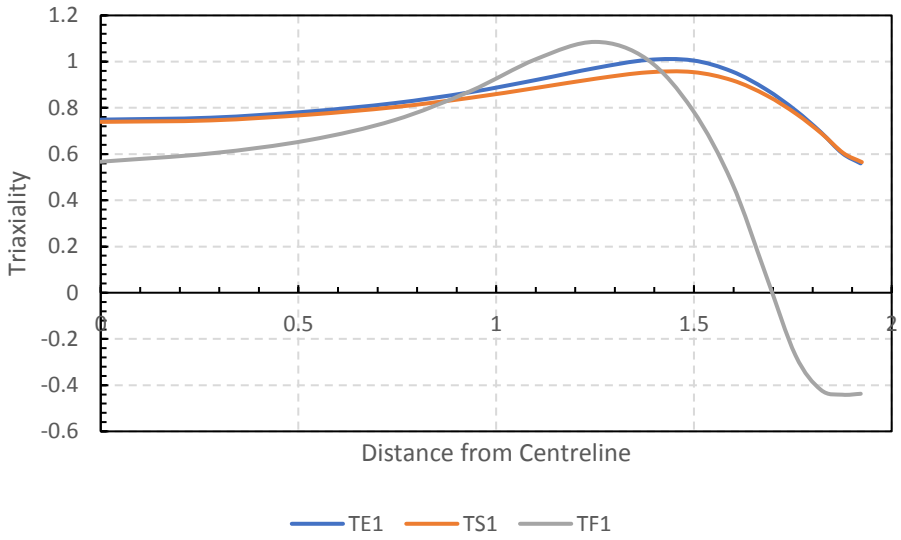

Figure 6.32– Triaxiality across the notch at the start of the relaxation dwell, end of relaxation dwell and at unload (peak fatigue) (24-hour creep fatigue dwell experiment) (where triaxiality is defined as the hydrostatic stress/von Mises equivalent stress)

Table 6.3 shows the dwells to failure predicted by all variations of the SMDE damage model used. Despite the finite element model showing that the specimen was subject to local compressive stresses during the fatigue cycle/unload of the specimen the number of dwells to failure predicted by the model was the almost the same as for the corresponding repeat relaxation experiments. This was because compressive stresses were assumed non-damaging in the damage model.

Table 6.3– Dwells to failure for repeat relaxation tests from all damage models used.

Dwell length (Hours)	Experimental	"Spindler" model Strain rate dependent ductility		SMDE			
				Type 1	Type 2	Type 1	Type 2
		PST	ST	PST	PST	ST	ST
1	8	12.8	20.0	7.4	19	5.1	15.1
12	6	6.9	5.7	1.9	5.5	0.5	2.5
24	4	5.5	4.6	1.3	5.1	0.3	2.1
168	2	4.4	2.6	1.1	3.5	0.1	1.1
500	2	3.2	2.1	1.1	3.1	0.1	1.1

6.5.3 Estimating Fatigue Damage

Comparing the dwells to failure from the FEA for creep fatigue and repeat relaxation it can be seen there is no difference. This is because the finite element models do not include fatigue damage whereas in the laboratory experiments conducted there was significant fatigue damage accumulated. The FEA does show that there are significant local compressive stresses in the creep fatigue experiments as well as a negative stress triaxiality during the fatigue cycle.

The following stage of analysis is to calculate the fatigue damage per cycle. Fatigue endurance data obtained from EDF Energy was fitted to the following expression (Note that the strain range used was based on an isotropic hardening creep damage model and if a kinematic hardening model had been used this strain range could have been significantly greater):

$$\log_{10}\left(\frac{N_f}{15}\right) = C_f\,(\Delta\,\varepsilon)^{n_f} \tag{6.1}$$

$$N_f = (10^{C_f\,(\Delta\,\varepsilon)^{n_f}}) * 15 = (10^{2.15(4)^{-0.63}}) * 15 = 118.52$$

where N_f was the number of cycles to fatigue failure, $\Delta\varepsilon$ is the strain range (% strain) and C_f and n_f are the coefficient and exponent of the fitted power law respectively (2.15 and -0.63' respectively). The strain range per cycle was 4% at the notch (4% increase in mises equivalent

strain between the minimum strain during the fatigue cycle when the specimen is unloaded and the maximum strain when the stress is re-applied).

The fatigue damage per cycle was calculated following the R5V2/3 procedure as follows:

$$N_i = N_f \exp\left(-8.06\, N_f^{-0.28}\right) = 118.52 \exp(-8.06 * 118.52^{-0.28}) = 14.27 \quad (6.2)$$

$$N_g = N_f - N_i = 118.52 - 14.27 = 104.25 \quad (6.3)$$

$$N_g' = N_g\, M = 104.25 * 0.3 = 31.27 \quad (6.4)$$

N_i was the number of cycles to crack initiation. N_g was the number of cycles from crack initiation to failure. N'_g was the adjusted number of cycles from initiation to failure. M was the crack depth adjustment factor, it is calculated from the initial crack depth. This was not measured in this situation, so a typical value of M was used, $M = 0.3$. Therefore, the fatigue damage per cycle (d_f) was:

$$d_f = \frac{1}{N_0} = \frac{1}{45.55} = 0.022 \quad (6.5)$$

where N_0 is given by (N_0 was the adjusted number of cycles to failure based on the crack depth adjustment factor):

$$N_0 = N_g' + N_i = 31.27 + 14.27 = 45.55 \quad (6.6)$$

The total damage (d) per cycle is:

$$d = d_c + d_f \quad (6.7)$$

To account for the fatigue damage at the notch caused by the compressive stresses that were not accounted for in the creep damage models, the fatigue damage values calculated previously were added between the finite element stress relaxation dwells. Table 6.4 shows the dwells to failure using the fatigue damage per dwell, calculated using the experimental strain range (d_f = 0.022 per cycle). This was calculated by looking at the creep damage accumulated over each dwell from every finite element model and adding 0.022 damage per fatigue cycle experienced.

Table 6.4– Dwells to failure for creep fatigue tests from all damage models used with fatigue damage being estimated from the experimental strain range.

Dwell length (Hours)	Experimental	"Spindler" model Strain rate dependent ductility (Type 1)		SMDE			
				Type 1	Type 2	Type 1	Type 2
		PST	ST	PST	PST	ST	ST
1	8	10.0	13.9	6.4	13.4	4.6	11.3
12	6	6.0	5.1	1.8	4.9	0.5	2.4
24	4	4.9	4.2	1.3	4.6	0.3	2.0
168	2	4.0	2.5	1.1	3.2	0.1	1.1
500	2	3.0	2.0	1.1	2.9	0.1	1.1

From Table 6.4 it can be seen that the fatigue dwells were more damaging experimentally than predicted in the R5 calculation. The fatigue damage per dwell experimentally was estimated from the experimental test with 1-hour dwells and the corresponding repeat stress relaxation test at this temperature with the same start of dwell stress so the only difference was the addition of the fatigue step between relaxation dwells. The test with 1-hour dwells was chosen as this had the most fatigue cycles so would provide the best estimate. For the test with purely relaxation dwells the specimen failed on the 17th dwell. For the experiment conducted with fatigue cycles between each dwell the specimen failed on the 8th relaxation dwell, having also been subject to 7 fatigue cycles. This suggested that the 7 fatigue cycles were as damaging as 9 relaxation dwells and contributed to 53% of the total damage within the specimen, meaning each fatigue cycle caused 0.076 fatigue damage. However, the additional damage caused by the fatigue cycle was not completely fatigue damage. The reverse plasticity has a subsequent effect on creep damage. Having calculated the fatigue damage per cycle above it can be seen

that the reverse plasticity does indeed have an effect on the subsequent creep damage, in fact it enhances it by (0.076-0.022) 0.054 per cycle. This underprediction of creep damage could also have been due to the fact that an isotropic hardening model was used and so the strain range and hence damage per cycle could have been underestimated.

6.7 Discussion

Figures 6.1a and b show the difference between the creep fatigue experiments and the repeat relaxation tests. It can be seen that the only difference between the two experiments is a removal of the load between relaxation dwells, this causes a slight negative extension in the specimen before the load is re-applied. When the load is re-applied a significant positive extension occurs. Figure 6.15 shows that the finite element models predict that this unloading between dwells results in a significant compressive stress at the notch tip causing a local fatigue cycle at the notch.

Table 6.1 shows the longer the duration of the dwell the lower the number of dwells to failure. This is expected as more creep strain was accumulated over the longer dwells. The tests with shorter dwell times fail in a shorter time than those with long dwells. This is because the most rapid accumulation of creep strain occurs at the start of the dwell and they are subject to more fatigue cycles as the number of dwells is higher. The creep strain on failure is significantly higher for the tests with short term dwells, this shows that rapidly accumulated strain is less damaging to the specimens than the creep strain accumulated more slowly towards the end of the long dwells. This agrees with previous research from Chapters 4 and 5 that showed that creep strain is more damaging for this cast of material at 550˚C the slower it is accumulated in forward creep and repeat stress relaxation.

Figure 6.2 shows the net section stress against normalised time for all the creep fatigue experiments conducted in this study. Figure 6.2 shows how the stress drops more per dwell in the longer-term dwell experiments, but the rate of stress drop is constantly reducing with time. There is only a 20MPa drop in stress between 168 and 500 hours of relaxation, approximately the same amount of stress drop that is seen in the first hour of relaxation. The experimental results suggest that this same stress drop is significantly more damaging when spread over a longer time period. Figure 6.3 shows the experiments with longer dwell lengths fail with a significantly lower amount of accumulated strain. This confirms previous findings that creep strain is accumulated far more rapidly at the start of the dwell than at the end. It also confirms

that the creep strain accumulated more slowly towards the end of the dwell is more damaging than the rapidly accumulated creep strain at the start of the dwell for a given level of creep strain (as is also suggested by the stress relaxation behaviour shown in Figure 6.2).

Figures 6.4 and 6.5 compare the creep fatigue experiments with the repeat relaxation tests in terms of number of dwells to failure and creep strain on failure respectively. Figure 6.4 shows that all creep fatigue tests failed in a lower number of dwells than the equivalent repeat relaxation experiment. This shows that removing the load between relaxation dwells has a definite damaging effect on notched bar specimens. Figure 6.5 shows that the diametric creep strain on failure is similar between both sets of experiments, perhaps slightly lower in creep-fatigue.

From the experimental results it was clear that the removal/ addition of a creep fatigue cycle of the load between dwells was having a damaging effect on the specimen. However, the creep damage models were not taking this into account as they did not include the effects of fatigue damage and so the number of dwells to failure predicted by the damage models was the same for the creep fatigue tests as it was for the corresponding repeat relaxation experiments. To estimate the fatigue damage between stress relaxation dwells two different methods were used. The damage was calculated using the experimental strain range implementing the method detailed in R5. The fatigue damage was also estimated using the experimental results from the 1-hour dwell experiments (fatigue and repeat relaxation). From the experiments the effect of the fatigue cycles could be isolated and the damage per cycle estimated. Table 6.4 shows the results from all finite element damage models with both these fatigue damage inclusions. From this table it can be seen that the best match with the experimental data came with the strain rate dependent Spindler damage model without primary creep, the same model that most accurately captured the stress drop behaviour and most accurately predicted the results from the repeat relaxation experiments.

6.8 Conclusions

The experimental results confirmed the previous finding from Chapters 4 and 5 that creep strain accumulated rapidly is less damaging than equal amounts of creep strain accumulated more slowly. In the case of the creep fatigue experiments this was confirmed because the creep strain rapidly accumulated at the start of stress relaxation dwells was shown to be less damaging than the creep strain accumulated more slowly towards the end of the dwell. Creep and fatigue are

not independent in notched specimens fabricated from austenitic stainless-steel specimens at 550˚C. Adding reverse loading/complete unloading between relaxation dwells via a creep fatigue cycle reduces the life of the specimen. This was most apparent in the short-term dwell tests were more fatigue cycles were applied and the difference in number of dwells to failure between the repeat relaxation tests and the creep fatigue tests was most pronounced. Taking the net section stress to zero in notched specimens after a period of loading is a way of applying a compressive stress in the notch tip without causing buckling of the specimen. A more accurate representation of experimental data was achieved by the addition of fatigue damage between dwells. However, the best agreement was obtained by acknowledging that the reversed plastic strains on unloading appeared to have an effect on enhancing subsequent creep damage. By judging the size of this effect from the one-hour dwell tests, best agreement was obtained for the remaining tests. The tentative conclusion is therefore that reverse plasticity increases subsequent creep damage in tension in creep-fatigue tests, and that this is additive to the effect of fatigue damage.

CHAPTER 7

Discussion

“Debate and divergence of our views can only enrich our history and culture” - Ibrahim Babangida

Chapter 7 Discussion

Several data sets, collected under a range of conditions, have been presented and discussed in previous chapters. This chapter brings together all of these data sets and observations.

7.1 Strain Rate Driven Failures

The constant load creep experiments on notched bar specimens reported in Chapter 4 showed that a higher applied stress/load led to reduced times to rupture. However, when comparing the highest load constant stress test (515MPa) at 550˚C with the 1-hour dwell repeat relaxation tests and creep fatigue tests also at 550˚C with a 500MPa start of dwell stress the results suggest the reduced time to rupture is not driven by the higher stress. Figure 7.1 shows the net section stress applied to the notch of the specimen (based on initial diameter) as a function of time during three different experiments. The red line shows a constant net section stress creep rupture experiment at 515MPa, the solid black line shows the net section stress for 1-hour dwell repeat relaxation and the green line shows the net section stress for a 1-hour dwell creep fatigue experiment (all conducted at 550˚C on notched bar specimens with acuity 5). Here it can be seen that in both the repeat relaxation tests and the creep fatigue tests the net section stress is never higher than it is in the creep rupture experiment but both experiments have a shorter time to failure.

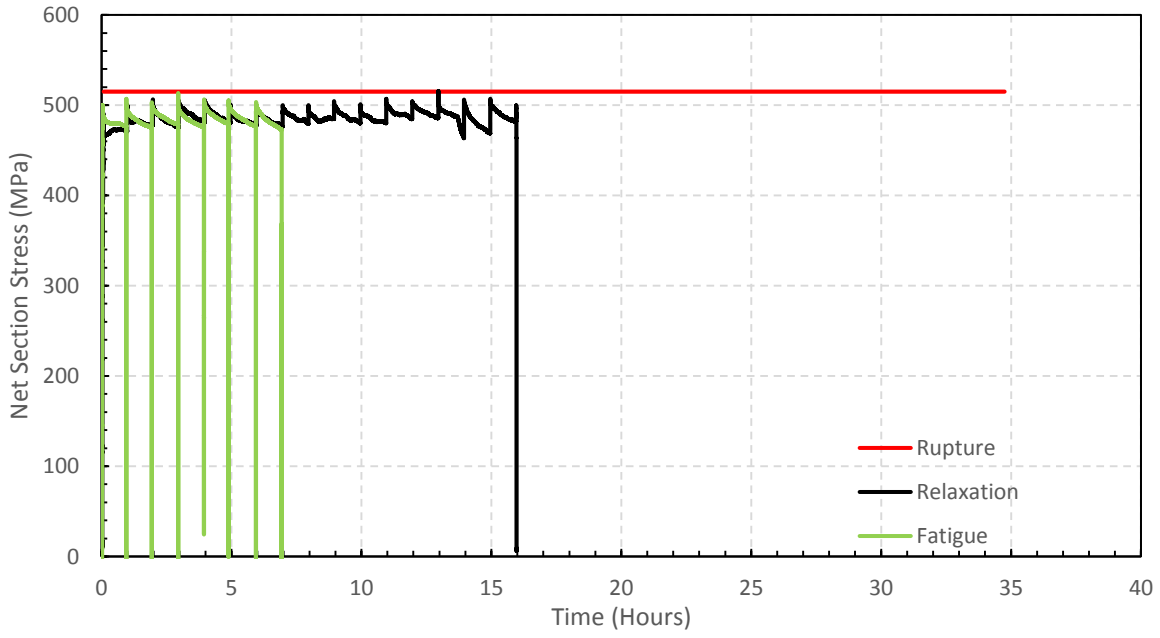

Figure 7.1 – Short term experimental data conducted at 550˚C (Creep rupture, repeat relaxation and creep fatigue). Net section stress against time.

Figure 7.2 shows the diametric creep strain at the notch on failure for each of the experiments being compared. Diametric creep strain was calculated as the change in diameter during creep divided by the diameter after initial load up. This Figure shows that the relaxation experiment had accumulated almost 3 times as much creep strain on failure as the rupture experiment and the fatigue experiment approximately 5 times as much creep strain on failure as the rupture experiment.

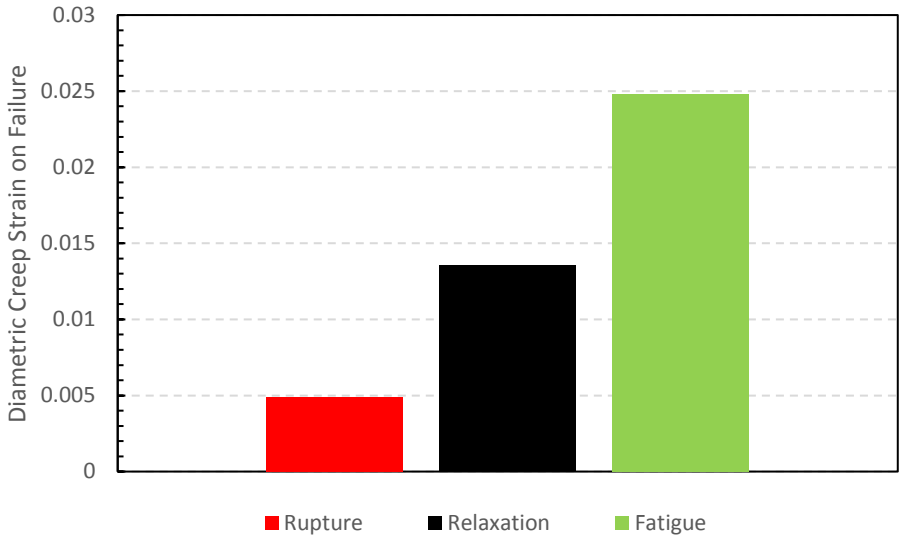

Figure 7.2 - Short term experimental data conducted at 550˚C (Creep rupture, repeat relaxation and creep fatigue). Diametric Creep Strain on Failure

Figure 7.3 shows the time to rupture plotted against the average creep strain rate for these three experiments. Here it can be seen that the higher the average diametric creep strain rate, regardless of experiment type, the shorter the time to rupture. These results imply that the time to rupture and the creep strain on failure are determined by the creep strain rate being applied to the specimen and not the load being applied.

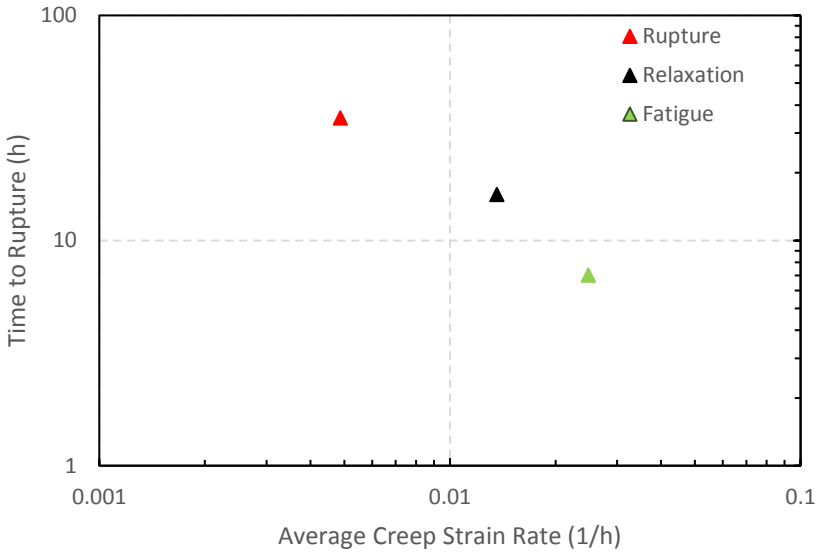

Figure 7.3 - Short term experimental data conducted at 550˚C (Creep rupture, repeat relaxation and creep fatigue). Time to rupture against average creep strain rate.

In creep rupture of notched bars the specimens failed more quickly and with greater creep strain on failure at increased loads because the increased loads result in the specimen being subject to a higher creep strain rate. In a relaxation experiment on an identical specimen, during the initial portion of relaxation the specimen was subject to high creep strain rates and in the 1-hour dwell test when the load was being rapidly re-established the average creep strain rate stayed above that of the rupture experiment. In the fatigue experiment removing the load between dwells and then re-applying it caused the creep strain rate to achieve an even higher rate than in the repeat relaxation or creep rupture experiments and hence the specimen failed in a shorter period of time and with a higher extension on failure (as this material exhibits a strain rate dependent ductility, as previously discussed (Chapter 5)).

7.2 Comparing the data as a whole

A summary of all of the experimental tests conducted on notched bar specimens (notch acuity 5) is shown below in Table 7.1. Figure 7.4 shows the average creep strain rate plotted against time to rupture for every experiment and Figure 7.5 shows the creep strain on failure against time to rupture for all experiments. Figure 7.4 shows just the experimental data with a line of best fit for the data as a whole and Figure 7.5 includes lines of best fit for each data set (split into creep rupture, creep fatigue, repeat relaxation at 550˚C and repeat relaxation at 515˚C).

Figures 7.6, 7.7 and 7.8 show the creep strain on failure for all experiments plotted against the average creep strain rate. Figure 7.6 shows just the experimental data, Figure 7.7 shows the experimental data with lines of best fit for each data set and Figure 7.8 shows the experimental data on a loglog scale with a line of best fit for all the data as a whole.

Table 7.1 - Notched bar experimental summary

Experiment Type	Temperature (˚C)	Dwell Length (Hours)	Stress (MPa) (start of dwell or constant)	Rupture Time (Hours)	Creep Strain on Failure	Average Diametric Creep Strain Rate (1/h)	Diameter on failure	Diameter after load up
Creep Rupture	550	-	342	11097	0.031	2.766E-6	3.79	3.91
Creep Rupture	550	-	390	480	0.026	5.482E-5	3.7	3.8
Creep Rupture	550	-	432	175	0.032	1.805E-4	3.68	3.8
Creep Rupture	550	-	436	307	0.025	8.076E-5	3.54	3.63
Creep Rupture	550	-	469	231	0.039	1.684E-4	3.46	3.6
Creep Rupture	550	-	500	16	0.038	2.397E-3	3.51	3.65
Creep Rupture	550	-	500	23	0.055	2.390E-3	3.61	3.82
Creep Rupture	550	-	515	35	0.049	1.392E-3	3.32	3.49
Stress Relaxation	550	1	500	16	0.136	8.523E-3	3.23	3.74
Stress Relaxation	550	12	500	72	0.115	1.597E-3	3.31	3.74

Stress Relaxation	550	24	500	96	0.102	1.058E-3	3.36	3.74
Stress Relaxation	550	168	500	336	0.061	1.830E-4	3.51	3.74
Stress Relaxation	550	500	500	507	0.045	8.965E-5	3.57	3.74
Stress Relaxation	550	1	440	55	0.122	2.220E-3	3.38	3.85
Stress Relaxation	550	12	440	144	0.106	7.395E-4	3.44	3.85
Stress Relaxation	550	24	440	168	0.101	6.030E-4	3.46	3.85
Stress Relaxation	550	168	440	672	0.078	1.160E-4	3.55	3.85
Stress Relaxation	550	500	440	1500	0.044	2.944E-5	3.68	3.85
Stress Relaxation	515	1	500	31	0.113	3.650E-3	3.37	3.8
Stress Relaxation	515	12	500	96	0.095	9.868E-4	3.44	3.8
Stress Relaxation	515	24	500	120	0.074	6.140E-4	3.52	3.8
Stress Relaxation	515	168	500	336	0.047	1.410E-4	3.62	3.8
Stress Relaxation	515	500	500	500	0.005	1.053E-5	3.78	3.8
Creep Fatigue	550	1	500	7	0.174	2.483E-2	3.09	3.74
Creep Fatigue	550	12	500	60	0.123	2.050E-3	3.28	3.74
Creep Fatigue	550	24	500	72	0.083	1.151E-3	3.43	3.74

Creep Fatigue	550	168	500	301	0.059	1.954E-4	3.52	3.74
Creep Fatigue	550	500	500	500	0.019	3.743E-5	3.67	3.74

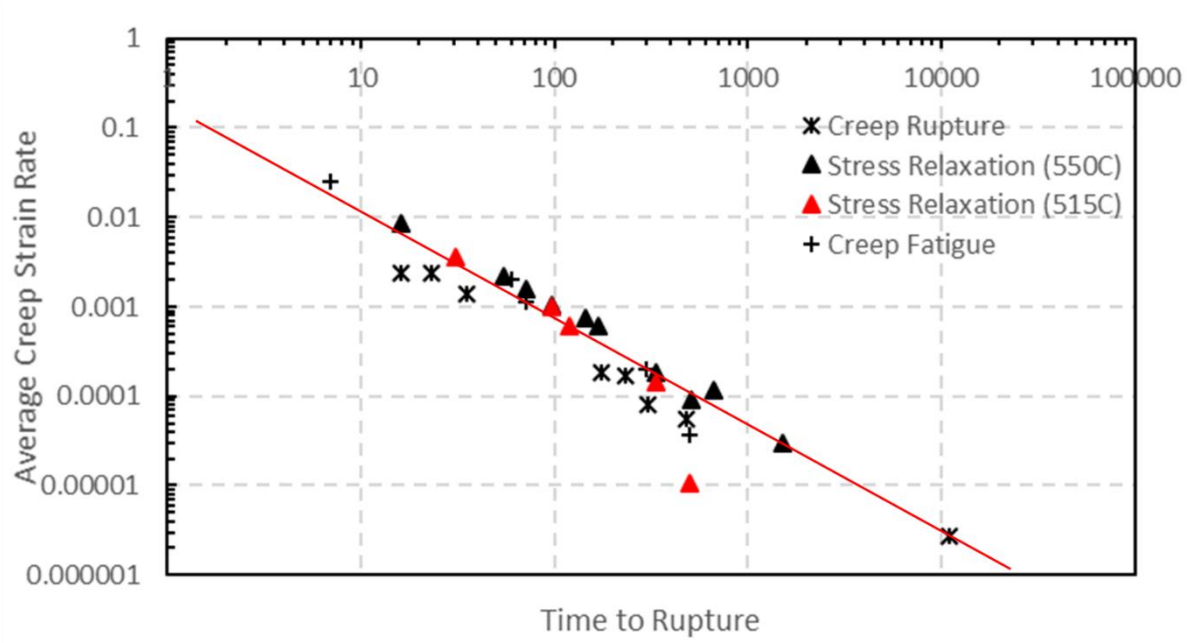

Figure 7.4 – Average diametric creep strain rate vs time to rupture for all notched bar experimental data plotted on a loglog scale with line of best fit for the entirety of the data

Figure 7.5 shows that for all the experiments conducted the general trend is an increased creep strain on failure with a reduced time to rupture.

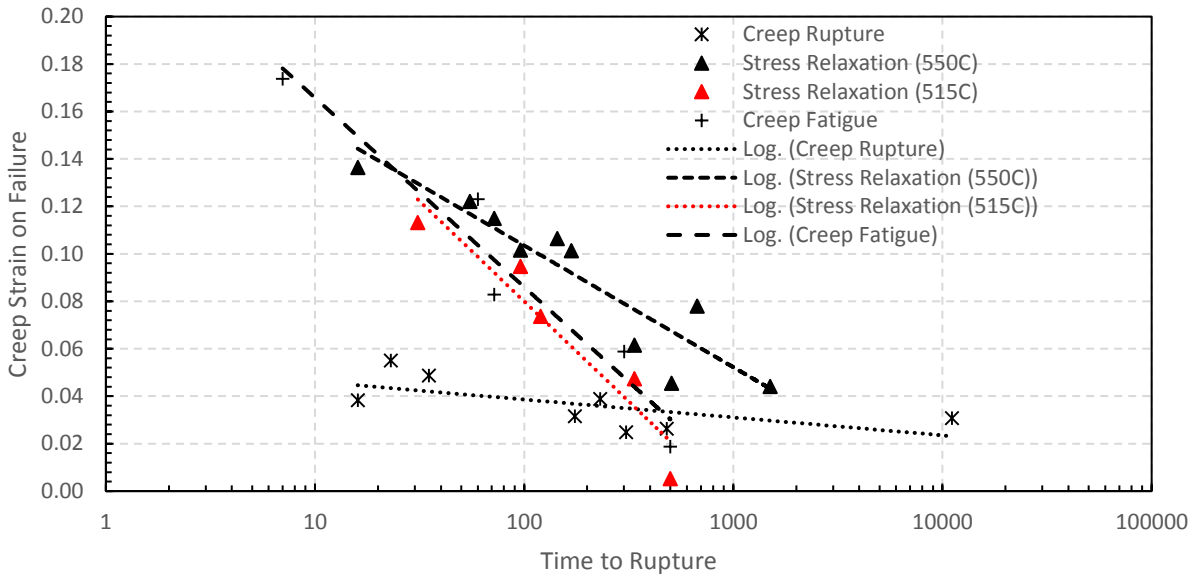

Figure 7.5 - Creep strain on failure vs time to rupture for all notched bar experimental data with lines of best fit for each data set

Figure 7.4 shows that for all experiment types as the creep strain rate is increased the time to rupture is reduced. Figure 7.7 shows that the creep strain on failure is increased with an increase in average creep strain rate. This is because this material exhibits a creep strain rate dependent creep ductility as previously discussed (Chapter 5). Here it can be seen that each data set has a slightly different line of best fit except the data set for rupture of notched bars. The creep strain on failure for the rupture of notched bar experiments tends to be lower than for the corresponding repeat relaxation and creep fatigue tests. This is because in the repeat relaxation and creep fatigue experiments at the start of the relaxation dwells there is a rapid accumulation of creep strain which is not very damaging to the specimen (see Chapter 5). In contrast there is a more steady rate of creep strain accumulation in the constant load experiments.

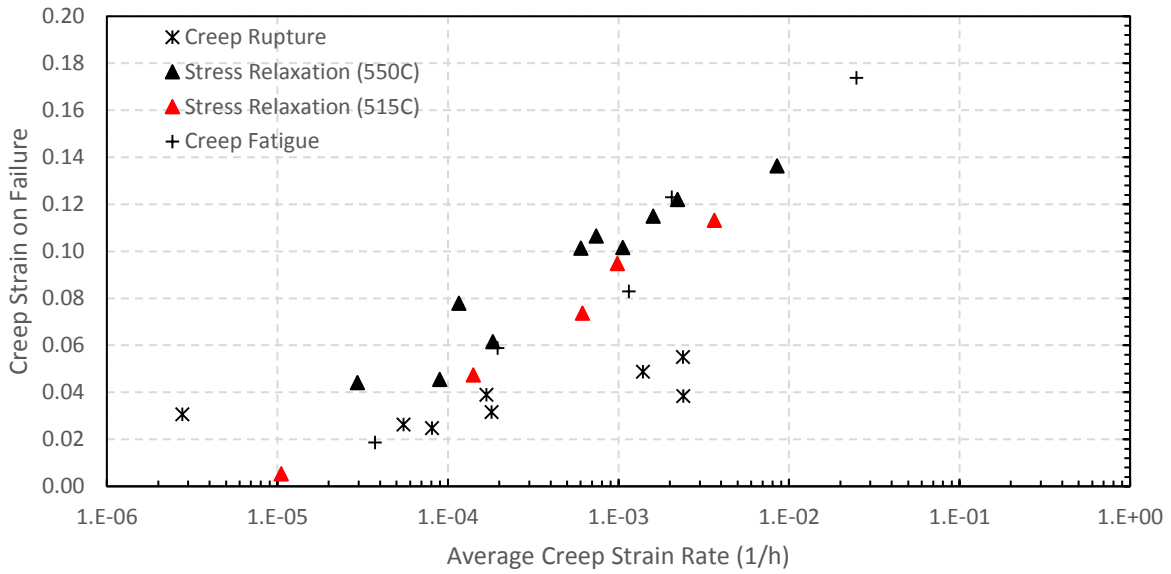

Figure 7.6 - Creep strain on failure vs average creep strain rate for all notched bar experimental data.

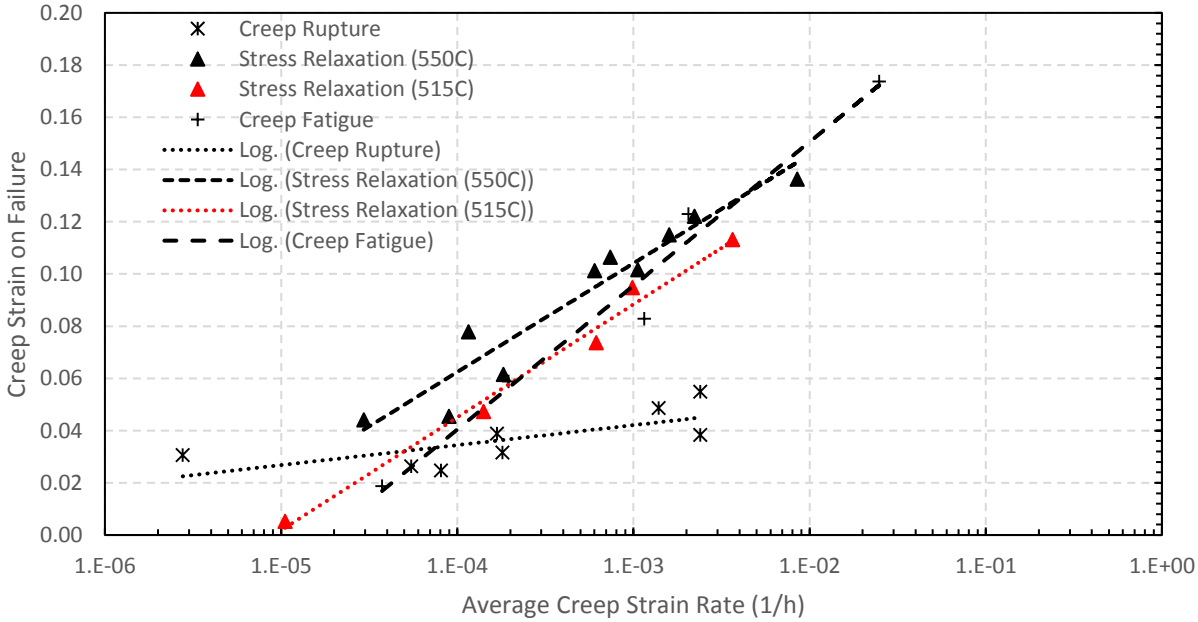

Figure 7.7- Creep strain on failure vs average creep strain rate for all notched bar experimental data (lines of best fit for each data set included)

Figure 7.7 shows the same experimental data from Figure 7.6 with lines of best fit for each data set. This shows all the tests show a similar line of best fit except the rupture experiments. This is for the same reason as discussed above for Figure 7.4. The rupture experiments are not subject to the rapid accumulations of creep strain at the start of dwells which cause negligible damage to the specimen.

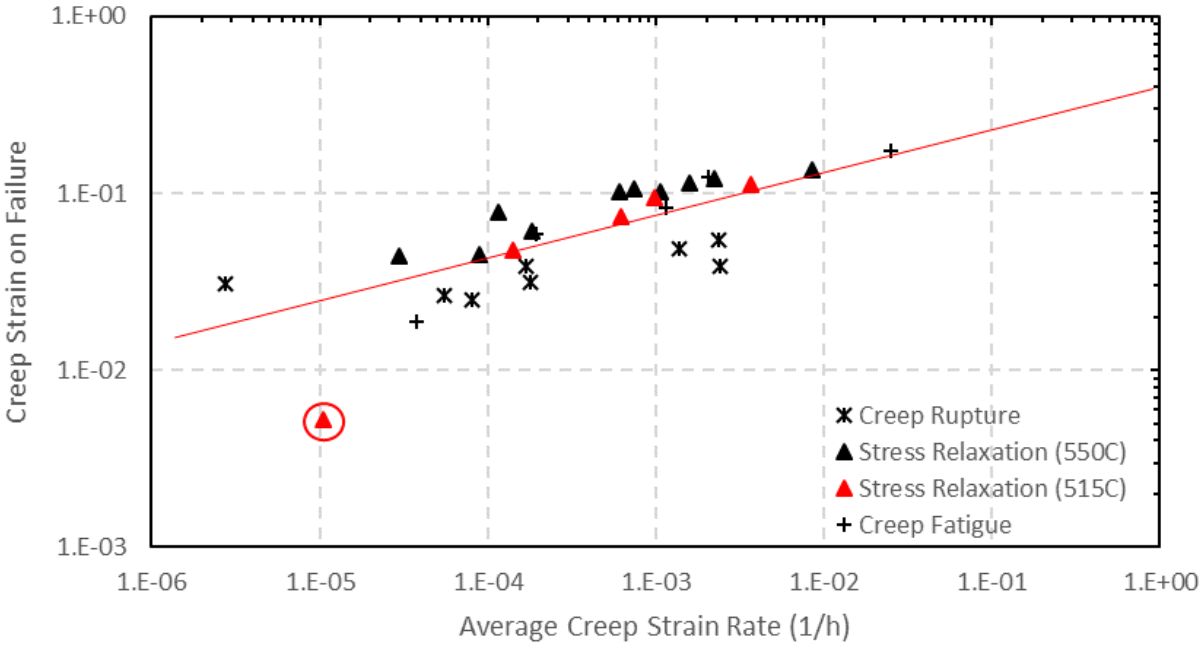

Figure 7.8- Creep strain on failure vs average creep strain rate for all notched bar experimental data plotted on a loglog scale with line of best fit for the entirety of the data

Figure 7.8 displays the same experimental data as Figure 7.6 plotted on a log log scale with a line of best fit for the entirety of the data displayed. Here it can be seen that all the data fits with limited scatter except for the 500-hour dwell stress relaxation test conducted at 515˚C (circled in red on the Figure). At first glance this looks like an anomalous result. However, referring back to Chapter 5 where the strain rate dependent ductility for this material was introduced and it was discussed that this material exhibited a reduced lower shelf ductility at 515˚C than at 550˚C (approximately 40% of the lower shelf ductility at 550˚C for notched bar specimens). The lower shelf ductility was for experiments conducted at a strain rate of 1E-5 (absolute per hour) and below. The 500 hour dwell experiment conducted at 515˚C was the

only test conducted at 515˚C with an average strain rate low enough to put it on the lower shelf and this is why the creep strain on failure for this experiment is approximately 40% of the value you would expect it to be were it not for the case of a reduced lower shelf ductility for this material at 515˚C.

It has been theorized by Stuart Holdsworth, a leading researcher in the field of creep, that the reason that this material exhibits a strain rate dependent ductility is because at low creep strain rates specimens fail via constrained cavity growth [72]. As creep strain rate is increased they start to fail via diffusion controlled cavity growth and these cavities are larger and result in more deformation before failure. At very high strain rates/approaching plastic failure then plastic holes appear in the specimen which result in a very large ductility on failure.

CHAPTER 8

Conclusions

“If it doesn’t challenge you it won’t change you” – Fred Devito

Chapter 8 Conclusions

8.1 Conclusions

In summary the following conclusions were made with regard to the behaviour of Type 316H austenitic stainless steel cast 69431 header 2C2/3 under various creep conditions based on the research described in this thesis:

1. In creep rupture of notched bars as the net section stress increases the time to failure reduces but the creep ductility on failure increases, implying the material has a time or strain rate dependent creep ductility. As net section stress is increased the overall extension of the specimen on failure is increased and specimen diameter on failure is reduced.
2. In creep rupture of notched bars the extension and diameter change attributable to creep also increase as the net section stress is increased, further confirming this material has an increased creep ductility at higher strain rates/stresses.
3. As net section stress is increased under constant load creep of notched bars (creep rupture), hoop and skeletal creep strains on failure are also increased. It has been shown that using creep constants derived from uniaxial creep data it is possible to accurately capture creep behaviour of notched bar specimens with a notch acuity of 5. The highest stress triaxiality factor (hydrostatic stress/Mises stress) occurs just away from the notch tip, 1.65mm from the centre line (15% of the distance from the edge of the notch to the centre line), the same point on the specimen where damage reaches 1 (unity) first. The higher the net section stress and therefore the higher the average creep strain rate in creep rupture tests, the higher the extension and creep ductility of the specimens on failure.
4. Repeat stress relaxation experiments conducted on notched bar specimens showed that austenitic stainless-steel type 316H has a lower creep ductility at 515˚C than at 550˚C. Creep strain accumulated rapidly at the start of the dwell is less damaging to a notched bar specimen than creep strain accumulated more slowly towards the end of a dwell. Creep strain accumulated more slowly because of the lower test temperature was also more damaging than creep strain accumulated at the higher temperature. This was shown in the long dwell repeat relaxation tests where the tests at 515˚C and 550˚C failed at the same time but the tests at 515˚C had accumulated significantly less creep strain.
5. The repeat relaxation experiments also showed that lowering the creep strain rate by reducing the start of dwell stress led to specimens failing with a lower accumulation of

creep strain, suggesting creep strain is more damaging when accumulated slowly due to a lower test stress or temperature. Regardless of whether the strain rate is altered by changing the test temperature or stress. A strain rate dependent ductility for this material has been indicated by previous unpublished work [4] however the work presented in this thesis is a conclusive demonstration of this behaviour.

6. A Spindler model with only secondary and tertiary creep more accurately predicts the behaviour than one with primary, secondary and tertiary creep when modelling stress relaxation of notched bars with an acuity of 5 with a high initial net section stress. It was also found that an adjusted model, with the stress drop lost through load up ignored in the finite element model and assumed to not be damaging, gives much better agreement than a model with primary, secondary and tertiary creep. This shows that strain accumulated very quickly, during the rapid stress drop present in the load up between rotations of the top wheel, is not damaging to the specimen.
7. From the creep fatigue experiments conducted on notched bar specimens it was found that creep and fatigue are not independent. Adding reverse loading/complete unloading between relaxation dwells via a creep fatigue cycle reduces the life of the specimen. This was most apparent in the short-term dwell tests where more fatigue cycles were applied and the difference in number of dwells to failure between the repeat relaxation tests and the creep fatigue tests was most pronounced. The finite element analysis showed that taking the net section stress to zero in notched specimens after a period of loading is a way of applying a compressive stress in the notch tip without causing buckling of the specimen.
8. When modelling creep of notched bars fabricated from austenitic stainless steel type 316H the Spindler damage model gives a more accurate representation of experimental behaviour that the stress modified ductility exhaustion model (SMDE).
9. The overall key conclusion is that a given creep strain is less damaging the faster it is accumulated. This is true under various high temperature loading conditions (creep rupture, stress relaxation and creep fatigue) and is supported by all experiments conducted within this work (this behaviour was also supported and accurately captured by the FEA using a strain rate dependent ductility). Smaller effective creep ductilities may therefore apply at the very slow strain rates relevant to plants operating for several decades.

8.2 Future Work

Based on the conclusions made the following recommendations for future work are suggested:

1. Conducting creep rupture experiments on specimens with varying notch acuities to see if reducing the time to failure by increasing the sharpness of the notch leads to an increased creep strain on failure as the results from this Thesis suggest.
2. Conducting creep rupture experiments on pre-strained notched bar specimens to determine whether adding plasticity prior to creep reduces the specimens creep life in the same way as adding plasticity during creep was shown to reduce creep life in the creep fatigue experiments.
3. Conducting creep fatigue experiments on round bar specimens to determine whether adding plasticity between dwells reduces the creep life in the same way as in the notched bar creep fatigue experiments conducted. Previous research by Tim Joseph [47] has shown the prior plasticity can improve a material's creep life in round bar specimens.
4. The most serious shortcoming of this work is the use of high stresses. The conclusions ideally need confirming for lower stresses – with the obvious problem the failure times will be far longer.

Chapter 9 References

1. Coleman, S.L., *Stress relaxation of ex-Heysham 1 Superheater Header Type 316H stainless steel.* Nuclear Electric Report: EPD/HYA/REP/0097/96, Nuclear Electric, Gloucester, 1996.
2. D, M., *The physics of high temperature creep in metals.* Reports on Progress in Physics, 1966. 29.
3. Smith, T.A., and R. G. Warwick, *A survey of defects in pressure vessels built to high standards of construction and its relevance to nuclear primary circuits.* International Journal of Pressure Vessels and Piping, 1974. 2.4: p. 283-322.
4. Spindler, M.W., *The multiaxial creep ductility of austenitic stainless steels.* Fatigue & Fracture of Engineering Materials & Structures, 2004. 27(4): p. 273-281.
5. E1351-96, A., *Standard practice for production and evaluation of metallographic replicas.* ASTM, 1996.
6. Gomez, G., T. Perez, and H.K.D.H. Bhadeshia, *Air cooled bainitic steels for strong, seamless pipes Part 2-properties and microstructure of rolled material.* Materials Science and Technology, 2009. 25(12): p. 1508-1512.
7. Bettinson, A.D., *The influence of constraint on the creep crack growth of 316H stainless steel.* PhD Thesis, Imperial College London, London, 2001.
8. Li, C.X. and T. Bell, *Corrosion properties of active screen plasma nitrided 316 austenitic stainless steel.* Corrosion Science, 2004. 46(6): p. 1527-1547.
9. Khayatzadeh, S., *Creep Deformation and Crack Incubation of Martensitic Steels under Different Boundary Conditions.* PhD Thesis, University of Bristol, UK, 2016.
10. Shaikh, H., N. Sivaibharasi, B. Sasi, T. Anita, R. Amirthalingam, B.P.C. Rao, T. Jayakumar, H.S. Khatak, and B. Raj, *Use of eddy current testing method in detection and evaluation of sensitisation and intergranular corrosion in austenitic stainless steels.* Corrosion Science, 2006. 48(6): p. 1462-1482.
11. Hayhurst, D.R., F. Vakili-Tahami, and J.Q. Zhou, *Constitutive equations for time independent plasticity and creep of 316 stainless steel at 550 degrees C.* International Journal of Pressure Vessels and Piping, 2003. 80(2): p. 97-109.
12. Oh, C.S., N.H. Kim, Y.J. Kim, C. Davies, K. Nikbin, and D. Dean, *Creep failure simulations of 316H at 550 degrees C: Part I - A method and validation.* Engineering Fracture Mechanics, 2011. 78(17): p. 2966-2977.

13. Davies, C.M., *Crack Initiation and Growth at Elevated Temperatures in Engineering Steels. PhD thesis, Imperial College London.* 2006.
14. Santos, T.G., P.L. Inacio, A.A. Costa, R.M. Miranda, and C.C.C.R. de Carvalho, *A New NDT Technique Based on Bacterial Cells to Detect Micro and Nano Surface Defects.* Soldagem & Inspecao, 2015. 20(2): p. 253-259.
15. Stoter, L.P., *Thermal Aging Effects in Aisi Type 316 Stainless-Steel.* Journal of Materials Science, 1981. 16(4): p. 1039-1051.
16. ODonnell, I.J., H. Huthmann, and A.A. Tavassoli, *The fracture toughness behaviour of austenitic steels and weld metal including the effects of thermal ageing and irradiation.* International Journal of Pressure Vessels and Piping, 1996. 65(3): p. 209-220.
17. Spindler, M.W., *Creep behavior of ex-service Type 316H.* Unpublished work.
18. Kim, N.H., C.S. Oh, Y.J. Kim, C.M. Davies, K. Nikbin, and D.W. Dean, *Creep failure simulations of 316H at 550 degrees C: Part II - Effects of specimen geometry and loading mode.* Engineering Fracture Mechanics, 2013. 105: p. 169-181.
19. Takahashi, Y., H. Shibamoto, and K. Inoue, *Long-term creep rupture behavior of smoothed and notched bar specimens of low-carbon nitrogen-controlled 316 stainless steel (316FR) and their evaluation.* Nuclear Engineering and Design, 2008. 238(2): p. 310-321.
20. Wang, Y.Q., M.W. Spindler, C.E. Truman, and D.J. Smith, *Critical analysis of the prediction of stress relaxation from forward creep of Type 316H austenitic stainless steel.* Materials & Design, 2016. 95: p. 656-668.
21. Fookes, A., S.X. Li, D.J. Smith, and M.W. Spindler, *Stress relaxation during dwells for creep and fatigue cycling of Type 316H stainless steel at 550° C.* 2nd International ECCC Conference, 2009.
22. Wang, Y., C.E. Truman, and D.J. Smith, *CREEP DEFORMATION OF TYPE 316H AUSTENITIC STAINLESS STEEL AT 550 C AND THE EFFECTS OF ELASTIC FOLLOW-UP*. 2009.
23. Energy, E., *High Temperature Behaviour of Austenitic Stainless Steels - Validation of creep damage models by FEA of Type 316H notched bar relaxation tests.* Systems and Engineering Technology.
24. Draper, J. *How to prevent plant fatigue creeping up on you*. 2008 10/08/2018]; Available from: https://www.powerengineeringint.com/articles/print/volume-16/issue-1/features/boiler-maintenance/how-to-prevent-plant-fatigue-creeping-up-on-you.html.

25. Yan, X.L., X.C. Zhang, S.T. Tu, S.L. Mannan, F.Z. Xuan, and Y.C. Lin, *Review of creep-fatigue endurance and life prediction of 316 stainless steels.* International Journal of Pressure Vessels and Piping, 2015. 126: p. 17-28.
26. Mamun, A.A., R.J. Moat, J. Kelleher, and P.J. Bouchard, *Generation of intergranular strains during high temperature creep fatigue loading of 316H stainless steel.* Materials at High Temperatures, 2014. 31(4): p. 378-382.
27. Takahashi, Y., *Evaluation of creep-fatigue life prediction methods for low-carbon nitrogen-added 316 stainless steel.* Journal of Engineering Materials and Technology-Transactions of the Asme, 1998. 120(2): p. 119-125.
28. Spindler, M.W. and C.C. Cotton, *Creep-fatigue crack growth in type 316h stainless steel through a zone of tensile residual stress.* Materials at High Temperatures, 1998. 15(2): p. 117-121.
29. Takahashi, Y., H. Shibarnoto, and K. Inoue, *Study on creep-fatigue life prediction methods for low-carbon nitrogen-controlled 316 stainless steel (316FR).* Nuclear Engineering and Design, 2008. 238(2): p. 322-335.
30. Takahashi, Y., *Further evaluation of creep-fatigue life prediction methods for low-carbon nitrogen-added 316 stainless steel.* Journal of Pressure Vessel Technology-Transactions of the Asme, 1999. 121(2): p. 142-148.
31. Shankar, V., K. Mariappan, R. Sandhya, and K. Laha, *Understanding low cycle fatigue and creep-fatigue interaction behavior of 316 L(N) stainless steel weld joint.* International Journal of Fatigue, 2016. 82: p. 487-496.
32. Hormozi, R., F. Biglari, and K. Nikbin, *Experimental and numerical creep-fatigue study of Type 316 stainless steel failure under high temperature LCF loading condition with different hold time.* Engineering Fracture Mechanics, 2015. 141: p. 19-43.
33. Valsan, M., A. Nagesha, K.B.S. Rao, and S.L. Mannan, *A comparative evaluation of low cycle fatigue and creep-fatigue interaction behaviour of 316L(N) stainless steel, 316 weld metal and 316L(N)/316 weld joint at 873 K.* Transactions of the Indian Institute of Metals, 2000. 53(3): p. 263-271.
34. Choi, B.G., S.W. Nam, and J. Ginsztler, *Life extension by cavity annihilation heat treatment in AISI 316 stainless steel under creep-fatigue interaction conditions.* Journal of Materials Science, 2000. 35(7): p. 1699-1705.
35. Marie, S. and C. Delaval, *Fatigue and creep-fatigue crack growth in 316 stainless steel cracked plates at 650 degrees C.* International Journal of Pressure Vessels and Piping, 2001. 78(11-12): p. 847-857.

36. Liu, D., D.J. Pons, and E.H. Wong, *The Unified Creep-Fatigue Equation for Stainless Steel 316.* Metals, 2016. 6(9).
37. R5, *Assessment procedure for the high temperature response of structures.* British Energy Generation Ltd., Gloucester., 2001.
38. Holmlund, D.E.W., *Physical-Properties of Surgical Suture Materials - Stress-Strain Relationship, Stress-Relaxation and Irreversible Elongation.* Annals of Surgery, 1976. 184(2): p. 189-193.
39. Cocks, A.C.F. and M.F. Ashby, *Intergranular Fracture during Power-Law Creep under Multiaxial Stresses.* Metal Science, 1980. 14(8-9): p. 395-402.
40. B.F, W.K.a.D., *Creep Fatigue Interactions in 316 Stainless Steel Under Torsional Loading.* Mechanical Behaviour and Nuclear Applications of Stainless Steel at Elevated Temperatures, 1982. Book 280, p136 140, The Metals Society, London.
41. Murakami S, K.M.a.Y.Y., *Creep After Cyclic Plasticity Under Multi Axial Conditions for Type 316 Stainless Steel at Elevated Temperature, Trans ASME, Vol 112, p346 352.* 1990.
42. Tavassoli, A.A., M. Mottot, and P. Petrequin, *Sequential Creep-Fatigue Interaction in Austenitic 316-L-Sph Stainless-Steel.* Theoretical and Applied Fracture Mechanics, 1988. 10(1): p. 49-57.
43. Fookes, A.J., S.X. Li, and D.J. Smith, *Influence of prior cyclic hardening on high temperature deformation and crack growth in type 316L (N) stainless steel.* Materials at High Temperatures, 1998. 15(3-4): p. 187-193.
44. Skelton, R.P. and C.A.P. Horton, *The effect of thermal ageing and mechanical exposure on low cycle creep-fatigue strength of 316 steel at 625 degrees C.* Materials at High Temperatures, 1999. 16(2): p. 87-97.
45. Rezgui B, P.P.a.M.M., *Hold Time Effects on Low Cycle Fatigue Properties of 316L Stainless Steel at 600°C and 650°C", in "Advances in Fracture Research, editor D François, Vol 5, p2393 2402, Pergamon, London* 1981.
46. B, R., *Interaction Fatigue Fluage Environnement dans un Acier Inoxydable Austenitique Z2 CND 17 13 (Type 316L) à 600 et 650C: Evolution Microstructurale et Endommagement, PhD Thesis, Universite de Paris Sud, CentreD'Orsay* 1982.
47. Joseph, T.D., Truman, C.E. and Smith, D.J., *British Energy High Temperature Centre End of Year Report 2010/2011.* Department of Mechanical Engineering, University of Bristol, Bristol, BS8 1TR, UK, 2011.

48. M, S., *Discussion document-creep constitutive models for type 316H.* British Energy, 2010.
49. MF, F.H.a.A., *Deformation-mechanism maps: the plasticity and creep of metals and ceramics.* Oxford: Pergamon Press, 1982.
50. WR, R.W.a.O., *Determination of stress-strain curves by three parameters.* National Advisory Committee on Aeromautics (NACA), 1941. 503.
51. DL, P.R.a.M., *Design for creep.* London: Chapman & Hall, 1995. 2nd Edition.
52. Brown, M.H., K.F. Hale, and Lagnebor.R, *Correlation between Observed Creep Behavior from in-Situ Experiments in Hvem and Predicted Behavior from Recovery Creep Theory.* Scripta Metallurgica, 1973. 7(12): p. 1275-1278.
53. Kachanov, L.M., *On Creep Stresses in a Bridgman Notched Bar.* Mechanics of Materials, 1986. 5(3): p. 229-234.
54. Kachanov, L.M., *Rupture time under creep conditions.* International Journal of Fracture, 1999. 97(1-4): p. Xi-Xviii.
55. Kachanov, L.M., N.V. Volkova, and E.A. Khein, *An Analysis of Methods for the Evaluation of the Limiting-Creep Stress in Metals.* Industrial Laboratory, 1962. 28(12): p. 1646-1648.
56. Kachanov, L., *Crack and Damage Growth in Creep - a Combined Approach.* International Journal of Fracture, 1980. 16(4): p. R179-R181.
57. Kachanov, L.M., *Growth of Cracks under Creep Conditions.* International Journal of Fracture, 1978. 14(2): p. R51-R52.
58. FH, N., *The creep of steel temperature at high temperature.* McGraw-Hill, New York, USA, 1929.
59. Blum, W., P. Eisenlohr, and F. Breutinger, *Understanding creep - a review.* Metallurgical and Materials Transactions a-Physical Metallurgy and Materials Science, 2002. 33(2): p. 291-303.
60. Estrin, Y. and H. Mecking, *A Unified Phenomenological Description of Work-Hardening and Creep Based on One-Parameter Models.* Acta Metallurgica, 1984. 32(1): p. 57-70.
61. Spindler, M.W., R. Hales, and R.P. Skelton, *The Multiaxial Creep Ductility of an Ex-Service Type 316H Stainless Steel.* 9th International Conference on Creep and Fracture of Engineering Materials and Structures, 2001: p. 679-688.

62. Alfaddagh, K.D., R.T. Fenner, and G.A. Webster, *Steady-State Stress Distributions in Circumferentially Notched Bars Subjected to Creep.* Journal of Strain Analysis for Engineering Design, 1982. 17(3): p. 123-132.
63. Liu, Y. and S. Murakami, *Damage localization of conventional creep damage models and proposition of a new model for creep damage analysis.* Jsme International Journal Series a-Solid Mechanics and Material Engineering, 1998. 41(1): p. 57-65.
64. *British Standards Institute, Metallic Materials – Uniaxial Creep Testing in Tension – Method of Test.* BS EN 10291:2000, London 2000.
65. Hyde, T.H., W. Sun, A.A. Becker, and J.A. Williams, *Creep continuum damage constitutive equations for the base, weld and heat-affected zone materials of a service-aged 1/2Cr1/2Mo1/4V:21/4Cr1Mo multipass weld at 640 degrees C.* Journal of Strain Analysis for Engineering Design, 1997. 32(4): p. 273-285.
66. Hyde, T.H., W. Sun, and C.J. Hyde, *Applied creep mechanics*. 2014, New York: McGraw-Hill. xiv, 370 pages.
67. Dyson, B.F., *Creep behaviour of advanced materials for the 21st century.* TMS Annual Meeting in San Diego, California, 1999.
68. Dyson, B.F. and M. Mclean, *Creep Deformation of Engineering Alloys - Developments from Physical Modeling.* Isij International, 1990. 30(10): p. 802-811.
69. Hyde, C.J., *Thermo-mechanical fatigue and creep at high temperature.* PhD Thesis, the University of Nottingham, 2010.
70. Kim, B.J. and B.S. Lim, *Effect of creep holding time on the fatigue behavior in P92 steel weldment at high temperature.* Pricm 5: The Fifth Pacific Rim International Conference on Advanced Materials and Processing, Pts 1-5, 2005. 475-479: p. 4211-4214.
71. Kowalewski, Z.L., D.R. Hayhurst, and B.F. Dyson, *Mechanisms-Based Creep Constitutive-Equations for an Aluminum-Alloy.* Journal of Strain Analysis for Engineering Design, 1994. 29(4): p. 309-316.
72. Webster, G.A., S.R. Holdsworth, M.S. Loveday, K. Nikbin, I.J. Perrin, H. Purper, R.P. Skelton, and M.W. Spindler, *A Code of Practice for conducting notched bar creep tests and for interpreting the data.* Fatigue & Fracture of Engineering Materials & Structures, 2004. 27(4): p. 319-342.
73. Spindler, M.W., Hales, R. and Skelton, R. P, *The Multiaxial Creep Ductility of an Ex-Service Type 316H Stainless Steel.* 9th International Conference on Creep and Fracture of Engineering Materials and Structures, 2001: p. 679-688.

74. Kassner, M.E. and T.A. Hayes, *Creep cavitation in metals.* International Journal of Plasticity, 2003. 19(10): p. 1715-1748.
75. Abaqus, *Abaqus 6.14. [ONLINE] Available at: http://abaqus.software.polimi.it/v6.14/index.html. [Accessed 9 October 2017]*. 2017.
76. Spindler, M.W., *The multiaxial and uniaxial creep ductility of Type 304 steel as a function of stress and strain rate.* Materials at High Temperatures, 2004. 21(1): p. 47-54.
77. Spindler, M.W. and M.C. Smith, *The effect of multiaxial states of stress on creep failure of Type 316h under displacement control.* Proc. PVP2009, 2009.
78. Oh CS, Nah-Hyun Kim, Sung-Hwan Min, and Y.-J. Kim, *Finite Element Damage Analysis for Predictions of Creep Crack Growth.* Proceedings of the ASME 2010 Pressure Vessels and Piping Division, 2010: p. 1-5.
79. R66, *AGR Materials data handbook, Issue 5. British Energy Generation Ltd., Gloucester*. 1999.
80. Spindler, M.W. and M.C. Smith, *High temperature creep properties of Type 316H stainless steel.* British Energy Generation Ltd., Gloucester., 2009.
81. Rice, J.R. and D.M. Tracey, *On Ductile Enlargement of Voids in Triaxial Stress Fields.* Journal of the Mechanics and Physics of Solids, 1969. 17(3): p. 201-+.
82. Hales, R., *The Role of Cavity Growth Mechanisms in Determining Creep-Rupture under Multiaxial Stresses.* Fatigue & Fracture of Engineering Materials & Structures, 1994. 17(5): p. 579-591.
83. Hayhurst, D.R., F.A. Leckie, and J.T. Henderson, *Design of Notched Bars for Creep-Rupture Testing under Triaxial Stresses.* International Journal of Mechanical Sciences, 1977. 19(3): p. 147-159.
84. Hayhurst, D.R., P.R. Dimmer, and C.J. Morrison, *Development of Continuum Damage in the Creep-Rupture of Notched Bars.* Philosophical Transactions of the Royal Society a-Mathematical Physical and Engineering Sciences, 1984. 311(1516): p. 103-+.
85. Hayhurst and Webster, *An overview on studies of stress state effects during creep of circumferentially notched bars.* , in: Gooch, D.J., How, I.M., editors. Techniques for multiaxial creep testing, Amsterdam: Elsevier, 137-143, 1986.
86. Spindler, M.W., *The Multiaxial Creep of Austenitic Stainless Steels.* Nuclear Electric Report TIGM/REP/0014/94., 1994.
87. Hares, E.A., C.E. Truman, M. Mostafavi, and R.A.W. Bradford, *The Influence of Creep Strain Rate on Creep Damage*

Formation in Austenitic Stainless Steel. Pressure Vessels and Piping Conference Prague. Technical Paper Publication: PVP2018-84635, 2018.

88. Webster, G.A., K.M. Nikbin, and F. Biglari, *Finite element analysis of notched bar skeletal point stresses and dimension changes due to creep.* Fatigue & Fracture of Engineering Materials & Structures, 2004. 27(4): p. 297-303.
89. Kang, G.Z., Q.H. Kan, J. Zhang, and Y.F. Sun, *Time-dependent ratchetting experiments of SS304 stainless steel.* International Journal of Plasticity, 2006. 22(5): p. 858-894.
90. Yatomi, M., et al., *Modelling of damage development and failure in notched-bar multiaxial creep tests.* Fatigue & Fracture of Engineering Materials & Structures 2004. 27.4: p. 283-295.
91. Mehmanparast, Davies, Dean, and Nikbin, *Effects of plastic pre-straining level on the creep deformation, crack initiation and growth behaviour of 316H stainless steel.* . International Journal of Pressure Vessels and Piping, 2016. 141: p. 1-10.
92. Yamashita, M. and Y. Wada, *The Stress-Relaxation Behavior of Type-304 Stainless-Steel.* International Journal of Pressure Vessels and Piping, 1990. 42(2): p. 203-216.
93. L, R.E., *The resistance to relaxation of materials at high temperature.* Trans ASME 1939;61:543-54., 1939.
94. Boyle, J.T. and K. Nakamura, *The Assessment of Elastic Follow-up in High-Temperature Piping Systems - Overall Survey and Theoretical Aspects.* International Journal of Pressure Vessels and Piping, 1987. 29(3): p. 167-194.
95. Wang Y, T.C.E.a.S.D.J., *Inelastic deformation and elastic follow-up.* PVP, Paris., 2013.
96. Boyle, J.T., *Stress relaxation and elastic follow-up using a stress range-dependent constitutive model.* Proceedings of the Institution of Mechanical Engineers Part C-Journal of Mechanical Engineering Science, 2012. 226(C6): p. 1472-1483.
97. Wang Y, T.C. E, and S.D. J., *Effect of elastic follow-up on the creep stress relaxation of Type 316H austenitic stainless steel at 550°C.* ECCC 2014, 2014.
98. K. Aoto, T. Koakutsu, Y. Wada, and M. Hirano, *The prediction of the stress relaxation behaviour of the high-temperature structural materials by creep–strain equations.* International Conference on Creep 1986, pp. 495–500., 1986.
99. Krempl, E., *An Experimental-Study of Room-Temperature Rate-Sensitivity, Creep and Relaxation of Aisi Type-304 Stainless-Steel.* Journal of the Mechanics and Physics of Solids, 1979. 27(5-6): p. 363-375.
100. Trumpler, W.E., *Relaxation of metals at high temperatures.* Journal of Applied Physics, 1941. 12(3): p. 248-253.

101. Wang, Y., Truman, C.E. and Smith, D.J., *CREEP DEFORMATION OF TYPE 316H AUSTENITIC STAINLESS STEEL AT 550 C AND THE EFFECTS OF ELASTIC FOLLOW-UP*. 2009.

102. Aoto, K., T. Koakutsu, Y. Wada, and M. Hirano, *The Prediction of The Stress Relaxation Behavior of The High-Temperature Structural Materials by Creep-Strain Equations*. Proceedings, International Conference on Creep, Tokyo, Japan, pp. 495–500., 1986.

APPENDIX I – Sub routines

The Spindler damage subroutine used is detailed below with areas that were changed for the various models highlighted in red.

```
**
C THIS SET OF ABAQUS USER SUBROUTINES CALCULATES CREEP DAMAGE IN TYPE 316H STAINLESS STEEL CAST 69431 HEADER 2C2/3
C THE RCC-MR CREEP DEFORMATION LAW, DUCTILITY EXHAUSTION AND THE SPINDLER FRACTION ARE ALL IMPLEMENTED.
      BLOCK DATA KDAT
      INCLUDE 'ABA_PARAM.INC'
C     INITIALISE DAMAGE ARRAYS
      REAL*4 SDAMAGE(30000,14),EDAMAGE(30000,14)
      INTEGER*4 KINCUV(30000,14)
      COMMON/KDAM/SDAMAGE,EDAMAGE,KINCUV
      DATA SDAMAGE/420000*0.E0/
           DATA EDAMAGE/420000*0.E0/
C     INITIALISE NAME AND PROPERTIES OF MATERIAL
      CHARACTER*8 CMN(10)
      REAL*8 RFAC(10),EFU(10),DL(10),SL(10),DU(10),SU(10),P(10),Q(10)
      COMMON/KPROPS/CMN,RFAC,EFU,DL,SL,DU,SU,P,Q
C     SET NAME OF MATERIAL IN ABAQUS MODEL
      DATA CMN/'C69431'/
C
C     SET RCC-MR CREEP LAW FACTORS
```

```
      DATA RFAC/1.0/
C     SET THE FIXED UNIAXIAL DUCTILITIES        <---------- This was set to 0.1 (10%)
      DATA EFU/0.0/                             for the model without strain rate dependency
C     IF EFU IS SET TO ZERO, DUCTILITY IS RATE DEPENDENT, SO SET
C     UP A LOWER/UPPER SHELF DESCRIPTION OF RATE DEPENDENCY
      DATA DL/0.10/
      DATA SL/1.0D-05/
      DATA DU/0.293/
      DATA SU/3.232/
C     SET THE SPINDLER FRACTION COEFFS
      DATA P/1.2/
      DATA Q/1.0/
      END
      SUBROUTINE CREEP(DECRA,DESWA,STATEV,SERD,ECO,ESWO,P,QTILD,
     +       TEMP,DTEMP,PREDEF,DPRED,TIME,DTIME,CMNAME,LEXIMP,
     +       LEND,COORDS,NSTATV,NOEL,NPT,LAYER,KSPT,KSTEP,KINC)
C+++++++++++++++++++++++++++++++++++++++++++++++++++++++++++++++++++++++++++++
C THIS SUBROUTINE USES THE RCC-MR EQUATIONS FOR PRI AND SEC CREEP DEFORMATION. TERTIARY CREEP IS MODELLED BY INCLUDING THE DAMAGE IN THE CREEP DEFORMATION FUNCTION.
C IN THE THEORETICAL FORMULATION, STRAIN RATES RISE TO INFINITY AS THE DAMAGE REACHES UNITY, BUT MAXIMUM STRAIN RATES ARE CAPPED BY THIS PROGRAM IN THE INTERESTS OF COMPUTATIONAL EFFICIENCY.
```

```
C A STRAIN HARDENING FORMULATION IS USED THROUGHOUT. STRESS MUST
BE IN MPa AND TIME MUST BE IN HOURS.
C THE SUBROUTINE IS VALID ONLY FOR 515 C AND 550 C.
      INCLUDE 'ABA_PARAM.INC'
      CHARACTER*8 CMNAME,CMN(10)
      REAL*4 SDAMAGE(30000,14),EDAMAGE(30000,14)
      INTEGER*4 KINCUV(30000,14)
      REAL*8 RFAC(10),DUMMY(21)
      DIMENSION DECRA(5),DESWA(5),PREDEF(*),DPRED(*),TIME(2),
     +          STATEV(*),COORDS(*)
      DIMENSION COEF(2,6)
C     ACCESS THE DAMAGE ARRAYS CREATED IN UVARM THROUGH A COMMON
BLOCK
      COMMON/KDAM/SDAMAGE,EDAMAGE,KINCUV
C     ACCESS THE NAME AND PROPERTIES OF THE MATERIAL
      COMMON/KPROPS/CMN,RFAC,DUMMY
C     DEFINE THE TEMPERATURE AND COEFFICIENT TABLE
C+++++++++++++++++++++++++++++++++++++++++++++++++++++++++++++++++++
++++++++++++++
      DATA COEF/
     +  515,  550,
     +  1.8803D-12, 1.89D-12,
     +  0.40053, 0.421,
     +  4.12500, 4.5,
     +  -28.382, -26.604,
```

```
     + 9.06,     9.1703,

C     ABAQUS SOMETIMES PROVIDES A VERY SMALL NEGATIVE CREEP STRAIN AT THE START OF THE INCREMENT (ECO) WHEN IT SHOULD BE ZERO. THIS LEADS TO NUMERICAL

C     PROBLEMS, SO TAKE A COPY AND SET THIS TO ZERO IF NEGATIVE

      ECO1=ECO

      IF (ECO1.LT.0.0D0) ECO1=0.0D0

C     IDENTIFY THE MATERIAL FROM ITS NAME

      MAT=0

      IF(CMNAME.EQ.CMN(1)) MAT=1

      IF(MAT.EQ.0) THEN

         WRITE (7,*)' ERROR - MATERIAL NAME DOES NOT MATCH ANY IN',

     +              ' THE CREEP SUBROUTINE'

         STOP

      ENDIF

C     FIND THE DAMAGE LEVEL FOR THIS ELEMENT INTEGRATION POINT AT THE START OF THE CURRENT INCREMENT. THE FOLLOWING CODING ENSURES THAT THE DAMAGE LEVEL IS THAT AT THE START OF THE CURRENT INCREMENT

      D=SDAMAGE(NOEL,NPT)

      IF (KINC.GT.KINCUV(NOEL,NPT)) D=EDAMAGE(NOEL,NPT)

      IF (QTILD.EQ.0.0D0) THEN

C     SET STRAIN INC AND DERIVS TO ZERO FOR ZERO MISES STRESS, TO AVOID COMPUTATIONAL DIFFICULTIES

      DECRA(1)=0.0D0

      DECRA(2)=0.0D0
```

```
      DECRA(5)=0.0D0
      ELSE
C                SET A MAXIMUM TO THE DAMAGE LEVEL IN ORDER TO AVOID
COMPUTATIONAL DIFFICULTIES
            IF (D.GT.0.999) D=0.999
C             CALCULATE PRIMARY/TERTIARY CREEP STRAIN INCREMENT
C++++++++++++++++++++++++++++++++++++++++++++++++++++++++++++++++++++
++++++++++++++
            EXP=1.0D0/C2                    <--------- These 3 lines were deleted to
remove primary creep
            U1=(C1/100.D0*QTILD**RN1)**EXP
            DE=((ECO1**EXP+U1*DTIME)**C2-ECO1)/(1.D0-D**3)
C             CALCULATE SECONDARY/TERTIARY CREEP STRAIN INCREMENT
            DES=0.0
            IF (T.GE.475) DES=(C*DTIME*QTILD**RN)/(1.D0-D**3)
C             CALCULATE LIMITING CREEP STRAIN INCREMENT (100*SECONDARY
INCREMENT WITHOUT DAMAGE)
            DEA=100.0*C*DTIME*QTILD**RN
C           SELECT THE LARGER OF THE PRIMARY AND SECONDARY INCREMENTS
            DECRA(1)=DE
            IF(DES.GT.DE) DECRA(1)=DES
C             CAP THE INCREMENT IF NECESSARY
            IF (DECRA(1).GT.DEA) DECRA(1)=DEA
            IF (LEXIMP.EQ.1) THEN
C                CALCULATE THE DERIVATIVES OF THE STRAIN INCREMENT FOR
IMPLICIT INTEGRATION
```

```
                IF (DECRA(1).EQ.DE) THEN
C                   STRAIN IN PRIMARY RANGE, CALC DERIVS BY DIFFERENCING
                  U2=(C1/100.D0*(QTILD+1.D-3)**RN1)**EXP
                  DE2=((ECO1**EXP+U2*DTIME)**C2-ECO1)
     +                /(1.D0-D**3)
                  DECRA(5)=(DE2-DE)/1.D-3
                  DE3=(((ECO1+1.D-9)**EXP+U1*DTIME)**C2
     +                -(ECO1+1.D-9))/(1.D0-D**3)
                  DECRA(2)=(DE3-DE)/1.D-9
                ENDIF
                IF (DECRA(1).EQ.DES) THEN
C                   STRAIN IN SECONDARY RANGE
                  DECRA(5)=(C*RN*DTIME*QTILD**(RN-1))
     +                /(1.D0-D**3)
                ENDIF
                IF (DECRA(1).EQ.DEA) THEN
C                   STRAIN RATE CAPPED BY PROGRAM
                  DECRA(5)=100.0*C*RN*DTIME*QTILD**(RN-1)
               ENDIF
             ENDIF
           ENDIF
         ENDIF
       ENDIF
c             STATEV(1)=D
```

```
      RETURN
      END
      SUBROUTINE UVARM(UVAR,DIRECT,T,TIME,DTIME,CMNAME,ORNAME,
     +     NUVARM,NOEL,NPT,NLAYER,KSPT,KSTEP,KINC,NDI,NSHR,
     +     COORD,JMAC,JMATYP,MATLAYO,LACCFLA)
C++++++++++++++++++++++++++++++++++++++++++++++++++++++++++++++++++++++++++
C THIS SUBROUTINE INTEGRATES A CREEP CRACKING DAMAGE FUNCTION FOR
MULTI-AXIAL STRESS STATES BASED ON SPINDLER'S FUNCTION
C THE FUNCTION IS ZERO FOR NO DAMAGE AND 1 FOR THE ONSET OF
CRACKING.
C THE DAMAGE IS INCLUDED IN THE CREEP DEFORMATION LAW CODED IN THE
THE MAX PRINCIPAL, VON MISES, HYDROSTATIC AND EQUIVALENT CREEP
STRAIN INCREMENT AT THE INTEGRATION POINT ARE EXTRACTED FROM
C ABAQUS. THESE ARE THEN COMBINED INTO THE FUNCTION, USING
MATERIAL CONSTANTS(P AND Q FOR THE SPINDLER FRACTION, DU AND DL
FOR THE UPPER AND LOWER SHELF UNIAXIAL DUCTILITIES, SU AND SL FOR
THE STRAIN RATES DEFINING THE LOWER
C LIMIT OF UPPER SHELF BEHAVIOUR AND THE UPPER LIMIT OF LOWER SHELF
BEHAVIOUR, RESPECTIVELY) DEFINED IN THIS ROUTINE, AND ADDED TO THE
PREVIOUS VALUE OF THE FUNCTION.
C THE DAMAGE FUNCTION IS STORED IN USER VARIABLE UVAR(1), AND THE
VALUE OF CREEP STRAIN IN THE PREVIOUS INCREMENT IS STORED IN
UVAR(2).THE CURRENT DAMAGE LEVEL FOR ALL ELEMENT INTEGRATION
POINTS IS ENTERED.
C THE ARRAYS 'SDAMAGE' AND 'EDAMAGE' FOR DAMAGE AT THE START AND
END OF THE INCREMENT RESPECTIVELY. THE ARRAY KINCUV RECORDS THE
CURRENT INCREMENT NO.
```

```
C THESE ARE IN A COMMON BLOCK SO THAT THEY CAN BE ACCESSED BY THE
CREEP USERSUB.
      INCLUDE 'ABA_PARAM.INC'
      REAL*8 MISES
      CHARACTER*8 CMNAME,ORNAME,FLGRAY(15),CMN(10)
      REAL*4 SDAMAGE(30000,14),EDAMAGE(30000,14)
      REAL*8 RFAC(10),EFU(10),DL(10),SL(10),DU(10),SU(10),P(10),Q(10)
      INTEGER*4 KINCUV(30000,14)
      DIMENSION UVAR(NUVARM),DIRECT(3,3),T(3,3),TIME(2)
      DIMENSION ARRAY(15),JARRAY(15),JMAC(*),JMATYP(*),COORD(*)
C     STORE THE DAMAGE ARRAYS IN A COMMON BLOCK SO THAT THEY ARE
ACCESSIBLE TO OTHER USER SUBROUTINES
      COMMON/KDAM/SDAMAGE,EDAMAGE,KINCUV
C     ACCESS THE NAMES AND PROPERTIES OF THE MATERIAL
      COMMON/KPROPS/CMN,RFAC,EFU,DL,SL,DU,SU,P,Q
C++++++++++++++++++++++++++++++++++++++++++++++++++++++++++++++++++++
++++++++++++++
C     IDENTIFY THE MATERIAL FROM ITS NAME
      MAT=0
      IF(CMNAME.EQ.CMN(1)) MAT=1
      IF(MAT.EQ.0) THEN
         WRITE (7,*)' ERROR - MATERIAL NAME DOES NOT MATCH ANY IN',
     +              ' THE CREEP SUBROUTINE'
         STOP
      ENDIF
```

```
C     INITIALISE THE USER VARIABLES IF THIS IS A NEW START OR A RESTART
      IF (EDAMAGE(NOEL,NPT).EQ.0.E0) THEN
        UVAR(1)=0.0D0
        UVAR(2)=0.0D0
      ENDIF
C     STORE THE DAMAGE AT THE START OF THE INCREMENT FOR THIS ELEMENT
INTEGRATION POINT
      SDAMAGE(NOEL,NPT)=UVAR(1)
C     RETRIEVE THE 3 PRINCIPAL STRESSES AND SELECT THE (ALGEBRAICALLY)
LARGEST
      CALL
GETVRM('SP',ARRAY,JARRAY,FLGRAY,JRCD,JMAC,JMATYP,MATLAYO,
     + LACCFLA)
      PRINC=ARRAY(3)
C     RETRIEVE THE STRESS INVARIANTS AND SELECT THE VON MISES AND
HYDROSTATIC STRESSES
      CALL
GETVRM('SINV',ARRAY,JARRAY,FLGRAY,JRCD,JMAC,JMATYP,MATLAYO,
     + LACCFLA)
      MISES=ARRAY(1)
      HYDRO=-ARRAY(3)
C     RETRIEVE THE CREEP STRAIN, SELECT THE EQUIVALENT CREEP STRAIN
AND FIND THE STRAIN INCREMENT BY SUBTRACTING THE CREEP STRAIN AT
THE END OF THE PREVIOUS INCREMENT. ALSO CALCULATE THE CREEP STRAIN
RATE
      CALL
GETVRM('CE',ARRAY,JARRAY,FLGRAY,JRCD,JMAC,JMATYP,MATLAYO,
```

```
     + LACCFLA)
      IF (JRCD.EQ.0) THEN
         E=ARRAY(7)-UVAR(2)
         ER=E/DTIME
      ELSE
C        AN ERROR HAS BEEN ENCOUNTERED. THIS WILL USUALLY BE BECAUSE THIS IS NOT A CREEP STEP, SO EXIT WITHOUT CHANGING USER VARIABLES
         RETURN
      ENDIF
C     CHECK FOR SMALL CREEP STRAIN RATE, TO AVOID NUMERICAL PROBLEMS IN CALCULATION. (A VERY SMALL OR ZERO RATE WILL OCCUR IN A NON-CREEPING STEP OR AT THE END OF STRESS RELAXATION.)
      IF (ER.LT.1.0D-11) RETURN
C     CHECK FOR SMALL MISES STRESS, TO OVERCOME POTENTIAL NUMERICAL PROBLEMS IN THE CALCULATION. IF MISES STRESS IS SMALL, THEN FAILURE FUNCTION INCREMENT NEGLIGIBLE (SINCE CREEP STRAIN INCREMENT IS VERY SMALL)
      IF (MISES.GT.0.0001D0) THEN
C        IF THE ELEMENT DAMAGE LEVEL ALREADY EXCEEDS UNITY, DO NOT INCREASE IT FURTHER (SINCE CREEP STRAINS ARE ARTIFICIAL THEREAFTER AND THE DAMAGE FUNCTION IS NOT MEANINGFUL)
         IF(UVAR(1).GE.1.D0) THEN
            CONTINUE
         ELSE
C           CALCULATE THE INVERSE OF THE SPINDLER FRACTION(BUT CAP AT A MAXIMUM OF 10,000)
            SLN=(P(MAT)*(PRINC/MISES-1))+(Q(MAT)/2*(3*HYDRO/MISES-1))
```

```
      IF(SLN.GT.9.21) SLN=9.21
      SPIND=DEXP(SLN)
C     FIND THE UNIAXIAL DUCTILITY FOR THE MATERIAL
C     FIRST ASSUME DUCTILITY IS RATE INDEPENDENT
      EFUNI=EFU(MAT)
      IF (EFUNI.EQ.0.0D0) THEN
C     DUCTILITY IS RATE DEPENDENT, SO CALCULATE THE EQUIVALENT
UNIAXIAL CREEP STRAIN RATE AND THE GRADIENT (IN NATURAL LOG
COORDINATES) OF THE RATE DEPENDENCY LINE IN THE LOWER TO UPPER
SHELF TRANSITION REGION
        ERATE=E/DTIME*SPIND
        GTR=(DLOG(DU(MAT))-DLOG(DL(MAT)))/
     +      (DLOG(SU(MAT))-DLOG(SL(MAT)))
C       CALCULATE THE RATE DEPENDENT UNIAXIAL CREEP DUCTILITY
USING THE LOWER/UPPER SHELF MODEL.
        IF (ERATE.LE.SL(MAT)) THEN
          EFUNI=DL(MAT)
        ELSE
          IF (ERATE.GE.SU(MAT)) THEN
            EFUNI=DU(MAT)
          ELSE
            EFUNI=EXP((DLOG(ERATE)-DLOG(SL(MAT)))*GTR
     +          +DLOG(DL(MAT)))
          ENDIF
        ENDIF
```

```
          ENDIF
C          INTEGRATE THE DAMAGE FUNCTION OVER THE CURRENT INCREMENT
          UT1=DLOG(E)+SLN-DLOG(EFUNI)
C                CHECK TO PREVENT INCREASE OF DAMAGE FUNCTION ABOVE
UNITY.(VERY LARGE DAMAGE INCREMENTS COULD OCCUR IF AN ELEMENT
HAS NOT BEEN ALLOWED TO FAIL AND THE MISES STRESS DROPS VERY LOW
DUE TO TERTIARY CREEP
          IF (UT1.GT.0.D0) UT1=0.D0
          UVAR(1)=UVAR(1)+DEXP(UT1)
          IF (UVAR(1).GT.1.D0) UVAR(1)=1.D0
        ENDIF
      ENDIF
C     STORE THE CURRENT VALUE OF CREEP STRAIN
      UVAR(2)=ARRAY(7)
C     ENSURE ARRAY 'DAMAGE' SIZE IS NOT EXCEEDED
      IF(NOEL.GT.30000.OR.NPT.GT.14) THEN
        WRITE(7,*)' ERROR IN USERSUB UVARM - TOO MANY ELEMENTS OR',
     +          'INTEGRATION POINTS TO BE MONITORED FOR FAILURE'
        STOP
C++++++++++++++++++++++++++++++++++++++++++++++++++++++++++++++++++++
++++++++++++++
      ENDIF
C     STORE THE CURRENT INCREMENT NUMBER AND THE DAMAGE AT THE END
OF THE INCREMENT FOR THIS ELEMENT INTEGRATION POINT
      KINCUV(NOEL,NPT)=KINC
      EDAMAGE(NOEL,NPT)=UVAR(1)
```

```
      RETURN
      END
C
**********************************************************************
**
```

APPENDIX II – A guide to conducting stress relaxation/elastic follow-up tests on rigs 7 and 9

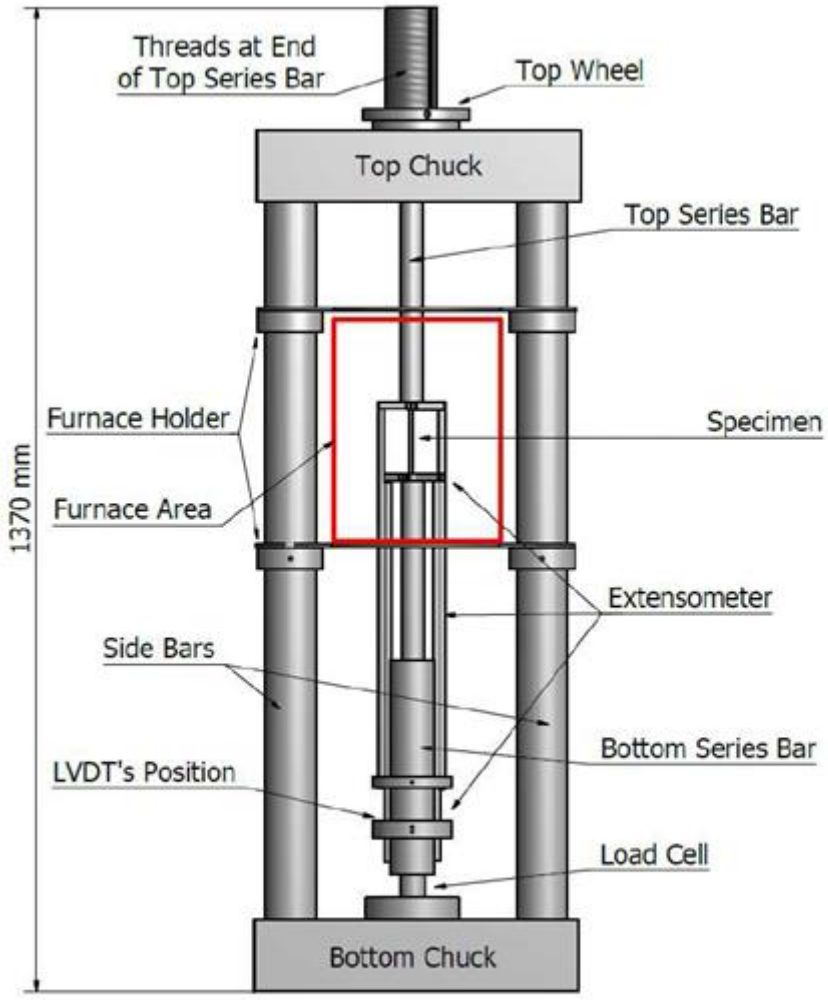

Uniaxial stress relaxation test rig

Ed Hares

General tasks

1. Check the specimen for manufacturing quality. Ensure that there are no radial tool marks/deep scratches, that the surface quality of the gauge length is adequate, that the threaded ends are machined correctly and a standard Ml0 nut turns smoothly along the entire length of the thread and that there are no burrs on the extensometry ridges.
2. Measure the dimensions of the specimen to ensure compliance with the tolerances specified for manufacture and correct calculation of stresses and strains. The diameter should be carefully measured using the digital micrometers, taking at least three readings along the gauge length of the sample to ensure that the diameter is constant along the gauge length. Measuring too close to the extensometry ridges may result in an erroneously high reading of the diameter due to the radii connecting the ridge to the gauge length.

3. Measure the gauge length of the sample using the shadowgraph. Consult with Steve Harding if you are not sure how to use this machine. Recommended practice is to measure the gauge length four times, rotating the specimen 45˚ between measurements and taking the average of the four measurements.
4. On the PC connected to the data logger, open the folder "Rig X" on the desktop corresponding to the creep rig that you intend to use. Within this folder there will be

a folder called "Templates Rig X" in addition to folders with names such as "01 - EXI", "02 ` EX6", etc. Create a copy of the "Templates Rig X" folder and rename it to place it at the end of the numerical sequence of the other folders with a name of the form "xx - yyy" where yyy is the name/code of the test to be started. Within this new test folder will be all of the template files required to calibrate and test the rig and to display the results of the test.

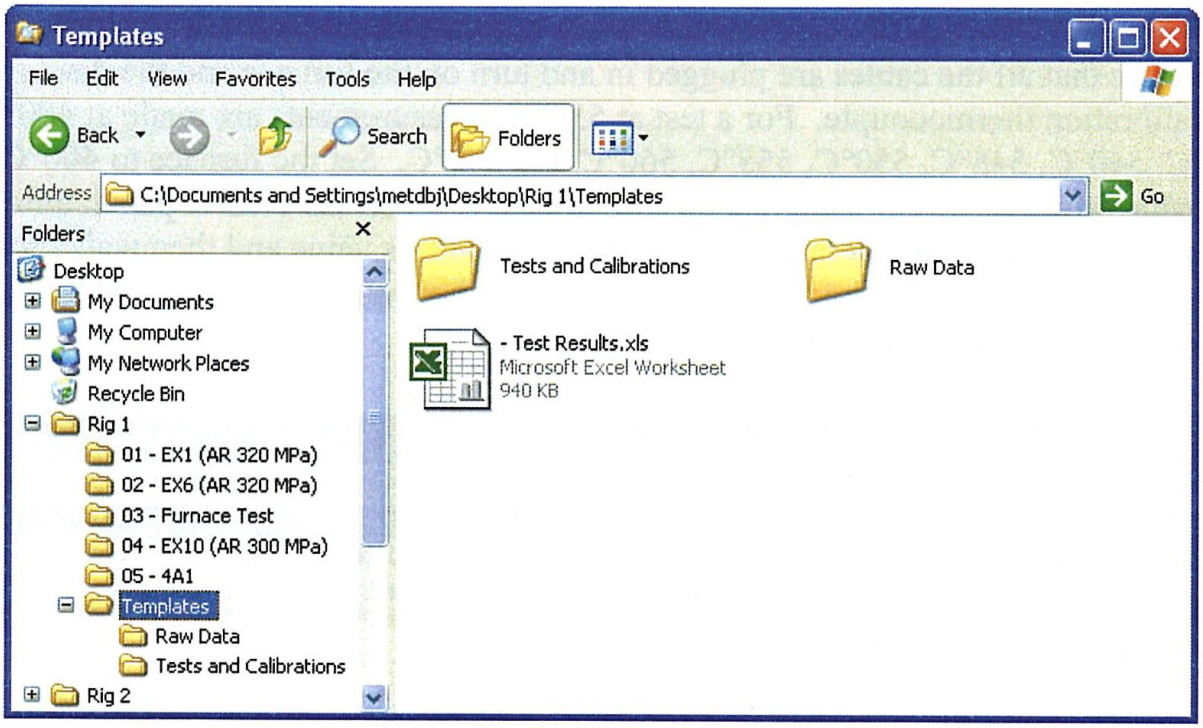

Calibrate the thermocouples

5. Calibrate the thermocouples on the rig to be used in the test. Insert the 6.4 mm diameter reference thermocouple into one of the larger wells in the calibration furnace. Straighten and insert the thermocouples to be calibrated. Make sure that the insulation on the thermocouples is not covering the tip and that the thermocouples are inserted all the way into the well so that the tip makes contact with the base. Fill the top of the calibration furnace with a small amount of insulation. In some cases it is possible to calibrate all the thermocouples from two adjacent rigs in one go. The calibration process will take an entire day and the furnace cannot be left on overnight as it does not have an over-temperature safety cut out. This means that it is best to start the furnace first thing in the morning (or arrange with Steve Harding for it to be started) and make sure that all readings are taken as soon as possible.


(5)

6. Open the "Tests and Calibrations" subfolder and open the file "TC Start.xls" (it can be helpful to rename the file as "yyyTC Start.xls" to avoid later confusion). The excel file is shown on the next page. Enter all the information requested such as the calibration date of the calibration thermocouple, rig number and the names of the preceding and following tests.

7. Ensure that all the cables are plugged in and tum on the furnace and the display for the calibration thermocouple. For a test at 550oC, measurements are made at 400oC, 500˚C, 540˚C, 545˚C, 550˚C, 555˚C, 560˚C and 600˚C. Set the furnace to 400oC (or the temperature required) using the up and down arrows on the control panel, allow the indicated furnace temperature to become stable at this value and then wait another 30 minutes before taking the first measurement for the temperature recorded by the calibration thermocouple to stabilise.

8. Open the channel monitor screen if it is not already open by going to the main Orchestrator menu programme, clicking on the "Channel monitor" menu and clicking on "Monitor selection".

(9)

In the window that opens select the file "DS7000" and click open.

Thermocouple Calibration

Date calibrated:
Calibrated by:

Rig No:

Previous Test:

Next Test:

Date of Reference Thermocouple Calibration 30/04/2010

Time	Celcius Aim	Calibration	Celcius Correction	Celcius True Temp	Room	Microvolts RTC1	Microvolts RTC2	Microvolts RTC3
	400		-0.74	-0.74				
	400		-0.74	-0.74				
	500		-0.89	-0.89				
	500		-0.89	-0.89				
	540		-1.14	-1.14				
	540		-1.14	-1.14				
	545		-1.09	-1.09				
	545		-1.09	-1.09				
	550		-1	-1				
	550		-1	-1				
	555		-1.09	-1.09				
	555		-1.09	-1.09				
	560		-1.15	-1.15				
	560		-1.15	-1.15				
	600		-0.26	-0.26				
	600		-0.26	-0.26				

	RTC1	RTC2	RTC3
Gradient (C/uV)	#DIV/0!	#DIV/0!	#DIV/0!
0uV Offset (C)	#DIV/0!	#DIV/0!	#DIV/0!

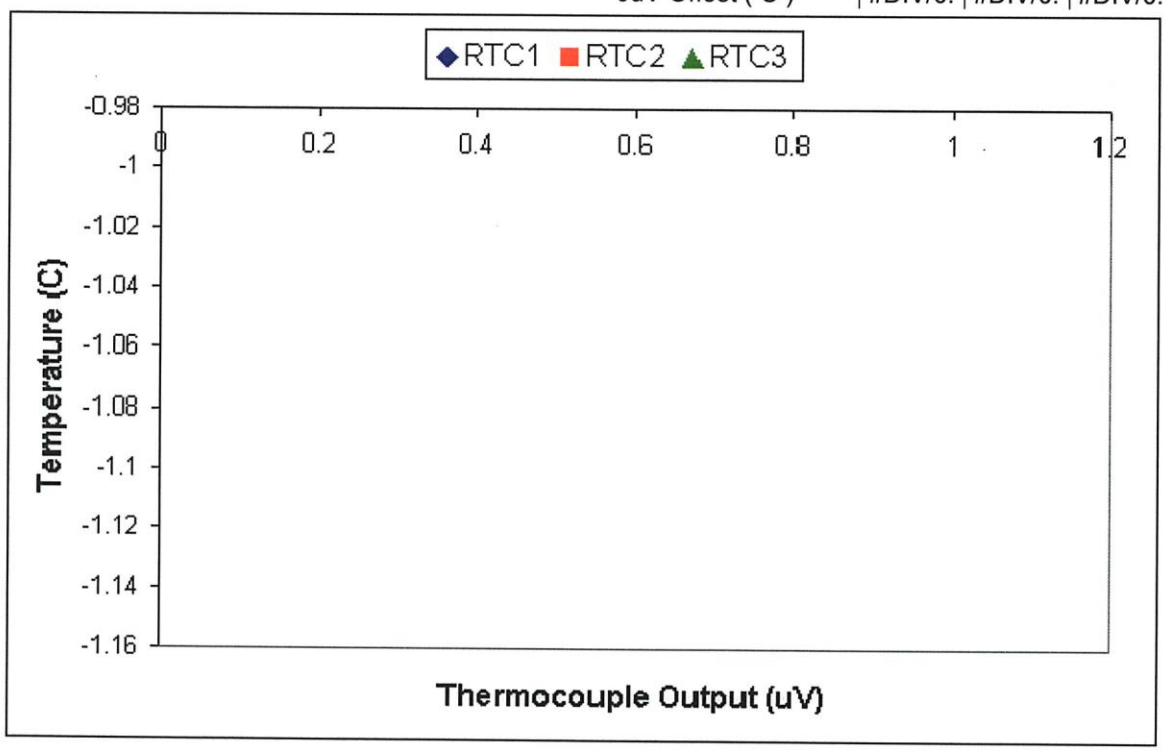

9. Find the four channels associated with the thermocouples on the rig that you are

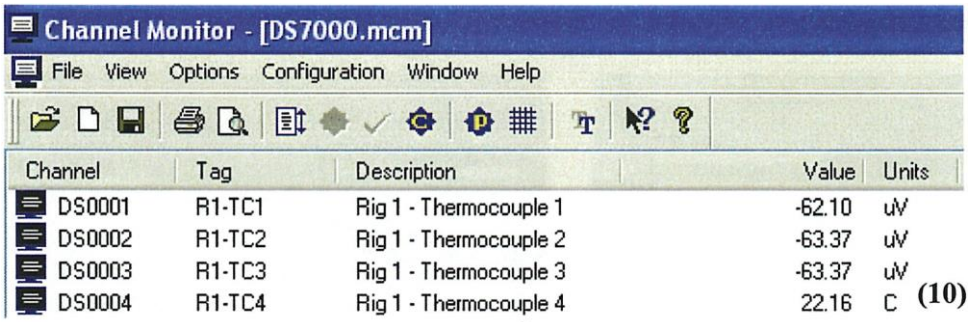

(10)

calibrating. Record the time of the measurement, the value recorded on the screen of the calibration thermocouple, room temperature (Rig X Thermocouple 4) and the values in microvolts recorded by the thermocouples 1 to 3.

10. Two measurements must be made at each temperature with a gap of 10 minutes between taking the measurements. After the second measurement has been made, raise the temperature of the furnace to the temperature of the next measurement and allow both the furnace temperature and the temperature recorded by the calibration thermocouple to stabilise. The following waiting times have been found to be appropriate for the temperature rises used to calibrate thermocouple for a test at 550˚C:

Temperature Rise	Time Until Next Reading
5°C	40 mins
40°C	60 mins
100°C	75 mins

11. Repeat step 11 for all the temperatures at which measurements are to be taken. When all the measurements are completed the "Gradient (˚C/mV)" and "omv offset (˚C)" boxes for each of the three thermocouples will display the values calculated for a best fit line (least squares regression) through the measurements taken between 540˚C and 560˚C. These are the values to be used for calculating the temperature from the thermocouple signal during the experiment.

Calibrating the LVDTs

12. Retrieve the tripod micrometer from the RS lab. Fit the brass LVDT holder into the hole in the end of the tripod micrometer and secure using the grub screw in the hole in one side of the end piece. Attach the aluminium LVDT core adaptor to the barrel of the micrometer and secure using the grub screw.

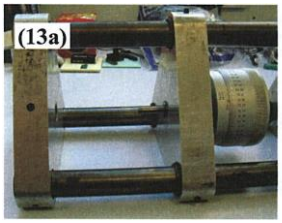

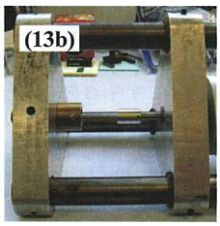

13. Make sure that the core of the LVDT is fully inserted into the body for safety and carefully push the LVDT into the brass LVDT holder, keeping the signal cable located in the slot on the side of the holder to avoid damaging it (fig 14a). Secure the LVDT by tightening the securing screw very gently. Overtightening the screw could cause damage to the case of the LVDT. Screw the LVDT core into the LVDT core into adaptor (fig 14b).
14. Open the channel monitor screen if it is not already open by going to the main Orchestrator menu programme, clicking on the "monitors" menu, opening the "channel monitor" menu and clicking on "monitor selection". In the window that opens select the file "DS7000" and click open. Find the channel associated with the LVDT that you are calibrating, named "RX-LVDTy".
15. Wind the barrel of the micrometer to the zero position by turning it clockwise. Undo the three grub screw at the comers of the central aluminium plate that secure it in position (fig l6a). Move the central plate towards the LVDT so that the value displayed for the LVDT is increasing (fig 16b). Do this until the value displayed starts to reach a minimum and the rate of increase drastically decreases (typically somewhere around 4800 to 5200 mV) - this should occur with approximately 2-.3 mm of the thinnest section of the LVDT core still exposed outside the LVDT (fig 16c).
16. Secure the central plate by tightening the three grub screws at the comers.

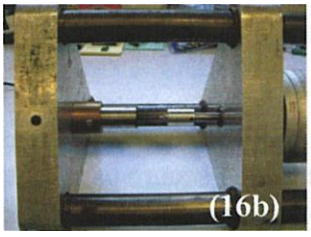

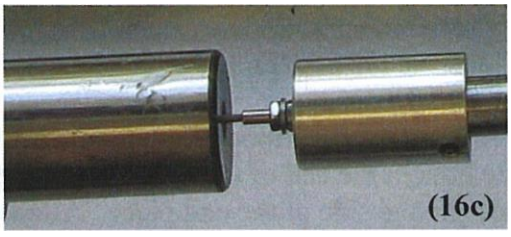

Set the micrometer barrel to the zero position by winding clockwise past zero and then

returning turning the barrel anti-clockwise. The zero lines on the rotating and stationary parts of the micrometer barrel must be aligned perfectly. From this point onwards all data readings must always be approached anti-clockwise. If you overshoot the position of the reading then you must turn back clockwise 1/4 to 1/2 a tum past it and approach it again to avoid backlash errors.

17. In the "Tests and Calibrations" folder for your test, rename the file "- LVDTx" as appropriate and open it. Fill in the details such as the date and the previous and next test.

LVDT Calibration **(18)**

Displacement (mm)	Voltage (mV) 1st Run	2nd Run
20		
19.5		
19		
18.5		
18		
17.5		
17		
16.5		
16		
15.5		
15		
14.5		
14		
13.5		
13		
12.5		
12		
11.5		
11		
10.5		
10		
9.5		
9		
8.5		
8		
7.5		
7		
6.5		
6		
5.5		
5		
4.5		
4		
3.5		
3		
2.5		
2		
1.5		
1		
0.5		
0		

Date calibrated:
Calibrated by:
Rig: 7
LVDT No: 1
Previous Test:
Next Test:

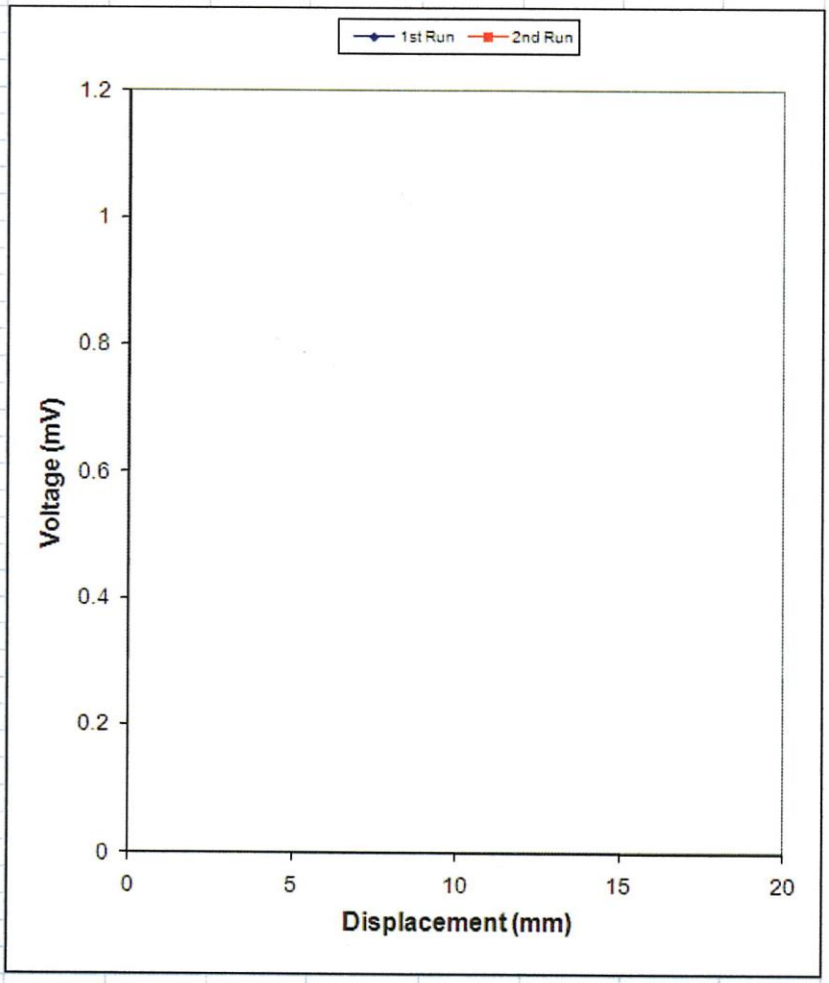

18. Enter the value recorded for the LVDT on the channel monitor screen in the Omm

box of the "1st Run" column. Tum the micrometer one full turn anti-clockwise and all 2-3 seconds for the reading on the channel monitor screen to refresh before recording the reading in the 0.5mm box. Repeat this until the reading is between -'4800 mV and -5200 mV and starting to flatten off on the graph. The more carefully the results are taken at this stage, the better the calculations from the creep results will be. The results are recorded starting from the bottom in this stage because the signal voltages must be recorded in order of increasing size for Excel to handle the calculations correctly later. In order for the calibration to comply with British Standards, the LVDT core must be drawn through the LVDT in the direction in which the test will take place, necessitating a start from positive signal voltages.

19. Wind the micrometer back to zero. Choose a position in the results of the first run where the signal voltage is approximately +3500 mV and wind the micrometer to this position. For the second run, results should be taken every 1 mm (two full anti-clockwise turns of the micrometer) from this position until the signal voltage is approximately -3500 mV. To comply with British Standards this should comprise at least 10 readings. During this run you should check that the results tally with the results of the first run to within a few mV.
20. Unscrew the LVDT core from the aluminium adaptor and store it carefully inside the body of the LVDT. Undo the LVDT securing screw and carefully remove the LVDT from the brass LVDT holder. Repeat steps 14-20 with the second LVDT. Note that the calibration is only valid for that specific combination of the LVDT and LVDT core. If the LVDT cores are mixed up then the calibration must be repeated.

Fitting a test specimen

21. Ensure that all thermocouples and LVDTs have been calibrated, that the load cell calibration is in date.
22. Screw the load cell into the base plate.

23. Use the 6 bolts to screw the base plate into the bottom chuck.

24. Lubricate both threaded ends of the test specimen and screw it into the upper and lower specimen grips.

25. Attach a pair of extensometry grips to the lower ridge on the specimen grip. Locate the grip with the thermocouple slot at the front of the rig and the two holes for the extensometry rods at the sides. Lubricate the bolts and place both in an anti-clockwise direction (this allows clearance for the upper extensometry rods). Tighten the two bolts fully and evenly.
26. Attach the longer of the extensometry rods to the grip on the lower ridge. Tighten the bolts tightly.

27. Attach a pair of extensometry grips to the upper ridge of the specimen grip. Locate the grip with the holes for the extensometry roughly above the shorter extensometry rods. It does not matter which side the thermocouple slot is on. Lubricate and tighten the bolts. Be sure not to overtighten grip should still be able to rotate.
28. Attach the shorter of the extensometry rods to the grip on the upper ridge, tighten bolts.
29. Rotate the upper extensometry grips so that the upper rods are vertical and the lower rods sit evenly located in the 10mm D holes in the upper extensometry disc. Tighten bolts.
30. Check all bolts sited within the furnace are evenly tightened.
31. Fit the bottom series bar through the central hole in the extensometry and screw into the load cell at the bottom of the rig. You will have to lift the loading rod/extensometry into the furnace before screwing it in. Take care not to knock the inside of the furnace.
32. Ensure metal plates that fix the top thread and top wheel in line are out of assembly. Remove top wheel and ball bearing that sits below it.

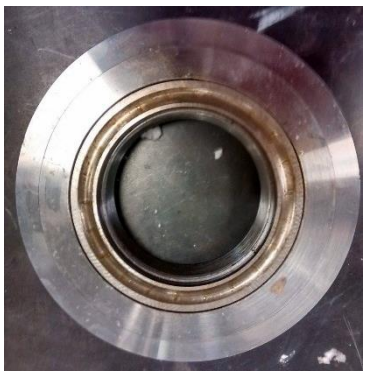

33. Screw top series bar into top end of specimen.

34. Place ball bearing around threads at top end bar.
35. Screw top wheel down to top check, keep a careful eye on the load to make sure none is being applied, this shouldn't be possible with hand screwing.
36. Once top wheel has screwed all the way down to the top chuck and any extra turns start adding stress to the specimen insert the metal plates down the side of the top thread and top wheel to hold in line.

Fitting the Thermocouples

37. Insert the tip of thermocouple 3 through the 8mm holes in the lower and upper extensometry discs. After thermocouple has been passed through holes bend the end of thermocouple into a U shape. Insert thermocouple into the lower extensometry grip. Ensure the insulation covers as much as possible of the exposed thermocouple within the furnace.
38. Bend the end of thermocouple 1 into a U shape and insert the end into the thermocouple slot in the upper extensometry grip. Ensure that the insulation covers as much as possible of the exposed length of the thermocouple that will lie within the furnace.
39. Carefully bend thermocouple 2 twice at right angles so that the tip is running parallel to the main length but approximately 2 cm to the side. The tip should be approximately 1cm in length. Be careful not to break thermocouple by bending too aggressively.
40. Tie thermocouple 2 to the gauge length of the specimen using a short length of stainless steel wire. In the confined space between the extensometry grips it will be necessary to make a few loose turns by hand and then tighten the wire using pliers. Use as many bits of wire as is necessary to secure the specimen.
41. Tie all thermocouples to the top series bar using lengths of stainless steel wire to keep them out the way.

Testing the Extensometry

42. Insert the LVDTs into the 19mm holes in the lower extensometry discs. Screw the LVDT cores into the bottom of the upper extensometry rods. Adjust the position of the LVDTs until the signal displayed on the "channel monitor" screen is within the linear range for the LVDT. For a specimen with a total expected extension of 10mm a good

starting value is between 2800 and 3000mV. For a specimen with a shorter expected extension a lower starting value may be appropriate. When the LVDTs are in the correct position, carefully tighten the securing screws using a 2mm allen key. Do not overtighten the screws as damage will occur to the LVDT.

43. Choose a testing stress that is known to be well within the elastic region of the specimen (100-150MPa for stainless steel).
44. Start the logger for the rig by going to the main Orchestrator screen on the logger PC, opening the "loggers" menu and clicking on the name of the relevant rig. Check that the logging rate is set to 2 seconds, Click on the save button and then click on the play button to start logging.
45. Allow approximately ten seconds for the datalogger to acquire readings before applying a stress. Rotate top wheel slowly using turning screws. Allow a gap of at least 10 seconds after every 20MPa of stress increased to give time for the data logger to take multiple readings.
46. When you have reached the required load, rotate the top wheel slowly in the opposite direction to remove the load.
47. Click the stop button on the logger screen. This will create a file called "Rig X - .DIF" in the folder "Rig X" on the desktop. Move this file into the "tests and calibrations" folder for your test and rename it "yyy-LVDTTest01.xls".
48. Open this file and copy the contents, excluding the header line, into the "Raw" tab of the "yyy-LVDTTest01.xls" file, starting on row 6. Note the number of the last line of the "Raw" tab that contains data and either delete rows or copy equations to new rows on the "Data" tab so that it finishes on the same row (Having too many rows will cause errors in the graph).

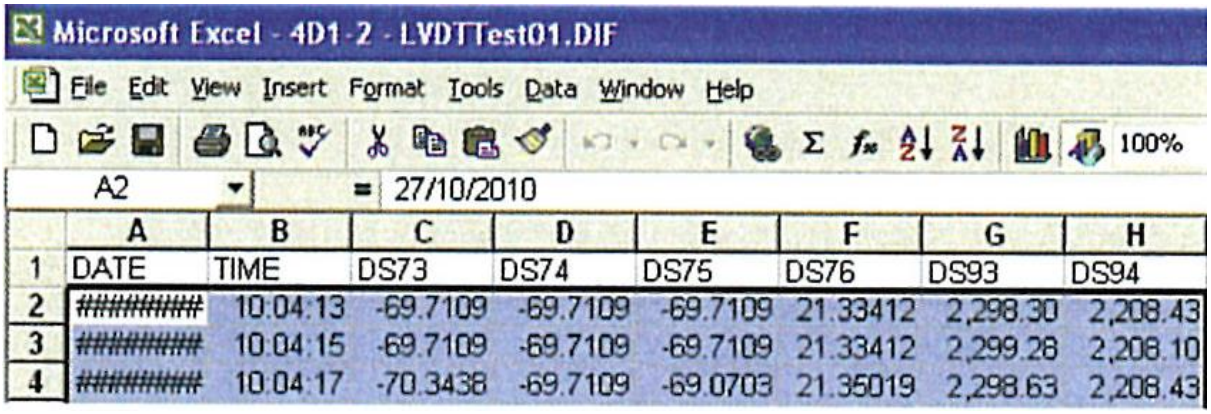

	A	B	C	D	E	F	G	H
1	DATE	TIME	DS73	DS74	DS75	DS76	DS93	DS94
2	##########	10:04:13	-69.7109	-69.7109	-69.7109	21.33412	2,298.30	2,208.43
3	##########	10:04:15	-69.7109	-69.7109	-69.7109	21.33412	2,299.28	2,208.10
4	##########	10:04:17	-70.3438	-69.7109	-69.0703	21.35019	2,298.63	2,208.43

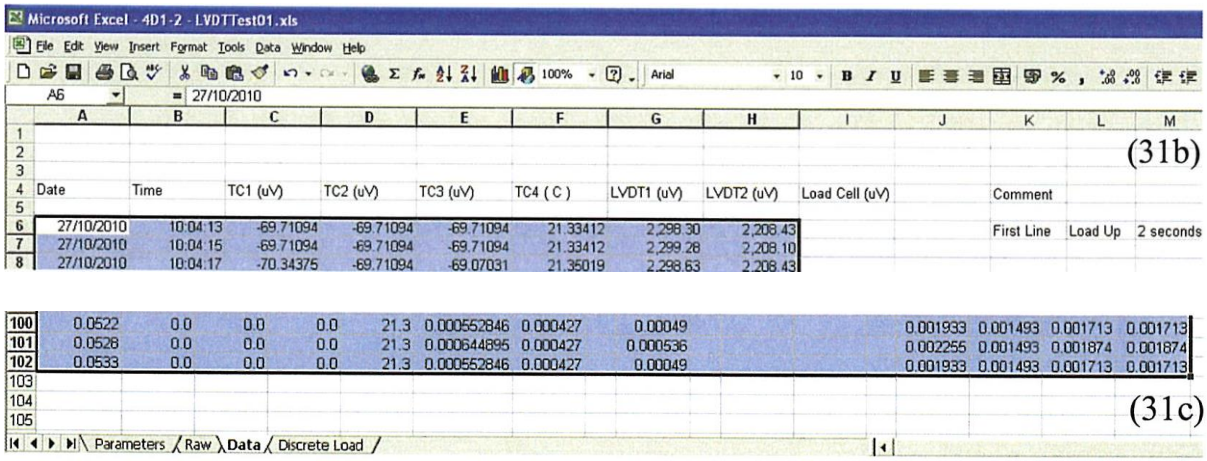

Heating up the specimen

********WHEN HEATING UP THE SPECIMEN ENSURE THAT THE RIG IS LOOSE, AND THE SPECIMEN IS UNDER NO STRESS********

49. Turn on the furnace controller but do not push the “Furnace On” button. The controller will light up like a merry little Christmas tree.
50. To update the temperature calculations in Orchestrator, go to the main Orchestrator screen. Open the calculated channels configuration window by going to r- ‘the “Processors” menu and click “Calculated channels” option.
51. Select the thermocouple channels for the rig in question by double—clicking on the channel tagged “Rig X TC Y”. This will open the configuration window. The formula is located at the bottom of this window in a box marked “Formula”. To calculate the temperature in OC, this takes the form: [Logger channel] x Thermocouple Gradient in OC/ uV + Thermocouple Offset in OC. Update the offset and gradient and click “Ok” to close the window.
52. Save the updated formulas by clicking on the save icon and restart the calculator by opening the “Control” menu and clicking on the “Restart Calculator” option. The calculated channels window can now be closed.

53. Open the “Configurable Monitor” application if not already open by going to the main Orchestrator menu Screen on the “Monitors” menu, opening the “Configurable monitor” menu and clicking on “Monitor selection”. In the window that opens, select the “RigXTC” monitor file and click open. If the Configurable Monitor screen is already open the, file can be opened by clicking on the “File” menu and click on “Open”. This will display three columns of graphs. In each column there are graphs for the top (TC1), middle (TC2) and bottom (TC3) of the specimen in order. The different columns display different temperature ranges for initial heating, temperature adjustment to reach approximately the right temperature and final fine tuning. These are initially set for a working temperature of 550°C but can be altered by right clicking on each graph, clicking on “Visual/Display Properties”, selecting the “Tracks” tab and changing the “Max”, “Min”, “Display Max” and “Display Min” settings. If changing the range of the graph, it may be necessary to go to the Monitor menu to check that it is in “Configure Mode” and that the “Lock Monitor” Option is not selected.

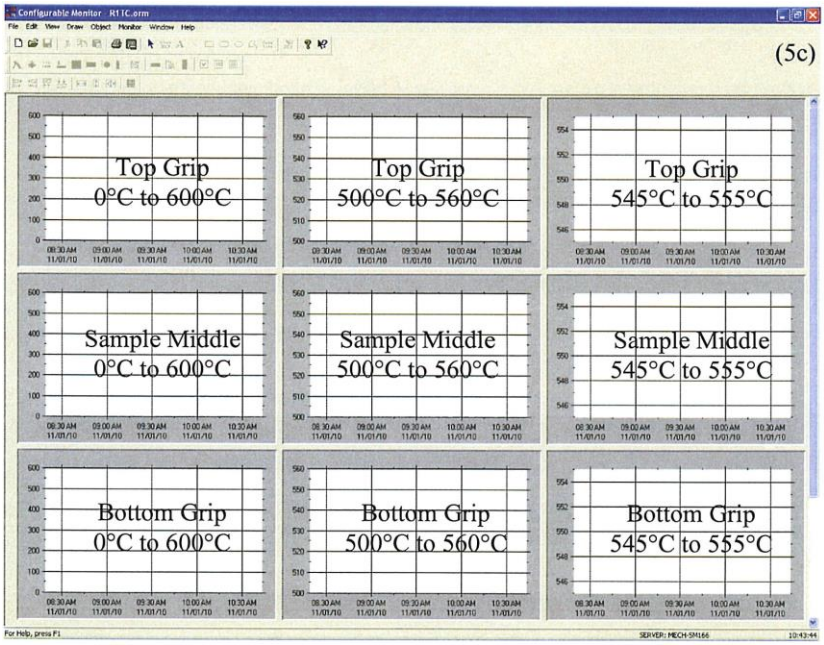

54. Set the controllers to a suitable initial temperature using the up and down arrows. In general more heat will be lost through the top and bottom so a suitable starting setting is top: test temp +10°C, mid: test temp - 10°C, bottom: test temp + 10°C. Settings from a previous run can also be lowered by a few degrees. Bear in mind that, in order to comply with British Standard BS EN 10291:2000, the temperature of the sample MUST at no time exceed the testing temperature +3°C.
55. Before starting the furnace itself, start and pause the three controllers. Do this by pressing the up and down arrows together once to start the controllers. Immediately press the up and down buttons together a second time to pause the controllers. Check that the setting of the overtemperature alarm (the bottom controller screen on each rig)

is suitable - this should be approximately 50°C above the temperature setting of the middle zone (the location of the over temperature thermocouple).

56. Start the logger for the rig by going to the main Orchestrator screen on the Control Loggers; logger PC, opening the "Loggers" menu and clicking on the name of the relevant rig. Check that the logging rate is set to 5 minutes. Click on the save button and then click on the play button to start.
57. Start the furnace by pressing the green "Furnace On" button. Start the three controllers as quickly as possible in order by pressing the up and down arrows together. The furnace will now climb to the target temperature at 5°C/min.
58. Each control unit will display the current measured temperature of the thermocouple at the top and the current target temperature at the bottom. Initially the measured temperature will race up to 50+°C while the target temperature is only up by two or three degrees. This is unavoidable, being caused by the time taken for the first input of power to give any heating, and is not a cause for alarm. The power input to the furnace will then be turned back off until the target temperature has caught up with the measured temperature.
59. While the furnace is heating to the target temperature, keep an eye on the graphs and also on the lever arm on rigs 4 to 9. Ensure that the lever arm is kept level to keep the sample in the correct position in the furnace. This will prevent a sudden change in thermocouple readings when the arm is levelled and the sample moves.
60. As the sample approaches the test temperature, adjust the three zones independently to approach the test temperature in a controlled manner while eliminating variations in temperature between the thermocouples on the specimen. If adjusting the settings of the zones significantly from the initial settings, check that the setting of the over temperature alarm is approximately 50°C than the setting of the middle zone.
61. Once the sample has reached the test temperature, adjust the three zones independently by 1 or 2 °C up or down at a time to try to eliminate variations in temperature between the thermocouples. British Standard BS EN 1029122000, calls for the temperature of the thermocouples on the sample to be within 3°C of the testing temperature and for a maximum variation of 3°C between the readings during the life of the test. A temperature of 1°C with a maximum variation of 1°C is normally easily achievable and is more likely to allow the natural fluctuation of temperatures during the test to remain within tolerances than a poor initial setup.

Loading Up

62. Open the logger for the rig by going to the main Orchestrator screen on the logger PC, opening the "Loggers" menu and clicking on the name of the relevant rig (fig 1a). Click the stop button to halt the logging of the heating up. This will create a file called "Rig X - .DIF" in the folder "Rig X" on the desktop. Move this file into the "Raw Data" folder for your test and rename it to "yyy ~— 01 Heat Up.DIF".
63. Change the logging rate to 2 seconds. Click on the save button and then click on the play button to start logging.
64. Open the "Configurable Monitor" application if not already open by going to the main Orchestrator menu screen, clicking on the "Monitors" menu.
65. Open the "Configurable monitor" menu and click on "Monitor selection". In the window that opens, select the "Loads and Stresses" monitor file and click open. If the Configurable Monitor screen is already open the each rig on screen.

66. Apply the load to the specimen by rotating the top wheel, you will need to screw the turning rods into the top wheel to be able to gain enough leverage to apply a high stress.
67. Apply 80% of the target stress very quickly (within 5 seconds), then over the next 5 seconds get as close to the target stress as possible.
68. When you have reached the required stress and at least 10 seconds have passed since you have finished turning the top wheel reset the logging interval to every 2 minutes, save the logger settings.
69. At the end of the dwell when re-applying the load be sure to change the logging interval back to every 2 seconds.
70. Then change this back to every 2 minutes once the stress has been applied.
71. When your specimen fails click the stop button on the logger screen. This will create a file called "Rig X — .DIF" in the folder "Rig X" on the desktop. Move this file into the "Raw Data" folder for your test and rename it to "yyy -- 02 Raw test data.DIF".

********IF RUNNING A TEST NOT TO FAILURE ENSURE THAT THE LOAD IS REMOVED AND THE SYSTEM IS LOOSE BEFORE LOWERING THE TEMPERATURE BACK TO ROOM TEMPERATURE********

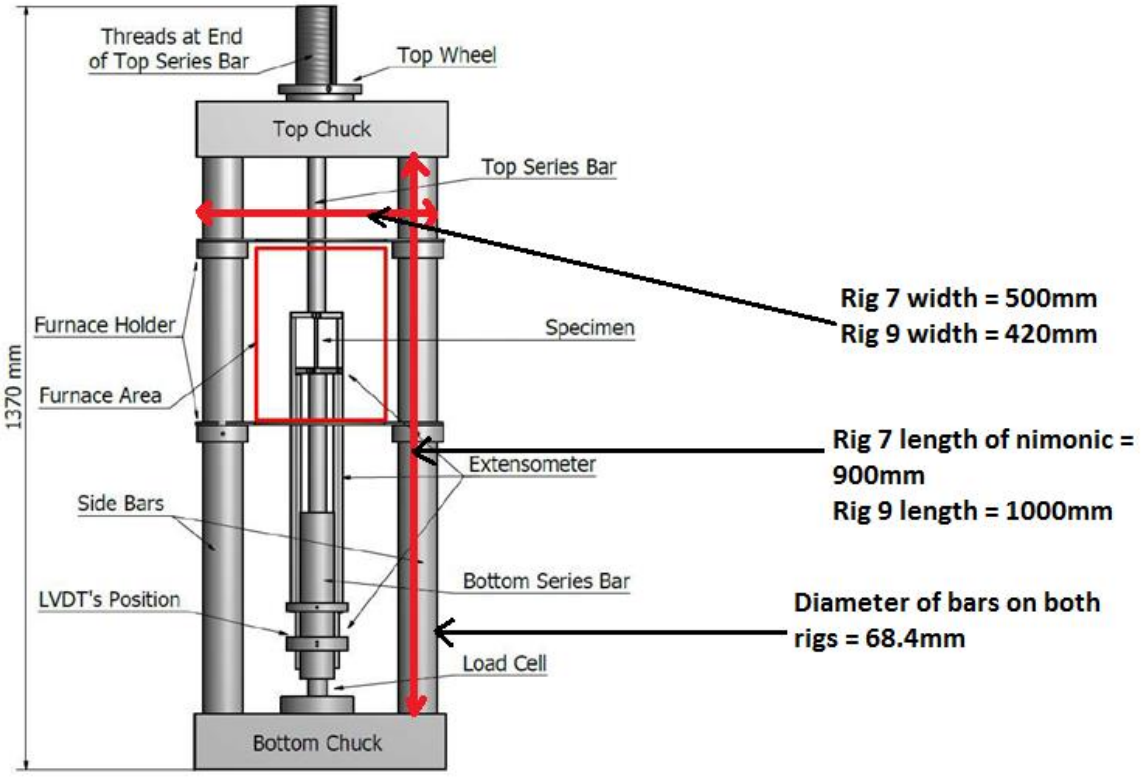

Uniaxial stress relaxation test rig

APPENDIX III - Stress strain tables used in Abaqus

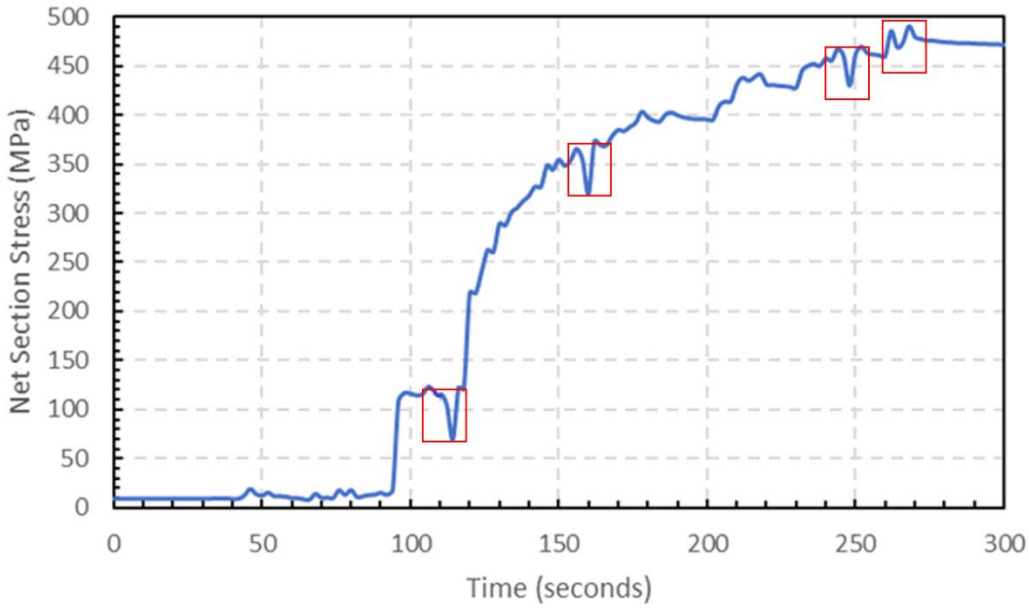

Figure showing the net section stress drop during load up in repeat stress relaxation experiments as manual rotations are applied to the loading wheel.

550˚C

σ (MPa)	ε
0.0	0.00000
30.1	0.00190
60.2	0.00383
90.5	0.00590
121.0	0.00832
128.7	0.00902
136.3	0.00976
144.0	0.01056
151.7	0.01143
188.1	0.01653
225.4	0.02414
264.2	0.03543
305.4	0.05177
350.2	0.07469
400.2	0.10575
457.3	0.14641
524.1	0.19792
603.8	0.26114
700.0	0.33647

515˚C

σ (MPa)	ε
0.0	0.00000
30.1	0.00190
60.2	0.00384
90.5	0.00593
121.0	0.00837
128.7	0.00906
136.3	0.00980
144.0	0.01059
151.7	0.01143
188.0	0.01627
225.2	0.02316
263.5	0.03292
303.8	0.04650
346.8	0.06491
393.6	0.08918
445.5	0.12030
504.2	0.15912
571.6	0.20634
650.0	0.26236